

IZVESTIYA VUZOV POROSHKOVAYA METALLURGIYA I FUNKTSIONAL'NYE POKRYTIYA

POWDER METALLURGY AND FUNCTIONAL COATINGS

Scientific and Technical Journal
Founded in 2007
4 numbers per year

Vol. 16 - № 4 - 2022

Journal is included into the list of the scientific journals recommended by the Highest Attestation Commission of the Ministry of Education and Science of the Russian Federation for publishing the results of doctoral and candidate dissertations.

Abstracting/Indexing: Scopus, RSCI (Russian Science Citation Index) to Web of Science platform, Ulrich's Periodicals Directory, VINITI Database (Abstract Journal).

Founder

National University of Science and Technology «MISIS»
Address: NUST «MISIS», Leninskiy pr. 4, Moscow, 119049 Russia
Internet address: <http://www.misis.ru>

Publisher

LLC «Kalvis»
Actual address: off. 405, Leninskiy pr. 4g, Moscow, 119049 Russia
Address for correspondence: p/o box 28, LLC «Kalvis», Moscow, 119049 Russia
Internet address: <http://www.kalvis.ru>

Editor-in-Chief

Levashov E.A. — Prof., Dr. Sci., Acad. of the RAS, Head of the Department of powder metallurgy and functional coatings, and Head of SHS Center, National University of Science and Technology «MISIS», Moscow, Russia

Editorial Board

Alymov M.I. — Dr. Sci., Corresponding Member of the RAS, Institute of Structural Macrokinetics and Materials Sciences, Moscow reg., Chernogolovka, Russia
Amosov A.P. — Prof., Dr. Sci., Samara State Technical University, Samara, Russia
Bagliuk G.A. — Prof., Dr. Sci., Acad. of the NASU, IPMS NASU, Kiev, Ukraine
Blinkov I.V. — Prof., Dr. Sci., National University of Science and Technology «MISIS», Moscow, Russia
Chen Pengwan — Prof., Dr., Beijing Institute of Technology, Beijing, P.R. China
Chukin M.V. — Prof., Dr. Sci., Magnitogorsk State Technical University, Magnitogorsk, Russia
Danninger H. — Prof., Dr., Vienna University of Technology, Austria
Derin Bora — Assoc. Prof., Dr., Istanbul Technical University, Maslak, Istanbul, Turkey
Dorofeyev V.Yu. — Prof., Dr. Sci., South-Russian State Polytechnical University (NPI), Novocherkassk, Russia
Estrin Yu.Z. — Prof., Dr., Monash University, Clayton, Australia
Feng Peizhong — Prof., Dr., China University of Mining and Technology, Xuzhou, P.R. China
Fu Zhengyi — Prof., Dr., Wuhan University of Technology, Wuhan, P.R. China
Ilyushchanka A.Ph. — Prof., Dr. Sci., Acad. of the NAS of Belarus, State Research and Production Powder Metallurgy Association, Minsk, Belarus
Kolobov Yu.R. — Prof., Dr. Sci., Belgorod National Research University, Belgorod, Russia
Komlev V.S. — Prof., Dr. Sci., Corresponding Member of the RAS, Institute of Metallurgy of the RAS, Moscow, Russia
Konyashin I. — Prof., Dr., Element Six GmbH, Burghaun, Germany
Korolyov Yu.M. — Prof., Dr. Sci., Scientific and Technical Association «Powder Metallurgy», Moscow, Russia
Kostikov V.I. — Prof., Dr. Sci., Corresp. Member of the RAS, National University of Science and Technology «MISIS», Moscow, Russia
Kovalev D.Yu. — Dr. Sci., Institute of Structural Macrokinetics and Materials Sciences, Chernogolovka, Russia
Kulinich S.A. — Associate Prof., PhD, Tokai University, Japan
Kuzmin S.V. — Prof., Dr. Sci., Corresponding Member of the RAS, Volgograd State Technical University, Volgograd, Russia
Kuznetsov V.P. — Prof., Dr. Sci., Ural Federal University, Ekaterinburg, Russia
Levinsky Yu.V. — Prof., Dr. Sci., Moscow Technological University (MITHT), Moscow, Russia

Ligachyov A.E. — Prof., Dr. Sci., Prokhorov General Physics Institute, Russian Academy of Sciences, Moscow, Russia
Lopatin V.Yu. — Cand. Sci., National University of Science and Technology «MISIS», Moscow, Russia
Lozovan A.A. — Prof., Dr. Sci., Moscow Aviation Institute (National Research University), Moscow, Russia
Lysak V.I. — Prof., Dr. Sci., Acad. of the RAS, Volgograd State Technical University, Volgograd, Russia
Makarov A.V. — Dr. Sci., Corresponding Member of the RAS, M.N. Mikheev Institute of Metal Physics of the Ural Branch of the Russian Academy of Sciences, Ural Federal University, Ekaterinburg, Russia
Mishnaevsky L.L. — Dr. habil., Technical University of Denmark, Roskilde, Denmark
Mukasyan A.S. — Prof., Dr., University of Notre Dame, USA
Oglezneva S.A. — Prof., Dr. Sci., Perm National Research Polytechnical University, Perm, Russia
Ordanian S.S. — Prof., Dr. Sci., St. Petersburg State Technological Institute (Technical University), St. Petersburg, Russia
Orrù Roberto — Prof., Dr., University of Cagliari, Cagliari, Italy
Panteleev I.B. — Prof., Dr. Sci., St. Petersburg State Technological Institute (Technical University), St. Petersburg, Russia
Petrzhik M.I. — Dr. Sci., National University of Science and Technology «MISIS», Moscow, Russia
Pogozhev Yu.S. — Cand. Sci., National University of Science and Technology «MISIS», Moscow, Russia
Polyakov V.V. — Prof., Dr. Sci., Altai State University, Barnaul, Russia
Popovich A.A. — Prof., Dr. Sci., Corresp. Member of the RAS, St. Petersburg State Polytechnical University (National Research University), St. Petersburg, Russia
Porozova S.E. — Dr. Sci., Perm National Research Polytechnical University, Perm, Russia
Rempel A.A. — Prof., Dr. Sci., Acad. of the RAS, Institute of Metallurgy of the Ural Branch of RAS, Ekaterinburg, Russia
Rustichelli F. — Prof., Dr., University of Marches, Ancona, Italy
Shlyapin S.D. — Prof., Dr. Sci., Moscow Aviation Institute (National Research University), Moscow, Russia
Shtansky D.V. — Dr. Sci., National University of Science and Technology «MISIS», Moscow, Russia
Shulov V.A. — Prof., Dr. Sci., Moscow Aviation Institute (National Research University), Moscow, Russia
Vityaz' P.A. — Prof., Dr., Acad. of the NAS of Belarus, Minsk, Belarus
Zaitsev A.A. — Cand. Sci., National University of Science and Technology «MISIS», Moscow, Russia
Zheng YongTing — Prof., Dr., Harbin Institute of Technology, Harbin, P.R. China

Editorial Staff

Editorial office address: off. 203, NUST «MISIS», Leninskiy pr. 4g, Moscow, 119049 Russia

Address for correspondence: «Izvestiya vuzov. Poroshkovaya metallurgiya i funktsional'nye pokrytiya» (box 164), NUST «MISIS», Leninskiy pr., 4, Moscow, 119049 Russia

Phone: (495) 638-45-35. **E-mail:** izv.vuz@misis.ru. **Internet address:** <http://powder.misis.ru>

Leading editor: Kudinova A.A.

Executive editor: Sosnina O.V.

Layout designer: Legkaya E.A.

Subscription: Ural-Press Agency

Format 60×88 1/8. Quires 11,75

Signed print 2.12.2022

Certificate of registration No. FS77-27955 (12.04.2007)

Re-registration PI No. FS77-79230 (25.09.2020)

Online version: <http://powder.misis.ru>; <http://www.kalvis.ru>

This publication may not be reproduced in any form without permission.

©  NUST «MISIS», LLC «Kalvis», 2007

© «Izvestiya Vuzov. Poroshkovaya Metallurgiya i Funktsional'nye Pokrytiya», NUST «MISIS», LLC «Kalvis», 2007

© «Izvestiya Vuzov. Poroshkovaya Metallurgiya i Funktsional'nye Pokrytiya», 2022

ИЗВЕСТИЯ ВУЗОВ ПОРОШКОВАЯ МЕТАЛЛУРГИЯ И ФУНКЦИОНАЛЬНЫЕ ПОКРЫТИЯ

POWDER METALLURGY AND FUNCTIONAL COATINGS

Научно-технический журнал
Основан в 2007 г. Выходит 4 раза в год

Том 16 - № 4 - 2022

Журнал включен в перечень научных журналов, рекомендованных ВАК Минобрнауки РФ для публикации результатов диссертаций на соискание ученых степеней. Журнал индексируется в международной базе данных Scopus, Russian Science Citation Index (RSCI) на платформе Web of Science, Ulrich's Periodicals Directory, РИНЦ, а также входит в базу данных (реферативный журнал) ВИНТИ.

Учредитель

ФГАУ ВО «Национальный исследовательский технологический университет «МИСиС»»

Адрес: 119049, Москва, Ленинский пр-т, 4
<http://www.misis.ru>

Издатель

ООО «Калвис»

Фактический адрес: 119049, Москва, Ленинский пр-т, 4 (корп. 4г, оф. 405)
Почтовый адрес: 119049, Москва, а/я 28 для ООО «Калвис»
<http://www.kalvis.ru>

Главный редактор

Левашов Е.А. — докт. техн. наук, акад. РАЕН, проф., НИТУ «МИСиС», Москва

Редакционная коллегия

Алимов М.И. — докт. техн. наук, чл.-кор. РАН, проф., ИСМАН, Черноголовка
Амосов А.П. — докт. физ.-мат. наук, проф., СамГТУ, Самара
Баглик Г.А. — докт. техн. наук, акад. НАНУ, проф., ИПМ НАН Украины, Киев
Блинов И.В. — докт. техн. наук, проф., НИТУ «МИСиС», Москва
Витязь П.А. — докт. техн. наук, акад. НАНБ, проф., НАН Беларуси, Минск
Дорофеев В.Ю. — докт. техн. наук, проф., ЮРГПУ (НПИ), Новочеркасск
Зайцев А.А. — канд. техн. наук, доцент, НИТУ «МИСиС», Москва
Ильющенко А.Ф. — докт. техн. наук, акад. НАН Беларуси, проф., ГНПО ПМ НАН Беларуси, Минск
Ковалев Д.Ю. — докт. физ.-мат. наук, ИСМАН, Черноголовка
Колобов Ю.Р. — докт. физ.-мат. наук, проф., НИУ «БелГУ», Белгород
Комлев В.С. — докт. техн. наук, чл.-кор. РАН, проф., ИМЕТ РАН, Москва
Королев Ю.М. — докт. техн. наук, проф., НТА «Порошковая металлургия», Москва
Костиков В.И. — докт. техн. наук, чл.-кор. РАН, проф., НИТУ «МИСиС», Москва
Кузнецов В.П. — докт. техн. наук, проф., УрФУ, Екатеринбург
Кузьмин С.В. — докт. техн. наук, чл.-кор. РАН, проф., ВолгГТУ, Волгоград
Левинский Ю.В. — докт. техн. наук, проф., МТУ (МИТХТ), Москва
Лигачев А.Е. — докт. физ.-мат. наук, проф., ИОФ РАН, Москва
Лозован А.А. — докт. техн. наук, проф., МАИ (НИУ), Москва
Лопатин В.Ю. — канд. техн. наук, доцент, НИТУ «МИСиС», Москва
Лысак В.И. — докт. техн. наук, акад. РАН, проф., ВолгГТУ, Волгоград
Макаров А.В. — докт. техн. наук, чл.-кор. РАН, ИФМ УрО РАН, УрФУ, Екатеринбург
Оглезнева С.А. — докт. техн. наук, проф., ПНИПУ, Пермь
Орданьян С.С. — докт. техн. наук, проф., СПбГТИ (ТУ), Санкт-Петербург
Пантелеев И.Б. — докт. техн. наук, проф., СПбГТИ (ТУ), Санкт-Петербург

Петржиж М.И. — докт. техн. наук, проф., НИТУ «МИСиС», Москва
Погожев Ю.С. — канд. техн. наук, доцент, НИТУ «МИСиС», Москва
Поляков В.В. — докт. физ.-мат. наук, проф., АлтГУ, Барнаул
Попович А.А. — докт. техн. наук, чл.-кор. РАЕН, проф., СПбГПУ, Санкт-Петербург
Порозова С.Е. — докт. техн. наук, проф., ПНИПУ, Пермь
Ремпель А.А. — докт. техн. наук, акад. РАН, проф., ИМЕТ УрО РАН, Екатеринбург
Чукин М.В. — докт. техн. наук, проф., МГТУ, Магнитогорск
Шляпин С.Д. — докт. техн. наук, проф., МАИ (НИУ), Москва
Штанский Д.В. — докт. физ.-мат. наук, НИТУ «МИСиС», Москва
Шулов В.А. — докт. физ.-мат. наук, проф., МАИ (НИУ), Москва
Chen Pengwan — Prof., Dr., Beijing Institute of Technology, Beijing, P.R. China
Danninger H. — Prof., Dr., Techn. University Wien, Austria
Derin Bora — Assoc. Prof., Dr., Istanbul Technical University, Maslak, Istanbul, Turkey
Estrin Yu. — Prof., Dr., Monash University, Clayton, Australia
Feng Peizhong — Prof., Dr., China University of Mining and Technology, Xuzhou, P.R. China
Fu Zhengyi — Prof., Dr., Wuhan University of Technology, Wuhan, P.R. China
Konyashin I. — Prof., Dr., Element Six GmbH, Burghaun, Germany
Kulimich S.A. — Associate Prof., PhD, Tokai University, Japan
Mishnaevsky L.L. — Dr. habil., Technical University of Denmark, Roskilde, Denmark
Mukasyan A.S. — Prof., Dr., University of Notre Dame, USA
Orrù Roberto — Prof., Dr., University of Cagliari, Cagliari, Italy
Rustichelli F. — Prof., Dr., University of Marches, Ancona, Italy
Zheng Yongting — Prof., Dr., Harbin Institute of Technology, Harbin, P.R. China

Редакция журнала

Фактический адрес: 119049, Москва, В-49, Ленинский пр-т, 4, НИТУ «МИСиС» (корп. 4г, оф. 203)

Почтовый адрес: 119049, Москва, В-49, Ленинский пр-т, 4, НИТУ «МИСиС», редакция журнала «Известия вузов. Порошковая металлургия и функциональные покрытия» (яч. 164)

Тел.: (495) 638-45-35. **E-mail:** izv.vuz@misis.ru. **Интернет:** <http://powder.misis.ru>

Ведущий редактор: Кудинова А.А.

Выпускающий редактор: Соснина О.В.

Дизайн и верстка: Легкая Е.А.

Подписка: Агентство «Урал-пресс»

Формат 60×88 1/8. Печ. л. 11,75. Подписано в печать 2.12.2022 г.
Свидетельство о регистрации № ФС77-27955 от 12.04.2007 г.
Перерегистрация 25.09.2020 г. ПИ № ФС77-79230

Электронные версии отдельных статей или журнала в целом доступны на сайтах: <http://powder.misis.ru>; <http://www.kalvis.ru>

Перепечатка материалов и использование их в любой форме, в том числе в электронных СМИ, возможны только с письменного разрешения редакции.

© ГМИ и ФП, НИТУ «МИСиС», ООО «Калвис», 2007 г.

© «Известия вузов. Порошковая металлургия и функциональные покрытия», НИТУ «МИСиС», ООО «Калвис», 2007 г.

© «Известия вузов. Порошковая металлургия и функциональные покрытия», 2022 г.

Contents

Production Processes and Properties of Powders

Lebedev V.A., Polyakov V.V.

Electrode processes in the production of microdispersed titanium powder by volumetric electrolytic reduction of its ions with sodium dissolved in the $\text{BaCl}_2\text{--CaCl}_2\text{--NaCl}$ melt in the absence of titanium halides in the initial melt 4

Cherezov N.P., Alymov M.I.

Structure and properties of titanium hydride powder obtained from titanium sponge by SHS hydrogenation 15

Theory and Processes of Formation and Sintering of Powder Materials

Linde A.V., Kondakov A.A., Studenikin I.A., Kondakova N.A., Grachev V.V.

MAX phase Ti_2AlN synthesis by reactive sintering in vacuum 25

Self-Propagating High-Temperature Synthesis

Amosov A.P., Titova Yu.V., Belova G.S., Maidan D.A., Minekhanova A.F.

SHS of highly dispersed powder compositions of nitrides with silicon carbide. Review 34

Kochetov N.A., Kovalev I.D.

Features of SHS of multicomponent carbides 58

Nanostructured Materials and Functional Coatings

Sharin P.P., Sivtseva A.V., Popov V.I.

Air-thermal oxidation of diamond nanopowders obtained by the methods of mechanical grinding and detonation synthesis 67

Materials and Coatings Fabricated Using the Additive Manufacturing Technologies

Kaysova A.O., Levashov E.A.

Features of the impact of hot isostatic pressing and heat treatment on the structure and properties of maraging steel obtained by selective laser melting method 84

Содержание

Процессы получения и свойства порошков

Лебедев В.А., Поляков В.В.

Электродные процессы при получении микродисперсного порошка титана объемным электролитическим восстановлением его ионов натрием, растворенным в расплаве $\text{BaCl}_2\text{--CaCl}_2\text{--NaCl}$, в отсутствие галогенидов титана в исходном расплаве 4

Черезов Н.П., Алымов М.И.

Структура и свойства порошка гидрида титана, полученного из титановой губки методом СВС-гидрирования 15

Теория и процессы формования и спекания порошковых материалов

Линде А.В., Кондаков А.А., Студеникин И.А., Кондакова Н.А., Грачев В.В.

Синтез MAX-фазы Ti_2AlN реакционным спеканием в вакууме 25

Самораспространяющийся высокотемпературный синтез

Амосов А.П., Титова Ю.В., Белова Г.С., Майдан Д.А., Минеханова А.Ф.

СВС высокодисперсных порошковых композиций нитридов с карбидом кремния. Обзор 34

Кочетов Н.А., Ковалев И.Д.

Особенности СВС многокомпонентных карбидов 58

Наноструктурированные материалы и функциональные покрытия

Шарин П.П., Сивцева А.В., Попов В.И.

Термоокисление на воздухе нанопорошков алмазов, полученных механическим измельчением и методом детонационного синтеза 67

Материалы и покрытия, получаемые методами аддитивных технологий

Каясова А.О., Левашов Е.А.

Особенности влияния горячего изостатического прессования и термообработки на структуру и свойства мартенситно-стареющей стали, полученной методом селективного лазерного сплавления 84

UDC 541.135.3 : 669.295

DOI dx.doi.org/10.17073/1997-308X-2022-4-14

Electrode processes in the production of microdispersed titanium powder by volumetric electrolytic reduction of its ions with sodium dissolved in the $\text{BaCl}_2\text{—CaCl}_2\text{—NaCl}$ melt in the absence of titanium halides in the initial melt

© 2022 г. **V.A. Lebedev, V.V. Polyakov**

Ural Federal University n.a. the first President of Russia B.N. Eltsin, Ekaterinburg, Russia

Received 01.03.2022, revised 17.06.2022, accepted for publication 21.06.2022

Abstract: The paper is devoted to a detailed study of cathodic processes, their influence on the anode process, and electrolysis performance. The polarization of a steel cathode in a $\text{CaCl}_2\text{—BaCl}_2\text{—NaCl}$ melt at $t = 610^\circ\text{C}$ was measured. The polarization curve clearly shows the potentials and current densities of the formation of a saturated sodium solution in the electrolyte ($E_{\text{sat}} = -2.97\text{ V}$, $i_c = 0.04\text{ A/cm}^2$, $\lg i_c = -1,4$), and the occurrence of sodium metal on the cathode ($E_{\text{Na}} = -3.22\text{ V}$, $i_{\text{Na}} = 0.12\text{ A/cm}^2$, $\lg i_{\text{Na}} = -0.92$). The value of E_{sat} was used to calculate the concentration of sodium in the electrolyte at $t = 610^\circ\text{C}$ ($1.3 \cdot 10^{-4}$ mol. fr.). The values of E_{sat} , E_{Na} , and their difference ($\Delta E = 0,25\text{ B}$) were confirmed by long-term electrolysis. These fundamental characteristics are the basis for process control and management. During long-term electrolysis, on the curve in the coordinates $E\text{ (V)} - \lg Q\text{ (A}\cdot\text{min)}$, 3 regions close to rectilinear ones were revealed: the discharge of sodium ions from supersaturated solutions at E more negative than E_{sat} (from E_{Na} to E_{sat}), from mixtures of supersaturated and saturated solutions (at a constant E equal to E_{sat}), from diluted solutions (with E more positive than E_{sat}). The activity coefficients of sodium in supersaturated solutions are close to 1, which ensures their increased reducing ability. Maximum degrees of supersaturation (>100) are created at formation and decomposition on the cathode of metallic sodium nuclei, which are sufficient to intensify and prolong electrolysis, to lower the lower temperature limit of its realization from 600 to 350°C . The formation of metallic titanium in the near-anode layer is explained by the disproportionation of Ti^{2+} ions entering the near-anode electrolyte from the anode surface and from the near-cathode melt.

Keywords: electrolytic bulk reduction of titanium, additive technologies, granulometry, potentials and current densities of formation of saturated solutions and metallic sodium on the cathode, nucleation and decay parameters of sodium nuclei, required degrees of supersaturation for their appearance on the cathode.

Lebedev V.A. — Dr. Sci. (Chem.), prof., Department of metallurgy of non-ferrous metals of Ural Federal University n.a. the first President of Russia B.N. Eltsin (UrFU) (620002, Russia, Sverdlovsk region, Ekaterinburg, Mira str., 19).
E-mail: v.a.lebedev@urfu.ru.

Polyakov V.V. — educational master, postgraduate student, Department of metallurgy of non-ferrous metals, UrFU.
E-mail: aheon@mail.ru.

For citation: Lebedev V.A., Polyakov V.V. Electrode processes in the production of microdispersed titanium powder by volumetric electrolytic reduction of its ions with sodium dissolved in the $\text{BaCl}_2\text{—CaCl}_2\text{—NaCl}$ melt in the absence of titanium halides in the initial melt. *Izvestiya Vuzov. Poroshkovaya Metallurgiya i Funktsional'nye Pokrytiya (Powder Metallurgy and Functional Coatings)*. 2022. Vol. 16. No. 4. P. 4—14 (In Russ.). DOI: dx.doi.org/10.17073/1997-308X-2022-4-14.

Электродные процессы при получении микродисперсного порошка титана объемным электролитическим восстановлением его ионов натрием, растворенным в расплаве $\text{BaCl}_2\text{—CaCl}_2\text{—NaCl}$, в отсутствие галогенидов титана в исходном расплаве

В.А. Лебедев, В.В. Поляков

Уральский федеральный университет (УрФУ) им. первого Президента России Б.Н. Ельцина,
г. Екатеринбург, Россия

Статья поступила в редакцию 01.03.2022 г., доработана 17.06.2022 г., подписана в печать 21.06.2022 г.

Аннотация: Работа посвящена детальному изучению катодных процессов, их влиянию на анодный процесс и показатели электролиза. Измерена поляризация стального катода в расплаве $\text{CaCl}_2\text{—BaCl}_2\text{—NaCl}$ при температуре $t = 610^\circ\text{C}$. На по-

ляризационной кривой отчетливо выделяются потенциалы ($E_{\text{нас}} = -2,97$ В) и плотности тока ($i_k = 0,04$ А/см², $\lg i_k = -1,4$) образования насыщенного раствора натрия в электролите и появления металлического натрия на катоде ($E_{\text{Na}} = -3,22$ В, $i_{\text{Na}} = 0,12$ А/см², $\lg i_{\text{Na}} = -0,92$). По величине $E_{\text{нас}}$ рассчитана концентрация натрия в электролите при $t = 610$ °С ($1,3 \cdot 10^{-4}$ мол. дол.). Величины $E_{\text{нас}}$, E_{Na} и их разность ($\Delta E = 0,25$ В) подтверждены при длительном электролизе. Эти фундаментальные характеристики являются основой для контроля и управления процессом. При длительном электролизе на кривой в координатах E (В) — $\lg Q$ (А·мин) выявлены 3 близких к прямолинейным участка: разряд ионов натрия из пересыщенных растворов при E отрицательнее $E_{\text{нас}}$ (от E_{Na} до $E_{\text{нас}}$), из смеси пересыщенных и насыщенных растворов (при постоянном E , равным $E_{\text{нас}}$), из разбавленных растворов (при E положительнее $E_{\text{нас}}$). Коэффициенты активности натрия в пересыщенных растворах близки к 1, что обеспечивает их повышенную восстановительную способность. Максимальные степени пересыщения (>100) создаются при образовании и распаде на катоде зародышей металлического натрия, которые достаточны для того, чтобы интенсифицировать и продлить электролиз, понизить нижний предел температур его реализации с 600 до 350 °С. Образование металлического титана в прианодном слое объяснено диспропорционированием ионов Ti^{2+} , поступающих в прианодный электролит от поверхности анода и из прикатодного расплава.

Ключевые слова: электролитическое объемное восстановление титана, аддитивные технологии, гранулометрия, потенциалы и плотности тока образования на катоде насыщенных растворов и металлического натрия, параметры зарождения и распада зародышей натрия, необходимые степени пересыщения для их появления на катоде.

Лебедев В.А. — докт. хим. наук, проф. кафедры металлургии цветных металлов УрФУ (620002, Свердловская обл., г. Екатеринбург, ул. Мира, 19). E-mail: v.a.lebedev@urfu.ru.

Поляков В.В. — учебный мастер, аспирант кафедры металлургии цветных металлов УрФУ. E-mail: aheon@mail.ru.

Для цитирования: Лебедев В.А., Поляков В.В. Электродные процессы при получении микродispersного порошка титана объемным электролитическим восстановлением его ионов натрием, растворенным в расплаве $\text{BaCl}_2\text{—CaCl}_2\text{—NaCl}$, в отсутствие галогенидов титана в исходном расплаве. *Известия вузов. Порошковая металлургия и функциональные покрытия*. 2022. Т. 16. No. 4. С. 4—14. DOI: dx.doi.org/10.17073/1997-308X-2022-4-14.

Introduction

The constant growth in the production and use of titanium alloys is due to their unique properties — such as corrosion resistance, low specific gravity, mechanical strength at high temperatures, and biocompatibility. Titanium-based alloys are widely used in aircraft and space construction, rocket and missile engineering, automotive engineering, shipbuilding, medicine [1—3], and the chemical industry.

The theoretical foundations of the process of volumetric electrolytic preparation of microstructural metal powders for modern technology have been developed under the guidance of Prof. M.V. Smirnov [4], who demonstrated high reactivity [5] and mobility [6] of this process.

The purpose of this work was to provide scientific justification for the possibility of implementing the process of volumetric intensive electrochemical method developed by the authors for obtaining microdispersed titanium powders for 3D technologies and powder metallurgy [7, 8]. The uniqueness of the process lies in the fact that it is carried out in the absence of dissolved sodium and titanium chlorides in the initial and final electrolytes (unlike the work [9]), with a stepwise increase in the electrolysis current and potentiometric control of the process [10].

To solve this problem, an original method for monitoring and controlling the process under development by measuring the RedOx-potential of the $\text{Ti}^{3+}/\text{Ti}^{2+}$ system in the near-anode layer was proposed and applied in practice. As a result, the mechanisms of the process realization at the initial, main and final stages of electrolysis are disclosed.

It is shown that in the first 12 min of electrolysis, the concentration of inactive Ti^{3+} complex ions increases in the near-anode layer, and sodium dissolved in the electrolyte restores mainly Ti^{2+} ions in the electrolyte volume. Starting from the 20th minute of electrolysis, as titanium powder accumulates in the electrolyte bulk, the concentration of Ti^{2+} ions begins to increase rapidly in the near-anode layer according to the reaction $2\text{Ti}^{3+} + \text{Ti} = 3\text{Ti}^{2+}$. At the same time, the proportion of sodium consumed for the reduction of Ti^{3+} to Ti^{2+} decreases. This contributes to an increase in the current output and stabilization of the cathode potential for 30 min at $E_c = -2.96$ V. After 50 min of electrolysis, the reactivity of the salt melt begins to decrease due to the low solubility of sodium in it. The cathode potential decreases sharply towards positive values. The concentration of Ti^{3+} ions in the near-anode layer increases steadily until it aligns at 85 min with the

concentration of Ti^{2+} ions. This dramatically increases the current consumption for ion recharge and leads to the need to stop electrolysis after a short-term (for 40 s) switching on the current of 12 A. After 10 s, judging by the change in the cathode potential, almost all of the sodium dissolved in the electrolyte is consumed for the reduction of titanium ions. After 6 min, the potentials of the electrodes returned to the initial value of the anode potential, indicating a return of the system to its initial state, where titanium salts and dissolved sodium were absent. More than 95 % of the powder is obtained in the volume of the electrolyte. The current yield was 84.0 % and was close to the calculated average valence of titanium ions in the near-anode layer and mass loss of the anode (87.0 %).

This paper is devoted to a detailed analysis of the mechanism of the cathode process, its effect on the anode process, and the results of electrolysis.

The methodology of the experiment

The experiments were carried out at $t = 610$ °C in a eutectic composition melt, mol. fr.: $BaCl_2$ — 0.16; $CaCl_2$ — 0.47; $NaCl$ — 0.37, with $t_{melt} = 452 \pm 2$ °C. Low-melting electrolytes similar in composition are used in industry to produce sodium with high current efficiency. The electrolyte was prepared from pre-dehydrated salts according to the method [11]. Titanium salts and metallic sodium were not added to the original electrolyte.

The design of the electrolytic cell is shown in Fig. 1.

Prior to the experiment, 228 g of electrolyte was loaded into the crucible. The anode is made of a titanium rod (current conductor) weighing 23.36 g and a titanium plate weighing 14.18 g. The walls of a steel crucible were used as the cathode. The working surface area of the anode was 14.4 cm^2 , the cathode was 100 cm^2 . To completely dry the electrolyte, the cell was heated under vacuum to 400° C, then argon purified by passing it through a titanium chip heated to 820 °C was supplied.

Polarization studies were carried out on the chassis of the NI PXIe 8108 instrument (National Instruments, USA) with NI PXI-4140, NI PXI-4072, and NI PXIe-6356 modules. The application for this device is written in the graphical programming language LabVIEW 10. The duration of the current pulse was 10 s, then the current was switched off for 10 s with measurement of the electrode potential value 0.5 ms after switching off, then the next current value was switched

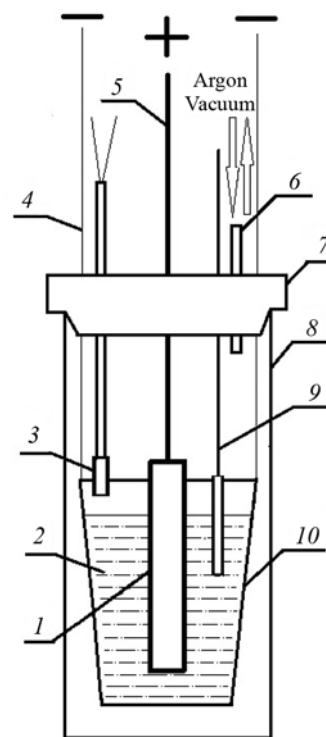


Fig. 1. Design of an electrolytic cell

1 — titanium plate (VT1-0); 2 — electrolyte; 3 — chromel-alumel thermocouple in BeO sheath; 4 — crucible steel suspension (cathode); 5 — titanium rod (current conductor); 6 — branch pipe for evacuating air and supplying argon; 7 — vacuum rubber stopper; 8 — quartz cell; 9 — reference electrode in BeO sheath; 10 — steel crucible

Рис. 1. Устройство электролитической ячейки

1 — титановая пластина (VT1-0); 2 — электролит; 3 — хромель-алюмелевая термопара в чехле из BeO; 4 — стальной подвес тигля (катод); 5 — титановый стержень (токоподвод); 6 — патрубок для откачки воздуха и подачи аргона; 7 — пробка из вакуумной резины; 8 — кварцевая ячейка; 9 — электрод сравнения в чехле из BeO; 10 — стальной тигель

on for 10 s. The sequential increase in current was uniform on a logarithmic scale: 1.0, 1.59, 2.51, 3.98, 6.31, 10.0 in each period.

A lead electrode $KCl-NaCl + 10 \text{ wt.}\% \text{ PbCl}_2$ was used as a reference electrode.

$$E [\text{V}] = -1.79 + 0.42 \cdot 10^{-3} T, \quad E_{883 \text{ K}} = -1,42 \text{ V.} \quad (1)$$

The results were recalculated on a chlorine electrode.

Results and discussion

The results of the cathode polarization study are shown in Fig. 2 in $E_c - \lg i_c$ coordinates.

At the current of $I_c = 4$ A (cathodic current density $i_c = 0.04$ A/cm², $\lg 0.04 = -0.92$) is obtained by sodium saturation of cathode electrolyte at $E_{\text{sat}} = -2.97$ V.

At $I_c = 12$ A ($i_c = 0.12$ A/cm², $\lg 0.12 = -1.4$) the cathode potential -3.22 V is close to the conditional standard sodium deposition potential -3.32 V, but doesn't reach it by 0.10 V. The sodium deposition potential (E^*) was calculated according to the procedure [12], using the values of standard potential of the Na^+/Na system in NaCl [4]:

$$E^0 = -3.903 + 0.60 \cdot 10^{-3}T, \quad (2)$$

$$E_{883\text{ K}}^0 = -3.373 \text{ V},$$

as well as mole fractions and ionic moments of cations, nm⁻¹: $\text{Na}^+ - 10.2$, $\text{Ca}^{2+} - 19.23$, and $\text{Ba}^{2+} - 14.5$ in the electrolyte used:

$$E^* = -3.829 + 0.58 \cdot 10^{-3}T, \quad (3)$$

$$E_{883\text{ K}}^* = -3.32 \text{ V},$$

$$E^* - E^0 = 0.074 - 0.02 \cdot 10^{-3}T, \quad (4)$$

$$\Delta E_{883\text{ K}} = 0.0563 \text{ V}.$$

By dividing the values given in equation (4) by the value of the pre-logarithmic coefficient ($2.3RT/F = 2.3 \cdot 8.314 \cdot 883/96485 = 0.175$, where R is the universal gas constant, F is the Faraday constant; T is temperature, K), the equation was obtained for calculating the value of activity coefficient of sodium ions in a salt melt (γ) and its value at $T = 883$ K:

$$\lg \gamma = 0.423 - 0.114 \cdot 10^{-3}T, \quad (5)$$

$$\lg \gamma = 0.322, \quad \gamma_{883\text{ K}} = 2.1.$$

The sodium activity in the melt used ($0.37 \cdot 2.1 = 0.78$) is close to 1, hence the activity of supercooled NaCl.

Information about the sequence and trends of electrode processes is obtained by measuring the changes in electrode potentials over time after the electrolysis current is switched off.

For the cathodic process (Fig. 3) at $I = 2, 4$, and 6 A, relatively stable (within 20 s) values of the cathode potentials are observed. At the same time, two processes occur on them: the decline in concentration polarization, which shifts the potential of the cathode toward positive values, and the influx of sodium dissolved in the salt from the electrolyte volume to the cathode surface, which shifts its potential in the opposite direction. For the first and second periods of electrolysis with a current of 2 A, the first process prevails.

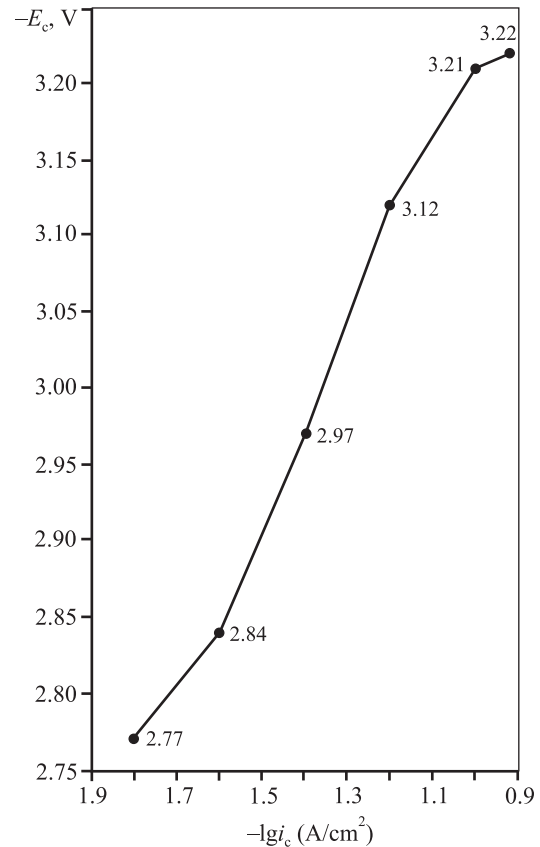


Fig. 2. Results of the cathode polarization study

Рис. 2. Результаты изучения поляризации катода

After electrolysis with 4 and 6 A currents, the process rates equalize, and the cathode potential stabilizes at -2.97 V. With the same value, the cathode potential begins to shift towards positive values after the current is turned off 8 A.

Studies carried out by different methods suggest that the cathode potential of -2.97 ± 0.01 V is a fundamental characteristic corresponding to a saturated sodium solution in the electrolyte used at $t = 610$ °C (E_{sat}). The sodium activity in a saturated solution (a_{sat}) was calculated based on the assumption that a change in the cathode potential from -3.22 to -2.97 V (i.e., by 0.25 V) is associated with a change in the activity of dissolved sodium. By substituting the corresponding values for the electrolyte used, we obtain $\lg a_{\text{sat}} = -0.25/0.175 = -1.486$, $a_{\text{sat}} = 0.0373$. Dividing this value by the activity coefficient of sodium (288), we obtain the sodium concentration in a saturated solution ($1.3 \cdot 10^{-4}$ mol. fr.).

Starting from $I = 8$ A, a sharper shift of the cathode potentials towards positive values is observed (see Fig. 3), which increases at $I = 10$ A. After the first switching off of 10 A current (see Fig. 5, per. 6), the potential

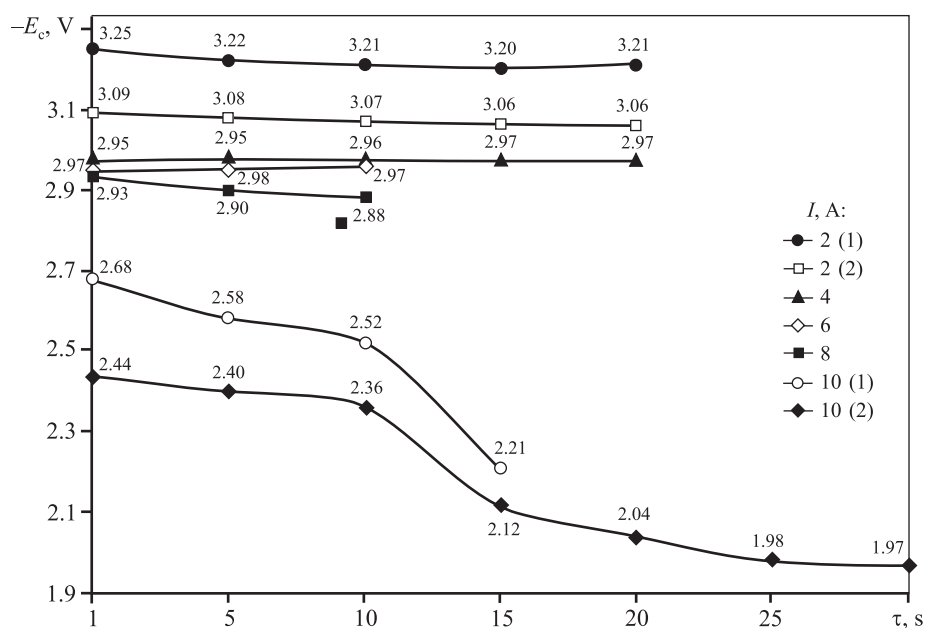


Fig. 3. Change in time of the cathode potential after the electrolysis current is switched off

Рис. 3. Изменение во времени потенциала катода после отключения тока электролиза

of -2.68 V corresponded to the concentration of dissolved sodium of $5 \cdot 10^{-3}$ mol. fr., which was enough to reduce the concentration of Ti^{2+} ions after 5 s down to $2.5 \cdot 10^{-7}$ mol. fr. ($E_c = -2.58$ V), and after 10 s — down to $6 \cdot 10^{-6}$ mol. fr. ($E_c = -2.52$ V). After the second switching off of 10 A current, the sodium concentration decreases down to $1 \cdot 10^{-5}$ mol. fr. ($E_c = -2.44$ V). After 5 s the concentration of Ti^{2+} ions was reduced down to $2 \cdot 10^{-5}$ mol. fr. ($E_c = -2.48$ V), after 10 s — down to $1 \cdot 10^{-5}$ mol. fr. ($E_c = -2.36$ V). With a further decrease in the cathode potential, the system under consideration passes into the area of coexistence of Ti^{2+} and Ti^{3+} ions. The ratio of Ti^{2+}/Ti^{3+} ion concentrations equal to 100 corresponds to the steady-state potential of -1.97 V. The appearance of the curves of the cathode potential change with time, observed when the current of 10 A is switched off, is similar at lower electrolysis currents as well. It is always necessary to wait for the transition of the system to the region of coexistence of Ti^{2+} and Ti^{3+} ions to exclude the presence of an alkali metal and noticeable amounts of titanium ions in the final electrolyte.

The time variation of the anode potentials after switching off the electrolysis current is shown in Fig. 4.

When currents 2, 4, and 6 A are switched off, the anode potentials naturally shift toward negative values under the influence of the richer Ti^{2+} ions of the melt in the pre-cathode space. For $I = 8$ A, the RedOx po-

tential does not exceed -1.75 V, which corresponds to 5-fold excess of the Ti^{2+} ion proportion. When switching off the current of 10 A, briefly, in 5–10 s, the maximum potential values are reached (-1.835 V, -1.831 V), corresponding to the ratio of ions $Ti^{2+}/Ti^{3+} = 20 \pm 17$. After $\tau = 5$ s, they decrease to -1.8 V, the ratio of ions $Ti^{2+}/Ti^{3+} = 10$. The presence of two fluxes of Ti^{2+} ions from the cathode side and the anode surface leads not to the expected increase, but to a rapid decrease in the concentration of Ti^{2+} ions due to the implementation of the disproportionation reaction:



We associate the formation of finely dispersed grains of metallic titanium in the form of linear and bulk aggregates in the near-anode electrolyte with the development of this reaction. This is due to the reaction taking place at a distance from the anode that is less than the thickness of the diffusion layer [13, 14].

Prolonged electrolysis was carried out with a step-by-step increase in current. Fig. 5 shows the operating voltage, cathode and anode potentials, inverse EMF, current values and duration of electrolysis in each of the 7 periods. All measurements were performed with an accuracy of 1 mV. This made it possible to trace the change in the ratio of Ti^{3+} and Ti^{2+} titanium ions in the near-anode layer and the change in the RedOx potential in the near-cathode layer of the electrolyte.

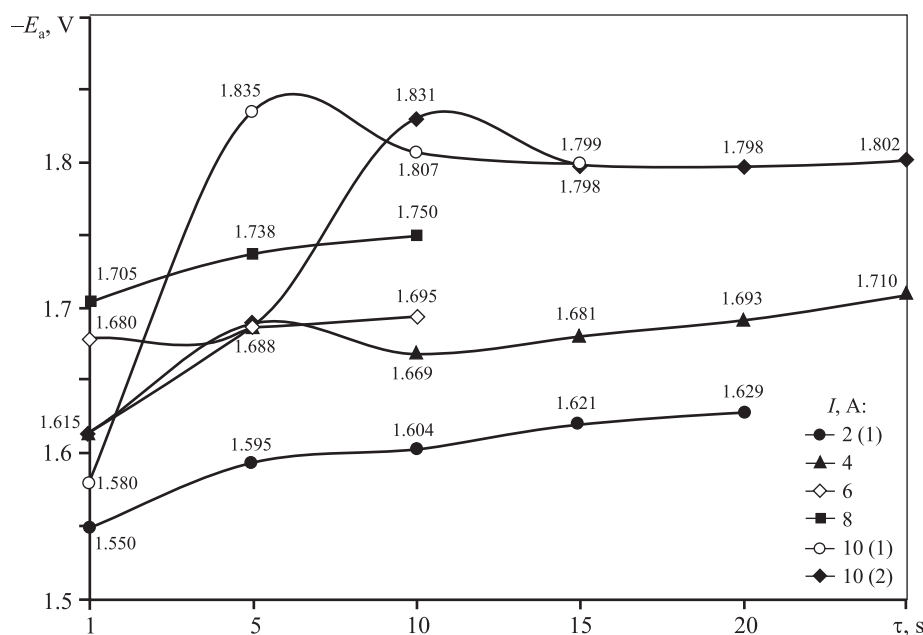


Fig. 4. Change of the anode potential in time after the electrolysis current is switched off

Рис. 4. Изменение потенциала анода во времени после отключения тока электролиза

Conditional standard potentials of systems Ti^{3+}/Ti , Ti^{2+}/Ti , Ti^{3+}/Ti^{2+} for $CaCl_2$, $BaCl_2$, $NaCl$ were taken from the monograph [4]. By multiplying the corresponding values by the mole fractions of the components and adding the results obtained, we obtained equations to calculate the conditional standard potentials of the corresponding systems in the electrolyte used. The coefficients of the equations $E^* = A + 10^{-3}BT$ are given in Table 1.

Based on the initial (before electrolysis) potentials of the cathode (-2.48 V) and anode (-1.87 V), the

concentrations of the corresponding ions in the electrode layers were calculated. For the cathode they are equal to, mol. fr.: $Ti^{2+} - 5.2 \cdot 10^{-7}$, $Ti^{3+} - 4.8 \cdot 10^{-12}$. Ti^{3+}/Ti^{2+} concentration ratio makes up $\sim 1 \cdot 10^{-5}$. For the anode this ratio equals to $3.7 \cdot 10^{-2}$, and average valency is 2.04.

The given values of conditional standard potentials made it possible to describe the processes occurring at the electrodes during electrolysis.

The reactivity of sodium dissolved in the electrolyte naturally decreases with an increase in the electricity

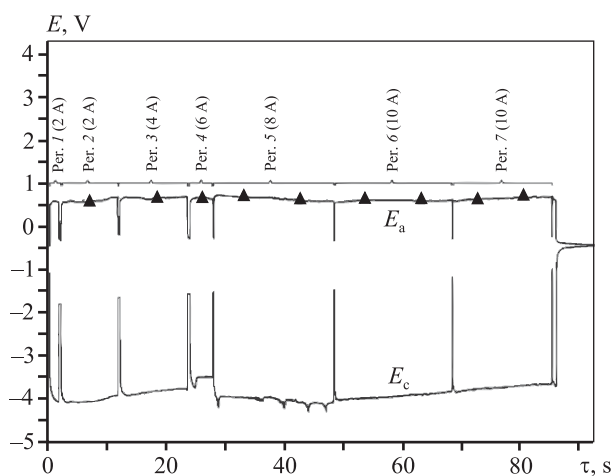


Fig. 5. Scheme of implementation of long-term electrolysis

Рис. 5. Схема реализации длительного электролиза

Table 1. Results of calculating the values of conditional standard potentials of the systems Ti^{2+}/Ti , Ti^{3+}/Ti , Ti^{3+}/Ti^{2+} in the electrolyte used

Таблица 1. Результаты расчета величин условных стандартных потенциалов систем Ti^{2+}/Ti , Ti^{3+}/Ti , Ti^{3+}/Ti^{2+} в используемом электролите

Salt	$E_{Ti^{2+}/Ti}^*$, V		$E_{Ti^{3+}/Ti}^*$, V		$E_{Ti^{3+}/Ti^{2+}}^*$, V	
	-A	B	-A	B	-A	B
$CaCl_2$	2.48	0.68	2.24	0.55	1.78	0.29
$BaCl_2$	2.60	0.73	2.36	0.59	1.87	0.31
$NaCl$	2.42	0.51	2.19	0.34	1.74	0.01
Electrolyte	2.49	0.63	2.24	0.48	1.78	0.18
$E_{883 K}^*$, V	-1.93		-1.82		-1.62	

passed, and hence the amount of titanium powder accumulating in the salt melt (Fig. 6).

It is no coincidence that the duration of our experiments and the authors of the work [15] was approximately the same and was ~2 h, which is due to the need to limit the accumulation of titanium powder in the electrolyte. The authors of [15] noted that when 8–10 % of titanium is accumulated in the electrolyte, an increase in current does not result in an increase in the amount of metal produced, and at 20 % Ti, a drop in the operating voltage down to 0 was detected when the anode was short-circuited to the bottom of the crucible. This may be due to the appearance of noticeable electronic conductivity in such melts.

On the dependence of the cathode potential on the logarithm of the electricity transmitted (see Fig. 6) there are three close to rectilinear regions.

The straight line equation in the region from -3.225 to -2.951 V is

$$E [\text{V}] = -3.32 + 0.185 \lg Q \pm 0.011. \quad (7)$$

The value of -3.32 coincides with the value of the conditional standard potential of sodium in the electrolyte used (3). The value of the prelogarithmic coefficient of 0.185 is close to its value for a single-electron process ($2.3 \cdot 8.314 \cdot 883 / 96484 = 0.175$), which indicates the constancy and proximity to 1 of the sodium activity coefficient in supersaturated solutions. The existence of the above region on the polarization curve was mentioned by the authors of [5] without explaining what processes it is associated with. In our opinion, it can be the formation (when current is flowing) and decay (when it is turned off for 10 s) of supersaturated solutions, the appearance and growth of electronic conductivity with the accumulation of powdered titanium in the salt melt. The deviation of the prelogarithmic coefficient from 0.175 may be considered as the occurrence and accumulation in the electrolyte of ions with a valency less than 1, for example, Na^{2+} . The first version seems to us the most probable on the considered part of the curve $E-\lg Q$.

In our opinion, the long-term region of potential constancy at $E_c = -2.97 \pm 0.01$ V is associated with the coexistence of saturated and supersaturated sodium solutions in the electrolyte in the near-cathode layer. The decomposition of the latter makes it possible to stabilize the cathode potential. At potentials negative to -2.97 V, only supersaturated solutions exist. At a potential of -2.951 V, a saturated solution appears, the proportion of which increases as the amount of electricity passes further. At $\lg Q = 2.41$ ($E_c = -2.962$ V) which is

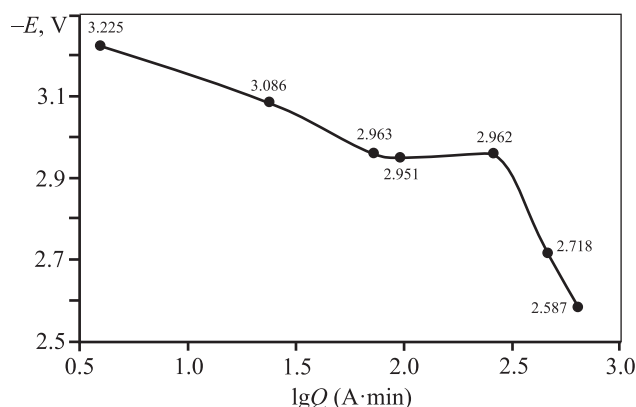


Fig. 6. The dependence of the cathode potential when the electrolysis current is switched off on the amount of electricity passed

Рис. 6. Зависимость потенциала катода при отключении тока электролиза от количества пропущенного электричества

in good agreement with the previously given value of 2.97 ± 0.01 V, all the supersaturated solution is consumed. The reactivity of sodium decreases hundreds of times, which is manifested in a sharp shift in the cathode potential towards positive values.

It should be noted that the characteristic points: $E_{\text{sat}} = -2.97$ V (formation of saturated solutions) and $E_{\text{Na}} = -3.22$ V (occurrence of a metallic sodium phase), were clearly manifested in the study of cathodic polarization with increasing electrolysis current and long-term electrolysis when the reducing ability of the melt decreased with an increase in the amount of electricity passed, and hence the amount of titanium powder accumulated in the electrolyte.

The most effective way to intensify and prolong electrolysis is the nucleation and decomposition of the metallic sodium phase at the cathode. It was observed at $I = 6$ and 8 A (see Fig. 5). An enlarged fragment of Fig. 5 is shown in Fig. 7. We associate the pulsating nature of the cathode potential change with the polarization accompanying the nucleation and decay of the liquid metallic sodium phase on the surface of the steel cathode.

When a current of 6 A is turned on ($i_c = 0.06$ A/cm² for the entire cathode surface bordering the melt), a voltage spike of 0.25 V, typical for phase polarization, is observed. The time to reach the maximum is 34 s, the decomposition time is 16 s, and the lifetime of the nucleus is 50 s. These parameters differ significantly from the respective values during the deposition of solid phases on a solid cathode, where the value of the maximum overvoltage varies from 20–30 to 70–100 mV, and the

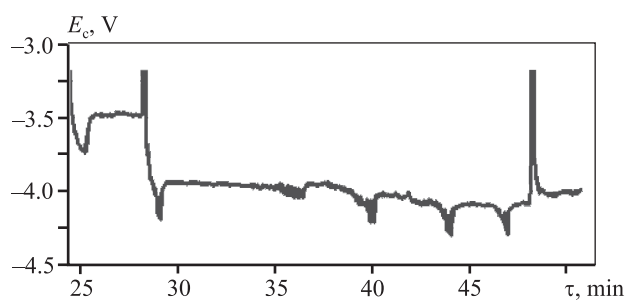


Fig. 7. Enlarged fragment of Fig. 5

Рис. 7. Увеличенный фрагмент рисунка 5

time to reach it varies from 10^{-2} до 10^{-4} s with a change in current density from 10^{-3} to 10^{-1} A·cm² [16]. The peculiarity of these curves is the slow reaching of the maximum and the rapid decay. After the decay of the nucleus in question, the cathode potential remained stable over time, and the difference between it and the maximum value remained 0.25 V.

When a current of 8 A ($i_c = 0.08$ A/cm²) was turned on, the magnitude of the maximum overvoltage (0.25 V) was maintained, the nucleus lifetime was 36 s, the time to reach the maximum overvoltage was 27 s, and the decay time was 9 s. The rapid and accelerating decay is due to the high mobility of the resulting decay products, which spread throughout the volume of the electrolyte. After the decay of this nucleus, the cathode potential began to shift toward negative values at a rate of 0.10–0.15 mV/s due to the entry of dissolved sodium into the interelectrode space from the electrolyte volume. The increasing supersaturation of the cathode

melt should have contributed to the formation of the following nuclei. Indeed, after 7 min, there was an attempt to nucleate the next nucleus, but it failed due to insufficient reactivity of the melt and a low degree of supersaturation in the pre-cathode space. For the occurrence of the next nucleus, the supersaturation of the melt increased up to 35 mV (the degree of supersaturation — 1.6), for the third one — 70 mV (the degree of supersaturation — 2.5), for the fourth one — 120 mV (the degree of supersaturation — 5.0). The maximum degree of saturation is observed during the formation and decay of sodium metal nuclei. In this case, the degree of supersaturation increases by more than 20 times ($10^{0.25/0.175} \approx 27$).

As a result of going through the stages of disintegration of supersaturated solutions, nucleation, and decay of metallic sodium nuclei in the volume of electrolyte the concentration of dissolved sodium was accumulated, which was enough to conduct electrolysis with 10 A current for 35 min and return the electrolyte composition to its original state.

In paper [5], the values of the solubility of Na in NaCl are given: at $t = 816$ °C — 2.42 mol.%, at $t = 864$ °C — 4.06 mol.%. Based on these data, the temperature dependence of the Na solubility (N , mol. fr.) and the value of N at $T = 1173$ K and for a supercooled melt at $T = 883$ K were calculated:

$$\lg N = 3.817 - (5920/T), \quad (8)$$

$$N_{1173 \text{ K}} = 0.059, \quad N_{883 \text{ K}} = 0.0013.$$

In the same paper, an equation was given for calcu-

Table 2. The results of calculating the sodium activity in the NaCl melt and the required degree of supersaturation to obtain metallic sodium on the cathode

Таблица 2. Результаты расчета активности натрия в расплаве NaCl и необходимой степени пересыщения для получения на катоде металлического натрия

T , K	N , mol. fr.	$\lg N$	$\lg \gamma$	γ	$\lg a$	a	Required degree of supersaturation
1173	0.059	-1.23	1.194	15.6	-0.04	0.92	1.09
1073	0.020	-1.700	1.879	75.7	-0.029	0.935	1.51
973	0.0055	-2.267	2.196	143	-0.123	0.79	1.27
873	0.0011	-2.962	2.498	315	-0.464	0.343	2.9
823	0.00042	-3.376	2.700	501	-0.68	0.211	4.8
773	0.00014	-3.841	2.927	845	-0.924	0.127	8.2
723	0.000043	-4.371	3.187	1540	-1.184	0.065	15
673	0.0000105	-4.979	3.486	3060	-1.49	0.032	31
623	0.0000021	-5.685	3.830	6761	-1.854	0.014	71

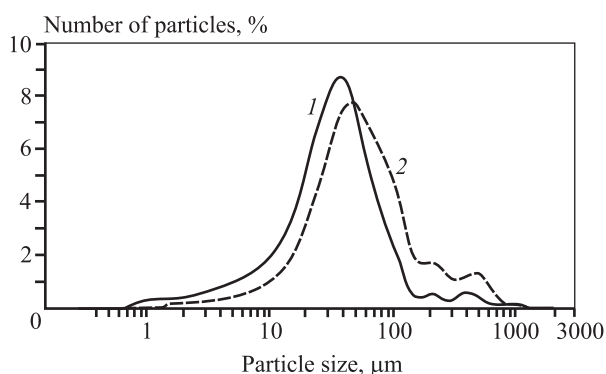


Fig. 8. Particle size distribution analysis of titanium powder

1 — after ultrasonic grinding; 2 — before ultrasonic grinding

Рис. 8. Гранулометрический анализ титанового порошка

1 — после ультразвукового измельчения
2 — до ультразвукового измельчения

lating the activity factor of sodium (γ) dissolved in the Na—NaCl melt:

$$\lg \gamma = (-0.823 + 2899/T)/(1 + 6.06(N_{\text{Na}}/(1 - N_{\text{Na}}))). \quad (9)$$

Maximum values of Na in NaCl activity factors (γ) are calculated at $N_{\text{Na}} = 0$, $\gamma = 44.5$ ($T = 1173$ K) and 288 ($T = 883$ K).

Table 2 summarizes the results of calculating the activity of sodium (a) in the NaCl melt depending on the temperature and concentration of dissolved sodium (N).

At temperatures above 973 K, the required degrees of supersaturation are negligible; below 873 K they increase markedly, but even at $T = 623$ K (71) they are inferior to the maximum degrees of supersaturation during the formation and decay of metallic sodium nuclei (100—123 times). This makes it possible to lower the lower temperature limit of the process implementation from 600 to 350 °C.

According to the granulometric analysis (Fig. 8) (Institute of Thermal Energy of Ural Branch of RAS, Ekaterinburg), 95 % of the obtained titanium powder is in the melt volume in the form of aggregates, easily crushed into individual crystals. More than 80 % of these crystals are in the range of 10—100 μm with an average size of 36 μm , which meets the requirements for the size of powders for additive technologies.

Conclusion

A preliminary study of the cathode polarization revealed the potentials and current densities of so-

dium saturation of the salt melt ($E_{\text{sat}} = -2.97$ V, $i = 0.04$ A/cm²) and the occurrence of sodium metal on the cathode ($E_{\text{Na}} = -3.22$ V, $i_c = 0.12$ A/cm²). The concentration of sodium in a saturated solution at $t = 610$ °C ($1.3 \cdot 10^{-4}$ mol. fr.) was calculated using the value of E_{sat} . The values of E_{sat} , E_{Na} , and the difference between them ($\Delta E = 0.25$ V) have been confirmed in long-term electrolysis and are the basis for monitoring and controlling the process.

During prolonged electrolysis, three regions close to rectilinear were identified on the curve in coordinates E (B) — $\lg Q$ (A·min). In the equation of the straight line $E = A + B \lg Q$ in the region from -3.22 to -2.963 V, the value of A (-3.32 V) coincides with the value of the conditional standard potential of sodium in the electrolyte used. The value of B (0.185 V) is close to its value for the one-electron process (0.175), which indicates the constancy and closeness to 1 of the activity coefficient of sodium in supersaturated solutions. The discharge of sodium ions from supersaturated solutions occurs when E is more negative than E_{sat} to E_{Na} . In the decomposition of supersaturated solutions, a 5-fold degree of supersaturation of the electrolyte in sodium is achieved. During the formation and decomposition of metallic sodium nuclei, it increases by more than 20 times and becomes sufficient to intensify and prolong the electrolysis process, to lower the lower limit of its realization temperature from 600 [17] to 350 °C.

The long-term region of potential constancy at $E_c = -2.97 \pm 0.01$ V is associated with the coexistence of saturated and supersaturated sodium solutions in the electrolyte in the near-cathode layer. The decomposition of the latter stabilizes the cathode potential. At $\lg Q = 2.41$, the entire supersaturated solution is consumed, the reactivity of sodium and the cathode potential drop sharply, and the discharge of sodium ions from diluted solutions starts at potentials from E_{sat} to values 0.25—0.35 V more positive.

It can be seen that the reducing ability of the melt decreases as the amount of electricity passed through, and hence as the amount of titanium powder accumulated in the electrolyte increases.

The formation of titanium metal in the near-anode space is explained by the disproportionation of Ti^{2+} ions entering the anode electrolyte from the near-anode layer and the near-cathode melt.

The resulting product is similar to powder [17], and after classification and spheroidization by gas atomization methods [18—24], it can be used for 3D printing as a starting material.

References

1. Niinomi M., Nakai M., Hieda J. Development of new metallic alloys for biomedical applications. *Acta Biomater.* 2012. Vol. 11. P. 3888–3903. DOI: 10.1016/j.actbio.2012.06.037.
2. Vaezi M., Yang S. Extrusion-based additive manufacturing of PEEK for biomedical applications. *Virtual Phys. Prototyp.* 2015. Vol. 10. No. 3. P. 123–135. DOI: 10.1080/17452759.2015.1097053.
3. Hiroyasu K., Yoshimasa T., Hideyuki I., Tatsushi K., Takayuki Y. Application of titanium and titanium alloys to fixed dental prostheses. *J. Prosthodontic Res.* 2019. Vol. 565. P. 266–270. DOI: 10.1016/j.jpor.2019.04.011.
4. Смирнов М.В. Электродные потенциалы в расплавленных хлоридах. М.: Наука, 1973. Smirnov M.V. Electrode potentials in molten chlorides. Moscow: Nauka, 1973 (In Russ.).
5. Smirnov M.V., Chebykin V.V., Tsiiovkina L.A. The thermodynamic properties of sodium and potassium dissolved in their molten chlorides, bromides, and iodides. *Electrochim Acta.* 1981. Vol. 26. No. 9. P. 1275–1288. DOI: 10.1016/0013-4686(81)85111-0.
6. Ковалевский Р.А., Чебыкин В.В. Транспортные характеристики восстановленных форм катионов растворителя в расплавах хлоридов щелочных металлов. *Расплавы.* 1992. No. 3. С. 36–42. Kovalevskii R.A., Chebykin V.V. Transport characteristics of reduced forms of solvent cations in melts of alkali metal chlorides. *Rasplavy.* 1992. No. 3. P. 36–42 (In Russ.).
7. Fang Z.Z., Paramore J.D., Sun P., Ravi Chandran K.S., Zhang Y., Xia Y., Cao F., Koopman M., Free M. Powder metallurgy of titanium — past, present, and future. *Int. Mater. Rev.* 2018. Vol. 63. No. 7. P. 407–459. DOI: 10.1080/09506608.2017.1366003.
8. Dutta B., Froes F.H. Additive manufacturing of titanium alloys. Butterworth-Heinemann, 2016. DOI: 10.1016/B978-0-12-804782-8.00002-1.
9. Polyakov V.V., Babin A.V., Lebedev V.A. Volumetric reduction of FeCl₂–CaCl₂ melt with calcium dissolved in calcium chloride. *Russ. J. Non-Ferr. Met.* 2019. Vol. 60. No. 4. P. 408–412. DOI: 10.3103/S1067821219040114.
10. Лебедев В.А., Поляков В.В. Способ получения микроструктурных порошков титана: Пат. RU2731950С2 (РФ). 2020. Lebedev V.A., Polyakov V.V. The method of obtaining microstructural titanium powders. Pat. RU2731950С2 (RF). 2020 (In Russ.).
11. Лебедев В.А., Бабин А.В., Поляков В.В., Рымкевич Д.А., Бездоля И.Н. Восстановление титана из его тетраоксида кальцием, растворенным в расплаве CaCl₂. *Титан.* 2017. No. 1. С. 4–9. Lebedev V.A., Babin A.V., Polyakov V.V., Rymkevich D.A., Bezdolya I.N. Reduction of titanium from its tetrachloride calcium dissolved in the melt of the CaCl₂. *Titan.* 2017. No. 1. P. 4–9 (In Russ.).
12. Лебедев В.А. Взаимосвязь стандартных и условных стандартных потенциалов в расплавленных галогенидах. *Докл. Акад. наук СССР.* 1993. Т. 330. No. 5. С 586–589. Lebedev V.A. Relationship of standard and conventional standard potentials in molten halides. *Doklady Akademii nauk SSSR.* 1993. Vol. 330. No. 5. P. 586–589 (In Russ.).
13. Храмов А.П., Чернышев А.А., Исаков А.В., Зайков Ю.П. Вторичное восстановление тугоплавкого металла у гладкого катода при электролизе солевого расплава. 1. Вывод базовых уравнений для модели процесса. *Электрохимия.* 2020. Т. 56. No. 9. С. 771–781. DOI: 10.31857/S0424857020090054. Khramov A.P., Chernyshev A.A., Isakov A.V., Zaykov Yu.P. Secondary reduction of a refractory metal near a smooth cathode during electrolysis of molten salt. 1. Derivation of basic equations for the process model. *Russ. J. Electrochem.* 2020. Vol. 56. P. 699–708. DOI: 10.1134/S1023193520090050.
14. Храмов А.П., Чернышев А.А., Исаков А.В., Зайков Ю.П. Вторичное восстановление тугоплавкого металла у гладкого катода при электролизе солевого расплава. 2. Расчеты для некоторых гипотетических экспериментов. *Электрохимия.* 2020. Т. 56. No. 9. С. 782–787. DOI: 10.31857/S0424857020090066. Khramov A.P., Chernyshev A.A., Isakov A.V., Zaykov Yu.P. Secondary reduction of a refractory metal near a smooth cathode during electrolysis of molten salt. 2. Calculations for some hypothetical experiments. *Russ. J. Electrochem.* 2020. Vol. 56. P. 709–714. DOI: 10.1134/S1023193520090062.
15. Вараксин А.В., Лисин В.Л., Костылев В.А. Влияние параметров электрохимического процесса на гранулометрический состав и морфологию титановых порошков. *Бутлеровские сообщения.* 2014. Т. 37. No. 1. С. 62–67. Varaksin A.V., Lisin V.L., Kostylev V.A. The influence of the parameters of the electrochemical process on the particle size distribution composition and the morphology of titanium powders. *Butlerovskie soobshcheniya.* 2014. Vol. 37. No. 1. P. 62–67 (In Russ.).
16. Барабошкин А.Н. Электрокристаллизация металлов из расплавленных солей. М.: Наука, 1976. Baraboshkin A.N. Electrocrystallization of metals from molten salts. Moscow: Nauka, 1976 (In Russ.).

17. Лебедев В.А., Поляков В.В. Получение тонкодисперсного порошка титана объемным восстановлением его ионов натрием, растворенным в расплаве $BaCl_2$ — $CaCl_2$ — $NaCl$. *Известия вузов. Порошковая металлургия и функциональные покрытия*. 2022. No. 1. С. 4—16. Lebedev V.A., Polyakov V.V. Production of finely dispersed titanium powder by volumetric reduction of its ions with sodium dissolved in the $BaCl_2$ — $CaCl_2$ — $NaCl$ melt. *Izvestiya Vuzov. Poroshkovaya Metallurgiya i Funktsional'nye Pokrytiya (Powder Metallurgy and Functional Coatings)*. 2022. Vol. 16. No. 1. P. 4—16 (In Russ.).
18. Boulos M. Plasma power can make better powders. *Met. Powder Report*. 2004. Vol. 59. No. 5. P. 16—21. DOI: 10.1016/S0026-0657(04)00153-5.
19. Sun P., Fang Z., Zhang Y., Xia Y. Review of the methods for production of spherical Ti and Ti alloy powder. *J. Miner. Met. Mater. Soc.* 2017. Vol. 69. No. 10. P. 1853—1860. DOI: 10.1007/s11837-017-2513-5.
20. Heidloff A.J., Rieken J.R., Anderson I.E., Byrd D., Sears J., Glynn M., Ward R.M. Advanced gas atomization processing for Ti and Ti alloy powder manufacturing. *J. Miner. Met. Mater. Soc.* 2010. Vol. 62. No. 5. P. 35—41. DOI: 10.1007/s11837-010-0075-x.
21. Larouche F., Balmayer M., Trudeau-lalonde F. Plasma atomization metal powder manufacturing processes and systems therefore: Pat. WO2017011900 A1 (WIPO). 2017. <https://patents.google.com/patent/WO2017011900A1/en?q=WO2017011900+A1>.
22. Dion C.A.D., Krekewetz W., Carabin P. Plasma apparatus for the production of high quality spherical powders at high capacity: Pat. WO2016191854 A1 (WIPO). 2016. <https://patents.google.com/patent/US20180169763A1/en?q=WO2016191854+A1>.
23. Sun P., Fang Z., Xia Y., Zhang Y., Zhou C. A novel method for production of spherical Ti—6Al—4V powder for additive manufacturing. *Powder Technol.* 2016. Vol. 301. P. 331—335. DOI: 10.1016/j.powtec.2016.06.022.
24. Chen G., Zhao S., Tan P., Wang J., Xiang C., Tang H. A comparative study of Ti—6Al—4V powders for additive manufacturing by gas atomization, plasma rotating electrode process and plasma atomization. *Powder Technol.* 2018. Vol. 333. P. 38—46. DOI: 10.1016/j.powtec.2018.04.013.

UDC 621.762.242

DOI dx.doi.org/10.17073/1997-308X-2022-4-15-24

Structure and properties of titanium hydride powder obtained from titanium sponge by SHS hydrogenation

© 2022 г. **N.P. Cherezov, M.I. Alymov**

Merzhanov Institute of Structural Macrokinetics and Materials Science of the Russian Academy of Sciences (ISMAN), Chernogolovka, Russia

Received 14.03.2022, revised 07.06.2022, accepted for publication 10.06.2022

Abstract: The results of the study of the structure and properties of titanium hydride powders obtained from titanium sponge by SHS hydrogenation and mechanical grinding are presented. Hydrogenation was carried out in a reactor at a constant hydrogen pressure of 3 MPa. After passing the combustion wave, the hot titanium sponge was cooled to room temperature in a hydrogen atmosphere. As a result, titanium hydride spongy granules with a hydrogen content of 4.2 wt.% were obtained. Titanium hydride was ground in a ball mill and divided into 4 fractions corresponding to the fractional composition of titanium powder PTK, PTS, PTM and PTOM. Particle size analysis showed that the samples of the PTK and PTOM powders have a narrower particle distribution in comparison with the PTS and PTM ones. Further, obtained powders chemical composition and surface morphology studies were carried out and bulk density, compaction, pycnometric density and specific surface area were determined. According to the chemical analysis results the content of carbon and oxygen impurities decreases during SHS-hydrogenation and the iron content slightly increases during mechanical grinding depending on the grinding time. The study of morphology showed that the hydride titanium particles have an irregular fragmentary shape, such morphology is characteristic of powders obtained by this technology. The surface structure has partially preserved structure of the initial titanium sponge and consists of elongated oriented grains. It is established that with a decrease in the particle size, the bulk density decreases, and the compaction increases. Pycnometric density and specific surface area values are approximately equal for all powder samples.

Keywords: titanium hydride, powder metallurgy, self-propagating high-temperature synthesis (SHS), hydrogenation, morphology, technological properties.

Cherezov N.P. — junior researcher of the Laboratory of high-energy methods of synthesis of ultrahigh-temperature ceramic materials of Merzhanov Institute of Structural Macrokinetics and Materials Science of the Russian Academy of Sciences (ISMAN) (142432, Russia, Moscow region, Noginsk district, Chernogolovka, Akademian Osip'yan str., 8).
E-mail: cherezovnikita@gmail.com.

Alymov M.I. — Dr. Sci. (Eng.), prof., corresponding member of the Russian Academy of Sciences, director of the ISMAN.
E-mail: alymov.mi@gmail.com.

For citation: Cherezov N.P., Alymov M.I. Structure and properties of titanium hydride powder obtained from titanium sponge by SHS hydrogenation. *Izvestiya Vuzov. Poroshkovaya Metallurgiya i Funktsional'nye Pokrytiya (Powder Metallurgy and Functional Coatings)*. 2022. Vol. 16. No. 4. P. 15—24 (In Russ.).
DOI: dx.doi.org/10.17073/1997-308X-2022-4-15-24.

Структура и свойства порошка гидрида титана, полученного из титановой губки методом СВС-гидрирования

Н.П. Черезов, М.И. Алымов

Институт структурной макрокинетики и проблем материаловедения им. А.Г. Мерджанова РАН (ИСМАН), г. Черноголовка, Россия

Статья поступила в редакцию 14.03.2022 г., доработана 07.06.2022 г., подписана в печать 10.06.2022 г.

Аннотация: Представлены результаты исследования структуры и свойств порошков гидрида титана, полученных из титановой губки СВС-гидрированием и механическим измельчением. Гидрирование осуществляли в реакторе при постоянном давлении водорода 3 МПа. После прохождения волны горения горячую титановую губку охлаждали до комнатной температуры в среде водорода. В результате были получены губчатые гранулы гидрида титана с содержанием водорода 4,2 мас.%. Их измельчали в шаровой мельнице и разделяли на 4 фракции, соответствующие фракционному составу по-

рошка титана: ПТК, ПТС, ПТМ и ПТОМ. Анализ размера частиц показал, что образцы порошков ПТК и ПТОМ имеют более узкое распределение частиц в сравнении с ПТС и ПТМ. Далее для полученных порошков были проведены исследования химического состава, морфологии поверхности и определены насыпная плотность, уплотняемость, пикнометрическая плотность и удельная поверхность. Из результатов химического анализа было установлено, что в ходе СВС-гидрирования происходит снижение содержания примеси углерода и кислорода, а при механическом измельчении, в зависимости от его времени, незначительно увеличивается содержание железа. Исследование морфологии показало, что частицы гидрида титана имеют неправильную осколочную форму, — такая морфология характерна для порошков, полученных по данной технологии. Структура поверхности частично сохранила структуру исходной титановой губки и состоит из вытянутых ориентированных зерен. Установлено, что с уменьшением размера частиц насыпная плотность снижается, а уплотняемость возрастает. Значения пикнометрической плотности и удельной поверхности приблизительно равны для всех образцов порошка.

Ключевые слова: гидрид титана, порошковая металлургия, самораспространяющийся высокотемпературный синтез (СВС), гидрирование, морфология, технологические свойства.

Черезов Н.П. — мл. науч. сотр. лаборатории высокоэнергетических методов синтеза сверхвысокотемпературных керамических материалов ИСМАН (142432, Московская обл., Ногинский р-н, г. Черноголовка, ул. Академика Осипьяна, 8). E-mail: cherezovnikita@gmail.com.

Алымов М.И. — докт. техн. наук, проф., чл.-кор. РАН, директор ИСМАН. E-mail: alymov.mi@gmail.com.

Для цитирования: Черезов Н.П., Алымов М.И. Структура и свойства порошка гидрида титана, полученного из титановой губки методом СВС-гидрирования. *Известия вузов. Порошковая металлургия и функциональные покрытия*. 2022. Т. 16. No. 4. С. 15—24. DOI: [dx.doi.org/10.17073/1997-308X-2022-4-15-24](https://doi.org/10.17073/1997-308X-2022-4-15-24).

Introduction

Titanium is one of the metals, capable of actively absorbing hydrogen and forming hydrides. Titanium hydride (TiH₂) is known as a titanium with hydrogen chemical compound where hydrogen atoms are randomly distributed in the cavities of the titanium tetrahedral lattice [1, 2]. Titanium hydride has a fairly wide practical application in aerospace, aviation, the chemical industry and nuclear power engineering. It serves for porous titanium and titanium filters production. Blowing agent technique is used for aluminum foam production. Recently, due to the high hydrogen capacity (4.04 wt.%), titanium hydrides have been used as a hydrogen storage material [3—9].

Hydrogen is also known to cause embrittlement of metals and alloys. The brittleness of titanium hydride is due to the fact that hydrogen reduces the stress required for the movement of dislocations, increases their speed of movement and promotes the formation of microcracks, as well as their growth and the propagation of avalanches. Hydrogenation of titanium also increases the volume of the space cell — approximately in 2.5 times [10].

This characteristic is taken into account in the production of titanium powders using titanium sponge or scrap and by implementing hydrogenation-dehydrogenation method. While hydrogenating, the initial titanium is saturated with hydrogen during the isothermal heat treatment in hydrogen atmosphere. The resulting titanium hydride is quite brittle and can be micro ground

within a short period of time implementing mechanical grinding. Afterwards titanium hydride can be dehydrogenated for producing a finely-dispersed titanium powder, which serves to create corrosion-resistant filters, medical implants, and fabricating products by using powder metallurgy methods [11—14]. The powder particles obtained by this method have an irregular splinter shape and the content of impurities depends on the content of impurities in the source raw material. Obtained titanium powder has the same granulometric size composition as the initial titanium hydride. Hydrogenation-dehydrogenation method is of moderate cost and has small impact on the final powder price. Furthermore, finely-dispersed titanium hydride powder can be used for the synthesis of binary and multicomponent alloys and intermetallics [15, 16].

Another way to obtain titanium hydride is with the help of self-propagating high-temperature synthesis (SHS) method. It consists in using the heat of exothermic reaction after the local activation of a combustion one. High temperatures develop in the combustion front, that moves along the source titanium from layer to layer due to thermal transmission. No additional energy inputs are required, the process develops due to the heat of the chemical reaction $\text{Ti} + \text{H}_2 \rightarrow \text{TiH}_2 + Q$ (39 kcal/mol.) [17].

Production of titanium powders by SHS sponge hydrogenation with posterior dehydrogenation is cost-effective. Application of such powders as a primary compo-

ment allows reducing significantly the cost price of titanium products [18].

Technological properties (bulk density, compressibility) of initial powders are of significant importance for products manufactured by means of the titanium powder metallurgy techniques [19, 20]. According to consumer requirements such powders should possess certain properties and characteristics. Therefore, the study of properties and particle structure of powders used in manufacturing products implementing solid-phase sintering method is a relevant objective for the development of the titanium powder metallurgy techniques. The quality parameters of powders should be stable and not change during the shelf time [21–23].

The object of the given research is to study the structure and determine the technological and chemical properties of titanium hydride powders produced by SHS titanium sponge hydrogenation in the reactor and subsequent mechanical grinding.

Research data and methods

Titanium hydride powders with the density composition corresponding to the granulometric size composition of powders PTK, PTS, PTM, PTOM types (Specifications TU 14-22-57-92), prepared by titanium sponge TG-100 hydrogenation (GOST Russian National Standard 17746-96). The particle size of the initial titanium sponge was from 5 to 20 mm. Hydrogen gas, type «A» grade (GOST (Russian National Standard) 3022-80) was used as the hydrogen source.

Hydrogenation of the sponge was carried out in a sealed reactor of 2 L (Fig. 1, *a*). Titanium sponge 0.5 kg in weight was loaded into a gas-permeable shell installed in the reactor. Further finely-dispersed titanium powder was placed in a paper envelope on top of the titanium sponge to ignite the sponge. The reaction started due to the nickel chrome spiral heating and by means of electricity flow passing through it. Before synthesis, the reactor was sealed and purged with hydrogen to remove

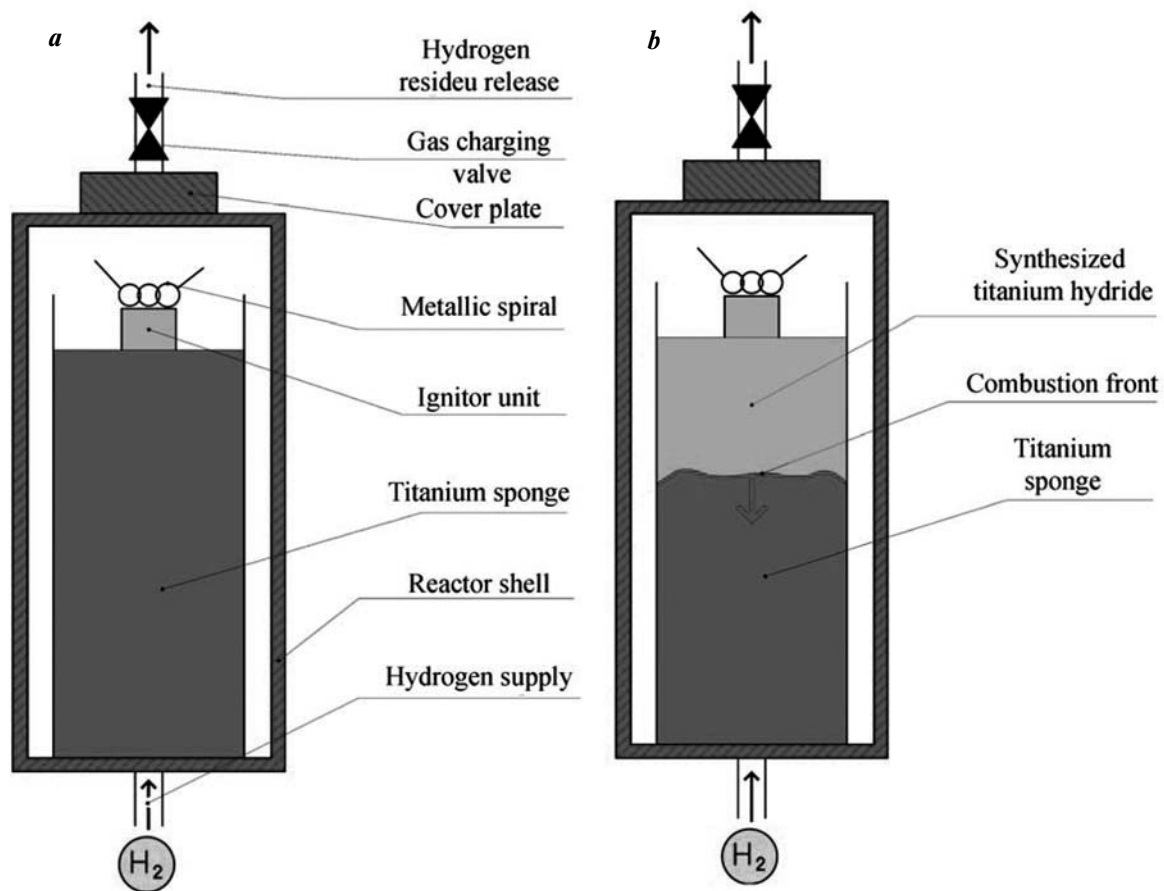


Fig. 1. High-pressure reactor schematic illustration (*a*) and SHS hydrogenation process (*b*)

Рис. 1. Схематическое изображение реактора высокого давления (*a*) и процесса СВС-гидрирования (*b*)

Table 1. Hydrogenated titanium sponge grinding modes

Таблица 1. Режимы измельчения гидрированной титановой губки

Grinding mode	Weight of the grinding sponge, kg	Drum rotation speed, rpm	Grinding time, min	Ratio of grinding bodies to titanium sponge
1	0.5	90	15	5 : 1
2	0.5	90	20	5 : 1
3	0.5	90	25	5 : 1

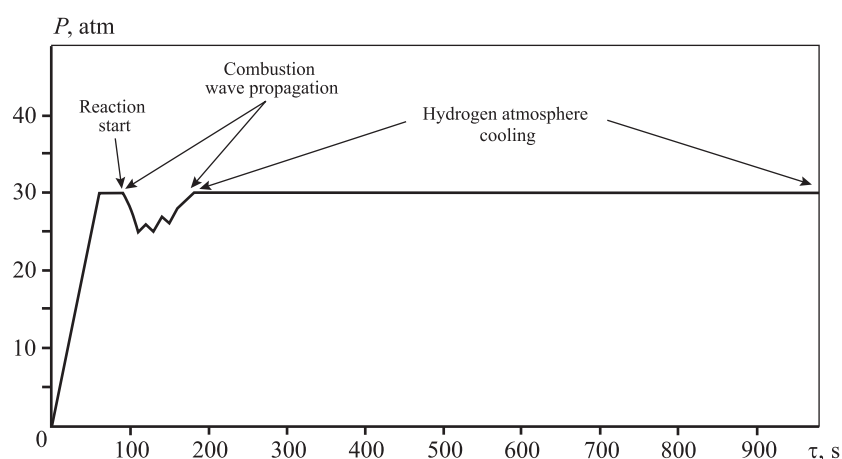


Fig. 2. Hydrogen pressure variation in the reactor during SHS hydrogenation

Рис. 2. Изменение давления водорода в реакторе в процессе СВС-гидрирования

air. Then it was filled with hydrogen until a hydrogen pressure of 30 atm was reached. While combusting, the pressure was maintained by the periodic supply of hydrogen in the direction opposite to the propagation of the combustion front (Fig. 1, b). The synthesis time was about 75 s. Then the heated titanium sponge was cooled to room temperature for 1 h in a hydrogen atmosphere (Fig. 2).

Derived titanium hydride sponge was mechanically ground in a steel ball mill with steel grinding bodies according to the modes given in Table 1.

Varying the grinding time resulted in obtaining titanium hydride powders with the particle distribution shown in Fig. 3.

For further study the ground powders were sieved (according to GOST Russian National Standard 18318-94) in order to obtain titanium hydride powders with the density composition corresponding to PTK, PTS, PTM, PTOM types. As a result, powders of 4 fractions were obtained: PTK (<40 μm — 10 wt.%; 40—280 μm — remaining wt.%), PTS (40—100 μm — 35 wt.%; <40 μm — remaining wt.%), PTM (40—100 μm —

25 wt.%; <40 μm — remaining wt.%), PTOM (40—100 μm — 5 wt.%; <40 μm — remaining wt.%).

Following technological characteristics of powders were determined for these fractions: bulk density, compressibility, pycnometric density and specific surface area. In addition, the morphology was studied, particle-size distribution by means of laser diffraction was carried out, and the main impurity content was determined for the obtained powders.

Powders bulk density was defined according to GOST Russian National Standard 19440-94, while their compressibility (compaction) — to GOST Russian National Standard 25280-90. Powder pycnometric density was determined according to GOST Russian National Standard 2211-2020: the method in use is based on determining the analytical sample weight and its true volume followed by density calculation. The true volume of the sample was estimated using a pycnometer with saturating liquid (toluene). Specific surface area was measured using the method of low-temperature nitrogen adsorption on Sorbi-M device designed for determining the specific surface area of porous materials.

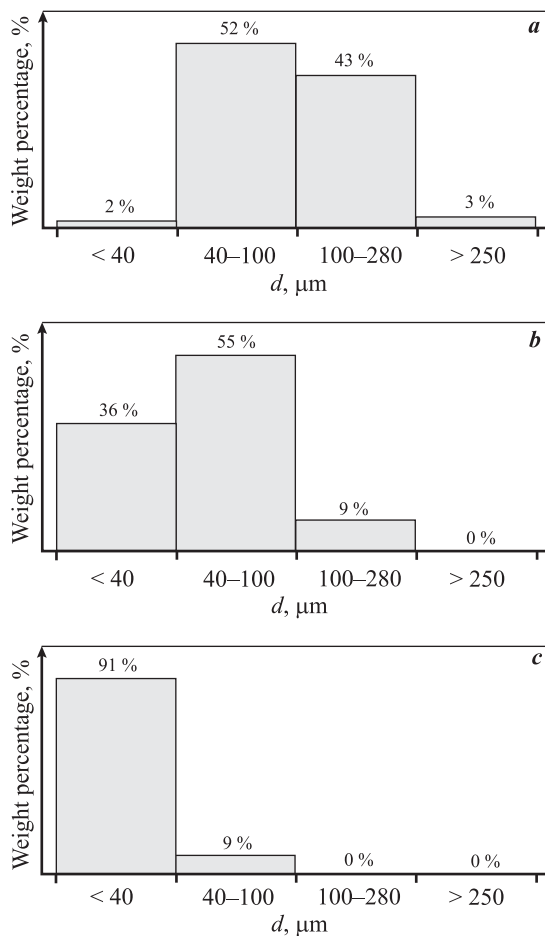


Fig. 3. Particles titanium hydride distribution at grinding modes 1 (a), 2 (b), 3 (c)

Рис. 3. Распределение частиц гидрида титана при режимах измельчения 1 (a), 2 (b), 3 (c)

Obtained titanium hydride powder particle morphology was studied with an electron-scan microscope LEO 1450. The particle size was studied with a laser particle analyzer MicroSizer 201. Impurity elements content of carbon, oxygen, nitrogen and hydrogen was determined using analyzers Leco CS-600, AK-7716P, TC-600 and RHEN-602 respectively. Powder iron content was estimated using Concentration photoelectric photometer-3-01.

Results and discussion

As a result of the SHS hydrogenation of the titanium sponge titanium hydride with hydrogen content of 4.2 wt.% was obtained. It is assumed that the high hydrogen content is recorded due to the concentration diffusion caused by high hydrogen reactor pressure

(30 atm) during synthesis. The large amount of dissolved hydrogen in the crystal lattice of titanium causes embrittlement of the latter and makes it possible to grind a large sponge with a particle size from 20 mm to 40 μm .

After grinding powders were divided into 4 density compositions, that correspond to the particle size distribution of PTK, PTS, PTM and PTOM types. Fig. 4 shows histograms of the investigated titanium hydride powders particle distribution. PTK and PTOM samples have narrower particle distribution in comparison with PTS and PTM.

Impurities play an important role in the quality of products made of the titanium powders. Final product presence of small amounts of metallic impurities, such as iron or aluminum, does not significantly affect its properties. The presence of non-metallic impurities such as oxygen, nitrogen and carbon should be strictly limited, as with the introduction of titanium they form solid solutions and chemical compounds that significantly reduce its moldability. A chemical analysis of the starting material and the synthesized powder was therefore carried out (Table 2). As a result, it was found that during SHS hydrogenation the carbon and oxygen content decreased, which indicates a self-cleaning of the titanium sponge. Supposedly, the impurities reduction occurs during the combustion process when the initial titanium sponge is sharply heated. It causes a significant increase in the diffusion coefficient and promotes the diffusion mass transfer of impurity atoms to the particle surface. Already on the surface, nitrogen and carbon impurities atoms can form molecules, which are subsequently desorbed into the gas state [24]. During mechanical grinding the iron content increases insignificantly due to the short grinding time.

A shape of the titanium powder particles largely determines its behavior at all stages of the technological process of obtaining products. It also significantly influences its technological properties. Fig. 5 (SEM-images) shows the general appearance of the obtained titanium hydride powders. The images clearly show that the hydride particles are of irregular splinter shape. This morphology characterizes the powders obtained by means of this technology [14].

Titanium hydride surface micro structure (Fig. 6) partially preserves the lamellar structure of the titanium sponge. As seen (Fig. 6, a, c), the surface structure is similar to that after annealing and consists of large elongated oriented grains. Traces of stress cracking caused by various titanium and titanium hydride specific volumes are noticeable on titani-

Table 2. Impurity content, wt.%, in the synthesized titanium hydride powder

Таблица 2. Содержание примесей, мас.%, в синтезированном порошке гидрида титана

Sample	C	N	O	Fe
Initial titanium sponge TG-100	0.52 ± 0.03	0.11 ± 0.01	0.51 ± 0.01	0.02 ± 0.001
PTK	0.18 ± 0.01	0.17 ± 0.01	0.26 ± 0.01	0.03 ± 0.001
PTS	0.11 ± 0.01	0.17 ± 0.01	0.21 ± 0.01	0.03 ± 0.001
PTM	0.13 ± 0.01	0.28 ± 0.01	0.32 ± 0.01	0.04 ± 0.001
PTOM	0.17 ± 0.01	0.27 ± 0.02	0.25 ± 0.01	0.04 ± 0.001

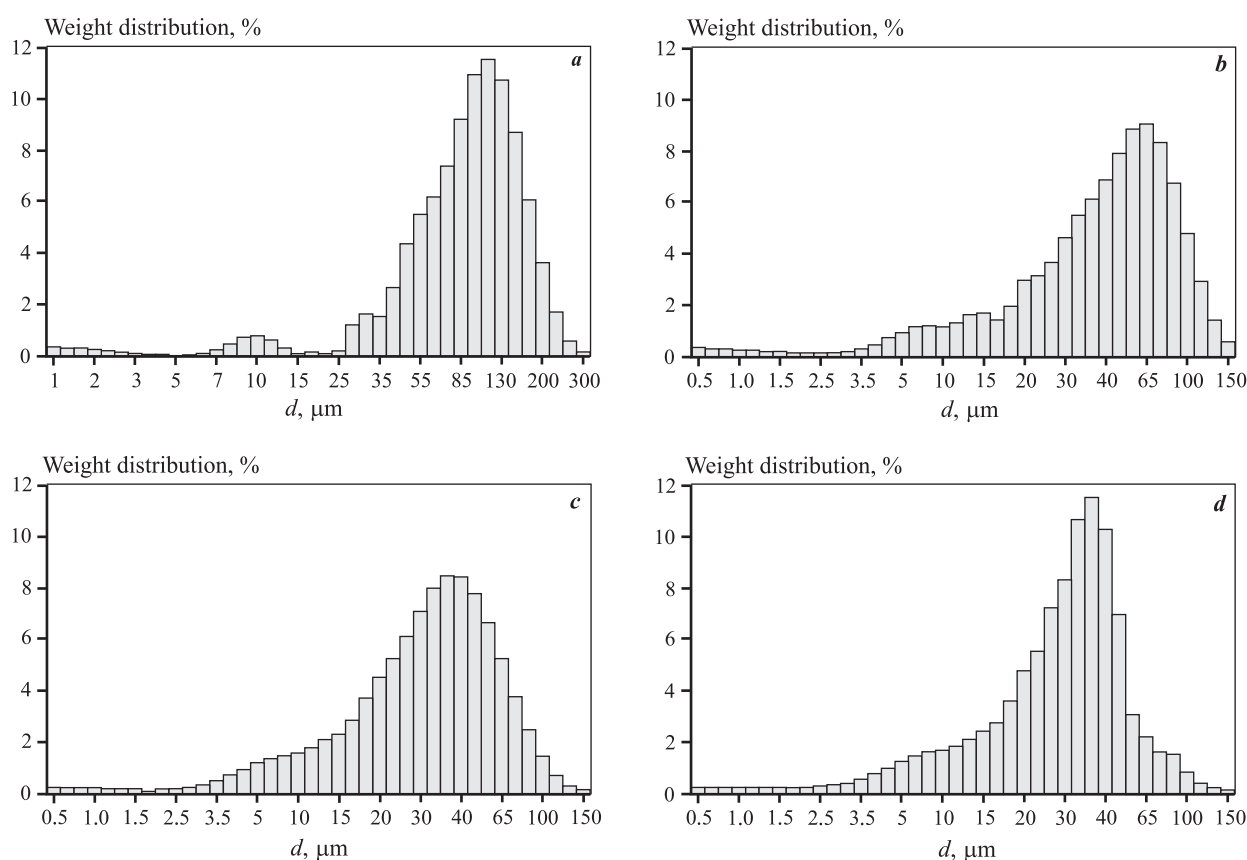


Fig. 4. Histograms of the synthesized titanium hydride powder particle distribution by size PTK (a), PTS (b), PTM (c), PTOM (d)

Рис. 4. Гистограммы распределения частиц синтезированного порошка гидрида титана по размерам. Изучены образцы ПТК (a), ПТС (b), ПТМ (c), ПТОМ (d)

um hydride surface layers (Fig. 6, b). Fig. 6, d shows a surface of an intergranular brittle fracture. Its appearance is characterized by relatively smooth surfaces.

Powders of the same chemical composition but with different physical characteristics can have different technological properties affecting the conditions of the further transformation of powders into products.

The technological properties of the synthesized titanium hydride powder are shown in Table 3.

Bulk density is a powder volumetric characteristic which represents a ratio of the powder mass to its volume in free-fall. Its value depends on the powder particles packing density considering certain freely filling volume. The greater the packing density, the coarser and more regular the powder particles and the greater their

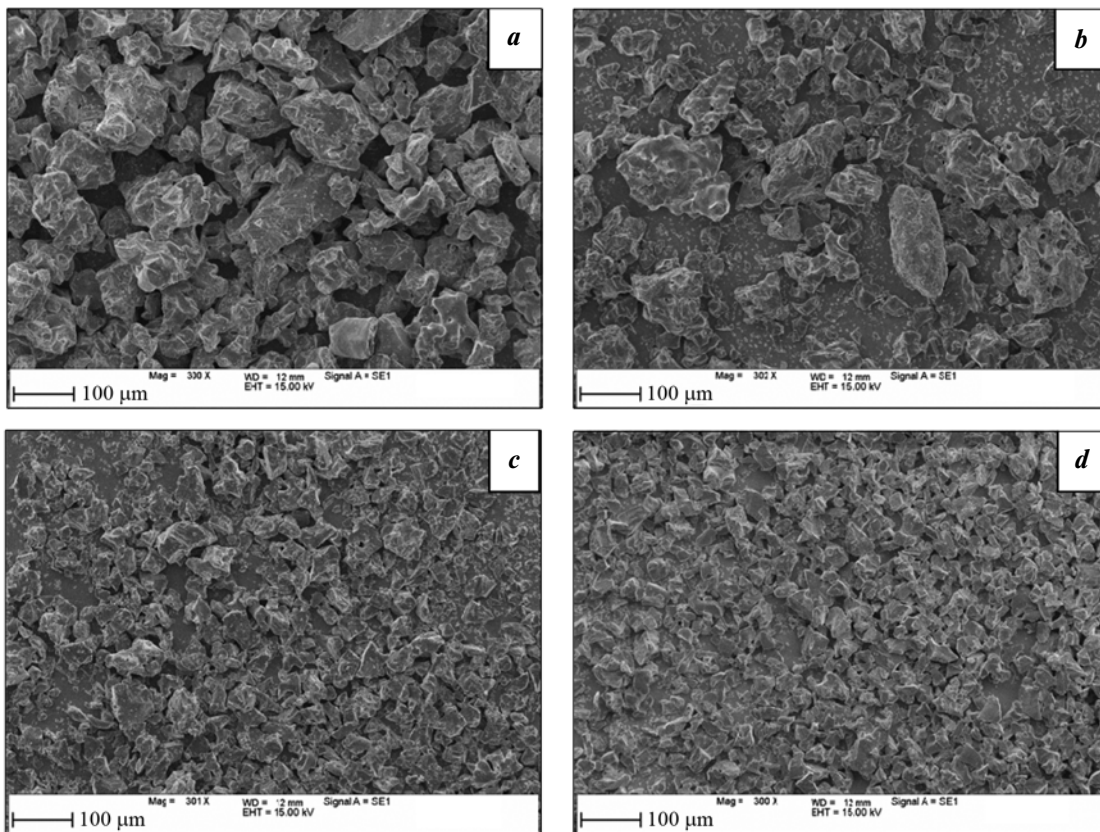


Fig. 5. Synthesized titanium hydride powder general appearance

a – PTK, *b* – PTS, *c* – PTM, *d* – PTOM

Рис. 5. Общий внешний вид синтезированного порошка гидрида титана

a – ПТК, *b* – ПТС, *c* – ПТМ, *d* – ПТОМ

pycnometric density. Obtained titanium hydride powders bulk density value reduces with decreasing particle size. The PTK sample has a wider fractional composition, which leads to a denser packing of particles: small particles fill the cavities formed by the packing of larger ones. The PTOM sample has a greater specific surface area due to the decreased particle size, which contributes to friction between particles, making it difficult for them to move relative to each other and leading to powders bulk density value reduction.

Powder compaction is the ability of a powder, under the influence of an external force, to acquire and retain a certain shape and size. Good compressibility makes the powder forming process easier and cheaper. The measured compaction values of the powders obtained are almost identical — this is because the titanium hydride particles are highly brittle and break apart during pressing to fill the voids.

Due to peculiarities of the production process, the particles of the metal powders may be characterized

by significant internal porosity and the presence of a large number of cavities in the lattice nodes. As a result, the actual density of the particles may differ significantly from the one calculated by using radiographic lattice-parameter determination data. Obtained titanium hydride particles density correlates with the theoretical one of 3.75 g/cm^3 , which indicates the practically total absence of cavities in the particle material.

The specific surface area of disperse bodies is the surface area of a powder unit mass or volume. The specific surface area depends not only on the particles size but also on the degree of the development of their surface, which is determined by the obtaining of powders conditions. The specific surface area is a very important characteristic of powders: determines the content of adsorbed gases in powders, their corrosion resistance, sintering ability, and a number of other characteristics. The obtained values for the specific surface area of titanium hydride powders are close to the values for spheri-

Table 3. Titanium hydride synthesized powder technological properties

Таблица 3. Технологические свойства синтезированного порошка гидрида титана

Sample	Bulk density, g/cm ³	Compaction, g/cm ³ , at 200 MPa	Pycnometric density, g/cm ³	Specific surface area, m ² /g
PTK	1.38 ± 0.04	2.83 ± 0.04	3.79 ± 0.01	0.6 ± 0.01
PTS	1.31 ± 0.03	2.85 ± 0.03	3.81 ± 0.01	0.6 ± 0.01
PTM	1.30 ± 0.02	2.86 ± 0.03	3.80 ± 0.01	0.6 ± 0.01
PTOM	1.16 ± 0.02	2.88 ± 0.03	3.72 ± 0.01	0.7 ± 0.01

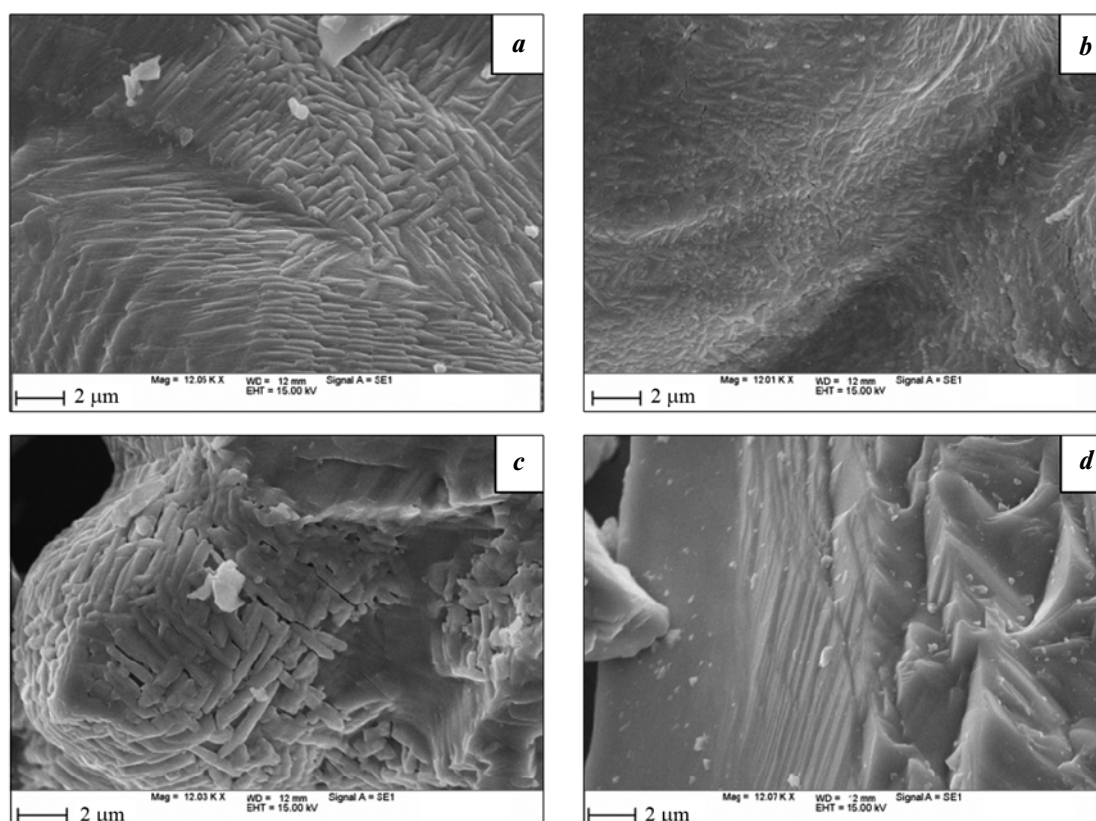


Fig. 6. Synthesized titanium hydride powder micro structure

a – PTK, *b* – PTS, *c* – PTM, *d* – PTOM

Рис. 6. Микроструктура синтезированного порошка гидрида титана

a – ПТК, *b* – ПТС, *c* – ПТМ, *d* – ПТОМ

cal powders (0.14 m²/g), therefore, the obtained hydride powder does not have a developed porous surface which coherent with the received data on the morphology of the particles.

Conclusion

Experimental studies of the structure and properties of titanium hydride powders obtained from titanium

sponge by the SHS method in a high-pressure reactor have been conducted.

It is found that due to high embrittlement of titanium hydride the hydrogenated titanium sponge is quickly and easily broken to a particle size of less than 40 μm. Iron impurity content increases insignificantly during the mechanical grinding process. The SHS hydrogenation leads to a product self-cleaning and also to carbon and oxygen impurities reduction.

Titanium hydride particles have an irregular splinter shape. Generally speaking, the shape and defects of particles are typical of the powders obtained by this method. Particles surface structure consists of elongated oriented grains. Due to stresses resulting from various specific volumes of titanium and titanium hydride the titanium hydride surface layers show traces of cracking.

A study of the technological properties demonstrated that the obtained powders possessed necessary parameters for application in powder metallurgy.

Acknowledgments: *The work was performed within the state assignment of ISMAN.*

Работа выполнена в рамках государственного задания ИСМАН.

References

- Xu J.J., Cheung H.Y., Shi S.Q. Mechanical properties of titanium hydride. *J. Alloys Compd.* 2007. Vol. 436. Iss. 1—2. P. 82—85. DOI: 10.1016/j.jallcom.2006.06.107.
- Левинский Ю.В., Патрикеев Ю.Б., Филянд Ю.М. Водород в металлах и интерметаллидах. М.: Научный мир, 2017.
Levinskii Yu.V., Patrikeev Yu.B., Filyand Yu.M. Hydrogen in metals and intermetallics. Moscow: Nauchnyi mir, 2017 (In Russ.).
- Ma M., Liang L., Wang L., Wang Y., Cheng Y., Tang B., Xiang W., Tan X. Phase transformations of titanium hydride in thermal desorption process with different heating rates. *Int. J. Hydrogen Energy.* 2015. Vol. 40. Iss. 29. P. 8926—8934. DOI: 10.1016/j.ijhydene.2015.05.083.
- Sakintuna B., Lamari-Darkrim F., Hirscher M. Metal hydride materials for solid hydrogen storage: A review. *Int. J. Hydrogen Energy.* 2007. Vol. 32. Iss. 9. P. 1121—1140. DOI: 10.1016/j.ijhydene.2006.11.022.
- Liu H., He P., Feng J.C., Cao J. Kinetic study on nonisothermal dehydrogenation of TiH₂ powders. *Int. J. Hydrogen Energy.* 2009. Vol. 34. Iss. 7. P. 3018—3025. DOI: 10.1016/j.ijhydene.2009.01.095.
- Erk K.A., Dunand D.C., Shull K.R. Titanium with controllable pore fractions by thermoreversible gelcasting of TiH₂. *Acta Mater.* 2008. Vol. 56. Iss. 18. P. 5147—5157. DOI: 10.1016/j.actamat.2008.06.035.
- Lehmhus D., Rausch G. Tailoring titanium hydride decomposition kinetics by annealing in various atmospheres. *Adv. Eng. Mater.* 2004. Vol. 6. Iss. 5. P. 1438—1656. DOI: 10.1002/adem.200300572.
- Yang C.C., Nakae H. Foaming characteristics control during production of aluminum alloy foam. *J. Alloys Compd.* 2000. Vol. 313. Iss. 1—2. P. 188—191. DOI: 10.1016/S0925-8388(00)01136-1.
- Kennedy A.R., Lopez V.H. The decomposition behavior of as-received and oxidized TiH₂ foaming-agent powder. *Mater. Sci. Eng. A.* 2003. Vol. 357. Iss. 1—2. DOI: 10.1016/S0921-5093(03)00211-9.
- Жарков А.Ю., Рудских В.В., Левченкова О.Н., Волкова Т.С., Светлаков С.В. Исследование процесса гидрирования дробы титана при пониженном давлении водорода. В сб. 2-й отрасл. конф.: *Титан в атомной промышленности*. Глазов: ОАО ЧМЗ, 2014.
Zharkov A.Yu., Rudskikh V.V., Levchenkova O.N., Volkova T.S., Svetlakov S.V. Investigation of the process of titanium shot hydrogenation at reduced hydrogen pressure In: *Titanium in the nuclear industry: 2-nd Industry Conf.* Glazov: ОАО ChMZ, 2014 (In Russ.).
- Bhosle V., Baburaj E.G., Miranova M., Salama K. Dehydrogenation of TiH₂. *Mater. Sci. Eng. A.* 2003. Vol. 356. Iss.1—2. P. 190—199. DOI: 10.1016/S0921-5093(03)00117-5.
- Zheng Y., Zhang J., Liu Y., Jia S., Tang R., Zhang D. Dehydrogenation and spheroidization of titanium hydride powder based on fluidization principle. *Heat Treat. Surf. Eng.* 2020. Vol. 2. No. 1. P. 22—29. DOI: 10.1080/25787616.2020.1845443.
- Yanko T., Brener V., Ovchinnikov O. Production of spherical titanium alloy powders used in additive manufacturing from titanium scrap. In: *MATEC Web Conf: 14th World Conf. on Titanium (Ti-2019)*. 2020. Vol. 321. DOI: 10.1051/mateconf/202032107008.
- Goso X., Kale A. Production of titanium metal powder by the HDH process. In: *Advanced Metals Initiative: Light Metals Conf.* 2010. Vol. 111. No. 3. P. 203—210.
- Huiping S., Zhi W., Tao L., Zhimeng G., Qing Y., Jun W., Sen S., Shaoyuan L. Method for preparing TiAl intermetallic compound powder by using titanium hydride powder: Pat. 102825259A (China). 2012.
- Ivasishin O., Moxson V. Low-cost titanium hydride powder metallurgy. *Titanium Powder Metallurgy.* 2015. P. 117—148. DOI: 10.1016/B978-0-12-800054-0.00008-3.
- Долуханян С.К. СВС-метод получения аккумуляторов водорода. *Альтерн. энергетика и экология.* 2005. No. 11. С. 13—16.
Dolukhanyan S.K. SHS method for obtaining hydrogen batteries. *Alternativnaya energetika i ekologiya.* 2005. No. 11. P. 13—16 (In Russ.).
- Ратников В.И., Прокудина В.К., Беликова А.Ф., Сачкова Н.В. Получение порошка титана из титановой губки СВС-гидрированием и дегидрированием. *Известия вузов. Порошковая металлургия и функциональные покрытия.* 2009. No. 4. С. 25—30.
Ratnikov V.I., Prokudina V.K., Belikova A.F., Sachkova N.V. Obtaining titanium powder from a titanium sponge by SHS hydrogenation and dehydrogenation. *Izves-*

- tiya Vuzov. Poroshkovaya Metallurgiya i Funktsional'nye Pokrytiya (Powder Metallurgy and Functional Coatings). 2009. No. 4. P. 25–30 (In Russ.).
19. Chen W., Yamamoto Y., Peter W.H., Gorti S.B., Sabau A.S., Clark M.B., Nunn S.D., Kiggans J.O., Blue C.A., Williams J.C., Fuller B., Akhtar K. Cold compaction study of Armstrong Process Ti–6Al–4V powders. 2011. *Powder Technol.* Vol. 214. Iss. 2. P. 194–199. DOI: 10.1016/j.powtec.2011.08.007.
 20. Machaka R., Chikwanda H.K. Analysis of the cold compaction behavior of titanium powders: A comprehensive Inter-model comparison study of compaction equations. *Metall. Mater. Trans. A.* 2015. Vol. 46. P. 4286–4297. DOI: 10.1007/s11661-015-3038-6.
 21. Павленко Д.В. Влияние параметров порошков титана на прочность спеченных полуфабрикатов. *Нові матеріали і технології в металургії і машинобудуванні.* 2014. No. 2. С. 87–92.
Pavlenko D.V. Influence of parameters of titanium powders on the strength of sintered semi-finished products. *Novi materiali i tekhnologii v metalurgii i mashinostroenii.* 2014. No. 2. P. 87–92 (In Ukr.).
 22. Князев А.Е., Неруш С.В., Алишин М.И., Куко И.С. Исследования технологических свойств металлопорошковых композиций титановых сплавов ВТ6 и ВТ20, полученных методом индукционной плавки и газовой атомизации. *Тр. ВИАМ.* 2017. Vol. 59. No. 11. С. 44–53. DOI: 10.18577/2307-6046-2017-0-11-6-6.
Knyazev A.E., Nerush S.V., Alishin M.I., Kuko I.S. Studies of technological properties of metal-powder compositions of titanium alloys VT-6 and VT-20 obtained by induction melting and gas atomization. *Trudy VIAM.* 2017. Vol. 59. No. 11. P. 44–53. DOI: 10.18577/2307-6046-2017-0-11-6-6 (In Russ.).
 23. Chen B., Shen J., Ye X., Umeda J., Kondoh K. Advanced mechanical properties of powder metallurgy commercially pure titanium with a high oxygen concentration. *J. Mater. Res.* 2017. Vol. 32. P. 3769–3776. DOI: 10.1557/jmr.2017.338.
 24. Потехин А.А., Горькаев Д.А., Постников А.Ю., Тарасова А.И., Мальшев А.Я. Изучение самоочистки реакционной системы в процессе СВС. *Тр. РФЯЦ–ВНИИЭФ.* 2015. Т. 20. Ч. 2. С. 618–619.
Potekhin A.A., Gorkaev D.A., Postnikov A.Y., Tarasova A.I., Malyshev A.Y. Self-purification from impurities during SHS of titanium hydride. *Int. J. SHS.* 2014. Vol. 23. No. 1. P. 58–61.

UDC 621.762.2

DOI dx.doi.org/10.17073/1997-308X-2022-4-25-33

MAX phase Ti₂AlN synthesis by reactive sintering in vacuum

© 2022 г. **A.V. Linde, A.A. Kondakov, I.A. Studenikin, N.A. Kondakova, V.V. Grachev**

Merzhanov Institute of Structural Macrokinetics and Materials Science of the Russian Academy of Sciences (ISMAN), Chernogolovka, Russia

Received 10.02.2022, revised 01.06.2022, accepted for publication 06.06.2022

Abstract: The synthesis of MAX phase Ti₂AlN from several mixtures of Ti, Al, TiN, and AlN powders by vacuum sintering of green samples in the form of dense compacts, bulk powder in silica tubes, and plain layer in a closed rectangular molybdenum boat was studied upon variation in charge composition and sintering temperature T_s. The sintering of 2 : 1 Ti—AlN mixture was carried out at 1100, 1200, 1300, 1400, and 1500 °C with exposure time of 60 min. The largest MAX phase content (94 wt.%) was reached at T_s = 1400 °C. The sintering of 1 : 1 TiAl : TiN composition at the same temperature gave 93 wt.% Ti₂AlN. The best result (single-phase Ti₂AlN in a 100-% yield) was achieved upon the sintering of 1 : 1 : 1 Ti—Al—TiN composition at T_s = 1400 °C. The scalability of our process was checked by the fabrication of a large (0.5 kg) and uniform cake of single-phase Ti₂AlN. In experiments we used green samples with shielded lateral surface (bulk powder in silica tubes, plain layer in a closed molybdenum boat) and without shield (dense compacts). It has been shown that shielding of Ti—Al—TiN samples restricts the escape of Al vapor from a sintered mixture, thus providing more favorable conditions for the synthesis of single-phase Ti₂AlN. Our process can be readily recommended for practical implementation.

Keywords: MAX phase, sintering, phase transitions, X-ray diffraction.

Linde A.V. — Cand. Sci. (Chem.), senior researcher of the Laboratory of macrokinetics of SHS-processes in chambers of Merzhanov Institute of Structural Macrokinetics and Materials Science of the Russian Academy of Sciences (ISMAN) (142432, Russia, Moscow Region, Noginsk district, Academician Osip'yan str., 8). E-mail: alex-linde@mail.ru.

Kondakov A.A. — researcher of the Laboratory of macrokinetics of SHS-processes in chambers of ISMAN. E-mail: kondakov_aleks@list.ru.

Studenikin I.A. — researcher of the Laboratory of macrokinetics of SHS-processes in chambers of ISMAN. E-mail: stivan@bk.ru.

Kondakova N.A. — junior researcher of the Laboratory of macrokinetics of SHS-processes in chambers of ISMAN. E-mail: natik1985@bk.ru.

Grachev V.V. — Cand. Sci. (Phys.-Math.), leading researcher, head of the Laboratory of macrokinetics of SHS-processes in chambers of ISMAN. E-mail: grachev@ism.ac.ru.

For citation: Linde A.V., Kondakov A.A., Studenikin I.A., Kondakova N.A., Grachev V.V. MAX phase Ti₂AlN synthesis by reactive sintering in vacuum. *Izvestiya Vuzov. Poroshkovaya Metallurgiya i Funktsional'nye Pokrytiya (Powder Metallurgy and Functional Coatings)*. 2022. Vol. 16. No. 4. P. 25—33 (In Russ.). DOI: dx.doi.org/10.17073/1997-308X-2022-4-25-33.

Синтез МАХ-фазы Ti₂AlN реакционным спеканием в вакууме

А.В. Линде, А.А. Кондаков, И.А. Студеникин, Н.А. Кондакова, В.В. Грачев

Институт структурной макрокинетики и проблем материаловедения им. А.Г. Мерджанова РАН (ИСМАН), г. Черноголовка, Россия

Статья поступила в редакцию 10.02.2022 г., доработана 01.06.2022 г., подписана в печать 06.06.2022 г.

Аннотация: Проведены исследования процесса синтеза МАХ-фазы Ti₂AlN спеканием в вакууме различных смесей порошков в зависимости от фазового состава исходных реагентов и режимов их термической обработки в вакуумной электропечи. На примере смеси порошков титана и нитрида алюминия в мольном соотношении Ti : AlN = 2 : 1 (состав 1) прослежена последовательность изменения фазового состава смеси при увеличении температуры изотермической выдержки длительностью 60 мин при t = 1100–1500 °C с шагом 100 °C и определено значение температуры 1400 °C, при которой в

продуктах спекания достигается максимальное значение содержания МАХ-фазы Ti_2AlN — 94 мас.%. При этой температуре изотермической выдержки для исходной смеси $TiAl : TiN = 1 : 1$ (состав 2) содержание МАХ-фазы составило 93 мас.%. Наилучший результат по синтезу МАХ-фазы (100 мас.% Ti_2AlN) был получен для смеси $Ti : Al : TiN = 1 : 1 : 1$ (состав 3). На примере смеси данного состава массой 500 г при определенном режиме термовакuumной обработки экспериментально показана принципиальная возможность масштабирования процесса получения однофазного продукта состава Ti_2AlN спеканием в вакууме. Эксперименты проводились с двумя типами образцов: с закрытой и открытой боковой поверхностью. К образцам с закрытой боковой поверхностью относились образцы в кварцевых трубках, заполненных исходной смесью порошков с насыпной плотностью, и образец массой 500 г, помещенный в молибденовый тигель с крышкой. Образцы с открытой боковой поверхностью — это цилиндрические таблетки, спрессованные из исходной порошковой смеси. Было показано, что закрытие боковой поверхности образца из смеси $Ti : Al : TiN$ (состав 3) блокирует выход паров алюминия из порового пространства образца при нагреве, благодаря чему образуется только Ti_2AlN .

Ключевые слова: МАХ-фаза, спекание, фазовые превращения, рентгенофазовый анализ.

Линде А.В. — канд. хим. наук, ст. науч. сотр. науч.-иссл. лаборатории «Макрокинетики процессов СВС в реакторах» ИСМАН (142432, Московская обл., Ногинский р-н, ул. Академика Осипьяна, 8).
E-mail: alex-linde@mail.ru.

Кондаков А.А. — науч. сотр. науч.-иссл. лаборатории «Макрокинетики процессов СВС в реакторах» ИСМАН.
E-mail: kondakov_aleks@list.ru.

Студеникин И.А. — науч. сотр. науч.-иссл. лаборатории «Макрокинетики процессов СВС в реакторах» ИСМАН.
E-mail: stivan@bk.ru.

Кондакова Н.А. — мл. науч. сотр. науч.-иссл. лаборатории «Макрокинетики процессов СВС в реакторах» ИСМАН.
E-mail: natik1985@bk.ru.

Грачев В.В. — канд. физ.-мат. наук, вед. науч. сотр., зав. науч.-иссл. лабораторией «Макрокинетики процессов СВС в реакторах» ИСМАН. E-mail: grachev@ism.ac.ru.

Для цитирования: Линде А.В., Кондаков А.А., Студеникин И.А., Кондакова Н.А., Грачев В.В. Синтез МАХ-фазы Ti_2AlN реакционным спеканием в вакууме. *Известия вузов. Порошковая металлургия и функциональные покрытия*. 2022. Т. 16. №. 4. С. 25—33. DOI: dx.doi.org/10.17073/1997-308X-2022-4-25-33.

Introduction

The Ti_2AlN compound belongs to the family of МАХ phases described by the general formula $M_{n+1}AX_n$, where M is a transition metal, A is an element of IIIA and IVA groups, X is carbon or nitrogen, $n = 1-3$ [1]. Recently, many researchers have investigated МАХ-phase based materials, as these materials simultaneously have a unique combination of metals and ceramic properties and a layered structure. Ti_2AlN -based materials also show an exceptional combination of properties: high elastic modulus, high thermal and electrical conductivity, low density, easy machinability and excellent thermal shock resistance [2—4]. This predetermines the use of Ti_2AlN -based materials as reinforcing agent in alloys, transition layers in semiconductors, etc. [5—7].

The Ti_2AlN compound was discovered in 1963 by Jeitschko [8]. Since then, researchers have made many attempts to obtain this compound by various methods.

In 2000 Barsoum et al. [4, 5] obtained Ti_2AlN by Ti and AlN mixture hot isostatic pressing (process parameters were the following: pressure 40 MPa, temperature 1400 °C and soaking for 48 h). However, they failed to achieve the purity of the final product, the content of other phases was 10—15 vol.%.

The authors [9, 10] synthesized Ti_2AlN from the Ti and AlN mixture of powders (in the molar ratio of 2 : 1) under isothermal annealing in argon atmosphere for 2 h at 1300 °C and pressure of 0.3 MPa. At the same time the TiN impurity fraction was not more than 1 wt.%. It was also found during the researches that the preparatory mechanical activation of the powder causes an increase in the content of the TiN secondary phase and that the synthesis in vacuum does not lead to the formation of a single-phase product.

The authors [11] obtained a Ti_2AlN single-phase material by hot pressing a mixture consisting of Ti, TiN and Al powders in an argon atmosphere at 25 MPa and 1400 °C. The resulting material characteristics were as close as possible to the theoretical evidence — this led to the conclusion that hot pressing is a promising way to obtain pure Ti_2AlN due to the short duration of the process, the low applied load and the final product high purity.

In the research [12] Ti_2AlN was obtained by titanium powders (2 mol.) and aluminum nitride (1 mol.) spark plasma sintering with soaking for 5 min. Provided that at 1400 °C Ti_2AlN МАХ-phase with an admixture of titanium nitride was obtained in the final product, and

Ti₂AlN was obtained practically pure after increasing the sintering temperature to 1450 °C — there were only traces of titanium nitride. The same method, but already at 1200 °C [13] let obtain the material consisting of one MAX-phase.

The authors [14] describe the Ti₂AlN production by 30 min microwave sintering a mixture of titanium, aluminum and titanium nitride powders (in an approximate molar ratio of 1 : 1.03 : 1) in an argon atmosphere at 1200 °C. A further increase in the sintering temperature to 1350 °C resulted in the MAX-phase destruction and the appearance of TiN (4 wt.%). This method is promising due to the lowest temperature for obtaining the pure MAX phase and the short process time.

In the research [15] the Ti₂AlN phase was obtained by thermal explosion of Ti, Al and TiN mixture of powders at 700 °C and $\tau = 2$ min. However, the content of the secondary TiN phase was 4 wt.%. The Ti₂AlN powder in the research [16] was synthesized by microwave sintering from a TiH₂, Al and TiN mixture of powders with a molar ratio of 1 : 1.15 : 1 at 1250 °C. The sample with the highest MAX phase content consisted of 96.68 wt.% Ti₂AlN and 3.32 wt.% Ti₄AlN₃.

Electrospark sintering in vacuum at 1200 °C [17] produced compressed pellets 15 mm in diameter with a Ti₂AlN content of about 98 wt.% from a initial Ti and AlN powders mixture. Ti₂AlN with TiAl admixture was obtained by two-stage annealing in an argon atmosphere [18] with holding temperatures of 600 °C ($\tau = 1$ h) and 1100 °C ($\tau = 3$ h) from mechanically activated Ti, Al and AlN powders mixed in a molar ratio of 2 : 0.8 : 1 and pressed into tablets of 13 mm in diameter. In research [19] Ti₂AlN (pellets 20 mm in diameter) was obtained by electrospark sintering from a Ti, Al and TiN powders mixture with a molar ratio of 1 : 1.02 : 1.

The analysis of literature data shows that virtually all of the above mentioned methods require expensive equipment, while allowing to obtain only a small amount of containing pure MAX-phase material and with impurity phases often present in the final products.

In this work the Ti₂AlN MAX-phase synthesis process by vacuum sintering of different powders mixtures depending on the initial chemical agents phase composition and their thermal treatment modes in a vacuum electric furnace was studied. However, the ultimate goal was to determine the optimum conditions for obtaining a Ti₂AlN single-phase product by such a relatively simple method, as well as the possibility of obtaining product significant batches weighing up to 0.5 kg.

Research preliminary results were previously published in concise form [20] — the phase composition of the products for quartz tubes samples filled with the initial powders mixture with bulk density was presented.

The present article describes more detailed experimental procedure giving the exact parameters of the samples and comparing the samples phase composition in quartz tubes and samples with open side surface in the cylindrical tablets form pressed from the initial powder mixture. The reason for the compared samples phase composition difference has been revealed and it has been established why under the same composition and the same heating conditions in one case (samples with closed side surface) the Ti₂AlN MAX-phase concentration is 100 %, and in the other case (pressed samples with open side surface) the MAX-phase content does not reach 100 %. A detailed analysis of the phase formation sequence during samples with open and buried lateral surface heating, which has not been investigated before, was out.

Experimental procedures

Initial chemical agents mixtures were prepared from AlN [21] and TiN [22] powders obtained by the SHS method at ISMAN, as well as Al (ASD-1 grade), Ti (PTS-1), and TiAl (PT65U35) powders.

The dispersibility of the initial components is presented in the table.

Three mixtures were prepared to obtain the Ti₂AlN single-phase product Ti : AlN = 2 : 1 (composition 1); TiAl : TiN = 1 : 1 (composition 2) and Ti : Al : TiN = 1 : 1 (composition 3). Initial powders were mixed in a planetary mill with a charge-to-ball mass ratio of 2 : 1 for 30 min. Tablets of 15 mm in diameter were pressed from compositions 1, 2 and 3 (mass of 15 g) with the

Dispersity of initial powders

Дисперсность исходных порошков

Chemical agent	Grade	Dispersity d_{50} , μm
Ti	PTS-1	60.5
Al	ASD-1	16.3
AlN	SHS ISMAN	2.05
TiN	SHS ISMAN	29.7
TiAl	PT65U35	23.3

same pressing force of 354 MPa, when the final height of tablets was 32.5; 29.2 and 28.7 mm (with porosity of 36, 34 and 32 %, respectively).

In order to exclude the tablet pressing stage, experiments with quartz tubes samples were carried out. To compare with the pressed tablets results, mixtures 2 and 3 with the same mass of 15 g were poured into quartz tubes with the same inner diameter of 15 mm as of the pressed tablets, consequently the samples bulk porosity was 59–61 %. According to the quartz tubes samples experiments results and in order to check the process scaling possibility, composition 3 samples of 500 g in weight and bulk porosity of 57 % were sintered in a rectangular molybdenum closed container 88 × 88 × 70 mm in size with a fill height of 35 mm.

Sintering was carried out in a vacuum electric resistance furnace SNVE-16/16 (OOO «NPPMosZETO», Moscow) at the following holding temperatures, °C: 1100, 1200, 1300, 1400 и 1500. In all experiments the samples soak time was 60 min at a minimum pressure of $7.73 \cdot 10^{-4}$ Pa. Since the sintering pressed tablets results at different holding temperatures determined the optimum temperature of 1400 °C, at which the Ti_2AlN MAX-phase maximum content in the final product was observed (see below), successive experi-

ments with quartz tubes samples in a molybdenum container were carried out at this holding temperature.

The sintering products phase composition was studied by X-ray diffraction analysis on diffractometer DRON-3M (NPP «Burevestnik», St. Petersburg). Phase identification on the diffractograms was carried out using the following standards: Ti (CAS number 5-672), Al (CAS number 4-787), TiN (CAS number 38-1420), AlN (CAS number 25-1133), TiAl (CAS number 5-678), Ti_3Al (CAS number 14-451), Ti_3AlN (PDF number 01-071-4029), Ti_2AlN (PDF number 00-055-0434). The quantitative phase content was determined by the corundum number method. The sintered samples fracture microstructure and the local elemental composition were studied on an ultra-high field emission scanning electron microscope «Zeiss Ultra Plus» based on «Ultra 55» (Carl Zeiss, Germany) with the X-ray microanalysis attachment «INCA Energy 350 XT» (Oxford Instruments, UK).

Results of experiments

Fig. 1 shows mixture 1 (Ti : AlN) pressed samples diffractograms, which show that at temperatures from 1100 to 1200 °C the product is multiphase and con-

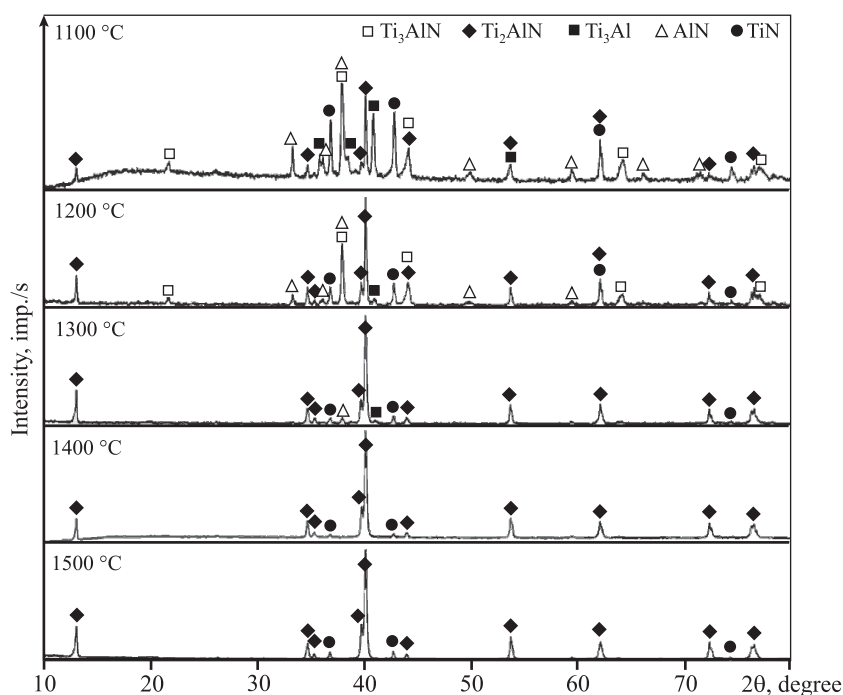


Fig. 1. Mixture 1 pressed samples diffractograms after sintering at different temperatures

Рис. 1. Диффрактограммы прессованных образцов смеси 1 после спекания при различных температурах

tains the following phases: Ti_2AlN , TiN , AlN , Ti_3AlN , Ti_3Al .

With increasing temperature up to 1200 °C the amount of Ti_2AlN MAX phase increases from 20 to 52 wt.% (see Fig. 2). At 1300 °C the product contains the following phases, wt.%: Ti_2AlN — 83, TiN — 12, AlN — 5. Further temperature rise to 1400 °C leads to the two-phase product formation consisting of Ti_2AlN (94 wt.%) and TiN (6 wt.%). After reaching 1500 °C

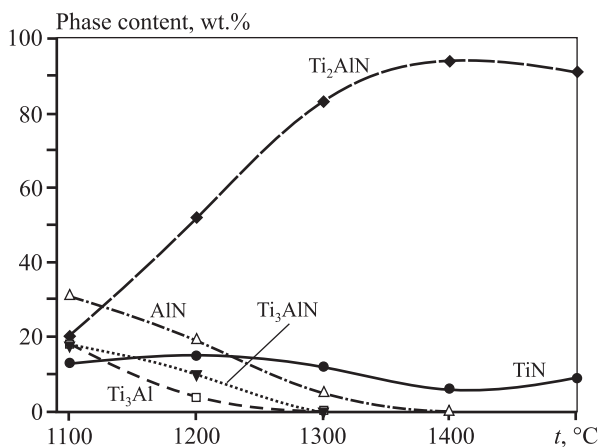


Fig. 2. Phases contents at composition 1 ($2Ti + AlN$) pressed samples various sintering temperatures

Рис. 2. Содержание фаз при различных температурах спекания прессованных образцов состава 1 ($2Ti + AlN$)

the product also remains biphasic, but there is a slight decrease of the Ti_2AlN MAX-phase to 91 wt.% and an increase of the titanium nitride proportion to 9 wt.%. Reducing the Ti_2AlN amount corresponds with the research data [23], which shows that in a dynamic vacuum at 1550 °C the aluminum evaporation from the MAX-phase with the titanium non-stoichiometric nitride formation is observed: $Ti_2AlN_{(s)} \rightarrow 2TiN_{0.5} + Al_{(g)}$. High-temperature aluminum evaporation in MAX-phase obtaining by sintering was also noted in the research [24].

By this means, the composition 1 ($2Ti + AlN$) maximum Ti_2AlN MAX-phase content of 94 wt.% was obtained at 1400 °C, which corresponds with Ti_2AlN obtaining results by spark plasma sintering [12], for that reason sintering of samples from mixtures 2 and 3 was performed at this very temperature.

After pressed sample from composition 2 mixture ($TiAl : TiN = 1 : 1$) sintering at 1400 °C a multiphase product (Fig. 3, a) with the following phase content (wt.%) was obtained: Ti_2AlN — 93; TiN — 4; Ti_3AlN — 2; Ti_3Al — 1.

After pressed sample from composition 3 mixture ($Ti : Al : TiN = 1 : 1 : 1$) sintering the product phase composition was as follows, wt.%: Ti_2AlN — 89, TiN — 9, %; Ti_3Al — 2 (Fig. 4, a).

To prevent the reactive volume aluminum vapor escape through the pressed samples surface during heating process and vacuum blowing experiments with quartz tubes samples were carried out. After composi-

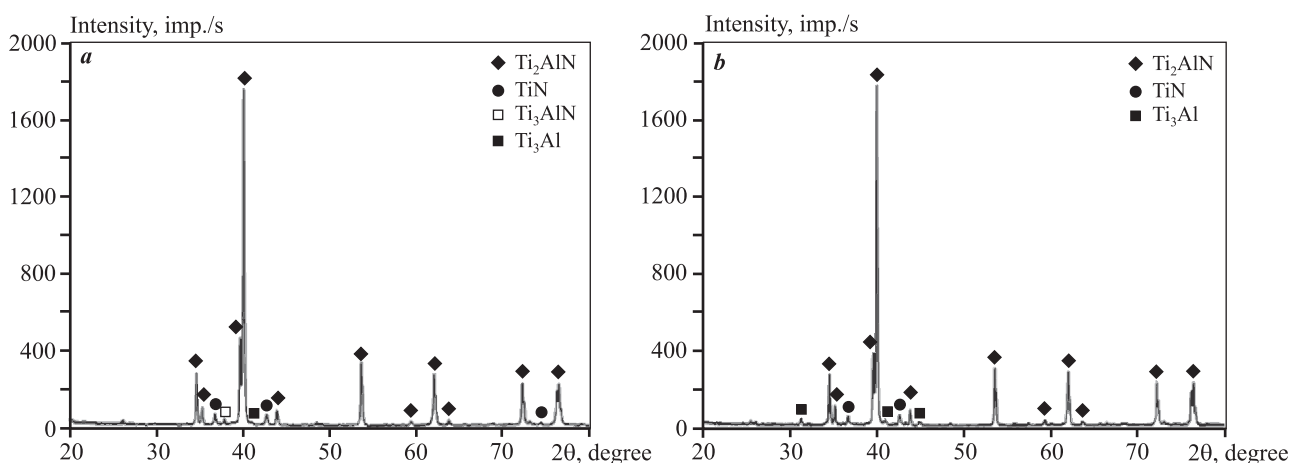


Fig. 3. Product diffractogram after composition 2 ($TiAl + TiN$) pressed sample (a) and the quartz tube sample (b) reactive sintering at 1400 °C in a vacuum

Рис. 3. Дифрактограмма продукта после реакционного спекания прессованного образца (a) и образца в кварцевой трубке (b) состава 2 ($TiAl + TiN$) при $t = 1400$ °C в вакууме

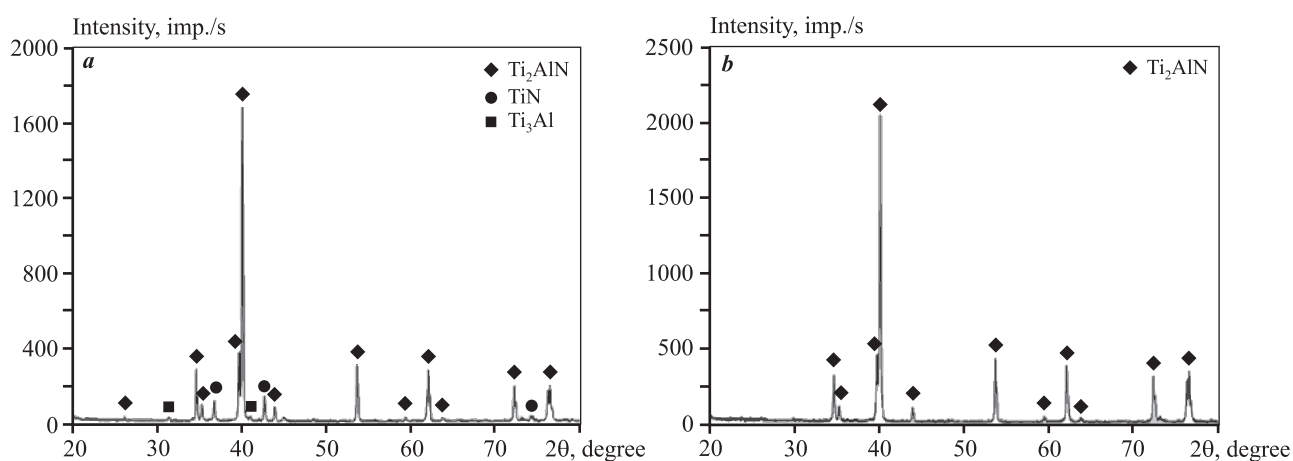


Fig. 4. Product diffractogram after composition 3 (Ti + Al + TiN) pressed sample (a) and a quartz tube sample (b) reactive sintering at 1400 °C in vacuum

Рис. 4. Дифрактограмма продукта после реакционного спекания прессованного образца (a) и образца в кварцевой трубке (b) состава 3 (Ti + Al + TiN) при $t = 1400$ °C в вакууме

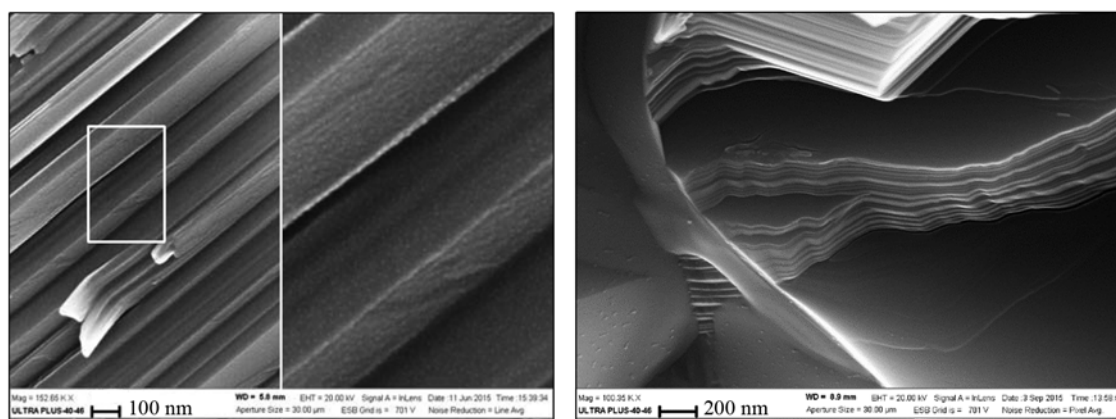


Fig. 5. Composition 3 sample photomicrograms at different scales

Рис. 5. Микрофотографии образца состава 3 с различным масштабом

tion 2 (TiAl : TiN = 1 : 1) sample sintering at 1400 °C a multiphase product (Fig. 3, b) with the following phase content (wt.%) was obtained: Ti₂AlN — 94, TiN — 4, Ti₃Al — 2. After the composition 3 (Ti : Al : TiN = 1 : 1 : 1) sample sintering the monophase product Ti₂AlN — 100 % was obtained as evidenced by the diffractogram in Fig. 4, b. The photomicrograms presented in Fig. 5 show that the composition 3 sample consists of so-called nanolaminates with the layers thickness of a few tens of nm.

Since the Ti₂AlN monophase product was obtained from mixture 3, it was interesting to make a point of the scale factor influence on this composition. The composition 3 initial charge 500 g in weight was poured into

a molybdenum container 88 × 88 × 70 mm in size in an even layer 35 mm in height. The container was covered with a lid and placed in a vacuum furnace. A view of the after-sintering mixture is shown in Fig. 6. The after-sintering composition was homogeneous over the entire cross section. The resulting product diffractogram was completely identical to the diffractogram in Fig. 4, b — 100 % Ti₂AlN MAX-phase without any other phases.

Fig. 7, a shows an after-sintering composition 3 fracture microphotograph, which shows the MAX-phases typical layered structure. Local elemental analysis data from approximately of the 5 mm² after-sintering product fracture area (marked by lines



Fig. 6. 500 g in weight after-sintering composition 3 photograph

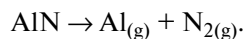
Рис. 6. Фотография полученного спека состава 3 массой 500 г

in Fig. 7, *b*) showed the following element content (at.%): N — 23.56, Al — 25.68, Ti — 50.76, which corresponds well with the Ti_2AlN MAX-phase elemental composition.

Results discussion

Basing on Ti—N and Al—N experimental data and phase diagrams the following sequence of composition 1 phase formation while heating in a dynamic vacuum can be suggested:

1. Extrapolating the aluminum nitride dissociation data [25] to the low pressure area, we obtain that at a pressure of $7.73 \cdot 10^{-4}$ Pa the dissociation temperature will be 913 °C. Therefore, it comes logical to assume that at the process initial stage dissociation occurs on the aluminum nitride particles surface:



2. The AlN dissociation products stream diffuses in the sample pore space to the titanium particles surface. Since both aluminum and nitrogen have considerable titanium dissolution and are α -stabilizers, solid solution $Ti(Al_x, N_y)$ is formed. At 1100–1200 °C it will be α - $Ti(Al_x, N_y)$ solution, and when the temperature rises to 1300–1500 °C — a β - $Ti(Al_x, N_y)$ solution.

3. From the α - $Ti(Al_x, N_y)$ solid solution, so far as it saturates with aluminum and nitrogen, and at < 1200 °C the TiN_x , Ti_3Al phases, the Ti_3AlN triple nitride and the Ti_2AlN MAX-phase crystallize.

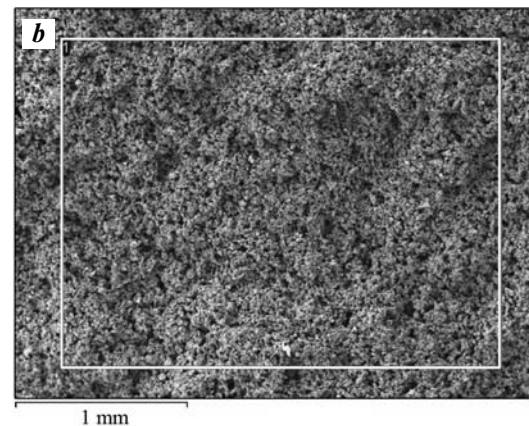
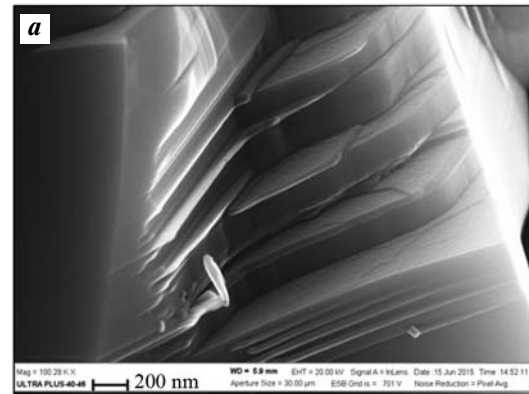


Fig. 7. After-sintering composition 3 sample fracture local microanalysis and microphotographs at different scales Spectrum, at.%: N — 23.56; Al — 25.68; Ti — 50.76

Рис. 7. Микрофотографии излома образца полученного спека состава 3 с различным масштабом

Спектр выделенной области, ат.%.: N — 23,56; Al — 25,68; Ti — 50,76

4. From the β - $Ti(Al_x, N_y)$ solid solution at > 1300 °C the TiN_x phases and the Ti_2AlN MAX-phase crystallize.

5. At 1400 °C the Ti_2AlN formation process completes and the MAX-phase sample content reaches its maximum value.

6. At further temperature increase up to 1500 °C and under dynamic vacuum conditions a MAX-phase partial decomposition occurs assisted by the titanium nitride phase and aluminum vapor formation which leave the sample pore space into the furnace volume.

Ti_2AlN MAX-phase content in the compositions 1 and 2 pressed samples sintering products practically do not differ (94 and 93 wt.% respectively), and in the composition 3 is noticeably lower (89 wt.%). It

can be assumed that this difference was noted due to the fact that in the mixtures 1 and 2 initial compositions aluminum is in a bound state in the form of compounds (AlN and TiAl respectively), and in mixture 3 — in the free state. Given the aluminum low melting temperature (660 °C), it goes under that logic that for mixture 3 aluminum vapor appears earlier than for mixtures 1 and 2 as the temperature rises in the furnace and they leave the samples pore space under open-side vacuuming through the side surface during a longer period of time. The lower Ti₂AlN MAX-phase content in the composition 3 pressed samples sintering products is explained by the formed aluminum deficit.

Closing the composition 2 samples side surface with the quartz tube walls had a relatively weak effect in terms of obtaining the Ti₂AlN MAX-phase, because its content in both samples (93 % in the pressed one and 94 % in a quartz tube) is almost the same. The products total phase composition changed insignificantly either. Apparently, when the reaction takes place at a holding temperature close to the TiAl melting temperature (~1450 °C), the aluminum mass transfer in mixture 2 takes place predominantly through the liquid phase. In the absence of aluminum vapor, closing the sample side surface does not lead to a significant change in the phase composition compared to the open side surface sample.

Closing the composition 3 sample side surface had a significant effect on the Ti₂AlN formation. Free aluminum present in the initial mixture, evaporating when heated, does not leave the reaction zone due to the closed side surface and reacts completely with the Ti₂AlN formation.

Conclusion

Summing up what has been stated, as a result of the sintering process research in a vacuum furnace the Ti₂AlN MAX-phase content dependence has been determined in the final product on the holding temperature and the composition of the initial charge. According to X-ray diffraction and energy-dispersive analyses a single-phase product with 100 % Ti₂AlN MAX-phase content was obtained for the composition Ti : Al : TiN = 1 : 1 : 1 at 1400 °C. It was shown that closing the Ti : Al : TiN mixture side surface blocked the aluminum vapor escape from the sample pore space resulting in the formation of Ti₂AlN only. The example of a 500 g filling sintering and obtaining a Ti₂AlN single-phase product the

fundamental possibility of sintering process scaling in a dynamic vacuum and the prospects of this method of production for industrial development have been demonstrated.

References

1. Barsoum M., Brodtkin D., El-Raghy T. Layered machinable ceramics for high temperature applications. *Scripta Mater.* 1997. Vol. 36. No. 5. P. 535—541. DOI: 10.1016/S1359-6462(96)00418-6.
2. Barsoum M. MAX phases: Properties of machinable ternary carbides and nitrides. Wiley-VCH Verlag GmbH & Co, KGaA, 2013. DOI: 10.1002/9783527654581.
3. Barsoum M.W., Radovic M. Elastic and mechanical properties of the MAX phases. *Annu. Rev. Mater. Res.* 2011. Vol. 41. P. 195—227. DOI: 10.1146/annurev-matsci-062910-100448.
4. Sokol M., Natu V., Kota S., Barsoum M. On the chemical diversity of the MAX phases. *Trends Chem.* 2019. Vol. 1. P. 210—223. DOI: 10.1016/j.trechm.2019.02.016.
5. Barsoum M., Ali M., El-Raghy T. Processing and characterization of Ti₂AlC, Ti₂AlN, and Ti₂AlC_{0.5}N_{0.5}. *Metall. Mater. Trans. A.* 2000. Vol. 31. No. 7. P. 1857—1865. DOI: 10.1007/s11661-006-0243-3.
6. Zhou Y., Sun Z. Electronic structure and bonding properties of layered machinable Ti₂AlC and Ti₂AlN ceramics. *Phys. Rev. B.* 2000. Vol. 61. No. 12. P. 12570. DOI: 10.1103/PhysRevB.61.12570.
7. Wang Z., Liu J., Wang L., Li X., Ke P., Wang A. Dense and high-stability Ti₂AlN MAX phase coatings prepared by the combined cathodic arc/sputter technique. *Appl. Surf. Sci.* 2017. Vol. 396. P. 1435—1442. DOI: 10.1016/j.apsusc.2016.11.183.
8. Jeitschko W., Nowotny H., Benesovsky F. Ti₂AlN, eine stickstoffhaltige H-Phase. *Monatsh. Chem.* 1963. Vol. 94. No. 6. P. 1198—2000.
9. Luginina M.A., Kovalev D.Yu., Sytshev A.E. Preparation of Ti₂AlN by reactive sintering. *Int. J. SHS.* 2016. Vol. 25. No. 1. P. 35—38. DOI: 10.3103/S1061386216010088/
10. Kovalev D.Yu., Luginina M.A., Sytshev A.E. Reaction synthesis of the Ti₂AlN MAX-phase. *Russ. J. Non-Ferr. Met.* 2017. Vol. 58. No. 3. P. 303—307. DOI: 10.3103/S1067821217030087.
11. Lin Z., Zhuo M., Li M., Wang J., Zhou Y. Synthesis and microstructure of layered-ternary Ti₂AlN ceramic. *Scr. Mater.* 2007. Vol. 56. No. 12. P. 1115—1118. DOI: 10.1016/j.scriptamat.2007.01.049.
12. Liu Y., Shi Z., Wang J., Qiao G., Jin Z., Shen Z. Reactive consolidation of layered-ternary Ti₂AlN ceramics by spark plasma sintering of a Ti/AlN powder mixture.

- J. Eur. Ceram. Soc.* 2011. Vol. 31. No. 5. P. 863–868. DOI: 10.3103/S1061386216010088.
13. Yan M., Mei B., Zhu J., Tian C., Wang P. Synthesis of high-purity bulk Ti_2AlN by spark plasma sintering (SPS). *Ceram. Int.* 2008. Vol. 34. No. 6. P. 1439–1442. DOI: 10.1016/j.ceramint.2007.04.009.
 14. Liu W., Qiu C., Zhou J., Ding Z., Zhou X., Du S., Han Y.-H., Huang Q. Fabrication of Ti_2AlN ceramics with orientation growth behavior by the microwave sintering method. *J. Eur. Ceram. Soc.* 2015. Vol. 35. P.1385–1391. DOI: 10.1016/j.jeurceramsoc.2014.11.020.
 15. Liu Y., Li Y., Li F., Cui H., Zhang L., Guo S. Synthesis and microstructure of Ti_2AlN ceramic by thermal explosion. *Ceram. Int.* 2017. Vol. 43. No. 16. P. 13618–13621.
 16. Chen W., Tang J., Lin X., Ai Y., Ye N. Formation mechanism of high-purity Ti_2AlN powders under microwave sintering. *Materials*. 2020. Vol. 13. No. 23. P. 5356. DOI: 10.3390/ma13235356.
 17. Christopher S., Ernesto Ch., Cristina G.-G., Rosalia P., José A.J. Mangalaraja R.V. Study of the influence of sintering atmosphere and mechanical activation on the synthesis of bulk Ti_2AlN MAX phase obtained by spark plasma sintering. *Materials*. 2021. Vol. 14. No. 16. P. 4574. DOI: 10.3390/ma14164574.
 18. Akhtar S., Roy Sh., Thu Tran T., Singh J., Anir S. Sharbirin, Kim J. Low temperature step annealing synthesis of the Ti_2AlN MAX phase to fabricate MXene quantum dots. *Appl. Sci.* 2022. Vol. 12. No. 9. P. 4154. DOI: 10.3390/app12094154.
 19. Li X., Gonzalez-Julian J., Malzbender J. Fabrication and mechanical performance of Ti_2AlN prepared by FAST/SPS. *J. Eur. Ceram. Soc.* 2020. Vol. 40. P. 4445–4453. DOI: 10.1016/j.jeurceramsoc.2020.05.017.
 20. Kondakov A.A., Studenikin I.A., Linde A.V., Kondakova N.A., Grachev V.V. Synthesis of Ti_2AlN MAX-phase by sintering in vacuum. *IOP Conf. Ser.: Mater. Sci. Eng.* 2019. Vol. 558. P.012017. DOI:10.1088/1757-899X/558/1/012017.
 21. Загоржевский В.В., Боровинская И.П., Сачкова Н.В. Синтез нитрида алюминия в режиме горения смеси $Al + AlN$. *Неорган. материалы*. 2002. Т. 38. No. 11. С. 1340–1350.
Zakorzhevskii V.V., Borovinskaya I.P., Sachkova N.V. Combustion synthesis of aluminum nitride. *Inorg. Mater.* 2002. Vol. 38. No. 11. P. 1131–1140. DOI: 10.1023/A:1020966500032.
 22. Zakorzhevskii V.V., Kovalev I.D., Barinov Y.N. Self-propagating high-temperature synthesis of titanium nitride with the participation of ammonium chloride. *Inorg. Mater.* 2017. Vol. 53. P. 278–286. DOI: 10.1134/S002016851703013X.
 23. Low I.M., Pang W.K., Kennedy S.J., Smith R.I. High-temperature thermal stability of Ti_2AlN and Ti_4AlN_3 : A comparative diffraction study. *J. Eur. Ceram. Soc.* 2011. Vol. 31. P. 159–166.
 24. Yang J., Liao C., Wang J., Jiang Y., He Y. Reactive synthesis for porous Ti_3AlC_2 ceramics through TiH_2 , Al and graphite powders. *Ceram. Int.* 2014. Vol. 40. P. 6739–6745. DOI: 10.1016/j.ceramint.2013.11.136.
 25. Zhou Z., Chen X., Yuan Y., Shi L., Jiang W., Yang B., Xu B., Liu D. A comparison of the thermal decomposition mechanism of wurtzite AlN and zinc blende AlN . *J. Mater. Sci.* 2018. Vol. 53. P. 11216–11227. DOI: 10.1007/s10853-018-2400-7.

UDC 621.762.2 + 666.3 + 544.452

DOI dx.doi.org/10.17073/1997-308X-2022-4-34-57

SHS of highly dispersed powder compositions of nitrides with silicon carbide. Review

© 2022 г. **A.P. Amosov, Yu.V. Titova, G.S. Belova, D.A. Maidan, A.F. Minekhanova**

Samara State Technical University (SamSTU), Samara, Russia

Received 19.04.2022, accepted for publication 22.04.2022

Abstract: The application of the process of self-propagating high-temperature synthesis (SHS) to prepare highly dispersed powder nitride-carbide compositions from the most common refractory nitride (Si_3N_4 , AlN, TiN) and carbide (SiC) compounds with a particle size of less than 1 μm is considered. The advantages of composite ceramics over single-phase ceramic materials and such trends of its development as the transition to nanostructured ceramics and the application of in situ processes of direct chemical synthesis of nanoparticles of components in the composite body are described. The attractiveness of the SHS process as one of the promising in situ processes characterized by simplicity and cost-effectiveness, the possibility of obtaining highly dispersed ceramic powders by burning mixtures of inexpensive reagents is shown. Considerable attention is paid to the consideration of the results of the application of azide SHS, based on the use of sodium azide and gasified halide salts as part of mixtures of initial powders of nitrated and carbidized elements during their combustion in nitrogen gas. The review of publications devoted to the application of SHS to obtain highly dispersed composite powders Si_3N_4 —SiC, AlN—SiC and TiN—SiC, promising for use in sintering of the corresponding composite ceramic materials of submicron and nano-sized structure with improved properties, lower brittleness, good machinability, lower sintering temperatures compared with single-phase ceramic materials made of nitrides or carbides as well as for other applications, is presented. The results of the application of azide SHS are presented in detail both in the form of the results of thermodynamic calculations and the results of experimental research of combustion parameters, combustion product structure and composition. The advantages and disadvantages of using the combustion process for the synthesis of nitride compositions with silicon carbide, the causes of the disadvantages and the directions of further research to eliminate them are discussed.

Keywords: composite ceramics, nitrides, silicon carbide, powder compositions, self-propagating high-temperature synthesis (SHS), combustion products, composition, structure.

Amosov A.P. — Dr. Sci. (Phys.-Math.), prof., head of the Department of physical metallurgy, powder metallurgy, nanomaterials (MPMN), Samara State Technical University (SamSTU) (443100, Russia, Samara, Molodogvardeiskaya str., 244).

E-mail: egundor@yandex.ru.

Titova Yu.V. — Cand. Sci. (Eng.), associate prof., Department of MPMN, SamSTU. E-mail: titova600@mail.ru.

Belova G.S. — postgraduate student, Department of MPMN, SamSTU. E-mail: galya.belova.94@mail.ru.

Maidan D.A. — Cand. Sci. (Eng.), associate prof., Department of MPMN, SamSTU. E-mail: mtm.samgtu@mail.ru.

Minekhanova A.F. — postgraduate student, Department of MPMN, SamSTU. E-mail: minekhanovaaf@mail.ru.

For citation: Amosov A.P., Titova Yu.V., Belova G.S., Maidan D.A., Minekhanova A.F. SHS of highly dispersed powder compositions of nitrides with silicon carbide. Review. *Izvestiya Vuzov. Poroshkovaya Metallurgiya i Funktsional'nye Pokrytiya (Powder Metallurgy and Functional Coatings)*. 2022. Vol. 16. No. 4. P. 34—57 (In Russ.).

DOI: dx.doi.org/10.17073/1997-308X-2022-4-34-57.

СВС высокодисперсных порошковых композиций нитридов с карбидом кремния Обзор

А.П. Амосов, Ю.В. Титова, Г.С. Белова, Д.А. Майдан, А.Ф. Минеханова

Самарский государственный технический университет (СамГТУ), г. Самара, Россия

Статья поступила в редакцию 19.04.22 г., подписана в печать 22.04.22 г.

Аннотация: Рассмотрено применение процесса самораспространяющегося высокотемпературного синтеза (СВС) для получения высокодисперсных порошковых нитридно-карбидных композиций из наиболее распространенных тугоплавких

нитридных (Si_3N_4 , AlN, TiN) и карбидного (SiC) соединений с размером частиц менее 1 мкм. Изложены преимущества композиционной керамики перед однофазными керамическими материалами и такие тенденции ее развития, как переход к наноструктурной керамике и использование *in situ* процессов прямого химического синтеза наночастиц компонентов в объеме композита. Показана привлекательность процесса СВС как одного из перспективных *in situ* процессов, характеризующегося простотой и экономичностью, возможностью получения высокодисперсных керамических порошков при сжигании смесей недорогих реагентов. Значительное внимание уделено рассмотрению результатов применения азидного СВС, основанного на использовании азидов натрия и газифицирующихся галоидных солей в составе смесей исходных порошков азотируемых и карбидизируемых элементов при их сжигании в газообразном азоте. Представлен обзор публикаций, посвященных применению СВС для получения высокодисперсных композиционных порошков Si_3N_4 —SiC, AlN—SiC и TiN—SiC, перспективных для использования при спекании соответствующих композиционных керамических материалов субмикронной и наноразмерной структуры с повышенными свойствами, меньшей хрупкостью, хорошей обрабатываемостью, меньшими температурами спекания по сравнению с однофазными керамическими материалами из нитридов или карбидов, а также для использования в других приложениях. Подробно представлены результаты применения азидного СВС как в виде показателей термодинамических расчетов, так и данных экспериментального исследования параметров горения, структуры и состава продуктов горения. Обсуждены достоинства и недостатки использования процесса горения для синтеза композиций нитридов с карбидом кремния, причины возникновения сдерживающих факторов и направления проведения дальнейших исследований по их устранению.

Ключевые слова: композиционная керамика, нитриды, карбид кремния, композиции порошков, самораспространяющийся высокотемпературный синтез (СВС), продукты горения, состав, структура.

Амосов А.П. — докт. физ.-мат. наук, проф., зав. кафедрой «Металловедение, порошковая металлургия, наноматериалы» (МПМН), СамГТУ (443100, г. Самара, ул. Молодогвардейская, 244).
E-mail: egundor@yandex.ru.

Титова Ю.В. — канд. техн. наук, доцент кафедры МПМН, СамГТУ. E-mail: titova600@mail.ru.

Белова Г.С. — аспирант кафедры МПМН, СамГТУ. E-mail: galya.belova.94@mail.ru.

Майдан Д.А. — канд. техн. наук, доцент кафедры МПМН, СамГТУ.
E-mail: mtm.samgtu@mail.ru.

Минеханова А.Ф. — аспирант кафедры МПМН, СамГТУ. E-mail: minekhanovaaf@mail.ru.

Для цитирования: Амосов А.П., Титова Ю.В., Белова Г.С., Майдан Д.А., Минеханова А.Ф. СВС высокодисперсных порошковых композиций нитридов с карбидом кремния. Обзор. *Известия вузов. Порошковая металлургия и функциональные покрытия*. 2022. Т. 16. № 4. С. 34—57. DOI: dx.doi.org/10.17073/1997-308X-2022-4-34-57.

Introduction

Refractory nitride (Si_3N_4 , AlN, TiN) and carbide (SiC) compounds are widely used to produce the corresponding non-oxide ceramic materials, both structural, due to their high melting point, hardness, wear resistance, heat resistance, chemical stability, and functional, due to their electrical and catalytic properties [1—5]. Such ceramic materials are conventionally produced of the corresponding ceramic powders by reactive sintering or hot pressing. Lately, they have been added by spark plasma sintering (SPS) and microwave sintering methods. However, single-phase ceramic materials made of individual refractory compounds may exhibit poor sinterability and machinability, high brittleness, high coefficient of friction (COF), etc. Several approaches are used to address these problems.

Firstly, multiphase (multi-component) composite ceramics are used. For example, conductive titanium nitride is added to non-conductive silicon nitride,

making it possible to use a significantly less expensive electrical discharge machining process when making ceramic products compared to machining with expensive diamond tools [6]. Titanium nitride TiN not only exhibits high electrical conductivity but also high melting point, hardness, wear resistance and corrosion resistance, it is compatible with Si_3N_4 , improves sintering and the properties of Si_3N_4 ceramics [7].

Secondly, the transition to nanostructured ceramics is used, since it has been extensively shown that powder size reduction, the transition to nanopowders and the production of nanostructured ceramics can significantly improve the properties of ceramics [5, 8—10]. Taking Si_3N_4 —TiN composite ceramics as an example, the ceramics of Si_3N_4 —30vol.%TiN composition obtained by spark plasma sintering of Si_3N_4 and TiN nanoparticles show the wear resistance being 3 times higher than the wear resistance of composite cera-

mics of the same composition obtained by hot pressing of commercially produced micron-sized powders [11]. Such composite ceramics with solid TiN nanoparticles cause significantly less frictional damage to the counterbody than ceramics containing micron-sized TiN particles, which is particularly important, for instance, for hybrid bearings having the balls made of ceramics and the rings made of metal [12].

Thirdly, *in situ* processes of obtaining composite ceramics by performing chemical synthesis of component nanoparticles in the composite body are applied. By far the simplest and most common approach to the production of composite nanoceramics involves mixing ready-made nanopowders, compacting and sintering them (*ex situ* processes). However, two problems are encountered at this point: the first one is the high cost of nanopowders (for example, the price of nitride and carbide nanopowders obtained by plasma-chemical synthesis, which are available on the market, is on average of 3 thous. euro per 1 kg [13]); the second one is that it is practically impossible to mix nanopowders homogeneously due to high tendency of nanoparticles to form quite solid agglomerates, which are extremely difficult to destroy when mixed [5, 9]. The presence of agglomerates impedes the homogeneous distribution of components and the compaction of the powder mixture, it requires higher temperatures for sintering, and results in the porosity of the sintered composite, it is the point of defects from which cracks can develop. In this context, in the case of highly dispersed powders, *in situ* chemical methods of direct synthesis of ceramic powders inside the desired composite body from a mixture of much cheaper initial reagents are preferable to *ex situ* mechanical methods of mixing the desired compositions of premixed ceramic powders [4, 8].

One of the advanced *in situ* processes is the process of self-propagating high-temperature synthesis (SHS) of the most diverse refractory compounds, including nitrides and carbides, which proceeds due to heat release during combustion in a simple, small-sized equipment and takes a little time [14–17]. Other known methods for obtaining Si, Al, Ti nitrides and Si carbide (the furnace method, plasma-chemical synthesis, carbothermal synthesis, gas-phase deposition, etc.) are characterized by high power consumption, complex equipment, and they do not always ensure the nanosize of Si_3N_4 , AlN, TiN, SiC powders, and even more so of nanopowder compositions. SHS process is attractive not only for its simplicity and cost-effectiveness, but it also provides considerable opportunities for controlling the disper-

sion and the structure of synthesized ceramic powders, as well as bringing them to the nanosized level [18, 19]. Various techniques are used for this purpose: the reduction of combustion temperature; the use of gasified halide salt additives, condensed and gaseous by-products of SHS reactions separating synthesized particles and preventing their growth; the application of chemical compounds of elements (precursors) rather than the powders of pure elements, e.g. the ones of metals, as initial reagents, etc.

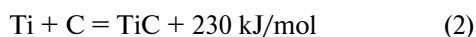
In particular, during the synthesis of nitrides, such opportunities are realized in the azide SHS process, designated as SHS-Az, where not nitrogen gas but sodium azide powder (NaN_3) is used as a nitrating reagent, which decomposes in a combustion wave, releasing active nitrogen [20, 21]. Pure elemental powders of silicon, titanium, aluminum, etc. are used as reagents to be nitrated. A certain halide salt is added to these basic reagents as an auxiliary additive, during the decomposition of which a large amount of vaporous and gaseous reaction products are formed during combustion. These products dilute the reaction body and thus preventing it from sintering, and as a result, the end product is synthesized in the form of a powder, which does not require additional reduction in size after the synthesis. Low combustion temperatures, the formation of condensed by-products and gases separating the desired nitride particles are the distinctive features of azide SHS, leading to the synthesis of nitride micropowders. Upon replacing the pure powders of the nitrated elements (Si, Ti, Al) with their halide salts, being the precursors that decompose in a combustion wave with entering of a nitrated element into reaction in the form of single atoms rather than the micron-sized particles of the condensed substance, the size of nitrides synthesized by azide SHS can be significantly reduced and brought to the nanosized level. Besides, in the case of the synthesis of nitride compositions, the gaseous and vaporous condition of reaction products allows for their prompt and homogeneous mixing, which is unobtainable by mechanical mixing of premix nanopowders. By this means, it is possible to solve the problem of the high cost of nitride nanopowders, obtain significantly (almost by one order of magnitude) cheaper nanopowders (since the most expensive component in the azide SHS is sodium azide, with a cost of up to 300 euros/kg) with minimum power consumption and simple, small-sized equipment if compared to plasma-chemical synthesis. Moreover, the nitride synthesis performed directly in composite powder body (*in situ*) rather than the one

performed in advance with subsequent mechanical mixing (*ex situ*), allows to achieve a high homogeneity of the nitride mixture, i.e. to solve the second problem, namely obtaining a homogeneous mixture of nitride nanopowders. The practical experience of using azide SHS for the production of TiN—BN, AlN—BN, Si₃N₄—TiN nitride composite powders with the use of precursors, the halide salts of both nitrated composite elements, has been accumulated [22, 23]. However, obtaining these results was not that easy though. It has been found that the replacement of elemental powders of nitrated elements with their precursors (halide salts) impedes the production of the desired nitrides, most often it results in the formation of undesired hard-to-remove by-products and incomplete reaction, for example, as in the case of compositions containing the by-product cryolite Na₃AlF₆ and free silicon impurity: AlN—BN—Na₃AlF₆, AlN—TiN—Na₃AlF₆, Si₃N₄—AlN—Na₃AlF₆—Si [23].

The positive results of studies on the application of SHS process for obtaining silicon carbide (SiC) nanopowders are known as well [24–26]. In the case of SiC synthesis from the elements, the reaction can be written as follows:



This reaction has a relatively small thermal effect of product formation compared, for example, with the reaction of titanium carbide formation from elements widely used in SHS:



and therefore has a relatively low adiabatic combustion temperature of 1860 K compared with 3290 K for the reaction of TiC formation. In this context, it is practically impossible to perform reaction (1) in combustion mode, i.e. to implement a self-sustaining SHS process in this system.

Several approaches have been developed to increase the reactivity of Si—C system: preheating of the reaction medium, electric field imposition, mechanical activation of the initial mixture of reagents, chemical activation of the reaction (1), for instance, using fluoroplastic powders, conducting the reaction (1) in a nitrogen gas or air medium. Almost all of these approaches can result in obtaining submicron SiC powders and some of them can result in obtaining nanosized SiC powders under the combustion mode. [24]. But it should be taken into account that when combusting Si + C mixture in nitrogen atmosphere, the combustion products can contain up to 3–7 wt.%

of silicon nitride impurities (Si₃N₄) along with silicon carbide.

This article presents the results of a review of publications devoted to the application of self-propagating high-temperature synthesis (SHS) to obtain highly dispersed (submicron and nanosized) powder nitride-carbide compositions from the most common refractory nitride (Si₃N₄, AlN, TiN) and carbide (SiC) compounds with a particle size of less than 1 μm. Considerable attention is paid to azide SHS method developed by the authors of the review. Synthesized highly dispersed composite powders Si₃N₄—SiC, AlN—SiC and TiN—SiC are promising for use in sintering of the corresponding composite ceramic materials of submicron and nanosized structure with improved properties, lower brittleness, good machinability, lower sintering temperatures compared to single-phase ceramic materials made of nitrides or carbides, as well as for other applications.

Si₃N₄—SiC composition

As it has already been mentioned, silicon nitride Si₃N₄ and silicon carbide SiC are known as high-temperature structural ceramics [1–3, 5]. Along with this, dielectric Si₃N₄ is applied as an insulator in microelectronics, as well as a storage medium in flash memory devices, and semiconductor SiC is used in high-power and high-temperature transistor devices and LEDs, as well as in electric heaters. Besides, silicon carbide is used as a catalyst in the oxidation of hydrocarbons, and silicon nitride is used as a catalyst carrier.

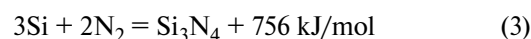
However, these ceramic materials differ markedly in certain characteristics (their specific values are highly dependent on the methods of ceramics production, therefore we will assume average values determined primarily at room temperature). For example, Si₃N₄ ceramics is not as brittle as SiC, and it exhibits high fracture toughness (5.3 MPa·m^{1/2} on average) and good flexural strength (at a level of 750 MPa), but it is characterized by low oxidation resistance at high temperatures (1.2 mg/cm³ weight increase at $T = 1573 \text{ K}$ per 100 h) [1, 27]. SiC ceramics, to the contrary, have high wear, creep and oxidation resistance at high temperatures (0.02 mg/cm³ weight increase under the same conditions), but it shows low values of flexural strength (450 MPa) and fracture toughness (2.8 MPa·m^{1/2}). Silicon carbide is the most important component of ultra-high-temperature ceramic materials (5–65 vol.%) for the achievement of their maximum oxidation resistance [28, 29].

The results of many of studies show that the combination of nitride and silicon carbide in composite material Si_3N_4 —SiC allows to use the advantages of each of these single-phase ceramics and obtain composite ceramics with significantly improved properties, primarily for high-temperature applications [5, 27, 30–32]. The introduction of minimum of 5 vol.% of SiC into Si_3N_4 matrix provides an opportunity of obtaining a composite with high fracture toughness ($6.5 \text{ MPa} \cdot \text{m}^{1/2}$) by spark plasma sintering [32]. Si_3N_4 —20vol.%SiC composite produced by hot isostatic pressing has fracture toughness of $9.5 \text{ MPa} \cdot \text{m}^{1/2}$ at $T = 1673 \text{ K}$ (compared with $5.3 \text{ MPa} \cdot \text{m}^{1/2}$ of Si_3N_4 single-phase ceramics), and it is considered as a promising material for gas turbine engines [31]. This conclusion is confirmed by the results of later studies, according to which hot-pressed nanocomposites Si_3N_4 —(20±30 vol.%)SiC have flexural strength up to 1500 MPa (compared with 850 MPa of common Si_3N_4 ceramics) and retain high strength up to $T = 1673 \text{ K}$ (compared with 1473 K of Si_3N_4 ceramics) [5]. The increase of SiC content up to 40 wt.% in hot-pressed composite Si_3N_4 —SiC results in binding strength improvement up to the level of 10.5 – $12.5 \text{ MPa} \cdot \text{m}^{1/2}$ [30]. Composite ceramics Si_3N_4 —SiC are highly perspective for their development and application due to the improvement of their composition, structure and properties, as well as the development of new methods of production and the reduction of manufacturing costs [9, 10].

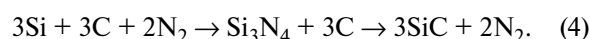
It has been noted before, that in the production of ceramic composites from highly dispersed powders, *in situ* chemical methods of direct synthesis of ceramic powder compositions from a mixture of initial reagents are more preferable than *ex situ* mechanical methods of mixing premixed powder components [5, 16]. Submicron and nanosized powder compositions Si_3N_4 —SiC can be synthesized by various chemical methods, including the coating of Si_3N_4 particles with highly dispersed carbon through methane pyrolysis [33], the pyrolysis of an organic silicon-containing precursor [34], carbothermal reduction of silicon dioxide under nitrogen gas [35], gas-phase reactions [36], plasma-chemical synthesis [37]. The listed chemical methods are characterized by high power consumption due to the high temperature heating required and the long exposures used, they also require the use of expensive equipment. In this regard, a simple energy-saving SHS method which is based on combustion of inexpensive initial components is promising.

The first studies on the use of combustion for the synthesis of powder compositions Si_3N_4 —SiC were

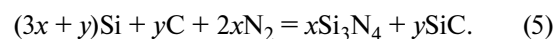
based on the combustion of mixtures of silicon and carbon black (soot) powders in nitrogen gas at a pressure ranging from 1 to 10 MPa [38–41]. The reaction (1) of synthesis of silicon carbide from elemental powders has a relatively low thermal effect and adiabatic temperature, which does not ensure a self-propagating combustion mode. However, the reaction of synthesis of silicon nitride from silicon powder in nitrogen gas



is highly exothermic with an adiabatic temperature of 2430 K, and it can proceed in self-propagating combustion mode. Therefore, the combustion of silicon and carbon powders mixture in nitrogen is initiated. Firstly, the silicon nitride is synthesized with a rise in temperature to high values exceeding 2273 K, at which the synthesized Si_3N_4 dissociates and then the resulting silicon reacts with carbon forming SiC, more stable at high temperatures. Thus, when reaction (1) is performed in nitrogen gas, silicon carbide can be obtained in the combustion mode as follows [38]:



In this system of reagents, the intermediate product is synthesized first in the combustion mode Si_3N_4 (the 1st reaction) with a rise in temperature to high values, upon which the subsequent transformation of silicon nitride into silicon carbide becomes thermodynamically favorable due to interaction with carbon (the 2nd reaction). If in the initial system of reagents silicon powder is taken in excess (4), i.e. in a larger amount than it is required for the complete conversion of Si_3N_4 into SiC, it is possible to perform the reaction in the combustion mode at a nitrogen pressure of 3 MPa, with the formation of a composition of nitride and silicon carbide powders [40]:



In this reaction, x and y coefficient values were used to obtain from 36.8 to 100 vol.% SiC in the composition, the combustion temperature values were from 1440 to 1880 °C. The results of the experiments were explained by the presence of an intermediate stage between the 1st and 2nd reactions, at which molten silicon appears (the melting temperature of 1414 °C) reacting simultaneously in nitridation и carbidization and ensuring the formation of SiC particles, being finer than the ones appearing upon further transformation of Si_3N_4 into SiC. A more detailed study of Si—nC—N₂ system using silicon powders of Kr1 grade (particle size $d < 15 \mu\text{m}$)

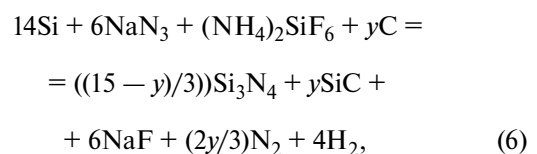
and carbon black of P803 grade ($d < 1 \mu\text{m}$) showed that at nitrogen gas pressure of 1–7 MPa, combustion can be initiated with the carbon black content of $n = 0.8$ maximum [41]. Upon that, the combustion temperatures are 1500–2000 °C, and the combustion product constitutes the composition of powders Si_3N_4 –SiC with SiC content of 5–60 wt.%, and Si_3N_4 constituting the rest, with a dominant content of β -modification, and a small amount of unreacted Si. The main part of the combustion product is comprised of particles with a size of 2–3 μm , although there are also larger ones with a size of up to 15 μm in the form of columnar crystals or agglomerates of fine particles. The application of polytetrafluoroethylene (PTFE) powder activator $(\text{C}_2\text{F}_4)_n$ in the amount of 5–15 wt.% expands the limits of combustion of Si–C–N₂ system and ensures obtaining the composites with any ratio of Si_3N_4 and SiC components from 0 to 100 %. Let us emphasize that these are the components of Si_3N_4 and SiC powders with micron particle sizes and a small amount of α -modification in silicon nitride Si_3N_4 .

Upon the combustion of a mixture of ferrosilicon Fe–Si and carbon black powders in nitrogen atmosphere at a pressure of 4–6 MPa and subsequent acid enrichment of the combustion product in dilute hydrochloric acid, composite submicron and nanosized Si_3N_4 –SiC powders with the content of 20 % SiC can be obtained [42]. At first, iron contained in ferrosilicon plays the role of a diluent that reduces the combustion temperature and separates the synthesized particles, as well as a catalyst for nitridation reaction, and then it is removed from the composite powder by being dissolved in acid. But the required acid treatment significantly complicates the process of obtaining Si_3N_4 –SiC powder composition and does not ensure the complete removal of iron (Fe) from the composition.

It has long been known that the higher is Si_3N_4 content of α -modification compared to β -modification in Si_3N_4 -based ceramics, the higher are the strength properties. However, not all production methods allow achieving high content of α - Si_3N_4 [1]. It has been shown that during the combustion of silicon powder in nitrogen gas, it is possible to significantly increase the amount of synthesized phase α - Si_3N_4 by diluting the charge with final product α - Si_3N_4 and using additives of gasified halide salts NH_4Cl and NH_4F [43, 44]. In the combustion wave, the decomposition products of these salts react with silicon particles and ensure the transition of silicon to the gas phase that allows conducting the low-temperature mode for the formation of a fine fiber α -modification of Si_3N_4 , which is stable

at temperatures below 1450 °C. In particular, to obtain α - Si_3N_4 content exceeding 95 wt.% it is necessary to carry out burning with minimum values of temperature and burning rate close to the limit of burning. For this purpose, it is necessary to use a charge with 28–40 % silicon content, with a high dilution with the desired product α - Si_3N_4 up to 65 % and with 6–8 % mixture of gasifying halide salts NH_4Cl and NH_4F at the ratio 1 : 1. In this case, the combustion product contains from 0.1 to 1.5 % of free silicon. The dispersity of synthesized α - Si_3N_4 depends on the dispersity of initial silicon powder: with micron Si powder of less than 30 μm in size, more than 96 % of α - Si_3N_4 is synthesized with 80 % of particles of a fibrous structure with fiber lengths over 10 μm , and diameter of 1 μm ; with submicron Si powder of less than 1 μm in size, up to 96.6 % of fibrous α - Si_3N_4 is synthesized with fiber lengths over 10 μm , and diameter of 0.1–0.2 μm and a small amount of elongated particles being 1–2 μm thick and up to 5 μm long. The carbon additive influences the mechanism of structure formation and allows synthesizing silicon nitride with an equiaxed shape of particles. Composite powders based on α - Si_3N_4 , containing up to 10 % SiC, with an average particle diameter of 300–400 nm and an equiaxed shape were obtained with the complex addition of carbon up to 3.5 % in the form of carbon black and gasifying salts [44].

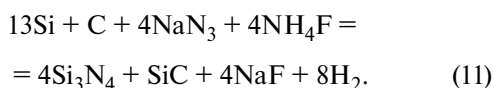
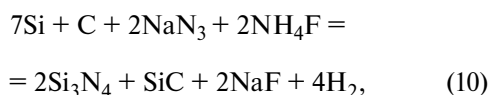
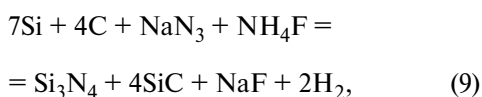
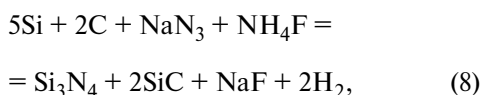
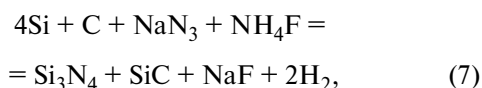
The marked increase of α - Si_3N_4 amount and particle size reduction in the powders of Si_3N_4 –SiC composition has been also ensured by azide SHS upon the combustion of the mixture of sodium azide (NaN_3) with silicon (Si) and carbon black (C) elemental powders and activating halide salt additive $(\text{NH}_4)_2\text{SiF}_6$ in nitrogen atmosphere [45]. The major reaction for obtaining Si_3N_4 –SiC was as follows:



where carbon black content made up 5 or 15 mol. The reagent combustion temperature of the system (6) reached 1850 °C for $y = 5$ and 1650 °C for $y = 15$. In case of $y = 5$ the cooled combustion product consisted of β - Si_3N_4 , α - Si_3N_4 , NaF and Si, and in case of $y = 15$ the combustion products included α - Si_3N_4 , SiC, NaF and Si. The X-ray diffraction (XRD) phase analysis showed that at $y = 5$ the content of β - Si_3N_4 superseded the content of α - Si_3N_4 , silicon carbide was not detected, and at $y = 15$, to the contrary, silicon

carbide SiC was present, while there was no β -Si₃N₄, i.e. silicon nitride consisted only of α -modification. A noticeable amount of unreacted silicon remains in the washed combustion product. (Unfortunately, the content of phases in the combustion product of the reagent system (6) was not quantified.) Silicon carbide was synthesized in the form of equiaxed particles with an average size of 100 nm, and silicon nitride was synthesized in the form of whiskers with a diameter of 100–200 nm.

The application of another halide salt, ammonium fluoride NH₄F, has been recently studied in order to obtain nitride-carbide powder composition Si₃N₄–SiC by azide SHS method over a wide range of phase ratios from 1 : 4 to 4 : 1 using the following chemical equations [46]:



In these equations, the composition of reaction products is expressed in moles; when passing to mass percent, the following ratios are obtained for the theoretical composition of the desired Si₃N₄–SiC composition, provided that water-soluble by-product salt NaF is removed from the reaction products:

$$(7): \text{Si}_3\text{N}_4 + \text{SiC} = 77.8\%\text{Si}_3\text{N}_4 + 22.2\%\text{SiC},$$

$$(8): \text{Si}_3\text{N}_4 + 2\text{SiC} = 63.6\%\text{Si}_3\text{N}_4 + 36.4\%\text{SiC},$$

$$(9): \text{Si}_3\text{N}_4 + 4\text{SiC} = 46.7\%\text{Si}_3\text{N}_4 + 53.3\%\text{SiC},$$

$$(10): 2\text{Si}_3\text{N}_4 + \text{SiC} = 87.5\%\text{Si}_3\text{N}_4 + 12.5\%\text{SiC},$$

$$(11): 4\text{Si}_3\text{N}_4 + \text{SiC} = 93.3\%\text{Si}_3\text{N}_4 + 6.7\%\text{SiC}.$$

The results of quantitative XRD phase analysis of the composition of synthesis products (after water washing and removal of NaF), which were obtained experimentally by combustion of the initial mixtures of powders (charges) in bulk form in a reactor at nitrogen gas pressure of 4 MPa, according to reactions (7)–(11), are presented in Table 1.

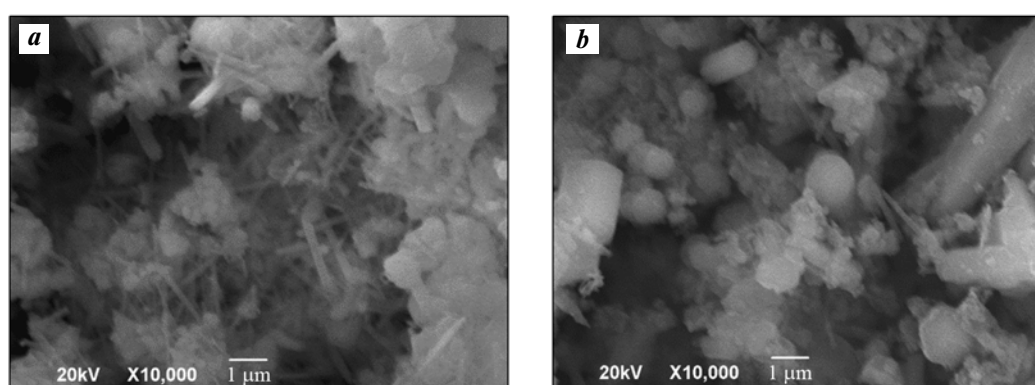
As Table 1 shows, the washed combustion products of all examined charge compositions consist of 4 phases: silicon nitride of two modifications (α -Si₃N₄ and β -Si₃N₄), silicon carbide (β -SiC) as well as silicon impurities (Si_{free}). It is obvious that experimental composition of Si₃N₄–SiC differs markedly from the calculated theoretical composition, first of all, by a significantly lower content of silicon carbide, particularly in the cases of mole ratios of nitride and carbide phases of 2 : 1 and 4 : 1 (by factor of 4). Besides, more silicon nitride and less silicon carbide are formed compared to reaction equations (7)–(11), but free carbon is not found in combustion products. Such a difference observed between the experimental and theoretical results can be explained by the peculiarities of silicon carbide formation according to the sequence of reactions (4) upon the combustion of silicon and carbon powders in a nitrogen atmosphere. A part of very fine light particles of carbon black (soot) can be removed (blown out) from a burning highly porous bulk charge sample by gases released during the synthesis of intermediate product Si₃N₄ (the 1st reaction), with the said particles not involved in further transformation of silicon nitride into silicon carbide through the interaction of Si₃N₄ with carbon (with the 2nd reaction). As a result, more silicon nitride and less silicon carbide are left in combustion products compared to reaction equations (7)–(11). The lower is the carbon content in the charge with respect to silicon content in these equations, the higher is the combustion temperature and the more considerable is the gas release, the greater is the relative loss of carbon due to the removal of gases, and the more differs the experimental composition of Si₃N₄–SiC from the theoretical one.

The results obtained in the work [46] confirmed the effectiveness of using halide salt NH₄F activating additive for obtaining the highly dispersed composition of Si₃N₄–SiC powders by azide SHS with different phase ratios in a wide range of silicon carbide content (from 1.6 to 41.8 %) without diluting the mixture with final product α -Si₃N₄. Synthesized compositions are characterized by a high content of α -Si₃N₄ (2.17–3.61 times more than of β -Si₃N₄). Upon high carbon content in the charge, leading to the synthesis of 23.9

Table 1. Combustion product compositions of charges of reactions (7)–(11), wt. %

Таблица 1. Составы продуктов горения шихт реакций (7)–(11), мас. %

The composition of charges of reactions (7)–(11)	α -Si ₃ N ₄	β -Si ₃ N ₄	α -Si ₃ N ₄ + β -Si ₃ N ₄	β -SiC	Si _{free}
4Si + C + NaN ₃ + NH ₄ F (7)	70.2	19.4	89.6	9.7	0.7
5Si + 2C + NaN ₃ + NH ₄ F (8)	50.9	19.5	70.4	23.9	5.7
7Si + 4C + NaN ₃ + NH ₄ F (9)	38.2	17.6	55.8	41.8	2.4
7Si + C + 2NaN ₃ + 2NH ₄ F (10)	68.4	27.4	95.8	3.6	0.6
13Si + C + 4NaN ₃ + 4NH ₄ F (11)	69.3	28.1	97.4	1.6	1.0

Fig. 1. Microstructure of combustion products of charges 7Si + C + 2NaN₃ + 2NH₄F (a) and 7Si + 4C + NaN₃ + NH₄F (b)Рис. 1. Микроструктура продуктов горения шихт 7Si + C + 2NaN₃ + 2NH₄F (a) и 7Si + 4C + NaN₃ + NH₄F (b)

and 41.8 % silicon carbide in the composition, α -Si₃N₄ is mainly formed in the form of equiaxed particles rather than the fibrous ones. The impurities of free silicon do not exceed 1.0 % for the compositions with SiC proportion of up to 10 %, but they reach 2.4–5.7 % for SiC content of 23.9 and 41.8 %, which is obviously associated with a large amount of silicon in the initial charge and incomplete reaction of SiC formation. Upon SiC content from 1.6 to 23.9 %, Si₃N₄–SiC compositions are submicron, and they consist of fibers with a diameter of 100–500 nm and a length of up to 5 μ m, as well as equiaxed particles with a size of 100–500 nm in the form of individual particles and their agglomerates (Fig. 1, a). Upon SiC content of 41.8 %, Si₃N₄–SiC composition is a mixture of submicron particles being 150–500 nm in size, with much larger particles up to 2 μ m in size (Fig. 1, b).

The obtained composite powders Si₃N₄–SiC distinguish from those synthesized earlier using the combustion process both by their higher dispersibility and higher α -Si₃N₄ content, and therefore they are pro-

ducing for use in the production of composite ceramic materials with improved properties at lower sintering temperatures.

AlN–SiC composition

Aluminium nitride (AlN) is distinguished in technical ceramics for its unique combination of physical, electrical and chemical properties at a relatively low cost: light weight, high thermal conductivity, good electrical insulation properties, moderate coefficient of thermal expansion, stability at high temperatures in an inert atmosphere, non-toxicity [1]. At present, aluminum nitride is mainly used in electronics, where heat dissipation from electronic devices is important with a high electrical resistance and a coefficient of thermal expansion (CTE) close to that of silicon [47]. In this respect, when it comes to the production of electronic components, aluminum nitride is being used in almost all areas where the highly toxic beryllium oxide was previously applied. Aluminum nitride is most intensively

used for the production of integrated circuit packages and substrates, high-power transistors, power absorbers, and LEDs. However, both in this regard and in the case of its application as a structural material at high temperatures, the application of aluminum nitride is limited by its brittleness, low fracture toughness, and heat resistance [48]. Therefore, much attention is being paid to the development of composite ceramics of aluminum nitride with silicon carbide (SiC), which in addition to good thermal conductivity and corrosion resistance possesses significantly better mechanical properties (hardness, fracture toughness, creep resistance) [49]. Silicon carbide is also attractive since it has a crystal structure similar to the one of aluminum nitride and it can form a single-phase homogeneous solid solution with it, thus resulting in improved flexural strength and fracture toughness, i.e. reduced brittleness [50, 51]. But AlN—SiC composites have significantly better toughness and heat resistance even without the formation of a solid solution, in a two-phase condition of sintered, spatially separated powder components AlN and SiC [52, 53]. AlN—SiC composites with high thermal conductivity can be obtained by adjusting the grain size of AlN and SiC [54]. AlN—SiC composite ceramics appeared to be promising for application not only in metallurgy and mechanical engineering as a structural material functioning under mechanical load at high temperatures, but also in electronics as a new high-temperature ceramic, which has a high capacity of microwave radiation absorption and can be used in high-power amplifiers and microwave components, sensors, thermoelectric elements, solar power receivers, RF resonators and filters, etc. [51, 55].

The following conventional energy-intensive methods for producing AlN—SiC ceramics are known: the carbothermal reduction of silica and alumina in nitrogen atmosphere; the pressureless sintering of SiC and AlN ceramic powders or the hot pressing of the ones, which require a high temperature of 2000 °C and a long holding time of up to several hours [51, 53, 56—58]. More advanced methods include spark plasma sintering (SPS), as well as self-propagating high-temperature synthesis (SHS), which is also called combustion synthesis [48, 55]. In the case of SPS method, the energy consumption is considerably lower since SPS process is conducted at a temperature of about 1600 °C and lasts about 10 minutes but requires expensive equipment. SHS method is much more cost-effective since the synthesis of AlN—SiC composite proceeds due to its own heat release during combustion in very simple equipment, and it is performed from cheap initial reagents, most of-

ten the powders of Al, Si, C (carbon black) and N₂ gas. Therefore, much attention is paid to the development of SHS method, various options for the combustion of mixtures of various powders are being studied to obtain AlN—SiC composition.

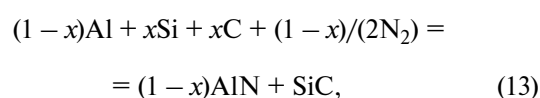
The application of the energy-efficient SHS method to obtain AlN—SiC was first studied in work [59]. Silicon nitride powder Si₃N₄ was used as a solid source of nitrogen, and the reaction equation was as follows:



Reaction (12) is highly exothermic with an adiabatic temperature of 2502 K, which was supposed to ensure its self-propagation in the combustion mode, still the combustion could not be conducted without the imposition of an electric field with an intensity (E) of at least 8 V/cm. As E increased, the combustion temperature and rate grew, and in the interval of $8 < E < 25$ V/cm the combustion products were the composition of two phases AlN and SiC with a gradual increase in their mutual solubility, and at $E = 25$ V/cm the combustion product was a stable single-phase solid solution AlN—SiC. The combustion process took several seconds, but the combustion product contained silicon and carbon impurities.

The application of microwave heating of reagent mixture specified in equation (12) allowed this mixture to be ignited and the SHS process to be implemented without the imposition of an electric field [60]. Depending on the weight of the mixture (from 0.5 to 16 g) and maximum combustion temperature (from 1027 to 1889 °C), the composition of the combustion products was different. At minimum combustion temperatures, it contained impurities of initial components Si₃N₄, Al, and C along with AlN and SiC phases, and at maximum temperatures, it included only Al and C impurities. As the combustion temperature increased, the grain size of combustion products grew. AlN—SiC solid solution could not be obtained since the combustion temperatures were below the critical value of 1960 °C, separating the areas of two-phase composite and single-phase solid solution.

In other studies, nitrogen gas N₂ was used as a source of nitrogen. In work [48], the formation of ceramics by the following reaction was studied:



where x varied from 0 to 0.85, and nitrogen pressure was 3, 8 or 12 MPa. The combustion led to the forma-

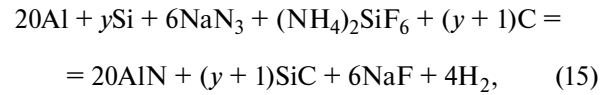
tion of AlN—SiC solid solution without unreacted Al and Si impurities only at considerably high nitrogen pressures: 12 MPa for $x = 0.3$ and 8 MPa for $x = 0.5$ and 0.6. Even higher nitrogen pressures (50 and 70 MPa) were used for SHS of AlN—SiC solid solution of other components [61]:



At the pressure of 50 MPa, the combustion temperature was 1400 °C, and the combustion product contained a large amount of unreacted Al (up to 12 %) and Si along with AlN_{0.7}SiC_{0.3} solid solution. An increase in pressure to 70 MPa resulted in the combustion temperature being increased up to 2050 °C and the Al impurity content being reduced to 0.5 %.

The possibility of implementing the SHS mode to obtain AlN—SiC solid solution at a low pressure of nitrogen gas (0.3–0.5 MPa) according to reaction (13) was studied in work [62]. The combustion temperature at a pressure of 0.3 MPa was ranging from 1972–2287 K, depending on the molar ratio of Al/Si components in the initial mixture from 0.5 to 2.5, which corresponded to x values from 0.665 to 0.286 in equation (13), and was low dependent on pressure. The maximum temperatures ranging from 2142 to 2287 K were obtained at Al/Si component ratios from 1 to 2 and allowed to synthesize AlN—SiC solid solution with residual Si. An almost pure and more homogeneous AlN—SiC solid solution was obtained by adding an additional amount of carbon black (20 %) to the initial powders. At the lower combustion temperatures, the SHS product was a composite of AlN and SiC phases being more contaminated with impurities of unreacted initial powders. In all cases, the synthesized AlN—SiC ceramics were powders with micron-sized particles.

In works [63, 64], the other SHS option, namely azide SHS using halide salt (NH₄)₂SiF₆ and the following common chemical reaction equation, was applied to obtain AlN—SiC powder composite:



where coefficient value y took the values from 1 to 10. The results of thermodynamic calculations of the adiabatic temperature perform by using the THERMO software (T_{ad}) and composition of reaction products (15) for different values of y are presented in Table 2.

As Table 2 shows, the adiabatic temperatures of reactions (15) are high enough for the combustion mode implementation, and the condensed reaction products are the desired phases of AlN and SiC with admixed water-soluble by-product salt NaF, which is easily removed by washing with water. According to the data of Table 2, after water washing, the synthesized AlN—SiC composition should contain from 2.8 to 24.0 wt.% of SiC.

The experimental studies of azide SHS process were conducted in laboratory reactor SHS-Az with a volume of 4.5 L at different contents of silicon and carbon powders in the initial charge, nitrogen pressure of 4 MPa, the relative bulk density of the charge of 0.4, and the diameter of the sample of 30 mm. Table 3 lists the results of quantitative XRD phase analysis of the composition of the synthesis products after water washing and removal of NaF.

Table 3 shows that the desired composition AlN—SiC can be synthesized during the combustion of mixtures of equation (15), however, the content of silicon carbide in the composition of the reaction products is much lower (from 1.3 to 5.9 wt.%) compared with

Таблица 2. Адиабатические температуры и состав продуктов реакций уравнения (15)

Table 2. Adiabatic temperatures and composition of reaction products of equation (15)

y	T_{ad} , K	Amount, mol.									
		Al _g	F _g	H _g	Na _g	H _{2g}	N _{2g}	NaF _g	NaF _l	AlN _g	SiC _s
1	2913	0.21	0.03	0.14	0.03	3.93	3.78	5.97	—	19.79	2.00
4	2858	0.13	0.03	0.12	0.03	3.94	3.78	5.97	—	19.87	5.00
6	2824	0.10	0.02	0.10	0.02	3.95	3.78	5.92	0.06	19.90	7.00
8	2812	0.09	0.02	0.10	0.02	3.95	3.78	5.56	0.42	19.91	9.00
10	2799	0.07	0.02	0.10	0.02	3.95	3.78	5.22	0.76	19.93	11.00

Table 3. The ratio of phases in washed combustion products of charges of equation (15)

Таблица 3. Соотношение фаз в промытых продуктах горения шихт уравнения (15)

Composition of charge	Composition of combustion products, wt. %					
	AlN	SiC	Na ₃ AlF ₆	Si	α-Si ₃ N ₄	β-Si ₃ N ₄
Si + 20Al + 6NaN ₃ + (NH ₄) ₂ SiF ₆ + 2C	90.3	1.3	7.7	0.7	—	—
4Si + 20Al + 6NaN ₃ + (NH ₄) ₂ SiF ₆ + 5C	86.0	2.6	10.5	0.9	—	—
6Si + 20Al + 6NaN ₃ + (NH ₄) ₂ SiF ₆ + 7C	81.5	4.2	12.3	0.7	1.3	—
8Si + 20Al + 6NaN ₃ + (NH ₄) ₂ SiF ₆ + 9C	78.8	4.5	13.8	0.7	1.2	1.0
10Si + 20Al + 6NaN ₃ + (NH ₄) ₂ SiF ₆ + 11C	76.0	5.9	15.5	0.8	1.1	0.5

the results of thermodynamic calculations, and water-insoluble by-product phase Na₃AlF₆ (cryolite) as well as free silicon impurity (0.7–0.9 wt.%) appear in the products. Upon that, the proportion of by-product cryolite Na₃AlF₆ is quite considerable and increases from 7.7 to 15.5 wt.% with an increase in carbon content from 2 to 11 mol in the initial mixture. The appearance of cryolite Na₃AlF₆ in SHS-Az products results in a decrease of AlN phase content in comparison with the results of thermodynamic calculations. Upon the proportion of silicon being ≥ 6 mol, the combustion products also contain a small amount of silicon nitride (less than 1.5 wt.%). Such a difference between the experimental and theoretical data can be explained by the fact that the results of the experimental study (Table 3) show the composition of the cooled products of SHS-Az reactions and thus differ markedly from the results of thermodynamic calculation (see Table 2) of the composition of the products at the maximum possible adiabatic temperature of SHS-Az reactions, in which there is no cryolite, and silicon carbide content is much higher (from 2.8 to 24.0 wt.%). When cooled, the composition of the products changes that leads to the formation of cryolite, which cannot exist at temperatures above 1000 °C as it melts and decomposes at this temperature [65]. It is worth emphasizing that despite high combustion temperatures (> 2200 °C), the product of SHS reaction is not a single-phase AlN—SiC solid solution, but a composition of two phases: AlN and SiC. This can be explained by considerable content of cryolite by-product, which separates AlN and SiC phases and prevents the formation of solid solution of the ones.

It is also worth noting that no free carbon is found in the experimental products although the content of SiC is much lower in the experimental combustion pro-

ducts compared with the one in the theoretical products, according to stoichiometric equation (15) and the results of thermodynamic calculations. As in the previous case of azide SHS of Si₃N₄—SiC composition, such a difference between experimental and theoretical results can also be explained by the peculiarities of silicon carbide formation according to the sequence of reactions (4) upon the combustion of silicon powder in nitrogen atmosphere. A considerable part of ultra-fine light carbon black particles can be removed from the burning highly porous bulk charge sample by gases released during the synthesis of intermediate product Si₃N₄ (the 1st reaction) and thus not involved in subsequent transformation of silicon nitride into silicon carbide due to the interaction of Si₃N₄ with carbon (the 2nd reaction). As a result, a part of intermediate product Si₃N₄ may remain in the final experimental combustion products, and less amount of silicon carbide is formed compared to the results of theoretical calculations, but free carbon may not be detected in the combustion products.

The results of the morphology and particle size study of the powder product synthesized are shown in Fig. 2.

As we can see in Fig. 2, *a* and *b*, predominantly equiaxed particles of aluminum nitride powder with a size from 150 nm to 1 μ m are formed during the combustion of mixtures with a silicon content of 1–4 mol. The combustion products of mixtures with silicon content ranging from 6 mol (Fig. 2, *c–e*) are equiaxed particles of aluminum nitride and silicon carbide of a smaller size being from 100 to 600 nm.

Thus, using the azide SHS method allows synthesizing the desired ceramic nitride-carbide powder composition AlN—SiC in the form of equiaxed particles ranging in size from 100 nm to 1 μ m with SiC

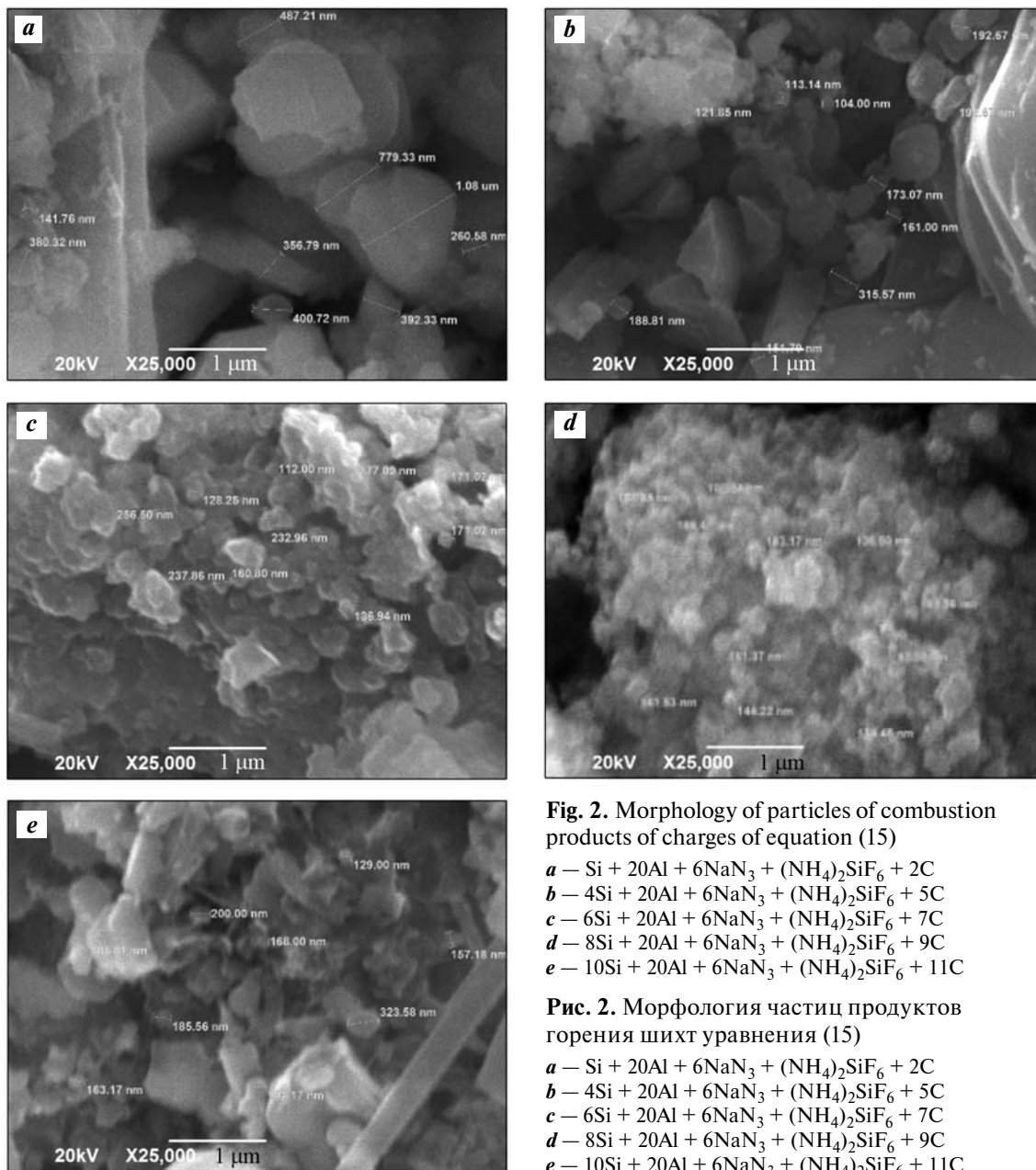


Fig. 2. Morphology of particles of combustion products of charges of equation (15)

- a* – $\text{Si} + 20\text{Al} + 6\text{NaN}_3 + (\text{NH}_4)_2\text{SiF}_6 + 2\text{C}$
b – $4\text{Si} + 20\text{Al} + 6\text{NaN}_3 + (\text{NH}_4)_2\text{SiF}_6 + 5\text{C}$
c – $6\text{Si} + 20\text{Al} + 6\text{NaN}_3 + (\text{NH}_4)_2\text{SiF}_6 + 7\text{C}$
d – $8\text{Si} + 20\text{Al} + 6\text{NaN}_3 + (\text{NH}_4)_2\text{SiF}_6 + 9\text{C}$
e – $10\text{Si} + 20\text{Al} + 6\text{NaN}_3 + (\text{NH}_4)_2\text{SiF}_6 + 11\text{C}$

Рис. 2. Морфология частиц продуктов горения шихт уравнения (15)

- a* – $\text{Si} + 20\text{Al} + 6\text{NaN}_3 + (\text{NH}_4)_2\text{SiF}_6 + 2\text{C}$
b – $4\text{Si} + 20\text{Al} + 6\text{NaN}_3 + (\text{NH}_4)_2\text{SiF}_6 + 5\text{C}$
c – $6\text{Si} + 20\text{Al} + 6\text{NaN}_3 + (\text{NH}_4)_2\text{SiF}_6 + 7\text{C}$
d – $8\text{Si} + 20\text{Al} + 6\text{NaN}_3 + (\text{NH}_4)_2\text{SiF}_6 + 9\text{C}$
e – $10\text{Si} + 20\text{Al} + 6\text{NaN}_3 + (\text{NH}_4)_2\text{SiF}_6 + 11\text{C}$

content of up to 5.9 wt.%, but the washed synthesis products, being condensed, include water insoluble cryolite impurity Na_3AlF_6 , upon that ranging in the amount from 7.7 to 15.5 wt.%, along the desired phases of AlN and SiC . An azide SHS product of such content can be applied for liquid-phase hybrid reinforcement of aluminum matrix composites with submicron AlN and SiC powders, upon which cryolite plays a positive role of flux and is not included in the final composition of the composite, without contaminating it [66].

TiN–SiC composition

It bears repeating that silicon carbide (SiC) based ceramics is widely used as a wear-resistant and high-temperature structural material due to its high hardness and rigidity, phase stability and heat resistance, low density and thermal expansion coefficient. Since SiC is a semiconductor, it has also found application in diodes and LEDs. But due to its semiconductor properties, SiC exhibits high electrical resistance ($2.0 \cdot 10^5 \text{ Ohm} \cdot \text{cm}$), which makes it impossible to use efficient electrical dis-

charge machining for the production of complex silicon carbide parts [67]. SiC based polycrystalline ceramics could find a wider application if they could be more easily machined to make them more electrically conductive. And the strengthening of SiC based ceramics would allow them to compete as a structural material with silicon nitride (Si_3N_4) based ceramics. [67].

In this context, the addition of electrically conductive titanium nitride particles (TiN) with low electrical resistivity ($22 \cdot 10^{-6}$ Ohm·cm) is of considerable interest for the improvement of the properties of SiC based ceramics. Upon that, titanium nitride has high values of melting temperature (3223 K) and hardness (20 GPa), good corrosion resistance [68]. It is used to create wear-resistant coatings for metal-cutting tools and protective and decorative coatings to imitate golden color, and it is also applied as a heat-resistant material, in particular, it is used to make crucibles for melting of metals in an oxygen-free atmosphere. Submicron and nanosized titanium nitride powders are used in ceramics based on silicon nitride and sialons to increase the hardness and strength of these materials [69].

A rich variety of methods for obtaining titanium nitride is known. The main industrial methods for obtaining titanium nitride powders with a particle size of up to 50 microns are the carbothermal reduction of titanium oxide in nitrogen atmosphere and direct nitridation of titanium powder. [70]. Submicron powders and nanopowders are obtained by plasma-chemical synthesis or by precipitation from the gas phase during the reduction of titanium tetrachloride vapor with ammonia at a temperature of 900–1000 °C [71, 72]. These methods are characterized by high energy consumption and the application of complex equipment. For the first time, titanium nitride was obtained by a simple energy-saving method of SHS by burning titanium powders in nitrogen atmosphere [14]. Due to high temperature of synthesis (2200–2500 °C), titanium nitride was formed in the form of porous cakes of sintered crystallites up to 100 μm in size. Nanostructured titanium nitride powders with particles of nanofibrous structure (the fiber diameter of 50–100 nm) and nanocrystalline structure (the average crystallite size of 100–200 nm) were obtained by azide SHS method [73]. To synthesize the ones, not titanium powder, but halide salt of ammonium hexafluorotitanate $(\text{NH}_4)_2\text{TiF}_6$ was used as the nitrated agent. In this case, the formation of titanium nitride proceeded in gas phase, from atomic titanium formed during the decomposition of halide salt at temperatures of 710–1080 °C. According to literature data analysis, in

order to synthesize titanium nitride nanopowders, it is necessary to create low-temperature conditions for synthesis (500–900 °C) and to conduct the reduction and nitridation of titanium source at the atomic level, i.e. in the gas phase [74].

A method for obtaining silicon carbide ceramics with the admixtures of titanium nitride nanoparticles by sintering under pressureless conditions is known [75]. The initial materials were α -SiC powder (particle size of 0.5–1.0 μm) in the form of matrix, Al_2O_3 and Y_2O_3 as sintering additives and TiN nanoparticles (0–15 wt.%, average particle size of 20 nm) as a strengthening phase. The initial powders were pressed until rectangular samples were formed, afterwards they were compacted by cold isostatic pressing at a pressure of 250 MPa. Further, the samples were subjected to liquid-phase sintering in a vacuum furnace at a temperature of 1950 °C for 15 min, and then at 1850 °C for 1 h. The study of the microstructure showed that TiN nanoparticles inhibited the compaction of silicon carbide ceramics and suppressed the growth of grains of silicon carbide ceramics. TiN reacted with SiC and Al_2O_3 to form new phases of TiC, AlN and some others. The formation of a new phase of titanium carbide (TiC), having higher hardness than the one of TiN, resulted in the fact that the hardness of sintered ceramics with 10 wt.% and 15 wt.% of TiN nanoparticles was higher than the hardness of the ones with 5 wt.% of TiN nanoparticles. However, the best combination of properties was obtained in silicon carbide ceramics with 5 wt.% of TiN nanoparticles, with a relative density of 92.8 %, flexural strength of 686 MPa, hardness of 92 HRA and fracture toughness of 7.04 $\text{MPa}\cdot\text{m}^{1/2}$. Adding up to 5 wt.% of SiC whiskers being 0.5–2.5 μm in diameter and 10–50 μm in length to such a ceramic composition resulted in flexural strength increase up to 1122 MPa together with some decrease in other mechanical characteristics [76]. Thus, the addition of TiN nanoparticles is an efficient technique for improving the mechanical characteristics of silicon carbide ceramics. The disadvantage of this method for manufacturing TiN–SiC ceramics is that it is multi-stage and quite complex, and expensive TiN nanopowder and silicon carbide fibers are used to obtain the composite.

SiC based composites with different content of coarser TiN powder (0–50 vol.%) were made of the mixture of α -SiC (0.7 μm) and TiN (0.8–1.2 μm) powders by hot pressing at $t = 1900$ °C with holding time of 60 min in flowing argon atmosphere under pressure 30 MPa, using

Al_2O_3 and Y_2O sintering additives (0.7 and 0.9 μm ; 6.0 and 4.0 wt.%, correspondingly) [67]. Electrical measurements showed that increase in TiN additions reduces the resistivity from $2.0 \cdot 10^5 \text{ Ohm} \cdot \text{cm}$ (0 % of TiN) to the plateau of $2.0 \cdot 10^{-4} \text{ Ohm} \cdot \text{cm}$ (40–50 vol.% of TiN). Flexural strength gradually increased with increase in TiN content. The maximum strength of 921 MPa was observed at the content of 40 vol.% of TiN compared to 616 MPa for initial SiC.

A method has been recently proposed for obtaining SiC–TiN composite material based on hot pressing of a powder mixture containing 53–83 wt.% of silicon carbide powder (< 25 μm), 5–40 wt.% of titanium powder (< 25 μm) and 7 wt.% of sintering additive powder in the form of Y_2O_3 – Al_2O_3 at the ratio of 3 : 5 [77]. In the process of hot pressing, the combination of sintering and nitridation of the powder mixture was ensured at $t = 1600 \text{ }^\circ\text{C}$ in nitrogen atmosphere within 30 minutes at a pressure of 30 MPa, then the temperature was increased to 1850 $^\circ\text{C}$ and held for 30 minutes to obtain a composite material with main phases SiC and TiN. As a result, the ceramic composite gained considerably high flexural strength, hardness, and density: 340–400 MPa, 22.8–34.4 GPa, and 91–97 %, correspondingly. The advantages of this method include less stages and duration, the use of inexpensive titanium powder with a particle size of 25 μm instead of expensive titanium nitride nanopowder.

The SHS process was applied to obtain more complex composition Si_3N_4 –TiN–SiC from TiSi_2 and SiC mixtures by combustion reaction at high nitrogen pressure of 10–130 MPa [78]. The analysis of mechanism of nitridation of TiSi_2 showed that upon the nitridation of TiSi_2 , TiN and Si are formed first, and upon further nitridation of Si, Si_3N_4 phase is formed. At a higher nitrogen pressure, the nitridation reaction is completed, and thus relatively dense composites Si_3N_4 –TiN–SiC are obtained.

The authors of this review studied the application of azide SHS method by using three halide salts $(\text{NH}_4)_2\text{TiF}_6$ (1), $(\text{NH}_4)_2\text{SiF}_6$ (2) and Na_2SiF_6 (3) to obtain highly dispersed powder composition TiN–SiC with five the following molar phase ratios given: 1 : 1, 1 : 2, 1 : 4, 2 : 1 and 4 : 1 [79]. Silicon powder of Kr0 grade (average particle size of 5 μm); fine titanium powder of PTM-3 grade (15 μm); halide salts (50 μm); sodium azide powder of «Pure» classification (100 μm); carbon black of P701 grade (70 nm, average size of agglomerates of 1 μm) were used in experiments as starting reagents. The combustion of mixtures of powders was conducted in laboratory reactor

SHS-Az with an operating volume of 4.5 l at nitrogen gas pressure of 4 MPa. THERMO software was applied to calculate the equilibrium compositions of products, adiabatic temperatures (t_{ad}) and the enthalpies of reactions of interaction of initial reagents (ΔH^0) for the synthesis of TiN–SiC composition with the above molar phase ratios and the use of the specified halide salts (Table 4–6).

As Table 4 shows, if salt 1 is used, the thermodynamic composition of the reaction products fully complies with all specified 5 mole ratios of phases TiN : SiC. If salts 2 and 3 (Table 5 and 6) are used, the thermodynamic composition of the reaction products complies with only two molar phase ratios: 2 : 1 and 4 : 1, i.e. TiN–SiC compositions with a high content of TiN phase, which are synthesized from mixtures with a high content of titanium powder. In the case of charges with a high content of silicon and carbon, which should have resulted in the formation of TiN–SiC with a mole ratio of phases 1 : 1, 1 : 2, and 1 : 4, i.e. with a high content of SiC phase, this phase is either not formed at all or is formed partially, with silicon nitride phase Si_3N_4 being formed instead. Such results can be explained by the sequence of reactions (4) of formation of silicon nitride and silicon carbide upon the combustion of a mixture of silicon and carbon powders in nitrogen gas. As Tables 4–6 show, the adiabatic temperature of reactions is high for the charges with high titanium content, it is close to the temperature of dissociation of Si_3N_4 (about 2000 $^\circ\text{C}$), therefore, silicon nitride is completely transformed into silicon carbide, and there is no free carbon in the final product of the synthesis. While in the case of mixtures with high silicon and carbon contents, the adiabatic temperature is markedly lower (particularly, in the case of salts 2 и 3), therefore, silicon nitride is not transformed into silicon carbide or is partially transformed, and silicon nitride (in whole or in part) and free carbon remain in the final product.

If we convert from mole ratios of phases to weight percentages with respect to the composition of TiN–SiC, we obtain the following expected compositional contents according to stoichiometric reaction equations after removal of the water-soluble impurity NaF from the reaction products, wt.%:

$$\text{TiN} : \text{SiC} = 60.7 : 39.3; \text{TiN} : 2\text{SiC} = 43.6 : 56.4;$$

$$\text{TiN} : 4\text{SiC} = 27.9 : 72.1; 2\text{TiN} : \text{SiC} = 75.6 : 24.4; \quad (16)$$

$$4\text{TiN} : \text{SiC} = 86.1 : 13.9.$$

Table 4. Results of thermodynamic calculations using $(\text{NH}_4)_2\text{TiF}_6$ Таблица 4. Результаты термодинамических расчетов при использовании $(\text{NH}_4)_2\text{TiF}_6$

Initial mixture of powders	Composition of products, mol.					$t_{\text{ad}}, ^\circ\text{C}$	$\Delta H^0, \text{kJ}$
	SiC	TiN	NaF	H ₂	N ₂		
2Si + Ti + 6NaN ₃ + $(\text{NH}_4)_2\text{TiF}_6$ + 2C	2.00	2.00	6.00	4.00	16.00	1691	-2308
4Si + Ti + 6NaN ₃ + $(\text{NH}_4)_2\text{TiF}_6$ + 4C	4.00	2.00	6.00	4.00	16.00	1704	-2440
8Si + Ti + 6NaN ₃ + $(\text{NH}_4)_2\text{TiF}_6$ + 8C	8.00	2.00	6.00	4.00	16.00	1712	-2704
2Si + 3Ti + 6NaN ₃ + $(\text{NH}_4)_2\text{TiF}_6$ + 2C	2.00	4.00	6.00	4.00	15.00	1974	-2984
2Si + 7Ti + 6NaN ₃ + $(\text{NH}_4)_2\text{TiF}_6$ + 2C	2.00	8.00	6.00	4.00	13.00	2277	-4336

Table 5. Results of thermodynamic calculations using $(\text{NH}_4)_2\text{SiF}_6$ Таблица 5. Результаты термодинамических расчетов при использовании $(\text{NH}_4)_2\text{SiF}_6$

Initial mixture of powders	Composition of products, mol.							$t_{\text{ad}}, ^\circ\text{C}$	$\Delta H^0, \text{kJ}$
	SiC	Si ₃ N ₄	TiN	NaF	H ₂	N ₂	C		
Si + 2Ti + 6NaN ₃ + $(\text{NH}_4)_2\text{SiF}_6$ + 2C	—	0.67	2.00	6.00	4.00	14.67	2.00	1557	-2057
3Si + 2Ti + 6NaN ₃ + $(\text{NH}_4)_2\text{SiF}_6$ + 4C	1.00	1.00	2.00	6.00	4.00	14.00	3.00	1666	-2373
7Si + 2Ti + 6NaN ₃ + $(\text{NH}_4)_2\text{SiF}_6$ + 8C	5.00	1.00	2.00	6.00	4.00	14.00	3.00	1667	-2638
Si + 4Ti + 6NaN ₃ + $(\text{NH}_4)_2\text{SiF}_6$ + 2C	2.00	—	4.00	6.00	4.00	15.00	—	1676	-2365
Si + 8Ti + 6NaN ₃ + $(\text{NH}_4)_2\text{SiF}_6$ + 2C	2.00	—	8.00	6.00	4.00	13.00	—	2127	-3718

Table 6. Results of thermodynamic calculations using Na_2SiF_6 Таблица 6. Результаты термодинамических расчетов при использовании Na_2SiF_6

Initial mixture of powders	Composition of products, mol.						$t_{\text{ad}}, ^\circ\text{C}$	$\Delta H^0, \text{kJ}$
	SiC	Si ₃ N ₄	TiN	NaF	N ₂	C		
Si + 2Ti + 4NaN ₃ + Na_2SiF_6 + 2C	—	0.67	2.00	6.00	10.67	2.00	1665	-1790
3Si + 2Ti + 4NaN ₃ + Na_2SiF_6 + 4C	1.75	0.75	2.00	6.00	10.50	2.25	1694	-1968
7Si + 2Ti + 4NaN ₃ + Na_2SiF_6 + 8C	5.60	0.80	2.00	6.00	10.40	2.40	1695	-2260
Si + 4Ti + 4NaN ₃ + Na_2SiF_6 + 2C	2.00	—	4.00	6.00	11.00	—	1799	-2098
Si + 8Ti + 4NaN ₃ + Na_2SiF_6 + 2C	2.00	—	8.00	6.00	9.00	—	2302	-3451

The experimentally found compositions of the washed combustion products of all initial mixtures of powders (charges) with three halide salts being used are presented in Table 7.

If we compare the experimental compositions of combustion products provided in Table 7 with the theoretical compositions given in Table 4–6 and ratios (16), it can be observed that the experimental

results differ significantly from the theoretical ones by the stable presence of silicon nitride (of α - and β -modifications) in the combustion products of all initial mixtures and the complete absence or a much smaller amount of silicon carbide phase in these products, along with the absence of free carbon in them. A noticeable amount of silicon carbide is formed only during the combustion of charge with a high car-

Table 7. Phase ratio in washed combustion products of charges

Таблица 7. Соотношение фаз в промытых продуктах горения шихт

Composition of charge	Composition of combustion products, wt. %					
	TiN	SiC	α -Si ₃ N ₄	β -Si ₃ N ₄	Si	C
2Si + Ti + 6NaN ₃ + (NH ₄) ₂ TiF ₆ + 2C	45.8	—	49.8	4.4	—	—
4Si + Ti + 6NaN ₃ + (NH ₄) ₂ TiF ₆ + 4C	41.2	6.4	43.9	7.6	0.9	—
8Si + Ti + 6NaN ₃ + (NH ₄) ₂ TiF ₆ + 8C	28.8	19.9	42.5	7.4	1.4	—
2Si + 3Ti + 6NaN ₃ + (NH ₄) ₂ TiF ₆ + 2C	80.0	—	14.0	6.0	—	—
2Si + 7Ti + 6NaN ₃ + (NH ₄) ₂ TiF ₆ + 2C	87.7	—	5.6	6.7	—	—
Si + 2Ti + 6NaN ₃ + (NH ₄) ₂ SiF ₆ + 2C	54.7	16.0	17.4	11.9	—	—
3Si + 2Ti + 6NaN ₃ + (NH ₄) ₂ SiF ₆ + 4C	40.0	31.0	19.0	9.0	1.0	—
7Si + 2Ti + 6NaN ₃ + (NH ₄) ₂ SiF ₆ + 8C	24.2	49.4	21.1	5.0	0.3	—
Si + 4Ti + 6NaN ₃ + (NH ₄) ₂ SiF ₆ + 2C	71.0	—	18.0	9.0	1.2	0.8
Si + 8Ti + 6NaN ₃ + (NH ₄) ₂ SiF ₆ + 2C	61.0	4.0	27.0	7.0	1.0	—
Si + 2Ti + 4NaN ₃ + Na ₂ SiF ₆ + 2C	54.0	20.0	15.0	11.0	—	—
3Si + 2Ti + 4NaN ₃ + Na ₂ SiF ₆ + 4C	42.0	34.0	16.0	8.0	—	—
7Si + 2Ti + 4NaN ₃ + Na ₂ SiF ₆ + 8C	23.0	49.0	21.0	6.0	1.0	—
Si + 4Ti + 4NaN ₃ + Na ₂ SiF ₆ + 2C	64.0	10.0	17.0	9.0	—	—
Si + 8Ti + 4NaN ₃ + Na ₂ SiF ₆ + 2C	76.0	—	19.0	5.0	—	—

bon content (4 and 8 mol), however, it is much less than the possible theoretical amount of SiC. In cases of combustion of charge with a low carbon content (2 mol), silicon carbide is either not formed at all, or it is formed in a small amount compared to the theoretically possible one. Upon that, in both cases (with large and small amounts of carbon in the charge), free carbon is practically undetectable in the composition of the final combustion product, although it is to remain entirely if SiC is not formed, or to be present partially if Si₃N₄ is partially transformed into SiC by reactions (4). As it has already been mentioned in two previous cases of using azide SHS to obtain compositions Si₃N₄—SiC and AlN—SiC, the absence of free carbon in the combustion products can be explained by the peculiarities of silicon carbide formation according to the sequence of reactions (4) during the combustion of silicon powder in nitrogen atmosphere. Ultrafine light particles of carbon black can be partially or even completely removed from a burning highly porous charge sample of bulk density by gases released during the formation of Si₃N₄ at the first stage of combustion, and

not involved in the transformation of Si₃N₄ into SiC. As a result, silicon nitride remains in the combustion products entirely or partially, and silicon carbide is not formed at all, or it is formed in a much smaller amount than it is to be according to the stoichiometric reaction equations for the initial mixtures of powders. The lower the amount of carbon in the charge in relation to the titanium content in these equations, the higher is the combustion temperature, the more is the gas release (and consequently also more significant is the relative loss of carbon due to its removal by the gases), as well as the lower is the formation of SiC (or it is not formed at all).

The microstructure of typical combustion products of charges with halide salt 2 is shown in Fig. 3.

As Fig. 3 shows, the synthesized ceramic compositions are a highly dispersed mixture of nanosized and submicron particles of equiaxed and fibrous forms.

Thus, despite the positive results of the theoretical thermodynamic analysis, the considered experimental application of the azide SHS method did not allow to synthesize the desired composition of TiN—

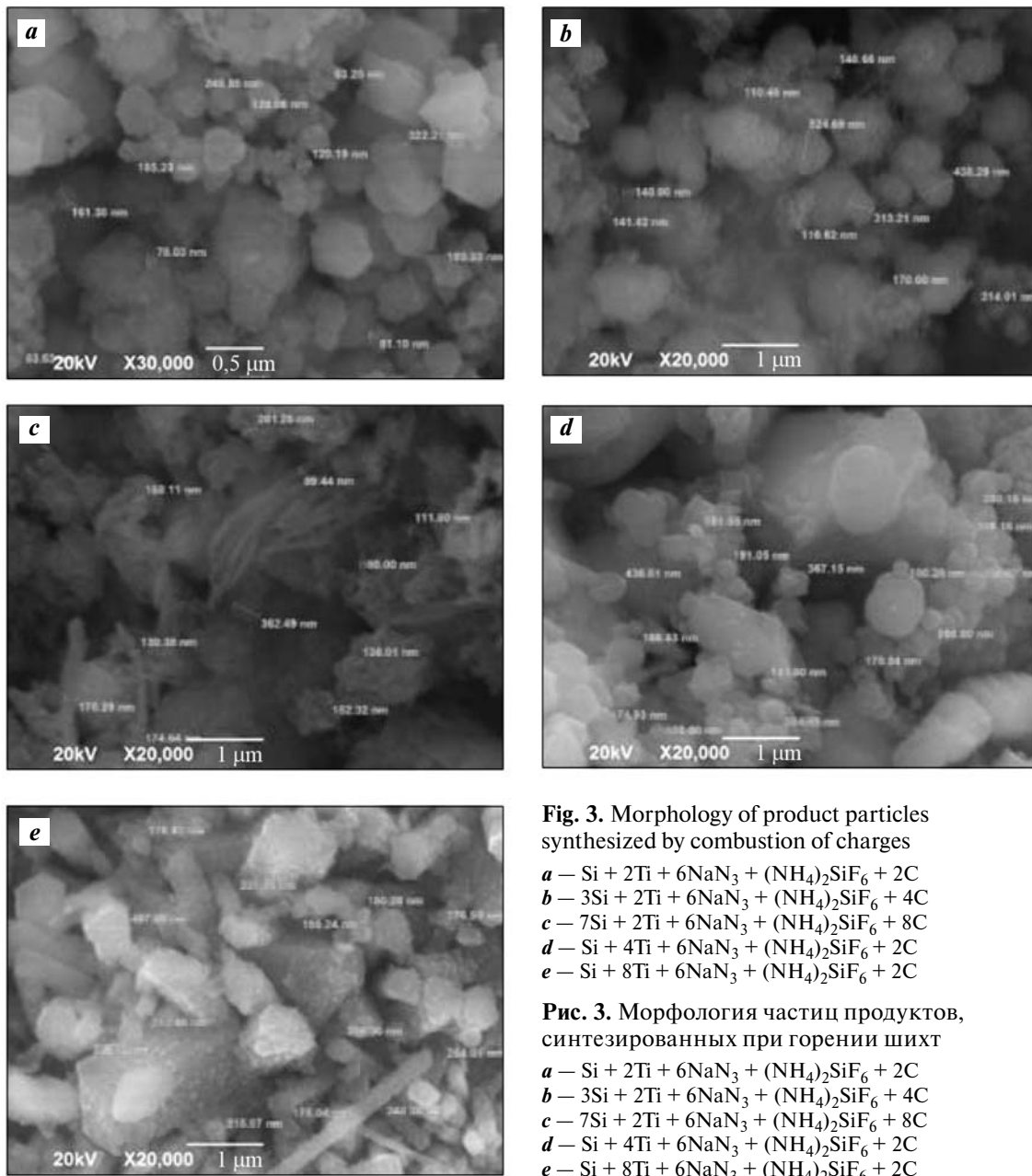


Fig. 3. Morphology of product particles synthesized by combustion of charges

- a** — $\text{Si} + 2\text{Ti} + 6\text{NaN}_3 + (\text{NH}_4)_2\text{SiF}_6 + 2\text{C}$
- b** — $3\text{Si} + 2\text{Ti} + 6\text{NaN}_3 + (\text{NH}_4)_2\text{SiF}_6 + 4\text{C}$
- c** — $7\text{Si} + 2\text{Ti} + 6\text{NaN}_3 + (\text{NH}_4)_2\text{SiF}_6 + 8\text{C}$
- d** — $\text{Si} + 4\text{Ti} + 6\text{NaN}_3 + (\text{NH}_4)_2\text{SiF}_6 + 2\text{C}$
- e** — $\text{Si} + 8\text{Ti} + 6\text{NaN}_3 + (\text{NH}_4)_2\text{SiF}_6 + 2\text{C}$

Рис. 3. Морфология частиц продуктов, синтезированных при горении шихт

- a** — $\text{Si} + 2\text{Ti} + 6\text{NaN}_3 + (\text{NH}_4)_2\text{SiF}_6 + 2\text{C}$
- b** — $3\text{Si} + 2\text{Ti} + 6\text{NaN}_3 + (\text{NH}_4)_2\text{SiF}_6 + 4\text{C}$
- c** — $7\text{Si} + 2\text{Ti} + 6\text{NaN}_3 + (\text{NH}_4)_2\text{SiF}_6 + 8\text{C}$
- d** — $\text{Si} + 4\text{Ti} + 6\text{NaN}_3 + (\text{NH}_4)_2\text{SiF}_6 + 2\text{C}$
- e** — $\text{Si} + 8\text{Ti} + 6\text{NaN}_3 + (\text{NH}_4)_2\text{SiF}_6 + 2\text{C}$

SiC powders in pure form, without the by-product silicon nitride phase of two modifications ($\alpha\text{-Si}_3\text{N}_4$ and $\beta\text{-Si}_3\text{N}_4$) in the composition. Moreover, at a high relative content of Ti in the charge, compared to the content of Si, only Si_3N_4 can be synthesized, and silicon carbide may not be synthesized at all. Upon that, the possibility of using combustion for the synthesis of compositions of highly dispersed nanosized and submicron ceramic powders TiN— Si_3N_4 and TiN— Si_3N_4 —SiC with a relatively low content of free silicon impurity (up to 1.4 %) was experimentally shown for the first time, and that is a remarkable achievement,

since earlier application of SHS method allowed to obtain these compositions only of much coarser powders with a particle size of 5–10 μm by combustion of titanium silicides and silicon carbide in nitrogen gas at high pressure [78, 80].

It is also worth noting that earlier an attempt was made to use the SHS-Az method to obtain a nanopowder composition TiN— Si_3N_4 by burning the charges of the following systems: $\text{Na}_2\text{SiF}_6\text{—NaN}_3\text{—Na}_2\text{TiF}_6$, $(\text{NH}_4)_2\text{SiF}_6\text{—NaN}_3\text{—}(\text{NH}_4)_2\text{TiF}_6$, $\text{Na}_2\text{SiF}_6\text{—NaN}_3\text{—}(\text{NH}_4)_2\text{TiF}_6$ and $(\text{NH}_4)_2\text{SiF}_6\text{—NaN}_3\text{—Na}_2\text{TiF}_6$ with different ratio of components [23]. The combustion

product was a mixture of highly dispersed powders, but a pure nitride composition consisting only of silicon nitride and titanium nitride could not be obtained since the final product contained a large amount (from 10 to 40 wt.%) of non-nitrided Ti and Si by-products, as well as TiSi_2 and Na_2TiF_6 by-products of the reaction.

Conclusion

The presented results of the review show that the application of the SHS process can significantly contribute to the development of methods for obtaining nitride-carbide powder compositions from the most common refractory nitride (Si_3N_4 , AlN , TiN) and carbide (SiC) compounds. The SHS process is attractive by its simplicity and cost-effectiveness, it is one of the promising *in situ* chemical methods for direct synthesis of ceramic powders in the desired composite body from the mixture of initial inexpensive reagents. Azide SHS using sodium azide NaN_3 and gasified fluoride halide salts NH_4F , Na_2SiF_6 , $(\text{NH}_4)_2\text{SiF}_6$ and $(\text{NH}_4)_2\text{TiF}_6$ has such distinctive features as relatively low combustion temperatures, the formation of a large amount of intermediate vapor and gas products of reaction, as well as final condensed and gas by-products that separate particles of the desired powders, making it possible to synthesize highly dispersed ($< 1 \mu\text{m}$) powder compositions $\text{Si}_3\text{N}_4\text{—SiC}$, AlN—SiC and TiN—SiC , where Si_3N_4 has a large ratio of α -modification.

However, in most cases, the amount of SiC phase synthesized in experiments appears to be considerably lower than the expected theoretical amount, and even no SiC at all may be present in the desired nitride-carbide composition. Upon that, almost all synthesized compositions contain Si_3N_4 phase as an undesirable by-product phase in AlN—SiC and TiN—SiC compositions and in excessive amount in $\text{Si}_3\text{N}_4\text{—SiC}$ compositions. Besides, the synthesized compositions may contain the impurities of unreacted free silicon. These disadvantages can be explained by the peculiarities of the formation of silicon carbide through the intermediate formation of silicon nitride during the combustion of a mixture of silicon and carbon powders in nitrogen atmosphere. (Combustion in nitrogen atmosphere is mandatory for *in situ* production of nitrides in composite body by SHS methods.) A considerable part of ultrafine light carbon black particles can be partially or entirely removed from the burning highly porous bulk charge sample by gases released during the

synthesis of intermediate product Si_3N_4 , and thus not involved in subsequent decomposition of Si_3N_4 and transformation into silicon carbide due to interaction with carbon. As a result, silicon nitride remains in the combustion products partially or entirely, and silicon carbide is formed in a smaller amount than it is to be according to the initial stoichiometric reaction equations and the results of thermodynamic calculations, or it is not formed at all. Upon that, an impurity of free silicon appears as well.

Several directions of further research of SHS process application to obtain highly dispersed compositions of nitrides with silicon carbide can be used for eliminating the specified disadvantages. Firstly, to charge an excessive amount of carbon black (soot) compared to the one required by the composition stoichiometry. As it has already been mentioned, almost pure (without Si_3N_4 and Si impurities) and more homogeneous AlN—SiC solid solution was obtained by adding an additional amount of carbon black (20 %) to the mixture of initial powders of Al—Si—C [62].

Secondly, to use polytetrafluoroethylene C_2F_4 (powder fluoroplast-4) as an activating and carbon-containing additive in the charge, which promotes the formation of SiC that was successfully done in work [41] by combustion synthesis of $\text{Si}_3\text{N}_4\text{—SiC}$ compositions with a high content of SiC phase, but with micron-sized particles and a small proportion of α -modification in silicon nitride (Si_3N_4). It was shown in works [26, 81] that upon the combustion of mixtures of silicon powder with carbon or polyethylene (in argon atmosphere) at a high content of C_2F_4 , silicon carbide is synthesized in the form of nanofibers and nanoparticles.

Thirdly, to burn charges in pressed rather than bulk form, in order to reduce the loss of carbon black from the charge due to its being blown out by gases released during the combustion. The pressed condition of the charge can hinder the filtration of nitrogen gas into it and the formation of nitrides, but when using sodium azide powder as a nitriding agent in the composition of the charge, a high degree of nitridation can be obtained even upon difficult filtration of nitrogen gas [20].

Fourthly, it is possible that when burning a pressed charge with sodium azide and polytetrafluoroethylene in an argon atmosphere rather than nitrogen, AlN—SiC and TiN—SiC compositions with a high content of SiC and without silicon nitride impurities will be synthesized.

Fifthly, to charge finely dispersed silicon carbide powder instead of carbon black in the amount required to obtain the desired nitride-carbide com-

position. In this case, the synthesis of SiC is not required as it is already present in the required amount, and all that is left to do is to synthesize nitride of the desired composition by combustion. For example, it was shown in work [42] that the introduction of SiC significantly expands the limits of stable combustion of ferrosilicon in nitrogen (50 % SiC instead of 10 % C) and increases the degree of nitridation of the synthesis products.

And sixthly the last, when synthesizing AlN—SiC composition, not to use sodium azide, but to use only ammonium halide salts and polytetrafluoroethylene in order to exclude the formation of by-product salt — cryolite Na_3AlF_6 during the combustion in nitrogen.

Acknowledgments: *The reported study was funded by RFBR, project numbers 20-08-00298 and 20-38-90158.*

Исследование выполнено при финансовой поддержке РФФИ в рамках проектов № 20-08-00298 и № 20-38-90158.

References

1. Косолапова Т.Я., Андреева Т.В., Бартницкая Т.Б., Гнезин Г.Г., Макаренко Г.Н., Осипова И.И., Прилуцкий Э.В. Неметаллические тугоплавкие соединения. М.: Metallurgiya, 1985.
Kosolapova T.Ya., Andreeva T.V., Bartnitskaya T.B., Gnesin G.G., Makarenko G.N., Osipova I.I., Prilutskii E.V. Non-metallic refractory compounds. Moscow: Metallurgiya, 1985 (In Russ.).
2. Самсонов Г.В. Нитриды. Киев: Наук. думка, 1969.
Samsonov G.V. Nitrides. Kiev: Naukova Dumka, 1969 (In Russ.).
3. Андриевский Р.А., Спивак И.И. Нитрид кремния и материалы на его основе. М.: Metallurgiya, 1984.
Andrievsky R.A., Spivak I.I. Silicon nitride and materials based on it. Moscow: Metallurgiya, 1984 (In Russ.).
4. Агеев О.А., Беляев А.Е., Болтовец Н.С., Киселев В.С., Конакова Р.В., Лебедев А.А., Миленин В.В., Охрименко О.Б., Поляков В.В., Светличный А.М., Чередниченко Д.И. Карбид кремния: технология, свойства, применение. Харьков: ИСМА, 2010.
Ageev O.A., Belyaev A.E., Boltovets N.S., Kiselev V.S., Konakova R.V., Lebedev A.A., Milenin V.V., Okhrimenko O.B., Polyakov V.V., Svetlichnyi A.M., Cherednichenko D.I. Silicon carbide: technology, properties, application. Kharkiv: ISMA, 2010 (In Russ.).
5. Basu B., Balani K. Advanced structural ceramics. Hoboken, New Jersey: John Wiley & Sons, Inc., 2011.
6. Liu C.C., Huang J.L. Effect of the electrical discharge machining on strength and reliability of TiN/Si₃N₄ composites. *Ceram. Int.* 2003. Vol. 29. No. 6. P. 679—687. DOI: 10.1016/S0272-8842(02)00217-1.
7. Huang J.L., Nayak P.K. Effect of nano-TiN on mechanical behavior of Si₃N₄ based nanocomposites by spark plasma sintering (SPS). In: *Nanocomposites — new trends and developments*. Ed. F. Ebrahimi. Rijeka: InTech, 2012. P. 421—436. DOI: 10.5772/50547.
8. Niihara K. New design concept of structural ceramics-ceramic nanocomposites. *J. Ceram. Soc. Jpn.* 1991. Vol. 99. P. 974—982. DOI: 10.2109/JCERSJ.99.974.
9. Palmero P. Structural ceramic nanocomposites: A review of properties and powders' synthesis methods. *Nanomaterials*. 2015. Vol. 5. P. 656—696. DOI: 10.3390/nano5020656.
10. Montanaro L., Palmero P. Advances in the field of nanostructured ceramic composites. *Ceramics*. 2019. Vol. 2. P. 296—297. DOI: 10.3390/ceramics2020024.
11. Yoshimura M., Komura O., Yamakawa A. Microstructure and tribological properties of nano-sized Si₃N₄. *Scr. Mater.* 2001. Vol. 44. P. 1517—1521. DOI: 10.1016/S1359-6462(01)00721-7.
12. Tatami J., Kodama E., Watanabe H., Nakano H., Wakihara T., Komeya K., Meguro T., Azushima A. Fabrication and wear properties of TiN nanoparticle-dispersed Si₃N₄ ceramics. *J. Ceram. Soc. Jpn.* 2008. Vol. 116. No. 6. P. 749—754. DOI: 10.2109/jcersj.2.116.749.
13. Nanomaterials and related products: catalogue and price-list. URL: http://www.plasmachem.com/download/PlasmaChem-General_Catalogue_Nanomaterials_2022 (accessed: 17.03.2022).
14. Амосов А.П., Боровинская И.П., Мержанов А.Г. Порошковая технология самораспространяющегося высокотемпературного синтеза материалов. М.: Машиностроение-1, 2007.
Amosov A.P., Borovinskaya I.P., Merzhanov A.G. Powder technology of self-propagating high-temperature synthesis of materials. Moscow: Mashinostroenie-1, 2007 (In Russ.).
15. Левашов Е.А., Рогачев А.С., Курбаткина В.В., Максимов Ю.М., Юхвид В.И. Перспективные материалы и технологии самораспространяющегося высокотемпературного синтеза. М.: Изд. дом МИСиС, 2011.
Levashov E.A., Rogachev A.S., Kurbatkina V.V., Maksimov Yu.M., Yukhvid V.I. Perspective materials and

- technologies of self-propagating high-temperature synthesis. Moscow: MISIS, 2011 (In Russ.).
16. *Рогачев А.С., Мукасян А.С.* Горение для синтеза материалов. М.: Физматлит, 2012.
Rogachev A.S., Mukasyan A.S. Combustion for material synthesis. New York: CRC Press, 2014.
 17. *Levashov E.A., Mukasyan A.S., Rogachev A.S., Shtansky D.V.* Self-propagating high-temperature synthesis of advanced materials and coatings. *Int. Mater. Rev.* 2016. Vol. 62 (4). P. 1—37. DOI: 10.1080/09506608.2016.1243291.
 18. *Амосов А.П., Боровинская И.П., Мерзханов А.Г., Сычев А.Е.* Приемы регулирования дисперсной структуры СВС-порошков: от монокристалльных зерен до наноразмерных частиц. *Известия вузов. Цветная металлургия.* 2006. No. 5. С. 9—22.
Amosov A.P., Borovinskaya I.P., Merzhanov A.G., Sychev A.E. Principles and methods for regulation of dispersed structure of SHS powders: From monocrystallites to nanoparticles. *Int. J. SHS.* 2005. Vol. 14. No. 1. P. 165—186.
 19. *Nersisyan H.H., Lee J.H., Ding J.-R., Kim K.-S., Manukyan K.V., Mukasyan A.S.* Combustion synthesis of zero-, one-, two- and three-dimensional nanostructures: Current trends and future perspectives. *Progr. Energy Comb. Sci.* 2017. Vol. 63. P. 79—118. DOI: 10.1016/j.precs.2017.07.002 0360-1285.
 20. *Амосов А.П., Бичуров Г.В.* Азидная технология самораспространяющегося высокотемпературного синтеза микро- и нанопорошков нитридов. М.: Машиностроение-1, 2007.
Amosov A.P., Bichurov G.V. Azide technology of self-propagating high-temperature synthesis of micro- and nanopowders of nitrides. Moscow: Mashinostroenie-1, 2007 (In Russ.).
 21. *Bichurov G.V.* Halides in SHS azide technology of nitrides obtaining. In: *Nitride ceramics: Combustion synthesis, properties, and applications.* Eds. A.A. Gromov, L.N. Chukhlomina. Weinheim, Wiley-VCH Verlag GmbH & Co. KGaA, 2015. P. 229—263.
 22. *Бичуров Г.В., Шиганова Л.А., Титова Ю.В.* Азидная технология самораспространяющегося высокотемпературного синтеза микро- и нанопорошков нитридных композиций М.: Машиностроение, 2012.
Bichurov G.V., Shiganova L.A., Titova Yu.V. Azide technology of self-propagating high-temperature synthesis of micro- and nanopowders of nitride compositions Moscow: Mashinostroenie, 2012 (In Russ.).
 23. *Amosov A.P., Bichurov G.V., Kondrat'eva L.A., Kerson I.A.* Nitride nanopowders by azide SHS technology. *Int. J. SHS.* 2017. Vol. 26. No. 1. P. 11—21.
 24. *Mukasyan A.S.* Combustion synthesis of silicon carbide. In: *Properties and applications of silicon carbide.* Ed. R. Gerhardt. Rijeka, Croatia: InTech, 2011. P. 361—388.
 25. *Нерсисян Г.А., Никогосов В.Н., Харатян С.Л., Мерзханов А.Г.* Химический механизм превращения и режимы горения в системе кремний—углерод—фторопласт. *Физика горения и взрыва.* 1991. No. 6. С. 77—81.
Nersisyan G.A., Nikogosov V.N., Kharatyan S.L., Merzhanov A.G. Chemical transformation mechanism and combustion regimes in the system silicon-carbon-fluoroplastic. *Combust. Explos. Shock Waves.* 1991. Vol. 27. P. 720—724. DOI: 10.1007/BF00814517.
 26. *Закоржевский В.В., Лорян В.Э., Акопджанян Т.Г.* Самораспространяющийся высокотемпературный синтез нановолокон карбида кремния. *Известия вузов. Порошковая металлургия и функциональные покрытия.* 2020. No. 2. С. 14—20. DOI: 10.17073/1997-308X-2020-2-14-20.
Zakorzhewsky V.V., Loryan V.E., Akopdzhanyan T.G. Self-propagating high-temperature synthesis of silicon carbide nanofibers. *Russ. J. Non-Ferr. Met.* 2020. Vol. 61. No. 6. P. 675—679. DOI: 10.3103/S106782122006022X.
 27. *Бобович Б.Б.* Неметаллические конструкционные материалы: Учеб. пос. М.: МГИУ, 2009.
Bobovich B.B. Nonmetallic structural materials: textbook. Moscow: MGIU, 2009 (In Russ.).
 28. *Justin J.F., Jankowiak A.* Ultra high temperature ceramics: densification, properties and thermal stability. *Aerospace Lab.* 2011. No. 3. P. 1—11.
 29. *Симоненко Е.П., Симоненко Н.П., Гордеев А.Н., Колесников А.Ф., Лысенков А.С., Нагорнов И.А., Севастьянов В.Г., Кузнецов Н.Т.* Окисление пористых ультравысокотемпературных керамических материалов HfB₂—SiC с повышенным содержанием карбида кремния (65 об.%) сверхзвуковым потоком воздуха. *Журн. неорган. химии.* 2020. Т. 65. No. 4. С. 564—573. DOI: 10.31857/S0044457X20040194.
Simonenko E.P., Simonenko N.P., Gordeev A.N., Kolesnikov A.F., Lysenkov A.S., Nagornov I.A., Sevast'yanov V.G., Kuznetsov N.T. Oxidation of porous HfB₂—SiC ultra-

- high-temperature ceramic materials rich in silicon carbide (65 vol.%) by a supersonic air flow. *Russ. J. Inorg. Chem.* 2020. Vol. 65. No. 4. P. 606—615. DOI: 10.1134/S0036023620040191.
30. Пилиповский Ю.Л., Грудина Т.В., Сапожникова А.Б., Листовничая С.П., Гриффен Л.А., Ступко А.В. Композиционные материалы в машиностроении. Киев: Техника, 1990. *Pilipovskii Yu.L., Grudina T.V., Sapozhnikova A.B., Listovnichaya S.P., Griffen L.A., Stupko A.V.* Composite materials in mechanical engineering. Kiev: Tekhnika, 1990 (In Russ.).
 31. Pezzotti G. Si₃N₄—SiC-platelet composite without sintering aids: a candidate for gas turbine engines. *J. Am. Ceram. Soc.* 1993. Vol. 76. P. 1313—1320. DOI: 10.1002/chin.199330007.
 32. Khajelakzay M., Bakhshi S.R. Optimization of spark plasma sintering parameters of Si₃N₄—SiC composite using response surface methodology (RSM). *Ceram. Int.* 2017. Vol. 43. P. 6815—6821. DOI: 10.1016/j.ceramint.2017.02.099.
 33. Yanai T., Ishizaki K. Mechanical properties of Si₃N₄ ceramics prepared from carbon coated powders. *J. Ceram. Soc. Jpn.* 1993. Vol. 101. P. 764—768. DOI: 10.2109/jcersj.101.764.
 34. Riedel R., Seher M., Becker G. Sintering of amorphous polymer-derived Si, N and C containing composite powders. *J. Eur. Ceram. Soc.* 1989. Vol. 5. P. 113—122. DOI: 10.1016/0955-2219(89)90018-6.
 35. Suri J., Shaw L., Zawrah M.F. Controlling the relative contents of Si₃N₄ and SiC through carbothermic reduction and nitridation of silica fume. *Int. J. Appl. Ceram. Tech.* 2012. Vol. 9. P. 291—303. DOI: 10.1111/j.1744-7402.2011.00710.x.
 36. Hojo J., Meada H., Kato A. Preparation of composite particles of SiC—Si₃N₄ system by vapor reaction method. *Yogyo-Kyokai-Shi.* 1987. Vol. 95. P. 45—49.
 37. Lee H.J., Eguchi K., Yoshida T.J. Preparation of ultrafine silicon nitride, and silicon nitride and silicon carbide mixed powders in a hybrid plasma. *J. Am. Ceram. Soc.* 2005. Vol. 73. P. 3356—3362. DOI: 10.1111/j.1151-2916.1990.tb06461.x.
 38. Yamada O., Hirao K., Koizumi M., Miyamoto Y. Combustion synthesis of silicon carbide in nitrogen atmosphere. *J. Am. Ceram. Soc.* 1989. Vol. 72 (9). P. 1735—38. DOI: 10.1111/j.1151-2916.1989.tb06315.x.
 39. Zeng J., Miyamoto Y., Yamada O. Combustion synthesis of Si₃N₄/SiC composite powders. *J. Am. Ceram. Soc.* 1991. Vol. 74. P. 2197—2200. DOI: 10.1111/J.1151-2916.1991.TB08283.X.
 40. Kata D., Lis J., Pampuch R., Stobierski L. Preparation of fine powders in the Si—C—N system using SHS method. *Int. J. SHS.* 1998. Vol. 7. No. 4. P. 475—485.
 41. Хачатрян Г.Л., Арутюнян А.Б., Харатян С.Л. Активированное горение смеси кремний—углерод в азоте и СВС композиционных керамических порошков Si₃N₄/SiC и карбида кремния. *Физика горения и взрыва.* 2006. Т. 42. No. 5. С. 56—62. *Khachatryan G.L., Arutyunyan A.B., Kharatyan S.L.* Activated combustion of a silicon—carbon mixture in nitrogen and SHS of Si₃N₄—SiC composite ceramic powders and silicon carbide. *Comb. Expl. Shock Waves.* 2006. Vol. 42. No. 5. P. 543—548. DOI: 10.1007/S10573-006-0086-7.
 42. Чухломина Л.Н., Максимов Ю.М., Верещагин В.И. Самораспространяющийся высокотемпературный синтез композиционных нитридсодержащих керамических материалов. Новосибирск: Наука, 2012. *Chukhlomina L.N., Maksimov Yu.M., Vereshchagin V.I.* Self-propagating high-temperature synthesis of composite nitride-containing ceramic materials. Novosibirsk: Nauka, 2012 (In Russ.).
 43. Боровинская И.П., Загоржевский В.В., Игнатьева Т.И., Мержанов А.Г., Савенкова Л.П. Способ получения нитрида кремния с повышенным содержанием альфа-фазы: Пат. 2137708 (РФ). 1998. *Borovinskaya I.P., Zakorzhevskii V.V., Ignat'eva T.I., Merzhanov A.G., Savenkova L.P.* A method for obtaining silicon nitride with an increased alpha-phase content: Pat. 2137708 (RF). 1998.
 44. Загоржевский В.В. Самораспространяющийся высокотемпературный синтез нитридов кремния, алюминия и композиционных порошков на их основе: Дис ... канд. техн. наук. Черногловка: ИСМАН, 2004. *Zakorzhevskii V.V.* Self-propagating high-temperature synthesis of silicon, aluminum nitrides and composite powders based on them: Dissertation of Cand. Sci. (Eng.). Chernogolovka: ISMAN, 2004 (In Russ.).
 45. Титова Ю.В., Амосов А.П., Ермошкин А.А., Марков Ю.М., Хусаинова Т.Н., Попова А.В. Получение нанопорошка

- карбида кремния и композиции на его основе по азидной технологии СВС. *Известия вузов. Порошковая металлургия и функциональные покрытия*. 2013. No. 3. С. 45—51.
- Titova Y.V., Amosov A.P., Ermoshkin A.A., Markov Y.M., Khushainova T.N., Popova A.V. Preparation of silicon-carbide nanopowder and compositions based on it using SHS azide technology. *Russ. J. Non-Ferr. Met.* 2014. Vol. 55. No. 6. P. 620—626. DOI: 10.3103/S1067821214060261.
46. Амосов А.П., Белова Г.С., Тутова Ю.В., Майдан Д.А. Синтез высокодисперсной порошковой керамической композиции Si_3N_4 —SiC при горении компонентов в системе Si—C— NaN_3 — NH_4F . *Журн. неорганической химии*. 2022. Т. 67. No. 2. С. 1—9. DOI: 10.31857/S0044457X22020027.
- Amosov A.P., Belova G.S., Titova Yu.V., Maidan D.A. Synthesis of highly dispersed powder ceramic composition Si_3N_4 —SiC by combustion of components in the Si—C— NaN_3 — NH_4F system. *Rus. J. Inorg. Chem.* 2022. Vol. 67. No. 2. P. 123—130. DOI: 10.1134/S0036023622020024.
47. Непочатов Ю., Земницкая А., Муль П. Разработка керамики на основе нитрида алюминия для изделий электронной техники. *Соврем. электроника*. 2011. No. 9. С. 14—16.
- Nepochatov Yu., Zemnitskaya A., Mul' P. Development of ceramics based on aluminum nitride for electronic products. *Sovremennaya elektronika*. 2011. No. 9. P. 14—16 (In Russ.).
48. Kexin C., Haibo J., Zhou H.P., Ferreira J.M.F. Combustion synthesis of AlN—SiC solid solution particles. *J. Eur. Ceram. Soc.* 2000. Vol. 20. P. 2601—2606. DOI: 10.1016/S0955-2219(00)00119-9.
49. Unni C.K., Gordon D.E. Mechanical properties of monolithic AlN and SiCw/AlN composites. *J. Mater. Sci.* 1995. Vol. 30. P. 1173—1179. DOI: 10.1007/BF00356116.
50. Zangvil A., Ruh R. Phase relationship in the silicon carbide-aluminum nitride system. *J. Am. Ceram. Soc.* 1988. Vol. 71. P. 884—890. DOI: 10.1111/J.1151-2916.1988.TB07541.X.
51. Besisa D.H.A., Ewais E.M.M., Ahmed Ya.M.Z., Elhosiny F.I., Fend T., Kuznetsov D.V. Investigation of microstructure and mechanical strength of SiC/AlN composites processed under different sintering atmospheres. *J. Alloys Compd.* 2018. Vol. 756. P. 175—181. DOI: 10.1016/J.JALLCOM.2018.05.020.
52. Miura M., Yogo T., Hirano S.-I. Phase separation and toughening of SiC—AlN solid-solution ceramics. *J. Mater. Sci.* 1993. Vol. 27. P. 3859—3865. DOI: 10.1007/BF00353191.
53. Besisa D.H.A., Ewais E.M.M., Ahmed Ya.M.Z., Elhosiny F.I., Fend T., Kuznetsov D.V. Thermal shock resistance of pressureless sintered SiC/AlN ceramic composites. *Mater. Res. Express.* 2018. Vol. 5. No. 1. P. 015506. DOI: 10.1088/2053-1591/AAA2C2.
54. Lee R.-R., Wei W.-C. Fabrication, microstructure, and properties of SiC—AlN ceramic alloys. *Ceram. Eng. Sci. Proc.* 1990. Vol. 11 (7/8). P. 1094—1121. DOI: 10.1002/9780470313008.CH39.
55. Gao P., Jia Ch.-Ch., Cao W.-B., Wang C.-C., Liang D., Xu G.-L. Dielectric properties of spark plasma sintered AlN/SiC composite ceramics. *Int. J. Miner. Metall. Mater.* 2014. Vol. 21. No. 6. P. 589—594. DOI: 10.1007/s12613-014-0946-1.
56. Cutler I.B., Miller P.D., Rafaniello W., Park H.K., Thompson D.P., Jack K.H. New materials in the Si—C—Al—O—N and related systems. *Nature*. 1978. Vol. 275. P. 434—435. DOI: 10.1038/275434A0.
57. Teusel I., Rossel C. Pressureless sintering of aluminium nitride/silicon carbide ceramics. *J. Mater. Sci. Lett.* 1992. Vol. 1 (1). P. 205—207. DOI: 10.1007/BF00741422.
58. Ruh R., Zangvil A. Composition and properties of hot-pressed SiC—AlN solid solution. *J. Am. Ceram. Soc.* 1982. Vol. 65. P. 260—265. DOI: 10.1111/J.1151-2916.1982.TB10429.X.
59. Xue H., Munir Z.A. The synthesis of composites and solid solutions of SiC—AlN by field-activated combustion. *Scr. Mater.* 1996. Vol. 35. No. 8. P. 919—982. DOI: 10.1016/1359-6462(96)00246-1.
60. Abbasi Z., Shariat M.H., Javadpour S. Microwave-assisted combustion synthesis of AlN—SiC composites using a solid source of nitrogen. *Powder Technol.* 2013. Vol. 249. P. 181—185. DOI: 10.1016/J.POWTEC.2013.08.012.
61. Borovinskaya I.P., Akopdzhanyan T.G., Chemagina E.A., Sachkova N.V. Solid solution $(\text{AlN})_x(\text{SiC})_{1-x}$ ($x = 0.7$) by SHS under high pressure of nitrogen gas. *Int. J. SHS*. 2018. Vol. 27. No. 1. P. 33—36. DOI: 10.3103/S1061386218010028.
62. Juang R.-C., Chen C.-C., Kuo J.-C., Huang T.-Y., Li Y.-Y. Combustion synthesis of hexagonal AlN—SiC solid solution under low nitrogen pressure. *J. Alloys Compd.* 2009. Vol. 480. P. 928—933. DOI: 10.1016/J.JALLCOM.2009.02.102.

63. Titova Yu.V., Amosov A.P., Maidan D.A., Belova G.S., Minekhanova A.F. Physical and chemical features of combustion synthesis of nanopowder composition AlN—SiC using sodium azide. *AIP Conf. Proc.* 2020. Vol. 2304. Art. 020008. DOI: 10.1063/5.0034318.
64. Amosov A., Smetanin K., Titova Yu., Maidan D. Preparation of ceramic nitride-carbide composition AlN—SiC by SHS method using halide salt and sodium azide. In: *Proc. 7th Intern. Congr. on energy fluxes and radiation effects (EFRE-2020)*. IEEE Xplore. 2020. P. 1110—1114. DOI: 10.1109/EFRE47760.2020.9241986.
65. Лидин Р.А., Молочко В.А., Андреева Л.Л. Химические свойства неорганических веществ. М.: Дрофа, 2007. Lidin R.A., Molochko V.A., Andreeva L.L. Chemical properties of inorganic substances. Moscow: Drofa, 2007 (In Russ.).
66. Titova Y.V., Sholomova A.V., Kuzina A.A., Maidan D.A., Amosov A.P. Azide SHS of aluminum nitride nanopowder and its application for obtaining Al—Cu—AlN cast nanocomposite. *IOP Conf. Ser. Mater. Sci. Eng.* 2016. Vol. 156. Art. 012037. DOI: 10.1088/1757-899X/156/1/012037.
67. Wing Z.N. TiN modified SiC with enhanced strength and electrical properties. *J. Eur. Ceram. Soc.* 2017. Vol. 37. No. 4. P. 1373—1378. DOI: 10.1016/j.jeurceramsoc.2016.11.007.
68. Самсонов Г.В., Виноцкий И.М. Тугоплавкие соединения: Справочник. М.: Metallurgiya, 1976. Samsonov G.V., Vinitskii I.M. Refractory compounds: Handbook. Moscow: Metallurgiya, 1976 (In Russ.).
69. Лысенков А.С., Ким К.А., Каргин Ю.Ф., Фролова М.Г., Титов Д.Д., Ивичева С.Н., Овсянников Н.А., Коновалов А.А., Перевилов С.Н. Композиты Si₃N₄—TiN, полученные горячим прессованием порошков нитрида кремния и титана. *Неорган. материалы*. 2020. Т. 56. No. 3. С. 324—328. DOI: 10.31857/S0002337X20030112. Lysenkov A.S., Kim K.A., Kargin Yu.F., Frolova M.G., Titov D.D., Ivicheva S.N., Ovsyannikov N.A., Konovalov A.A., Perevislov S.N. Si₃N₄—TiN composites obtained by hot pressing of silicon and titanium nitride powders. *Inorg. Mater.* 2020. Vol. 56. No. 3. P. 324—328.
70. Самсонов Г.В., Кулик О.П., Полищук В.С. Получение и методы анализа нитридов. Киев: Наук. думка, 1978. Samsonov G.V., Kulik O.P., Polishchuk V.S. Obtaining and methods of analysis of nitrides. Kiev: Naukova Dumka, 1978 (In Russ.).
71. Kiesler D., Bastuck T., Theissmann R., Kruis F.E. Plasma synthesis of titanium nitride, carbide and carbonitride nanoparticles by means of reactive anodic arc evaporation from solid titanium. *J. Nanopart. Res.* 2015. Vol. 17. Art. 152. DOI: 10.1007/s11051-015-2967-8.
72. Dekker J.P., Van der Put P.J., Veringa H.J., Schoonman J. Vapor-phase synthesis of titanium nitride powder. *J. Mater. Chem.* 1994. Vol. 4. No. 5. P. 689—694. DOI: 10.1039/JM9940400689.
73. Шиганова Л.А., Бичуров Г.В., Амосов А.П., Титова Ю.В., Ермошкин А.А., Бичурова П.Г. Самораспространяющийся высокотемпературный синтез наноструктурированного порошка нитрида титана с использованием азиды натрия и галоидной титаносодержащей соли. *Известия вузов. Порошковая металлургия и функциональные покрытия*. 2010. No. 1. С. 18—22. Shiganova L.A., Bichurov G.V., Amosov A.P., Titova Yu.V., Ermoshkin A.A., Bichurova P.G. The self-propagating high-temperature synthesis of a nanostructured titanium nitride powder with the use of sodium azide and haloid titanium containing salt. *Russ. J. Non-Ferr. Met.* 2011. Vol. 52. No. 1. P. 91—95. DOI: 10.3103/S1067821211010238.
74. Загоржевский В.В. Разработка СВС-технологий порошков нитридов Al, Si, Zr, Ti и композиций на их основе: Дис. ... докт. техн. наук. Черноголовка: ИСМАН, 2022. Zakorzhnevsky V.V. Development of SHS technologies for Al, Si, Zr, Ti nitride powders and compositions based on them: Dissertation of Dr. Sci. (Eng.). Chernogolovka: ISMAN, 2022 (In Russ.).
75. Guo X., Yang H., Zhang L., Zhu X. Sintering behavior, microstructure and mechanical properties of silicon carbide ceramics containing different nano-TiN additive. *Ceram. Int.* 2010. Vol. 36. Iss. 1. P. 161—165. DOI: 10.1016/j.ceramint.2009.07.013.
76. Zhang L., Yang H., Guo X., Shen J., Zhu X. Preparation and properties of silicon carbide ceramics enhanced by TiN nanoparticles and SiC whiskers. *Scr. Mater.* 2011. Vol. 65. No. 3. P. 186—189. DOI: 10.1016/j.scriptamat.2011.03.034.
77. Леонов А.В., Севостьянов М.А., Лысенков А.С., Царева А.М., Насакина Е.О., Баукин А.С., Сергиенко К.В., Колмаков А.Г., Опарина И.Б. Способ получения композиционного материала SiC—TiN: Пат. 2681332 (РФ). 2019. Leonov A.V., Sevost'yanov M.A., Lysenkov A.S., Tsareva A.M.,

- Nasakina E.O., Baikin A.S., Sergienko K.V., Kolmakov A.G., Oparina I.B.* Method of obtaining SiC—TiN composite material: Pat. 2681332 (RF). 2019 (In Russ.).
78. *Han J.-C., Chen G.-Q., Du S.-Y., Wood J.V.* Synthesis of Si₃N₄—TiN—SiC composites by combustion reaction under high nitrogen pressures. *J. Eur. Ceram. Soc.* 2000. Vol. 20. No. 7. P. 927—932. DOI: 10.1016/S0955-2219(99)00230-7.
79. *Титова Ю.В., Амосов А.П., Майдан Д.А., Белова Г.С., Минеханова А.Ф.* Азидный самораспространяющийся высокотемпературный синтез высокодисперсных керамических нитридно-карбидных порошковых композиций TiN—SiC. *Известия вузов. Порошковая металлургия и функциональные покрытия.* 2022. Т. 16. No. 2. С. 22—37.
- Titova Yu.V., Amosov A.P., Maidan D.A., Belova G.S., Minekhanova A.F.* Azide self-propagating high-temperature synthesis of highly dispersed ceramic nitride-carbide powder compositions TiN—SiC. *Izvestiya Vuzov. Poroshkovaya Metallurgiya i Funktsional'nye Pokrytiya* (*Powder Metallurgy and Functional Coatings*). 2022. Vol. 16. No. 2. P. 22—37 (In Russ.).
80. *Manukyan K.V., Kharatyan S.L., Blugan G., Kuebler J.* Combustion synthesis and compaction of Si₃N₄/TiN composite powder. *Ceram. Int.* 2007. Vol. 33. Iss. 3. P. 379—383. DOI: 10.1016/j.ceramint.2005.10.006.
81. *Воротыло С., Левашов Е.А., Потанин А.Ю., Логинов П.А., Швындина Н.В.* Особенности синтеза керамических композитов, дискретно армированных углеродными волокнами и формирующимися в волне горения *in situ* волокнами карбида кремния. *Известия вузов. Порошковая металлургия и функциональные покрытия.* 2020. No. 1. С. 41—54. DOI: 10.17073/1997-308X-2020-41-54.
- Vorotilo S., Levashov E.A., Potanin A.Yu., Loginov P.A., Shvyndina N.V.* Features of synthesizing ceramic composites discretely reinforced by carbon fibers and SiC nanowires formed *in situ* in the combustion wave. *Russ. J. Non-Ferr. Met.* 2020. Vol. 61. No. 5. P. 559—570. DOI: 10.3103/S1067821220050168.

UDC 536.46

DOI dx.doi.org/10.17073/1997-308X-2022-4-58-66

Features of SHS of multicomponent carbides

© 2022 г. **N.A. Kochetov, I.D. Kovalev**

Merzhanov Institute of Structural Macrokinetics and Materials Science of the Russian Academy of Sciences (ISMAN), Chernogolovka, Russia

Received 14.04.2022, revised 14.07.2022, accepted for publication 18.07.2022

Abstract: Combustion of powders of transition metals of titanium PTS (average particle size 57 μm), zirconium PCRK-1 (12 μm), tantalum Ta PM-3 (8 μm), hafnium GFM-1 (4 μm), niobium NBP-1a (21 μm) with carbon black grade P-803 dispersion 1–2 μm was studied. The combustion process of the compressed samples (mass 2.5–6.9 g, height 1.2–1.7 cm, relative density 0.55–0.61) was performed in an inert argon medium at a pressure of 760 mmHg in the constant pressure chamber. Combinations were studied, Me1 + Me2 + Me3 + Me4 + 4C, Me1 + Me2 + Me3 + Me4 + Me5 + 5C. XRD patterns of the mixtures were recorded on a DRON-3M diffractometer ($\text{CuK}\alpha$ -radiation). Combustion product sections were studied using a LEO 1450 VP scanning electron microscope (Carl Zeiss, Germany). The fractional composition and particle size distribution of the mixture were determined according to standard procedure using a Microsizer-201C laser particle size analyzer. Combustion velocity, elongation of samples, phase composition of products were determined. The maximum combustion temperature of the mixture (Ti + Hf + Zr + Nb + Ta) + 5C was measured experimentally for the first time. The morphology and microstructure of the reaction products were also observed. Combustion products of mixtures (Ti + Zr + Nb + Ta) + 4C and (Ti + Zr + Nb + Hf) + 4C contain high entropy carbides, which are solid solutions with the same structural type B1 (space group Fm-3m) and having different cell parameters. Product samples of mixtures (Ti + Zr + Hf + Ta) + 4C and (Ti + Hf + Zr + Nb + Ta) + 5C contain high entropy and medium entropy carbides, also representing solid solutions with the same structural type B1 (space group Fm-3m). The results of this work can be used in the production of high-entropy and medium-entropy multicomponent carbides.

Keywords: SHS, combustion, high-entropy multicomponent carbides, medium entropy carbides, high-entropy ceramics, transition metals, refractory metals.

Kochetov N.A. — Cand. Sci. (Phys.-Math.), senior researcher of the Laboratory of dynamics of microheterogeneous processes of Merzhanov Institute of Structural Macrokinetics and Materials Science of the Russian Academy of Sciences (ISMAN) (142432, Russia, Moscow region, Noginsk district, Chernogolovka, Academician Osip'yan str., 8).
E-mail: kolyan_kochetov@mail.ru.

Kovalev I.D. — Cand. Sci. (Phys.-Math.), researcher of the Laboratory of X-ray investigation, ISMAN.
E-mail: i2212@yandex.ru.

For citation: Kochetov N.A., Kovalev I.D. Features of SHS of multicomponent carbides. *Izvestiya Vuzov. Poroshkovaya Metallurgiya i Funktsional'nye Pokrytiya (Powder Metallurgy and Functional Coatings)*. 2022. Vol. 16. No. 4. P. 58–66 (In Russ.). DOI: dx.doi.org/10.17073/1997-308X-2022-4-58-66.

Особенности СВС многокомпонентных карбидов

Н.А. Кочетов, И.Д. Ковалев

Институт структурной макрокинетики и проблем материаловедения им. А.Г. Мерджанова РАН (ИСМАН), г. Черноголовка, Россия

Статья поступила в редакцию 14.04.22 г., доработана 14.07.22 г., подписана в печать 18.07.22 г.

Аннотация: Изучено горение порошков переходных металлов: титана марки ПТС (средний размер частиц 57 мкм), циркония ПЦРК-1 (12 мкм), тантала Та ПМ-3 (8 мкм), гафния ГФМ-1 (4 мкм), ниобия НБП-1а (21 мкм) — с сажей марки П-803 дисперсностью 1–2 мкм. Процесс горения спрессованных образцов (масса 2,5–6,9 г, высота 1,2–1,7 см, относительная плотность 0,55–0,61) осуществляли в инертной среде аргона при давлении 760 мм рт. ст. в камере постоянного давления. Исследовали комбинации Me1 + Me2 + Me3 + Me4 + 4C и Me1 + Me2 + Me3 + Me4 + Me5 + 5C. Рентгенограммы смесей регистрировали на дифрактометре «Дрон-3М» ($\text{CuK}\alpha$ -излучение). Шлифы продуктов горения изучали на сканирующем электронном микроскопе LEO 1450 VP (Carl Zeiss, Германия). Фракционный состав и распределение частиц смеси по размеру устанавливали по стандартной методике на лазерном анализаторе размера частиц «Микросайзер-201С» (РФ). Определяли скорость горения, удлинение образцов, фазовый состав продуктов. Впервые экспериментально измерена максималь-

ная температура горения смеси (Ti + Hf + Zr + Nb + Ta) + 5C. Также наблюдали за морфологией и микроструктурой продуктов реакции. Продукты горения смесей (Ti + Zr + Nb + Ta) + 4C и (Ti + Zr + Nb + Hf) + 4C содержат высокоэнтропийные карбиды, представляющие собой твердые растворы с одинаковым структурным типом B1 (пространственная группа Fm-3m) и обладающие различными параметрами ячейки. Образцы продуктов смесей (Ti + Zr + Hf + Ta) + 4C и (Ti + Hf + Zr + Nb + Ta) + 5C содержат в составе высокоэнтропийные и среднеэнтропийные карбиды, также представляющие собой твердые растворы с одинаковым структурным типом B1 (пространственная группа Fm-3m). Результаты данной работы могут найти применение при получении высокоэнтропийных и среднеэнтропийных многокомпонентных карбидов.

Ключевые слова: СВС, горение, высокоэнтропийные многокомпонентные карбиды, среднеэнтропийные карбиды, высокоэнтропийная керамика, переходные металлы, тугоплавкие металлы.

Кочетов Н.А. — канд. физ.-мат. наук, ст. науч. сотр. лаборатории динамики микрогетерогенных процессов ИСМАН (142432, Московская обл, Ногинский р-н, г. Черноголовка, ул. Академика Осипьяна, 8). E-mail: kolyan_kochetov@mail.ru.

Ковалев И.Д. — канд. физ.-мат. наук, науч. сотр. лаборатории рентгеноструктурных исследований ИСМАН. E-mail: i2212@yandex.ru.

Для цитирования: Кочетов Н.А., Ковалев И.Д. Особенности СВС многокомпонентных карбидов. *Известия вузов. Порошковая металлургия и функциональные покрытия.* 2022. Т. 16. No. 4. С. 58—66.
DOI: dx.doi.org/10.17073/1997-308X-2022-4-58-66.

Introduction

The combustion of transition metals with carbon was the subject of scientific research as recently as several decades ago [1—5].

Self-propagating high-temperature synthesis (SHS) in Zr + C, Ta + C and Hf + C systems was first implemented by A.G. Merzhanov and I.P. Borovinskaya [1].

In work [2], it has been demonstrated that the combustion process in Nb + C system is initiated in a much more complicated way compared to Zr + C system, and the combustion limit for Nb in Nb + Zr + C system was 0.7 at. fr. Upon a higher content of niobium, the samples did not flare up at any concentration of carbon. It is noted by the authors [3] that the combustion parameters of Zr + C system depend heavily on the grade of powders being used. In work [4], the substantial impact of impurity gas release on the combustion of Ta + C system was established, which is expressed in the dependence of the combustion rate on the pressure of inert gas, as well as in the elongation and delamination of the sample during combustion. Besides, the combustion at a sample diameter of $d > 1$ cm was implemented successfully [4]. There was no combustion in Ta + C system at $d \leq 1$ cm. The considerable elongation of the compressed samples of Ti + C mixture during combustion was also noted earlier [5]. In work [6], it is mentioned that combustion in Ta + C system is possible at temperatures below the melting temperature, upon which it is necessary to use metal powders with a submicron particle size. The authors [7, 8] determined the influence of the particle size of the titanium powder used on the combustion rate of samples made from a Ti + C mixture.

The synthesis and study of the properties of high-entropy alloys (HEAs), which represent a new class of metallic materials, have been a popular and promising line of scientific research in recent times. HEAs include compounds containing several (usually 5) metals and forming a single-phase solid solution [9]. The works devoted to the production and study of medium entropy alloys, containing 3 metals, appear [10]. The mechanical properties of medium entropy alloys can exceed the properties of HEAs [11, 12].

The works devoted to the production of high-entropy ceramics [13, 14] and, in particular, high-entropy carbides (HECs) [15—21] have been published relatively recently. HECs were obtained by mechanical alloying in ball mills and spark plasma sintering.

The combustion of powders of transition metals with carbon black in Me1 + Me2 + Me3 + Me4 + 4C (4 metals with carbon, 5 combinations) and Me1 + Me2 + Me3 + Me4 + Me5 + 5C (5 metals with carbon, 1 combination) combinations, where Me_i is Ti, Hf, Nb, Zr, Ta, was studied. The objective of obtaining a high-entropy metal carbide by using SHS was set.

Research methods

The powders of titanium PTS (average particle size 57 μm), zirconium PCRK-1 (12 μm), tantalum Ta PM-3 (8 μm), hafnium GFM-1 (4 μm), niobium NBP-1a (21 μm) and carbon black grade P-803 dispersion 1—2 μm were used as initial materials. The X-ray phase analysis (XRD) of initial metals revealed that all powders are single-phase, except for Hf, which exhibits HfH_{1.63} phase impurity.

The initial powders were thoroughly mixed in a porcelain mortar in the required weight proportions for the purpose of obtaining Me + C mixtures. Me1 + Me2 + Me3 + Me4 + 4C (4 metals with carbon, 5 combinations) and Me1 + Me2 + Me3 + Me4 + Me5 + 5C (5 metals with carbon, 1 combination) mixtures, where Me_i is Ti, Hf, Nb, Zr, Ta, were mixed in a ball mill for 2 h.

The combustion process of the compressed samples (mass 2.5–6.9 g, height 1.2–1.7 cm, relative density 0.55–0.61) was carried out in an inert argon medium at a pressure of 760 mmHg in a constant pressure chamber [22]. The process was recorded on the camera through a viewing glass. The combustion of samples was initiated from the upper end with an ignite tablet consisting of Ti + 2B by means of heated tungsten coil, which ensured stable ignition conditions. Upon stop motion viewing of video records, the combustion rate of the samples was determined. The maximum combustion temperature was measured with a tungsten-rhenium thermocouple.

The measurements of combustion rate, maximum combustion temperature and relative elongation of the samples had an error within 10 %.

Thermodynamic calculations were performed

using THERMO software — <http://www.ism.ac.ru/thermo/>.

Combustion product sections were studied using a LEO 1450 VP scanning electron microscope (Carl Zeiss, Germany). To obtain the sections, combustion product powders were impregnated with epoxy resin diluted with acetone to reduce viscosity. Metallographic sections were made after the resin hardened.

The X-ray phase analysis (XRD) of initial powders and combustion products was performed with DRONE-3M diffractometer (the RF) upon copper radiation being in the range of angles 2θ from 20 to 80°. The obtained data were analyzed using PDF-2 database [14].

The fractional composition and particle size distribution of the mixture were determined according to a standard procedure using a Microsizer-201C laser particle size analyzer (the RF). The measurement error did not exceed 1.2 %.

Results and discussions

The values of combustion rates, elongation of samples during the SHS, as well as the phase composition of the products of synthesis of metal powders with carbon black in various combinations are provided in the table.

Combustion rate, elongation of samples, phase composition of products, and adiabatic temperature of SHS of metal powders with carbon black

Скорость горения, удлинение образцов, фазовый состав продуктов и адиабатическая температура СВС порошков металлов с сажей

System	Combustion rate, cm/s	Composition of the products	Elongation of the sample during combustion, %	Adiabatic combustion temperature, K
Ti + C	1.3	TiC	94	3289
Ta + C				2721
Hf + C				3899
Zr + C	1.0	ZrC	224	3777
Nb + C				2835
(Ti + Hf + Zr + Nb + Ta) + 5C	0.24	[Ti,Hf,Zr,Nb,Ta]C, [Ti,Hf,Zr,Ta]C, [Ti,Hf,Ta]C	181	3290
(Ti + Zr + Nb + Ta) + 4C	0.35	[Ti,Zr,Nb,Ta]C	96	3180
(Ti + Zr + Nb + Hf) + 4C	0.35	[Ti,Hf,Zr,Nb]C	331	3309
(Ta + Hf + Zr + Nb) + 4C				3360
(Ti + Hf + Nb + Ta) + 4C				3286
(Ti + Zr + Hf + Ta) + 4C	0.55	[Ti,Hf,Zr,Ta]C, [Ti,Hf,Ta]C	213	3290

Among Me + C systems, the SHS without preheating was initiated in samples compressed from Ti + C and Zr + C mixtures. Samples of other mixtures (Nb + C, Hf + C, Ta + C) did not burn at room temperature under the present experimental conditions (the component particle size and the sample size). The values of the combustion rates of samples of Ti + C and Zr + C mixtures appeared to be close to: 1.3 and 1.0 cm/s (see the table). Due to the release of impurity gas, the samples often elongate during the combustion [23, 24]. The samples of Zr + C mixture elongated significantly compared with the samples of Ti + C mixture (for comparison, 224 and 94 %, respectively), which is similar to the results obtained earlier upon the combustion of mixtures of Zr and Ti powders with boron [14]. According to XPhA results, the combustion products of Me + C systems exhibited the reflections of the only carbide phase MeC (ZrC and TiC, respectively).

Among the mixtures containing 4 metals with carbon (where Me is Ti, Hf, Nb, Zr, Ta), the combustion process without preheating was successfully conducted (and the sample burned completely) in the systems containing Ti and Zr, i.e. (Ti + Zr + Nb + Ta) + 4C, (Ti + Zr + Nb + Hf) + 4C, (Ti + Zr + Hf + Ta) + 4C.

The combustion of samples compressed from (Ti + Hf + Nb + Ta) + 4C mixture could not be initiated without preheating. The samples of (Ta + Hf + Zr + Nb) + 4C mixture did not burn out completely. The design adiabatic combustion temperature of the compositions varied in the range of 3180 to 3360 K. Upon that, the samples of (Ti + Zr + Hf + Ta) + 4C mixture appeared to be the fastest burning ones as their combustion rate was 0.55 cm/s. The samples of (Ti + Zr + Nb + Ta) + 4C and (Ti + Zr + Nb + Hf) + 4C mixtures had the same combustion rate of 0.35 cm/s.

According to XRD results, the products of synthesis of (Ti + Zr + Nb + Ta) + 4C and (Ti + Zr + Nb + Hf) + 4C slow burning systems contain 3 carbide phases based on solid solutions with the same structural type B1 (spatial group Fm-3m), having different cell parameters (Fig. 1).

Phase 1 is the closest to HfC, phase 2 is the closest to ZrC, phase 3 is the closest to NbC or TaC in cell parameter (see below). The combustion products of the faster burning system (Ti + Zr + Hf + Ta) + 4C already contain 4 carbide phases, are distinguished by their cell parameters (see Fig. 1), where phase 4 is the closest to phase TaTiC₂ by its cell parameter. Below are the unit cell parameters of the synthesized

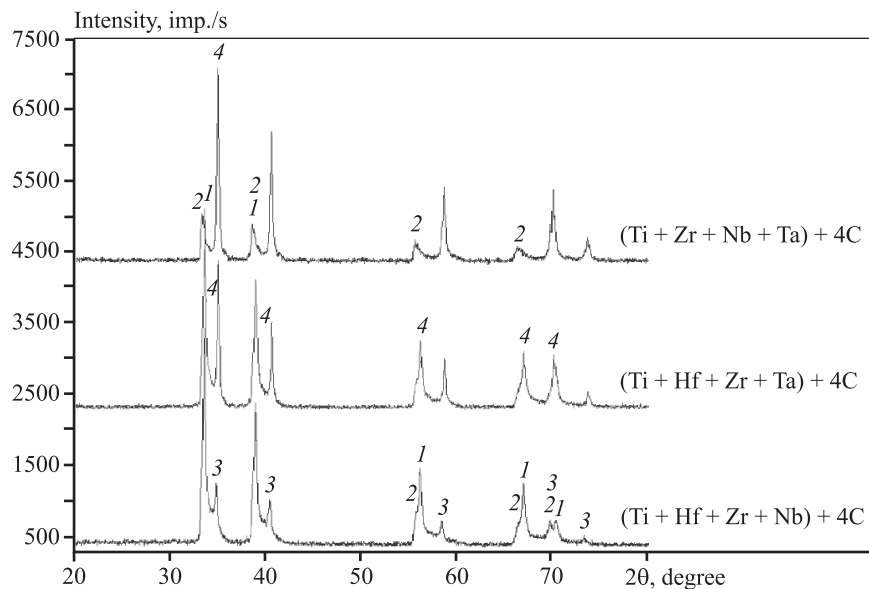


Fig. 1. XRD patterns of products of synthesis of Me₁ + Me₂ + Me₃ + Me₄ + 4C mixtures (where Me is Ti, Ta, Zr, Hf, Nb)

1–4 — FCC phases; a , Å = 4.6360 (1), 4.6737 (2), 4.4748 (3), 4.4526 (4)

Рис. 1. Рентгенограммы продуктов синтеза смесей Me₁ + Me₂ + Me₃ + Me₄ + 4C (Me — Ti, Ta, Zr, Hf, Nb)

1–4 — ГЦК-фазы; a , Å = 4,6360 (1), 4,6737 (2), 4,4748 (3), 4,4526 (4)

solid solutions and the cell parameters of monocarbides (a), Å:

NbC	4.4698
HfC	4.6377
ZrC	4.6930
TaC	4.4547
TiC	4.3274
Phase 1	4.6360
Phase 2	4.6737
Phase 3	4.4748
Phase 4	4.4526

To identify metals in carbide phases, sections were made of product samples and local elemental analysis was performed (Fig. 2). According to XPhA and elemental analysis results, the combustion products of

(Ti + Zr + Nb + Ta) + 4C and (Ti + Zr + Nb + Hf) + 4C slow-burning systems contain the phases of high-entropy carbides ([Ti,Zr,Nb,Ta]C and [Ti,Hf,Zr,Nb]C, respectively), differing in the ratio of components (Fig. 2, a, b). The products of a faster burning system (Ti + Zr + Hf + Ta) + 4C include medium entropy carbides [Ti,Hf,Ta]C, containing 3 metals (Fig. 2, c), along with high-entropy carbides [Ti,Hf,Zr,Ta]C.

It appears that considerably high combustion rate of the sample made of (Ti + Zr + Hf + Ta) + 4C mixture (0.55 cm/s) and its small size result in a lack of time for the homogenization of the product.

Similar to the samples of Me + C mixtures, the samples made of Me1 + Me2 + Me3 + Me4 + 4C mixtures grew during combustion and dispersed into separate fragments due to impurity gas release. Upon that, the minimum elongation was observed during the combustion of samples made of a mixture without haf-

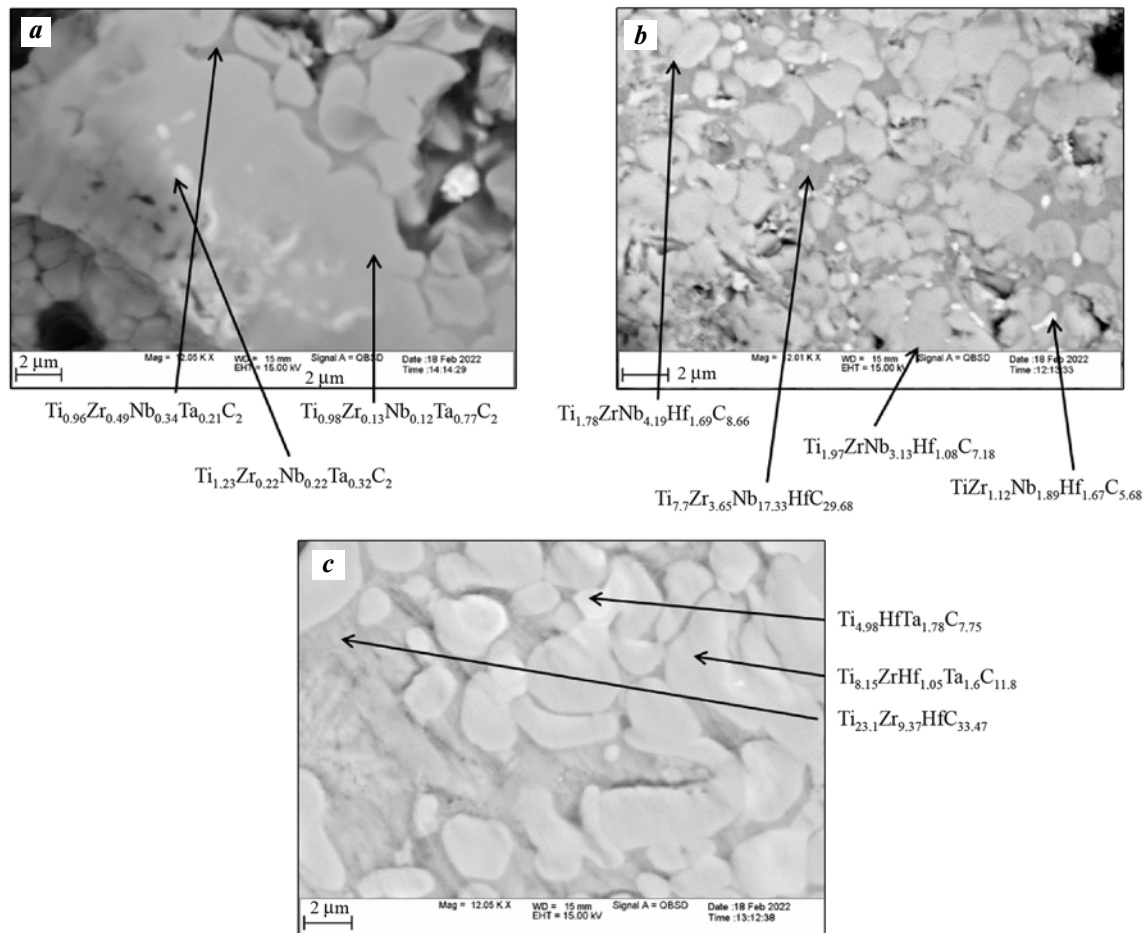


Fig. 2. Microstructure of combustion products of samples of Ti + Zr + Nb + Ta + 4C (a), Ti + Hf + Zr + Nb + 4C (b) and Ti + Zr + Hf + Ta + 4C (c) mixtures

Рис. 2. Микроструктура продуктов горения образцов из смесей Ti + Zr + Nb + Ta + 4C (a), Ti + Hf + Zr + Nb + 4C (b) и Ti + Zr + Hf + Ta + 4C (c)

niium — (Ti + Zr + Nb + Ta) + 4C, i.e. 96 % (see the table). The samples made of mixtures containing hafnium ((Ti + Zr + Nb + Hf) + 4C and (Ti + Zr + Hf + Ta) + 4C) elongated much more, namely 331 and 213 %, respectively. This suggests that hafnium, containing hydride $\text{HfH}_{1.63}$, results in an increase in impurity gas release during the combustion of samples.

The photograph of the microstructure of the combustion products of Ti + Hf + Zr + Nb + 4C mixture, as well as the element distribution map are presented in Fig. 3. One can see that all the elements contained in the product are quite uniformly distributed over the cross-sectional area of the section.

Combustion of Me1 + Me2 + Me3 + Me4 + Me5 + 5C mixture

The sample made of (Ti + Hf + Zr + Nb + Ta) + 5C mixture burned out completely without preheating. Upon that, its combustion rate appeared to be lower than the one of burned samples made of Me + C and Me1 + Me2 + Me3 + Me4 + 4C mixtures and amounted to only 0.24 cm/s. The design adiabatic combustion temperature of (Ti + Hf + Zr + Nb + Ta) + 5C mixture

amounted to $T_{ad} = 3290$ K, which coincides with T_{ad} for the fastest burning mixture of 4 metals with carbon (Ti + Zr + Hf + Ta) + 4C (see the table).

According to XPhA results, the composition of combustion products of (Ti + Hf + Zr + Nb + Ta) + 5C mixture, exhibit three carbide phases based on solid solutions with the same structural type B1 (spatial group Fm3m), having different cell parameters (Fig. 4), in the same way as for mixtures of 4 metals with carbon. The first phase is the closest to HfC, the second phase is the closest to ZrC, and the third phase is the closest to NbC or TaC in cell parameter (the same has been specified above).

The elemental analysis of sections of combustion products allowed to identify these carbide phases (Fig. 5). They turned out to be high-entropy carbide [Ti,Hf,Zr,Ta]C, containing 4 metals, and medium entropy carbide [Ti,Hf,Ta]C, containing 3 metals, there are also the traces of high-entropy carbide [Ti,Hf, Zr,Nb,Ta]C, including all 5 metals.

Similar to the samples of previous systems (containing 1 or 4 metals), a sample made of (Ti + Hf + Zr + Nb + Ta) + 5C mixture significantly elongated and dispersed into separate fragments during combustion. The relative elongation of the sample accounted for 181 %,

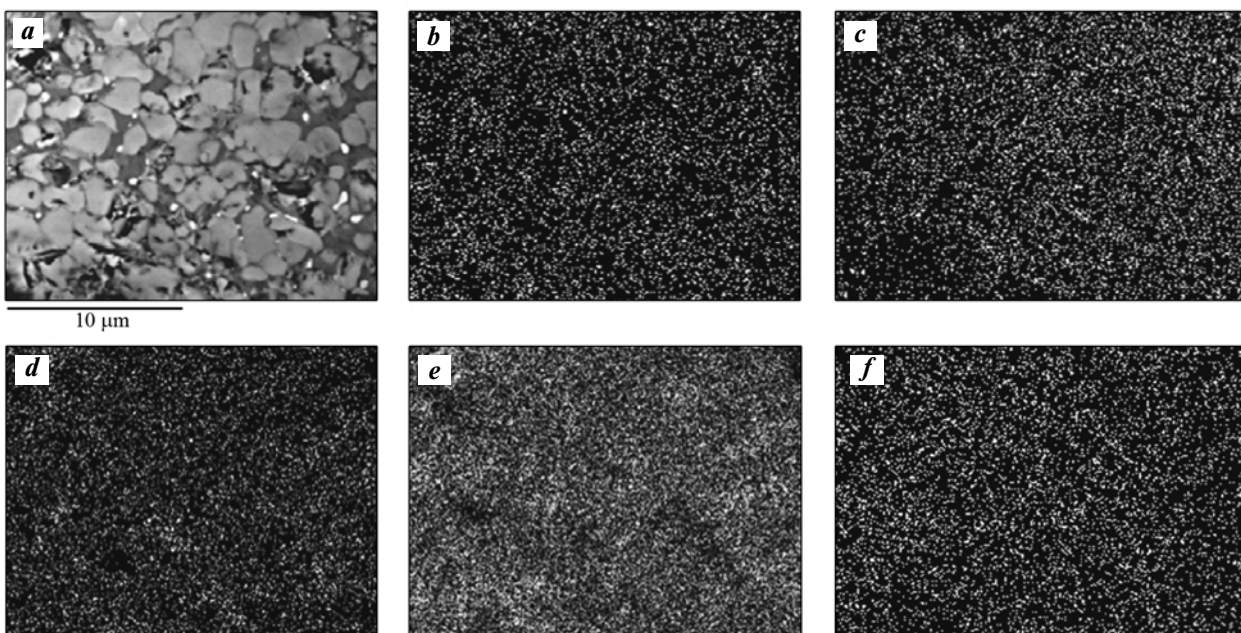


Fig. 3. Microstructure of combustion products of Ti + Hf + Zr + Nb + 4C mixture (*a*) and element distribution map (*b–f*)
b – C, *c* – Ti, *d* – Zr, *e* – Nb, *f* – Hf

Рис. 3. Микроструктура продуктов горения смеси Ti + Hf + Zr + Nb + 4C (*a*) и карта распределения элементов (*b–f*)
b – C, *c* – Ti, *d* – Zr, *e* – Nb, *f* – Hf

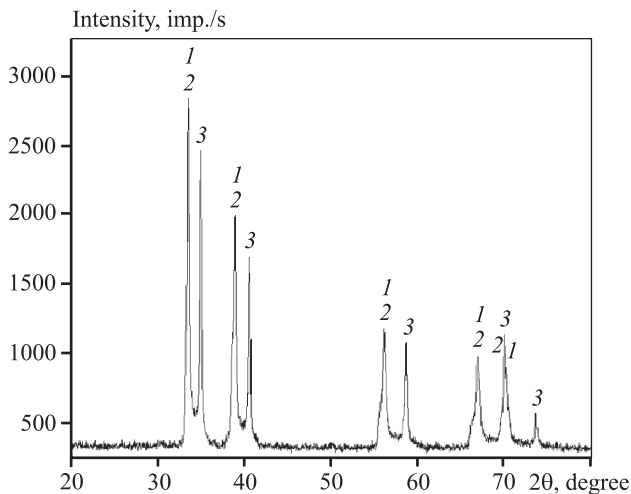


Fig. 4. XRD of products of synthesis of Me1 + Me2 + Me3 + Me4 + Me5 + 5C mixture (where Me is Ti, Ta, Zr, Hf, Nb)
 1–3 – FCC phases; a , Å = 4.6360 (1), 4.6737 (2), 4.4748 (3)

Рис. 4. Рентгенограмма продуктов синтеза смеси Me1 + Me2 + Me3 + Me4 + Me5 + 5C (Me – Ti, Ta, Zr, Hf, Nb)
 1–3 – ГЦК-фазы; a , Å = 4,6360 (1), 4,6737 (2), 4,4748 (3)

which falls within the interval between maximum and minimum elongation values for the studied systems containing 1 or 4 metals.

Considerable elongation of the sample during combustion made it difficult to determine maximum combustion temperature by means of a thermocouple. To measure the maximum combustion temperature, experiments were carried out on the combustion of compressed samples. The sample was pre-compressed, and

that limited its elongation. As a result, it decreased by an order of magnitude (15 %) that allowed to measure the maximum combustion temperature, the value of which was 1950 °C. The measured maximum combustion temperature appeared to be significantly lower than the design adiabatic one, probably due to the fact that the heat loss is not taken into account during the calculation. At such a combustion temperature, only two of five initial metals (Ti and Zr) melt in the combustion wave. The rest of the metals (Hf, Nb, Ta) have a melting temperature higher than the experimentally measured maximum combustion temperature of (Ti + Hf + Zr + Nb + Ta) + 5C mixture, below are the melting temperatures of the components of the mixture, °C:

Zr	1855
Ti.....	1668
Hf.....	2227
Nb.....	2468
Ta	3017

Furthermore, the compression of the sample and a decrease by an order of magnitude of its growth resulted in a combustion rate increase by a several-fold factor, namely from 2.4 to 8.8 mm/s, which correlates well with a pioneer work on the study of the compression of samples by combustion rate [25]. As it is shown in works [23, 24], the elongation of the sample during combustion occurs behind the combustion front due to impurity gas release. In the case of compression of the sample, hindering its elongation, the pressure of these gases, being released behind the front during combustion, increases. According to the findings of the con-

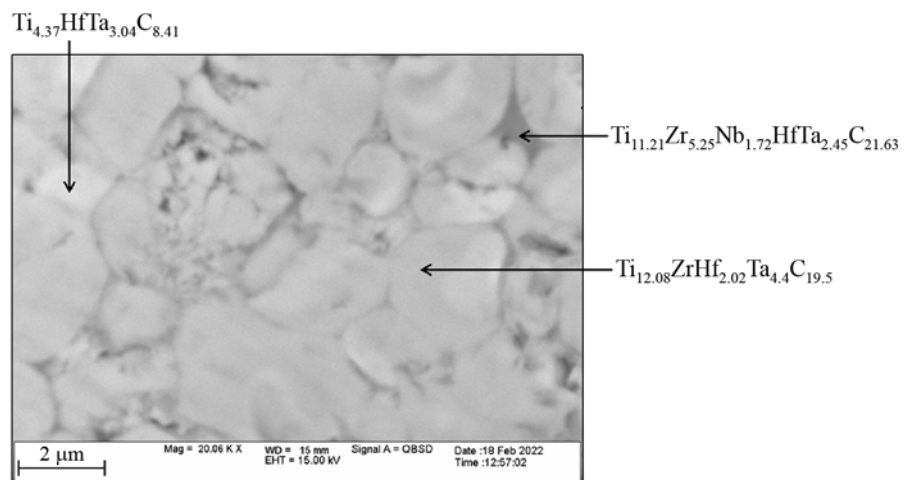


Fig. 5. Microstructure of combustion products of the sample made of Ti + Zr + Nb + Ta + Hf + 5C mixture

Рис. 5. Микроструктура продуктов горения образца из смеси Ti + Zr + Nb + Ta + Hf + 5C

vective-conductive combustion model, this results in an increase in the propagation velocity of the combustion front [26].

It is further planned to obtain compact samples of high-entropy carbides from the combustion products of mixtures of 4 metals with carbon and 5 metals with carbon by SPS method.

Conclusion

The combustion and composition of the products of Me + C, Me₁ + Me₂ + Me₃ + Me₄ + 4C (4 metals with carbon in 5 combinations) and Me₁ + Me₂ + Me₃ + Me₄ + Me₅ + 5C (5 metals with carbon, 1 combination) mixtures, where Me_i is Ti, Hf, Nb, Zr, Ta, were studied.

Multicomponent carbides, belonging to the class of high-entropy compounds, were synthesized in the combustion mode.

Among the mixtures of 4 metals with carbon, combustion was achieved in the samples containing Ti and Zr.

The measured maximum combustion temperature of (Ti + Hf + Zr + Nb + Ta) + 5C mixture was 1950 °C.

The conclusions of the work can be used in obtaining new materials such as high-entropy and medium entropy carbides.

Acknowledgments: This work was supported by a grant from the Russian Science Foundation (Project No. 20-13-00277).

The authors are grateful to N.I. Mukhina, S.G. Vadchenko, M.L. Busurina for their assistance in experiments and to A.S. Rogachev, D.Yu. Kovalev and B.S. Seplyarskii for the discussion.

Работа выполнена за счет гранта Российского научного фонда (проект № 20-13-00277).

Авторы благодарны Н.И. Мухиной, С.Г. Вадченко, М.Л. Бусуриной за помощь в экспериментах и А.С. Рогачеву, Д.Ю. Ковалеву и Б.С. Сеплярскому за обсуждение.

References

1. Мержанов А.Г., Боровинская И.П. Самораспространяющийся высокотемпературный синтез тугоплавких неорганических соединений. *ДАН СССР*. 1972. Т. 204. No 2. С. 366—369.
Merzhanov A.G., Borovinskaya I.P. Self-spreading high-temperature synthesis of refractory compounds. *Dokl. Chem.* 1972. Vol. 204. No. 2. P. 429—431.
2. Агаджанян Н.Н., Долуханян С.К. Влияние реакционной среды на процесс горения системы Zr—Nb—C *Физика горения и взрыва*. 1996. Т. 32. No. 2. С. 31—37.
Agadzhanyan N.N., Dolukhanyan S.K. Effects of reaction medium on combustion of the Zr—Nb—C system. *Combust. Explos. Shock Waves*. 1996. Vol. 32. No. 2. P. 145—150. <https://doi.org/10.1007/BF02097083>.
3. Епишин К.Л., Пютюлин А.Н. Влияние некоторых параметров на горение системы Zr + C. *Физика горения и взрыва*. 1991. Т. 27. No. 4. С. 27—30.
Epishin K.L., Pityulin A.N. Effect of certain parameters on combustion of zirconium and carbon. *Combust. Explos. Shock Waves*. 1991. Vol. 27. No. 4. P. 415—418. <https://doi.org/10.1007/BF00789549>.
4. Шкиро В.М., Нерсисян Г.А., Боровинская И.П. Исследование закономерностей горения смесей тантала с углеродом. *Физика горения и взрыва*. 1978. Т. 14. No. 4. С. 58—64.
Shkiro V.M., Nersisyan G.A., Borovinskaya I.P. Principles of combustion of tantalum-carbon mixtures. *Combust. Explos. Shock Waves*. 1978. Vol. 14. No. 4. P. 455—460. <https://doi.org/10.1007/BF00742950>.
5. Курдяшкин А.И., Максимов Ю.М., Некрасов Е.А. О механизме взаимодействия титана с углеродом в волне горения. *Физика горения и взрыва*. 1981. Т. 17. No. 4. С. 33—36.
Kirdyashkin A.I., Maksimov Y.M., Nekrasov E.A. Titanium-carbon interaction mechanism in a combustion wave. *Combust. Explos. Shock Waves*. 1981. Vol. 17. No. 4. P. 377—379. <https://doi.org/10.1007/BF00761204>.
6. Рогачев А.С. О микрогетерогенном механизме безгазового горения. *Физика горения и взрыва*. 2003. Т. 39. No. 2. С. 38—47.
Rogachev A.S. Microheterogeneous mechanism of gasless combustion. *Combust. Explos. Shock Waves*. 2003. Vol. 39. No. 2. P. 150—158. <https://doi.org/10.1023/A:1022956915794>.
7. Сеплярский Б.С., Абзалов Н.И., Кочетков Р.А., Лисина Т.Г. Влияние содержания поливинилбутирала на режим горения гранулированной смеси (Ti + C) + xNi. *Хим. физика*. 2021. Т. 40. No. 3. С. 23—30. DOI: 10.31857/S0207401X21030109.
Seplyarskii B.S., Abzalov N.I., Kochetkov R.A., Lisina T.G. Effect of the polyvinyl butyral content on the combustion mode of the (Ti + C) + xNi granular mixture. *Russ. J. Phys. Chem. B*. 2021. Vol. 15. No. 2. P. 242—249. DOI: 10.1134/S199079312102010X.
8. Seplyarskii B.S., Kochetkov R.A., Lisina T.G., Abzalov N.I. Combustion of Ti—C powders and granules: Impact of carbon allotropy and Ti particle size. *Int. J. SHS*. 2022. Vol. 31. No. 1. P. 54—56. DOI: 10.3103/S1061386222010071.
9. Cantor B., Chang I.T.H., Knight P., Vincent A.J.B. Microstructural development in equiatomic multicomponent

- alloys. *Mater. Sci. Eng. A*. 2004. Vol. 375—377. P. 213—218. <https://doi.org/10.1016/j.msea.2003.10.257>.
10. Rogachev A.S., Fourmont A., Kovalev D.Yu., Vadchenko S.G., Kochetov N.A., Shkodich N.F., Baras F., Politano O. Mechanical alloying in the Co—Fe—Ni powder mixture: Experimental study and molecular dynamics simulation. *Powder Technol.* 2022. Vol. 399. P. 117187. <https://doi.org/10.1016/j.powtec.2022.117187>.
 11. Zhang Z., Sheng H., Wang Z., Gludovatz B., Zhang Z., George E.P., Yu Q., Mao S.X., Ritchie R.O. Dislocation mechanisms and 3D twin architectures generate exceptional strength-ductility-toughness combination in CrCoNi medium-entropy alloy. *Nat. Commun.* 2017. Vol. 8. Art. 14390. P. 1—8. <https://doi.org/10.1038/ncomms14390>.
 12. Laplanche G., Kostka A., Reinhart C., Hunfeld J., Eggeler G., George E.P. Reasons for the superior mechanical properties of medium-entropy CrCoNi compared to high-entropy CrMnFeCoNi. *Acta Mater.* 2017. Vol. 128. P. 292—303. <https://doi.org/10.1016/j.actamat.2017.02.036>.
 13. Liu D., Wen T., Ye B., Chu Y. Synthesis of superfine high-entropy metal diboride powders. *Scr. Mater.* 2019. Vol. 167. P. 110—114. <https://doi.org/10.1016/j.scriptamat.2019.03.038>.
 14. Kochetov N.A., Rogachev A.S., Kovalev I.D., Vadchenko S.G. Combustion of transition metal—boron mixtures in argon gas. *Int. J. SHS*. 2021. Vol. 30. No. 4. P. 223—228. DOI: 10.3103/S106138622104004X.
 15. Braic V., Vladescu A., Balaceanu M., Luculescu C.R., Braic M. Nanostructured multi-element (TiZrNbHfTa)N and (TiZrNbHfTa)C hard coatings. *Surf. Coat. Technol.* 2012. Vol. 211. P. 117—121. DOI: 10.1016/j.surfcoat.2011.09.033.
 16. Yan X., Constantin L., Lu Y.F., Silvain J.-F., Nastas M., Cui B. (Hf_{0.2}Zr_{0.2}Ta_{0.2}Nb_{0.2}Ti_{0.2})C high-entropy ceramics with low thermal conductivity. *J. Am. Ceram. Soc.* 2018. Vol. 101. No. 10. P. 4486—4491. DOI: 10.1111/jace.15779.
 17. Zhang Q., Zhang J., Li N., Chen W. Understanding the electronic structure, mechanical properties, and thermodynamic stability of (TiZrHfNbTa)C combined experiments and first-principles simulation. *J. Appl. Phys.* 2019. Vol. 126. No. 2. Art. 025101. P. 1—7. <https://doi.org/10.1063/1.5094580>.
 18. Csanádi T., Castle E., Reece M., Dusza J. Strength enhancement and slip behaviour of high-entropy carbide grains during micro-compression. *Sci. Rep.* 2019. Vol. 9. P. 10200. DOI: 10.1038/s41598-019-46614-w.
 19. Castle E., Csanádi T., Grasso S., Dusza J., Reece M. Processing and properties of high-entropy ultra-high temperature carbides. *Sci. Rep.* 2018. Vol. 8. P. 8609. DOI: 10.1038/s41598-018-26827-1.
 20. Moskovskikh D.O., Vorotilo S., Sedegov A.S., Kuskov K.V., Bardasova K.V., Kiryukhantsev-Korneev Ph.V., Zhukovskiy M., Mukasyan A.S. High-entropy (HfTaTiNbZr)C and (HfTaTiNbMo)C carbides fabricated through reactive high-energy ball milling and spark plasma sintering. *Ceram. Int.* 2020. Vol. 46. P. 19008—19014. <https://doi.org/10.1016/j.ceramint.2020.04.230>.
 21. Kovalev D.Yu., Kochetov N.A., Chuev I.I. Fabrication of high-entropy carbide (TiZrHfTaNb)C by high-energy ball milling. *Ceram. Int.* 2021. Vol. 47. P. 32626—32633. <https://doi.org/10.1016/j.ceramint.2021.08.158>.
 22. Kochetov N.A., Sytshev A.E. Effects of magnesium on initial temperature and mechanical activation on combustion synthesis in Ti—Al—Mg system. *Mater. Chem. Phys.* 2021. Vol. 257. P. 123727. <https://doi.org/10.1016/j.matchemphys.2020.123727>.
 23. Kamynina O.K., Rogachev A.S., Sytshev A.E., Umarov L.M. Spontaneous deformation during self-propagating high-temperature synthesis. *Int. J. SHS*. 2004. Vol. 13. No. 3. P. 193—204.
 24. Камынина О.К., Рогачев А.С., Умаров Л.М. Динамика деформации реагирующей среды при безгазовом горении. *Физика горения и взрыва*. 2003. Т. 39. No. 5. С. 69—73.
Kamynina O.K., Rogachev A.S., Umarov L.M. Deformation dynamics of a reactive medium during gasless combustion. *Combust. Explos. Shock Waves*. 2003. Vol. 39. No. 5. P. 548—551. <https://doi.org/10.1023/A:1026161818701>.
 25. Вершинников В.И., Филоненко А.К. О зависимости скорости безгазового режима горения от давления. *Физика горения и взрыва*. 1978. Т. 14. No. 5. С. 42—47.
Vershinnikov V.I., Filonenko A.K. Pressure dependence of rate of gas-free combustion. *Combust. Explos. Shock Waves*. 1978. Vol. 14. No. 5. P. 588—592. <https://doi.org/10.1007/BF00789716>.
 26. Сеплярский Б.С. Природа аномальной зависимости скорости горения безгазовых систем от диаметра. *Докл. РАН*. 2004. Т. 396. No. 5. С. 640—643.
Seplyarskii B.S. The nature of anomalous dependence of burning velocity in «gasless» systems on sample diameter. *Dokl. Phys. Chem.* 2004. Vol. 396. No. 4—6. P. 130—133.

UDC 621.921.34:666.233

DOI dx.doi.org/10.17073/1997-308X-2022-4-67-83

Air-thermal oxidation of diamond nanopowders obtained by the methods of mechanical grinding and detonation synthesis

© 2022 г. P.P. Sharin¹, A.V. Sivtseva¹, V.I. Popov²

¹ Institute of Physical and Technical Problems of the North n.a. V.P. Larionov of Siberian Branch of Russian Academy of Sciences (SB RAS) under Federal Research Center «Yakutsk Scientific Center» of SB RAS, Yakutsk, Russia

² North-Eastern Federal University n.a. M.K. Ammosov, Yakutsk, Russia

Received 24.01.2022, revised 02.06.2022, accepted for publication 06.06.2022

Abstract: In this work, using the methods of X-ray phase analysis, transmission electron microscopy, X-ray photoelectron spectroscopy and Raman spectroscopy, the features of the impact of annealing in air within the temperature range of $t = 200\text{--}550$ °C on the morphology, elemental and phase composition, chemical state and structure of primary particles of nanopowders obtained by grinding natural diamond and the method of detonation synthesis are studied. It is shown that heat treatment in air at given values of temperature and heating time does not affect the elemental composition and atomic structure of primary particles of nanopowders obtained both by the methods of detonation synthesis (DND) and natural diamond grinding (PND). Using XPS, Raman spectroscopy, and transmission electron microscopy, it has been found that annealing in air within the temperature range of 400—550 °C results in the effective removal of amorphous and graphite-like carbon atoms in the sp^2 - and sp^3 -states from diamond nanopowders by oxidation with atmospheric oxygen. In the original DND nanopowder, containing about 33.2 % of non-diamond carbon atoms of the total number of carbon atoms, after annealing for 5 h at a temperature of 550 °C, the relative number of non-diamond carbon atoms in the sp^2 -state decreased to ~21.4 %. In this case, the increase in the relative number of carbon atoms in the sp^3 -state (in the lattice of the diamond core) and in the composition of oxygen-containing functional groups ranged from ~39.8 % to ~46.5 % and from ~27 % to ~32.1 %, respectively. In the PND nanopowder, which prior to annealing contains about 10.6 % of non-diamond carbon atoms in the sp^2 -state of the total number of carbon atoms, after annealing under the same conditions as the DND nanopowder, their relative number decreased to 7.1 %. The relative number of carbon atoms in the sp^3 -state increased from 72.9 % to 82.1 %, and the proportion of carbon atoms in the composition of oxygen-containing functional groups also slightly increased from 10.2 % to 10.8 %. It is demonstrated that the annealing of PND and DND nanopowders in air leads to a change in their color, they become lighter as a result of oxidation of non-diamond carbon by atmospheric oxygen. The maximum effect is observed at a temperature of 550 °C and an annealing time of 5 h. In this case, the weight loss of PND and DND nanopowders after annealing was 5.37 % and 21.09 %, respectively. The significant weight loss of DND nanopowder compared to PND is primarily caused by the high content of non-diamond carbon in the initial state and the high surface energy of primary particles due to their small size.

Keywords: natural diamond nanopowder, detonation nanodiamond, thermal oxidation of nanopowders, morphology, elemental composition, atomic structure of diamond nanoparticles, chemical state of nanopowders, oxygen-containing functional groups.

Sharin P.P. — Cand. Sci. (Phys.-Math.), lead researcher of the Department of physicochemistry of the Institute of Physical and Technical Problems of the North n.a. V.P. Larionov of Siberian Branch of Russian Academy of Sciences (RAS) (677980, Russia, Rep. Sakha, Yakutsk, Oktyabrskaya str., 1). E-mail: psharin1960@mail.ru.

Sivtseva A.V. — researcher of the Department of material science of the Institute of Physical and Technical Problems of the North n.a. V.P. Larionov of Siberian Branch of RAS. E-mail: sianva@yandex.ru.

Popov V.I. — Cand. Sci. (Phys.-Math.), senior researcher of the scientific and technological laboratory «Graphene nanotechnologies» of the Physical and Technical Institute of the North-Eastern Federal University n.a. M.K. Ammosov (677000, Russia, Rep. Sakha, Yakutsk, Belinskii str., 58). E-mail: volts@mail.ru.

For citation: Sharin P.P., Sivtseva A.V., Popov V.I. Air-thermal oxidation of diamond nanopowders obtained by the methods of mechanical grinding and detonation synthesis. *Izvestiya Vuzov. Poroshkovaya Metallurgiya i Funktsional'nye Pokrytiya (Powder Metallurgy and Functional Coatings)*. 2022. Vol. 16. No. 4. P. 67—83 (In Russ.). DOI: dx.doi.org/10.17073/1997-308X-2022-4-67-83.

Термоокисление на воздухе нанопорошков алмазов, полученных механическим измельчением и методом детонационного синтеза

П.П. Шарин¹, А.В. Сивцева¹, В.И. Попов²

¹ Институт физико-технических проблем Севера (ИФТПС) им. В.П. Ларионова СО РАН при Федеральном исследовательском центре «Якутский научный центр» (ФИЦ ЯНЦ) СО РАН, г. Якутск, Россия

² Северо-Восточный федеральный университет им. М.К. Аммосова, г. Якутск, Россия

Статья поступила в редакцию 24.01.22 г., доработана 02.06.22 г., подписана в печать 06.06.22 г.

Аннотация: Методами рентгеноструктурного фазового анализа (РФА), просвечивающей электронной микроскопии (ПЭМ), рентгеновской фотоэлектронной спектроскопии (РФЭС) и спектроскопии комбинационного рассеяния исследованы особенности влияния отжига на воздухе в интервале температур $t = 200\text{--}550\text{ }^\circ\text{C}$ на морфологию, элементный и фазовый составы, химическое состояние и структуру первичных частиц нанопорошков, полученных измельчением природного алмаза (ПНА) и методом детонационного синтеза (ДНА). Показано, что термообработка на воздухе при заданных значениях температуры и времени нагрева не оказывает влияние на элементный состав и атомную структуру первичных частиц нанопорошков, полученных как методом ДНА, так и методом ПНА. По результатам РФЭС, ПЭМ и спектроскопии комбинационного рассеяния установлено, что отжиг на воздухе при $t = 400\text{--}550\text{ }^\circ\text{C}$ приводит к эффективному удалению из нанопорошков алмаза атомов аморфного и графитоподобного углерода в sp^2 - и sp^3 -состояниях путем окисления кислородом воздуха. В исходном нанопорошке ДНА, содержащем около 33,2 % атомов неалмазного углерода от общего количества атомов углерода, после отжига в течение 5 ч при $t = 550\text{ }^\circ\text{C}$ относительное количество атомов неалмазного углерода в sp^2 -состоянии уменьшилось до ~21,4 %. При этом относительное количество атомов углерода в sp^3 -состоянии (в решетке алмазного ядра) и в составе кислородсодержащих функциональных групп увеличилось соответственно с ~39,8 до ~46,5 % и с ~27 до ~32,1 %. В нанопорошке ПНА, содержащем до отжига около 10,6 % атомов неалмазного углерода в sp^2 -состоянии от общего количества атомов углерода, после отжига при тех же условиях, что и для нанопорошка ДНА, их относительное количество снизилось до 7,1 %. При этом относительное количество атомов углерода в sp^3 -состоянии повысилось с 72,9 до 82,1 %, также незначительно (с 10,2 до 10,8 %) возросла доля атомов углерода в составе кислородсодержащих функциональных групп. Показано, что отжиг на воздухе нанопорошков ПНА и ДНА приводит к изменению их цвета: в результате окисления неалмазного углерода кислородом воздуха они становятся более светлыми. Максимальный эффект наблюдается при температуре $550\text{ }^\circ\text{C}$ и времени отжига 5 ч. При этом потери массы нанопорошков ПНА и ДНА после отжига составили, соответственно, 5,37 и 21,09 % — значительная потеря в массе нанопорошка ДНА обусловлена, в основном, высоким содержанием в исходном состоянии неалмазного углерода и высокой поверхностной энергией первичных частиц вследствие их малого размера.

Ключевые слова: нанопорошок природного алмаза, детонационный наноалмаз, термическое окисление нанопорошков, морфология, элементный состав и атомная структура наночастиц алмаза, химическое состояние нанопорошков, кислородсодержащие функциональные группы.

Шарин П.П. — канд. физ.-мат. наук, вед. науч. сотр. отдела физикохимии материалов и технологий ИФТПС им. В.П. Ларионова СО РАН (677980, Респ. Саха (Якутия), г. Якутск, ул. Октябрьская, 1).
E-mail: psharin1960@mail.ru.

Сивцева А.В. — науч. сотр. отдела материаловедения ИФТПС СО РАН.
E-mail: sianva@yandex.ru.

Попов В.И. — канд. физ.-мат. наук, ст. науч. сотр. учебной научно-технологической лаборатории «Графеновые нанотехнологии» Физико-технического института Северо-Восточного федерального университета им. М.К. Аммосова (677000, Респ. Саха (Якутия), г. Якутск, ул. Белинского, 58).
E-mail: volts@mail.ru.

Для цитирования: Шарин П.П., Сивцева А.В., Попов В.И. Термоокисление на воздухе нанопорошков алмазов, полученных механическим измельчением и методом детонационного синтеза. *Известия вузов. Порошковая металлургия и функциональные покрытия*. 2022. Т. 16. No. 4. С. 67—83. DOI: dx.doi.org/10.17073/1997-308X-2022-4-67-83.

Introduction

Diamond nanoparticles are a unique class of nano-sized materials with a variable structure and unstable physical and chemical properties [1—4]. Regardless of the method of obtaining, each primary particle of

diamond nanopowders consists of a diamond core having a cubic crystal lattice and being surrounded by a shell with a complex structure formed predominantly of non-diamond carbon and non-carbon impuri-

ties [4–6]. Due to the ultra-small size and, consequently, the high proportion of surface atoms with partially non-compensated electronic bonds, the primary particles of diamond nanopowders exhibit enormous surface activity, therefore in addition to segments of non-diamond carbon structures, the shell contains various functional groups, including C–H, oxygen-containing groups [7–9] imparting various physicochemical properties to it.

At present, diamond nanopowders are used as various functional components in polishing compounds [10], lubricating oils [1, 11], composite materials [12], elements of microelectronics [13, 14], as well as selective adsorbents and catalysts [15, 16]. A large number of other potential applications of nanodiamonds, including their application as drug carriers [17, 18], immobilizers of biologically active substances, a sorbent for the purification of blood, lymph, etc. [19, 20], are still at the examination stage. Most of these promising applications are hindered by the impossibility of obtaining diamond nanoparticles with controlled and reproducible surface chemistry depending on (being determined by) the extreme conditions of their production and the purification methods being used. The relative content of non-diamond carbon, the composition of functional groups and impurity atoms of primary particles of diamond nanopowders produced even by one manufacturer may differ from one batch to another [1–3].

In this context, the study of the processes of modification of diamond nanoparticles constitutes an urgent task, the solution of which will reveal the regularities of changes in their morphology, composition and structure under directed external influence, which contributes to obtaining diamond nanoparticles with controlled and reproducible properties, thus being important for their high-tech applications including biology, medicine etc. In works [4, 7, 21–23], the efficient and environmentally friendly method of purification of non-diamond carbon and impurities as well as modification of detonation synthesis diamond nanopowders by means of thermal oxidation with atmospheric oxygen without significant losses of diamond component are proposed and studied. Despite a significant number of works devoted to the study of thermal annealing in air, many issues and aspects of the formation of the composition and content of functional structures impacting the chemistry of diamond nanopowders are still unresolved and require clarification and additions.

The purpose of this paper is to study the features of the impact of modification by oxidation with atmospheric oxygen within the temperature range of 200–

550 °C on the morphology, elemental and phase composition, chemical state and structure of primary particles of nanopowders obtained by natural diamond grinding and by the method of detonation synthesis.

The subjects, methodology and methods of research

The samples of diamond nanopowders, obtained by two methods — the mechanical grinding of natural diamond and detonation synthesis from trinitrotoluene, were taken for the research. The procedure for obtaining nanopowders from natural diamond (PND) and their chemical purification are described extensively in work [6]. Highly purified nanopowder was used as samples of detonation synthesis nanodiamond (DND) of UDA-S-GO grade produced by Federal Research and Production Center «Altai» (Biysk).

A total of 12 samples of nanopowders, namely 6 samples of PND and DND were prepared. All samples of PND and DND were prepared from the same batch of the corresponding types of nanopowders. The staged heating of samples in air at atmospheric pressure was carried out as follows. All 12 samples of nanopowders were poured into separate ceramic corundum cups placed in a furnace chamber and heated in air at the following set temperature values (°C): 200, 300, 400, 500, and 550. After being held for 1 hour at each given temperature value, one sample of PND and DND was removed from the furnace for subsequent research, and the remaining samples were retained in the furnace chamber, the temperature of which was increased by the next given value at a rate of ~50 °C/min. Thus, the total time of staged heating of samples of PND and DND nanopowders in air at a temperature of 200 °C was 1 h, at a temperature of 300 °C — 2 h, at a temperature of 400 °C — 3 h, at a temperature of 500 °C — 4 h, and temperature of 550 °C — 5 h.

Morphological and structural characteristics of primary particles of nanopowders were studied by the methods of scanning electron microscopy (SEM) by means of JSM-6480LV instrument (JEOL, Japan) and high-resolution transmission electron microscopy (TEM) by means of «Titan 80-300» instrument (FEI, USA) with the following resolution: STEM; HREM ~0,08 nm. Digital processing of TEM images (Fourier transform, Fourier filtering, the determination of interplanar distances by FFT spectra) was performed using GMS-2.3.2 software package (GATAN, USA). The study of the phase composition and structural parameters of the samples of primary particles of nanopowders

was performed by means of «D8 Discover» powder diffractometer available from «Bruker» Company (USA) in $\text{CuK}\alpha$ radiation ($\lambda = 1.54 \text{ \AA}$). X-ray diffraction measurements were performed in the range of 2θ angles from 17° to 96° . The measurement data were processed and analyzed using Microcal Origin and Crystallographica Search Match applications.

The elemental and phase compositions, the chemical state of primary particles of nanopowders were studied by the methods of X-ray photoelectron spectroscopy (XPS) and Raman spectroscopy. XPS measurements were performed by means of SPECS photoelectron spectrometer (Germany) using PHOIBOS-150-MCD-9 hemispherical analyzer and FOCUS-500 X-ray monochromator ($\text{AlK}\alpha$ radiation, $h\nu = 1486.74 \text{ eV}$, 200 W). Binding energy scale (E_{bind}) was precalibrated by the position of the peaks of the core levels $\text{Au}4f_{7/2}$ (84.00 eV) and $\text{Cu}2p_{3/2}$ (932.67 eV). The samples of nanopowders were applied onto a double-sided copper conductive tape 3M (USA). The panoramic spectra were recorded at a transmission energy of the analyzer of 50 eV, and certain spectral areas were recorded at the energies of 10 or 20 eV. The determination of the relative content of elements on the samples of nanopowders and their atomic ratios was performed in accordance with the integral intensities of photoelectron lines (C1s, O1s and N1s) adjusted for the corresponding atomic sensitivity coefficients [24].

The Raman spectra (Raman) of nanopowder samples were studied using Solar TII Raman spectrometer being an integral part of Integra Spectra measuring complex (NT-MDT, JSC, Zelenograd). This spectrometer is equipped with a microscope with an objective of $100\times$ with a number aperture of $\text{NA} = 0.7$, a TV camera and a cooled CCD detector (-70°C). Laser radiation with the wavelengths of 473, 532, and 632 nm was used for Raman spectra excitation. When registering Raman spectra, a diffraction grating with a density of 600 lines/mm was used in the spectrometer. The Raman spectra of the samples were measured in the signal accumulation mode at room temperature.

The specific surface area of the samples was determined by BET method (Brunauer—Emmett—Teller) according to measurements of the low-temperature adsorption of nitrogen molecules (77 K) using SORBI-MS instrument (Meta, JSC, Novosibirsk) equipped with GSO 7912-2001 standard sample ($S_{\text{sp}} = 98.42 \text{ m}^2/\text{g}$) developed at G.K. Boreskov Institute of Catalysis, SB RAS (Novosibirsk). The density of diamond nanopowders was estimated by the pycnometric method.

Results and discussions

Table 1 provides the basic physical characteristics of the original PND and DND nanopowders. The pycnometric densities of both nanopowders are significantly lower than the theoretical density of diamond (3.5154 g/cm^3) and the density of massive natural diamond crystals, which, as it is known, varies in the range of $3.30\text{--}3.60 \text{ g/cm}^3$ depending on their impurity content [25].

In the daylight, dry PND nanopowder in its initial state exhibits a light gray color (Fig. 1, a), while after annealing in air at a temperature of 550°C for 5 h, the color of the sample changed and became almost white with a slightly grayish tint (Fig. 1, c). After annealing in air under the same conditions, the dark brown color of the original dry nanopowder of DND sample (Fig. 1, b) changed to light gray (Fig. 1, d).

X-ray phase analysis. 3 clear lines, corresponding to X-ray diffraction on (111), (220) and (311) planes of the crystal lattice of the diamond core of the primary particles of PND and DND nanopowders, were identified on the diffraction spectra in the studied range of angles $2\theta \sim 17\text{--}96 \text{ deg}$. (Fig. 2). The ratios of intensity of three diffraction peaks $I_{111} : I_{220} : I_{311}$ for all the samples of PND and DND, including the samples subjected to staged heating in air, are about $100 : 51 : 18$ and $100 : 21 : 12$, respectively.

There is a line observed in the spectrum of the original DND sample in the range of $2\theta \sim 18\text{--}28 \text{ deg}$. (spectrum 1 in Fig. 2, a), which is caused by the dif-

Table 1. Main physical characteristics of diamond nanopowders

Таблица 1. Основные физические характеристики алмазных нанопорошков

Powder	Size, nm (X-ray phase analysis)	Pycnometric densities, g/cm^3	Specific surface area, m^2/g	Non-combustible residue, %
PND	19.88 ± 3.0	3.05	32.98 ± 2.0	0.95
DND	4.98 ± 0.74	2.95	339.5 ± 20	1.1

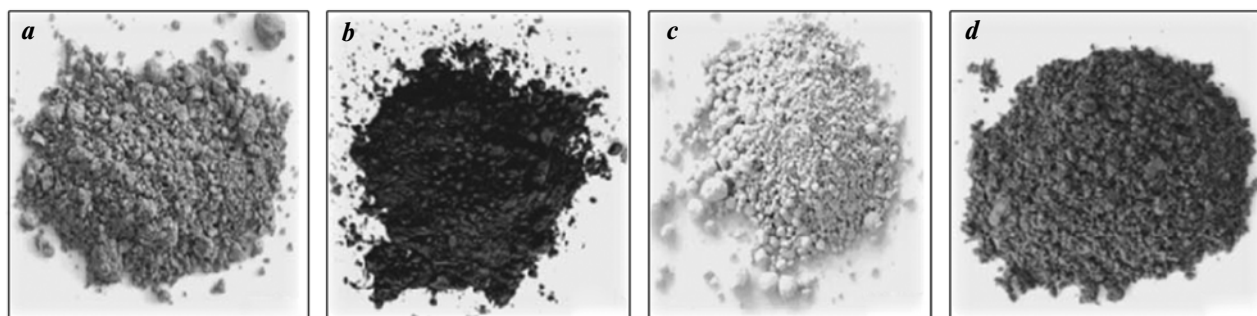


Fig. 1. The photographs of samples of PND and DND nanopowders in the initial state (*a, b*) and after annealing in air for 5 h at a temperature of 550 °C (*c, d*)

Рис. 1. Фотографии образцов нанопорошков ПНА и ДНА в исходном состоянии (*a, b*) и после отжига на воздухе в течение 5 ч при температуре 550 °C (*c, d*)

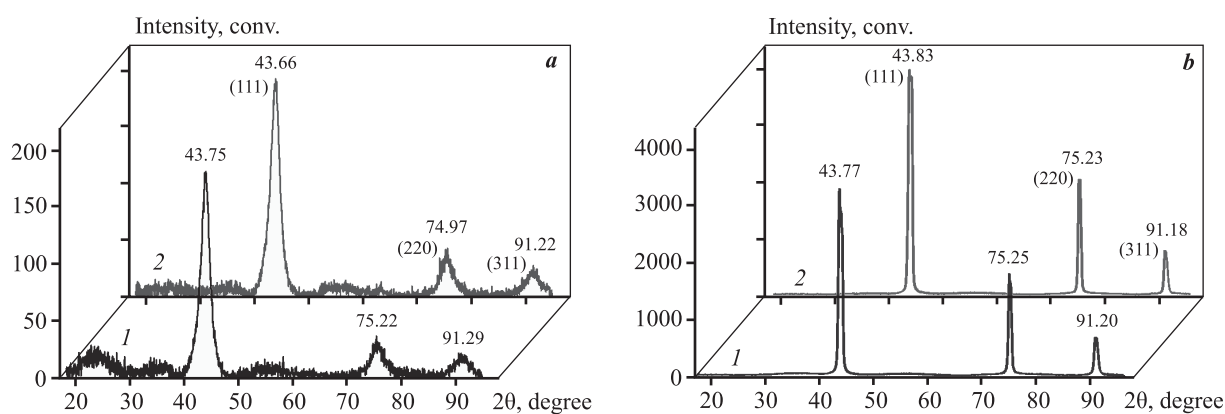


Fig. 2. X-ray diffraction spectra of DND nanopowders (*a*) and PND nanopowders (*b*) before annealing (*1*) and after annealing in air at a temperature of 550 °C (*2*)

Рис. 2. Рентгеновские дифракционные спектры нанопорошков ДНА (*a*) и ПНА (*b*) до отжига (*1*) и после отжига на воздухе при температуре 550 °C (*2*)

fuse scattering of X-rays from formations without long-range order. The presence of such a line in the spectrum is commonly associated with amorphous structural groups consisting mainly of non-diamond carbon and located around the diamond core and in the space between the adjacent primary particles of the nanopowder. [21, 26]. While in the spectrum of the DND sample (spectrum 2 in Fig. 2, *a*), subjected to heating in air, such a line is virtually absent, or, upon annealing in air, the content of amorphous formations of non-diamond carbon decreased to such an amount that is not detectable by X-ray phase analysis. Fig. 2 also reveals that the diffraction peaks of the samples of both nanopowders are broadened, upon that the ones of DND are much more broadened compared to the ones of PND due to the smaller size of its crystallites.

It is known that the broadening of the diffraction lines of any powder made of crystalline grains can be contributed by secondary microstresses in their crystals [27]. In a number of works [3, 5, 28], it was experimentally demonstrated that in the case of nanodispersed diamond particles, the contribution of secondary microstresses is insignificant [28]. This is explained by the fact that any microstresses in crystallites caused by thermal or mechanical impact are efficiently relaxed due to the combination of high-modulus of diamond with the nanoscale of its particles [6]. In this context, the line broadening in the diffraction spectrum is primarily contributed by the small size of nanodiamond crystallites; therefore, when calculating the size of the coherent scattering region (D_{CSR}), which essentially corresponds to the size of the diamond core of primary

particles of nanopowders (without taking into account their shells), we used a simplified formula $D_{CSR} = \lambda/(\beta \cos \theta)$.

The data provided in Table 2 suggest that the physical broadening (β) of the diffraction lines of DND samples (the original ones and the ones heat-treated in air), depending on the value of the heating temperature, is on average approximately 3.9 times higher than the line broadening of PND samples. The comparative analysis of the angles of maxima of diffraction lines, interplanar spacings, and physical broadening for the original samples and the PND and DND samples subjected to annealing in air reveals that heat treatment at the temperatures and heating duration speci-

fied in the experiment does not impact the structural state of primary particles of nanopowders of both DND and PND.

The elemental composition and chemical state of the samples. Panoramic X-ray photoelectron spectra of DND and PND samples before heating and after annealing in air at a temperature of 550 °C provide general information on the chemical composition of nanopowder samples and the presence of impurities or contaminants in them. (Fig. 3).

It is worth noting that XPS method, as applied to the nanopowder samples under study, provides information not only from the surface of their primary particles, but also from the entire volume of the ones

Table 2. The values of heating temperature (t), angles of maximum of diffraction lines (2θ), interplanar distances (d_{hkl}), physical broadening (β) and the size of coherent scattering regions (D_{CSR}) samples of PND and DND nanopowders before and after the staged heat treatment in air

Таблица 2. Значения температуры нагрева (t), углов максимума дифракционных линий (2θ), межплоскостных расстояний (d_{hkl}), физического уширения (β) и размера областей когерентного рассеяния ($D_{ОКР}$) образцов нанопорошков ПНА и ДНА до и после ступенчатой термообработки на воздухе

$t, ^\circ\text{C}$	Miller indices	PND				DND			
		$2\theta, \text{deg.}$	$d_{hkl}, \text{Å}$	$\beta, \text{deg.}$	D_{CSR}, nm	$2\theta, \text{deg.}$	$d_{hkl}, \text{Å}$	$\beta, \text{deg.}$	D_{CSR}, nm
Orig.	(111)	43.77	2.067	0.66	14.08	43.75	2.068	2.23	4.16
	(220)	75.25	1.262	0.43	25.48	75.22	1.263	2.00	5.44
	(311)	91.20	1.079	0.61	20.08	91.29	1.078	2.30	5.36
200	(111)	43.79	2.066	0.60	15.49	43.82	2.065	2.26	4.11
	(220)	75.26	1.262	0.43	25.41	75.25	1.262	1.99	5.47
	(311)	91.22	1.078	0.65	18.96	90.94	1.081	2.30	5.34
300	(111)	43.78	2.067	0.55	16.92	43.68	2.071	2.14	4.34
	(220)	75.23	1.262	0.48	22.74	75.34	1.261	2.14	5.10
	(311)	91.21	1.078	0.61	20.33	91.00	1.080	2.20	5.59
400	(111)	43.80	2.066	0.65	14.20	43.68	2.071	2.18	4.25
	(220)	75.24	1.262	0.43	25.34	75.20	1.263	2.05	5.31
	(311)	91.20	1.078	0.60	20.68	91.50	1.076	2.10	5.88
500	(111)	43.79	2.066	0.64	14.42	43.57	2.076	2.12	4.38
	(220)	75.25	1.262	0.43	25.34	74.91	1.267	2.10	5.17
	(311)	91.17	1.079	0.60	20.68	91.13	1.079	2.04	6.05
550	(111)	43.83	2.065	0.65	14.23	43.66	2.072	2.11	4.40
	(220)	75.23	1.262	0.42	25.91	74.97	1.266	1.98	5.49
	(311)	91.18	1.079	0.60	20.50	91.22	1.078	2.09	5.90

or a significant part of it, since the mean free path of electrons ($\lambda \sim 3$ nm) is comparable to or slightly less than the average size of the studied primary particles of DND and PND nanopowders. Taking into account the fact that about 95 % of the informative signal in XPS comes from a depth of 3λ , the depth of analysis for carbon constitutes $\sim 9\div 10$ nm. In Fig. 3, *a*, it can be seen that the spectra of the original samples of both nanopowders contain the lines being specific for carbon (C1s and C KVV) and oxygen (O1s and O KLL). Besides, the spectrum of the DND sample includes a nitrogen line (N1s), while the spectrum of the PND sample includes additional low-intensity peaks of titanium and sodium (practically at the level of noises). No other elements were found in all samples of nanopowders within the sensitivity of XPS method. The photoelectron spectra of DND and PND samples subjected to heat treatment in air at a temperature of 550 °C (Fig. 3, *b*) contain the same lines as the corresponding original samples. Table 3 provides the results of measurements of the relative content of basic elements (C, O and N), as well as the ratio of their atomic concentrations in the samples of DND and PND nanopowders.

The relative content of elements in the samples of nanopowders and their atomic ratios were determined by the integral intensities of photoelectron lines adjusted for the corresponding atomic sensitivity coefficients [24].

According to Table 3, the ratio of the number of oxygen atoms and carbon atoms is practically the same for the particles of PND and DND nanopowders.

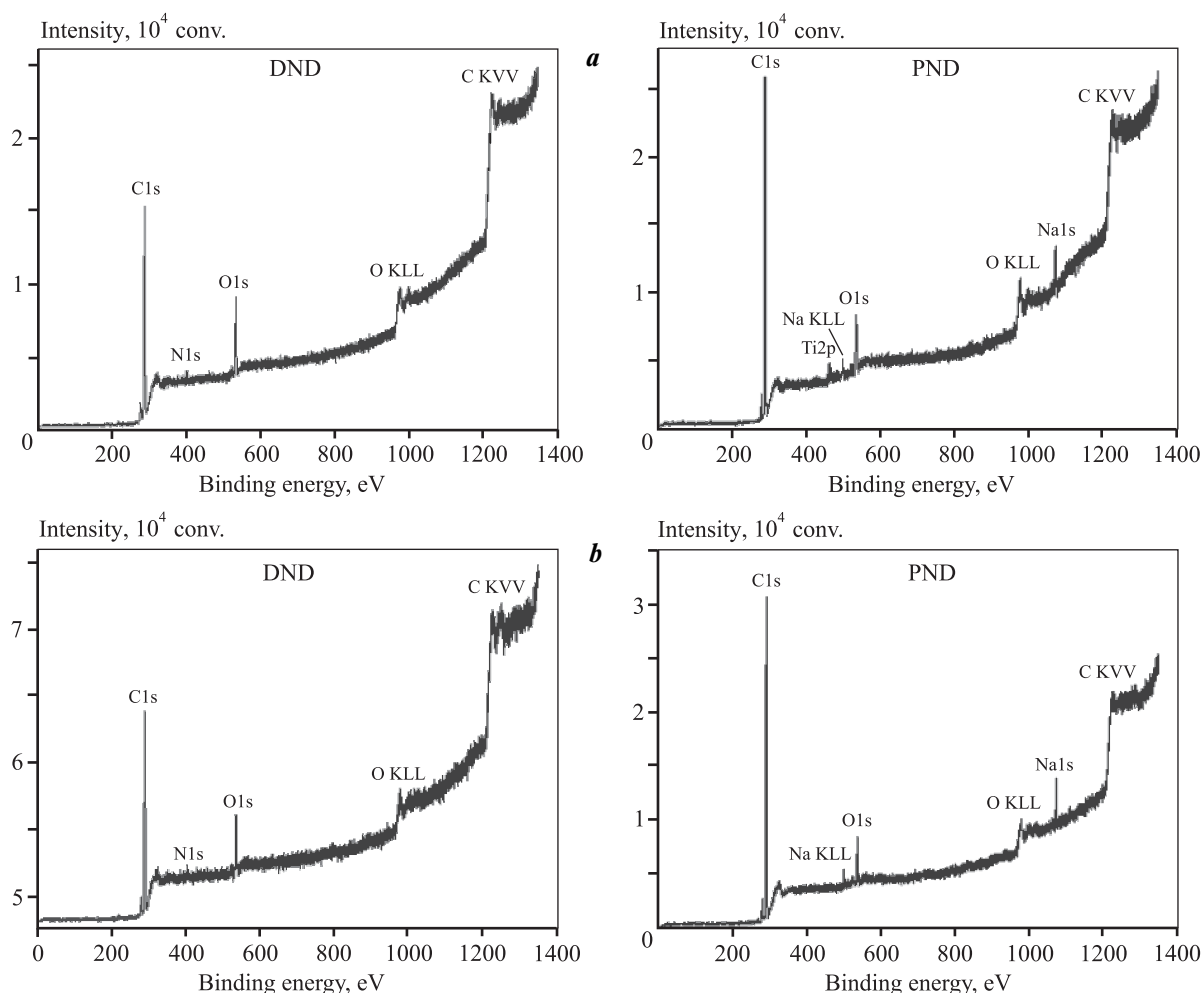


Fig. 3. The panoramic X-ray photoelectron spectra of DND and PND samples before heating (*a*) and after annealing in air at a temperature of 550 °C (*b*)

Рис. 3. Обзорные рентгеновские фотоэлектронные спектры образцов ДНА и ПНА до нагрева (*a*) и после отжига на воздухе при температуре 550 °C (*b*)

Table 3. The relative content of elements in PND and DND samples and their atomic ratios

Таблица 3. Относительное содержание элементов в образцах ПНА и ДНА и их атомные соотношения

<i>t</i> , °C	PND					DND				
	C	O	N	O/C	N/C	C	O	N	O/C	N/C
Orig.	90.6	9.4	—	0.10	—	89.4	9.1	1.5	0.10	0.02
400	90.8	9.2	—	0.10	—	89.0	9.5	1.5	0.11	0.02
500	91.2	8.8	—	0.10	—	89.4	9.0	1.6	0.10	0.02
550	90.8	9.2	—	0.10	—	90.6	7.8	1.6	0.19	0.02

For a detailed analysis, the main lines of C1s carbon, O1s oxygen, and N1s nitrogen were decomposed into separate spectral components using XPSPeak 4.1 software [29].

Fig. 4 shows that the carbon C1s lines of both nanopowder samples consist of separate spectral components, indicating that the carbon within the samples appears in 4 different chemical states. An analysis of binding energies of individual components in C1s spectra of both samples allows to conclude that the most intensive peaks with binding energies of 285.3 ± 0.2 eV correspond to sp^3 -hybridized carbon forming a diamond crystal lattice [7, 30–33].

The binding energies of peaks of 284.1 ± 0.1 eV are specific for carbon atoms in the sp^2 -state (graphite-like carbon atoms) [30–33]. The peaks with the binding energies of 286.6 eV correspond to carbon atoms in the composition of hydroxyl and ether groups (C—OH, C—O—C) [30–33]. The least intensive lines with the binding energies of 287.9 ± 0.3 eV characterize the states of carbon atoms in the composition of carboxyl groups (O=C—O, COOH). Table 4 provides relative contributions of each state of carbon atoms to the total C1s spectrum and sp^2/sp^3 ratio for all measured samples. According to Table 4, in the original sample of PND nanopowder, about 79.2 % of the total number of carbon atoms are in the sp^3 -state. ~10.6 % of the total number of carbon atoms correspond to graphite-like carbon atoms in the sp^2 -hybridized state, while other carbon atoms are in the composition of hydroxyl (or ether) (~8.0 %) and carboxyl (~2.2 %) groups.

The original sample of DND nanopowder, 33.2 % of the total number of carbon atoms are graphite-like carbon atoms in the sp^2 -hybridized state. The carbon atoms in the sp^3 -hybridized state account for ~39.8 %, while other carbon atoms are in the composition of hydroxyl (or ether) (~24.8 %) and carboxyl (~2.2 %) groups.

Table 4 also shows that as the temperature (starting from 400 °C) and the time of annealing in air increases, the content of non-diamond carbon atoms in the sp^2 -hybridized state both in PND samples and in DND samples gradually decreases as a result of air oxidation, while the proportion of carbon atoms in the sp^3 -hybridized state increases.

Fig. 5 shows O1s oxygen spectra of the samples of nanopowders measured before heating and after it ($t = 550$ °C). It can be seen that O1s spectra of DND and PND samples contain various oxygen-containing functional groups, which are commonly localized on the surface of carbon materials, including diamond nanopowders. According to the literature data, the peaks of oxygen atoms in the carbonyl groups of ketones, aldehydes and quinones are in the range of binding energies of ~531.3–531.5 eV [34–36]. The binding energy of 532.6 eV is characteristic of peaks of oxygen in the composition of phenolic [34] and hydroxyl groups [35], as well as carbonyl oxygen in esters and carboxylic anhydrides [35]. The peaks of oxygen with the binding energy of 533.8 eV correspond to the non-carbonyl atom of oxygen in esters or anhydrides and carboxyl group [34, 36, 37]. The peaks of oxygen with the binding energy of 530 eV can be attributed to oxygen in the composition of inorganic compounds [35]. The relative contributions of different states of oxygen atoms to the total O1s spectrum in all measured PND and DND samples are provided in Table 5.

Table 5 shows that the PND samples annealed in air exhibit a noticeable tendency to an increase in the proportion of oxygen atoms in the composition of ester, carbonyl, and carboxyl functional groups compared to the initial state, while the DND samples annealed in air exhibit a somewhat decrease in the proportion of oxygen atoms of the hydroxyl and carbonyl groups in the composition of ester, anhydride and carboxyl groups compared to the original sample.

A certain increase in the fraction of oxygen atoms of the non-carbonyl group is also noticeable only in the composition of carboxyl, anhydride, and ester groups

in DND samples after annealing. The analysis of the binding energies of spectral components presented in the spectrum of main line N1s in Fig. 6 allows

Table 4. The contribution of carbon states (%) to the total spectrum of C1s in PND and DND samples before their annealing and after heating in air at different temperatures

Таблица 4. Вклад состояний углерода, %, в суммарный спектр C1s в образцах ПНА и ДНА до их отжига и после нагрева на воздухе при разных значениях температуры

$t, ^\circ\text{C}$	PND					DND				
	sp^2	sp^3	C-O, C-O-C	COOH	sp^2/sp^3	sp^2	sp^3	C-O, C-O-C	COOH	sp^2/sp^3
Orig.	10.6	79.2	8.0	2.2	0.13	33.2	39.8	24.8	2.2	0.83
400	10.1	78.9	8.5	2.5	0.13	31.7	38.9	25.1	4.3	0.81
500	8.2	81.5	8.4	1.9	0.10	29.8	42.8	23.2	4.2	0.70
550	7.1	82.1	9.1	1.7	0.09	21.4	46.5	27.8	4.3	0.46

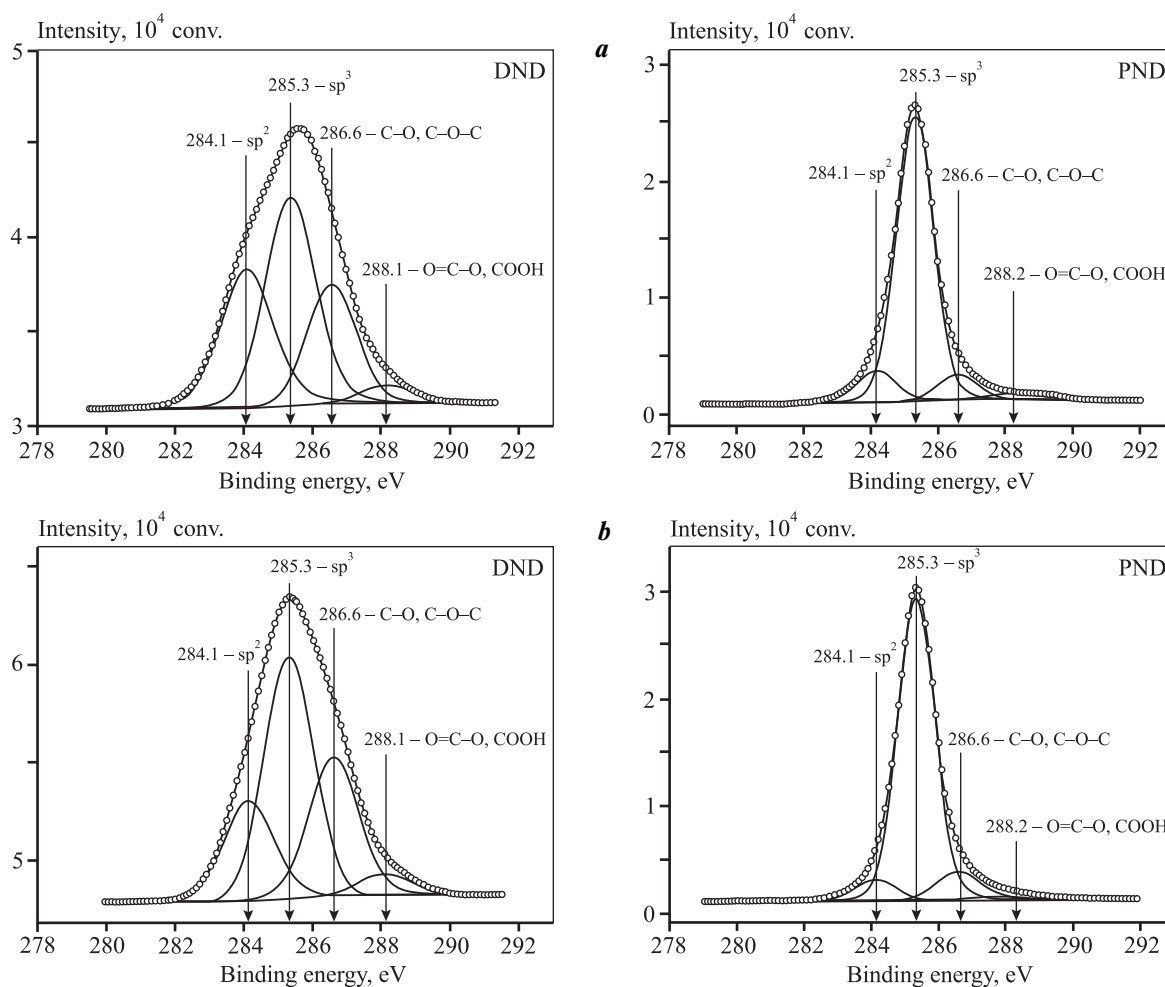


Fig. 4. The spectra of C1s carbon of DND and PND samples before heating (a) and after annealing in air at a temperature of 550 °C (b)

Рис. 4. Спектры углерода C1s образцов ДНА и ПНА до нагрева (a) и после отжига на воздухе при температуре 550 °C (b)

Table 5. The contribution of the states of oxygen atoms (%) to the total spectrum of O1s

Таблица 5. Вклад состояний атомов кислорода, %, в суммарный спектр O1s

t, °C	PND				DND			
	O=C—O—C, —C—OH	—C=O	—O—C=O	NaOH + TiO ₂	O=C—O—C, —C—OH	—C=O	—O—C=O	NaOH + TiO ₂
Orig.	36.7	18.6	14.2	30.5	64.6	27.7	7.7	—
400	46.8	21.6	16.7	14.9	58.6	31.0	10.4	—
500	49.3	21.9	16.6	12.2	57.6	29.4	12.9	—
550	49.9	21.7	21.1	7.3	55.2	27.0	17.8	—

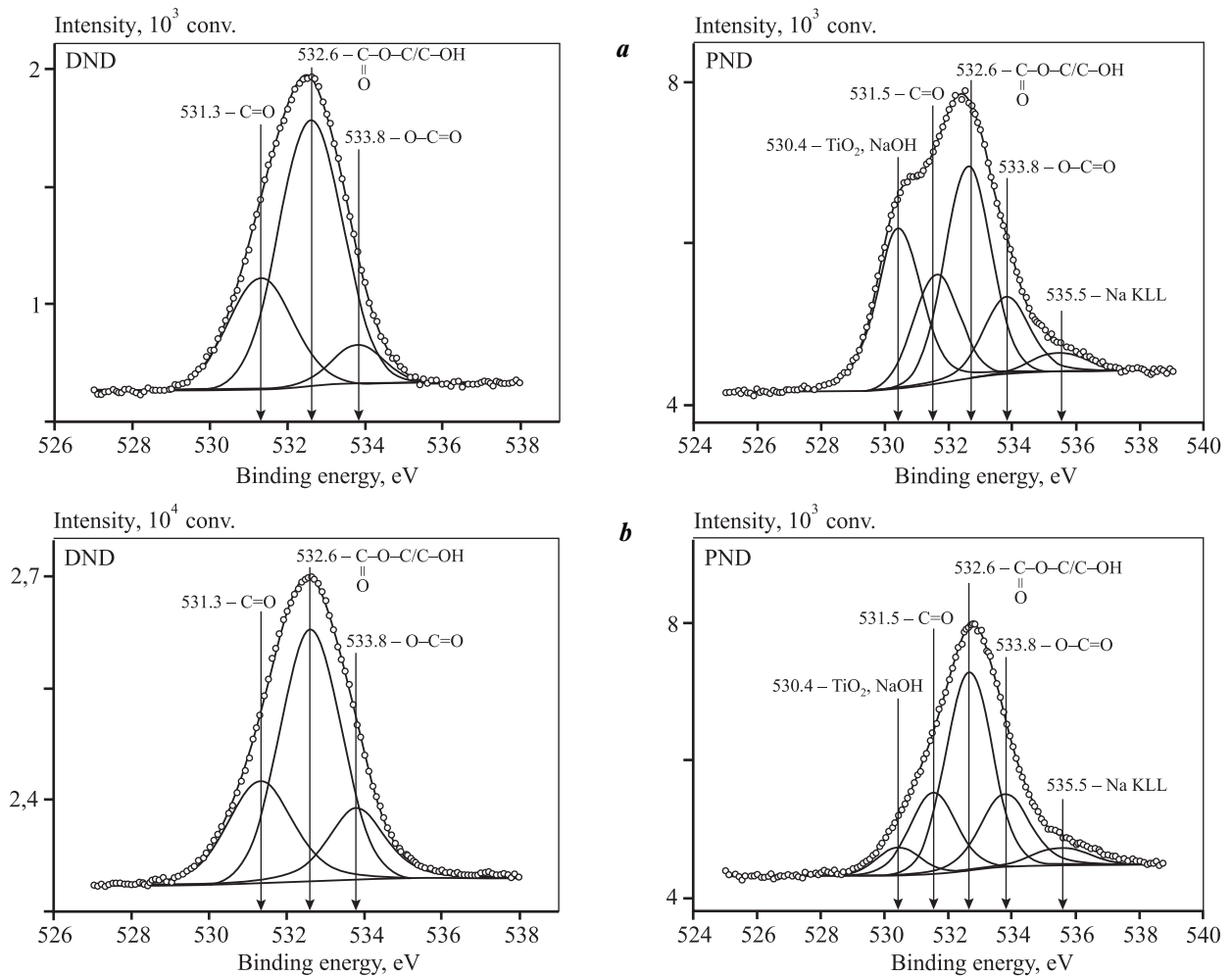


Fig. 5. The spectra of O1s oxygen of the samples of DND and PND nanopowders before heating (a) and after annealing in air at a temperature of 550 °C (b)

Рис. 5. Спектры кислорода O1s образцов нанопорошков ДНА и ПНА до нагрева (a) и после отжига на воздухе при температуре 550 °C (b)

to suggest that nitrogen is present on the surface in the composition of the following functional groups: 398.6 eV —C—N=C and 399.6 eV —C—N—C. Peak with the binding energy value of 402.8 ± 0.1 eV may belong to oxidized nitrogen (NO_x).

The contribution of nitrogen states in N1s spectra of the studied samples is provided in Table 6. The analysis of the binding energies of spectral components presented in N1s spectrum allows to suggest that nitrogen is present on the surface in the composition of

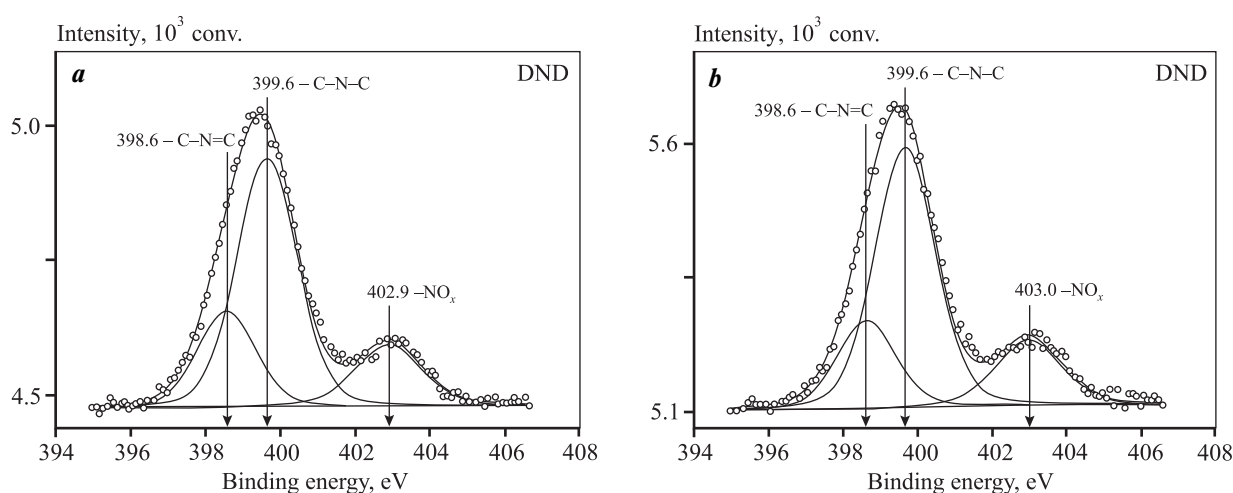


Fig. 6. The main lines of N1s nitrogen of the samples of DND nanopowder before heating (a) and after annealing in air at a temperature of 550 °C (b)

Рис. 6. Основные линии азота N1s образцов нанопорошка ДНА до нагрева (a) и после отжига на воздухе при температуре 550 °C (b)

Table 6. The contribution of the states of nitrogen atoms (%) to the total spectrum of N1s in DND samples

Таблица 6. Вклад состояний атомов азота, %, в суммарный спектр N1s в образцах ДНА

<i>t</i> , °C	C–N=C	C–N–C	NO _x
Orig.	27.3	55.6	17.1
400	25.2	57.5	17.3
500	22.3	60.4	17.3
550	21.3	61.3	17.4

the following functional groups: 398.6 eV —C–N=C and 399.6 eV — C–N–C. Peak with the binding energy value of 402.8 ± 0.1 eV may belong to oxidized nitrogen (NO_x).

Transmission electron microscopy. Fig. 7 shows the images of the structure of primary particles of DND and PND nanopowder samples in their initial state and after annealing in air at a temperature of 550 °C.

The interplanar distances of the crystals of the diamond core of the primary particles of nanopowders are distinctly visible in all the high-resolution images in Fig. 7. Both in DND nanopowder and in PND nanopowder, the shells consisting mainly of graphite-like carbon in sp²-hybridized state and amorphous carbon in sp³-state are clearly visible together with the cores of primary particles [4, 7]. The space between the adjacent primary particles is also filled with formations of non-diamond carbon and segments of amorphous

carbon in sp³-hybridized state (see Fig. 7). The comparative analysis of high-resolution images of primary DND and PND particles obtained before annealing and after heating in air in the temperature range of 400–550 °C is indicative of a noticeable decrease in non-diamond carbon both on the shells surrounding the cores of primary particles and in the space between the adjacent primary particles.

Thus, the results obtained by direct TEM observation are in qualitative line with the analysis data established on the basis of XPS measurements of C1s carbon, which show that the relative content of graphite-like carbon atoms in the sp²-hybridized state decreases as a result of their being oxidized with atmospheric oxygen upon annealing of nanopowder samples at a temperature above 400 °C (see Table 4). A decrease in the relative content of non-diamond carbon in the samples during annealing in air as a result of oxidation is also observed in the Raman spectra of PND and DND nanopowders.

Raman spectroscopy. Fig. 8 shows the normalized Raman spectra (RS) of PND and DND nanopowders in their states before and after annealing (in air at *t* = 550 °C). It can be observed that the Raman spectra of the samples of PND and DND nanopowders in their initial state and after annealing differ significantly (see Fig. 8). Thus, in the Raman spectrum of PND sample, *D* line being the line of low-ordered carbon in sp²-state, from which a sharp diamond peak, caused by the vibrations of carbon atoms in the sp³-state, emerges at a frequency about 1331 cm⁻¹, and *G* line being the line

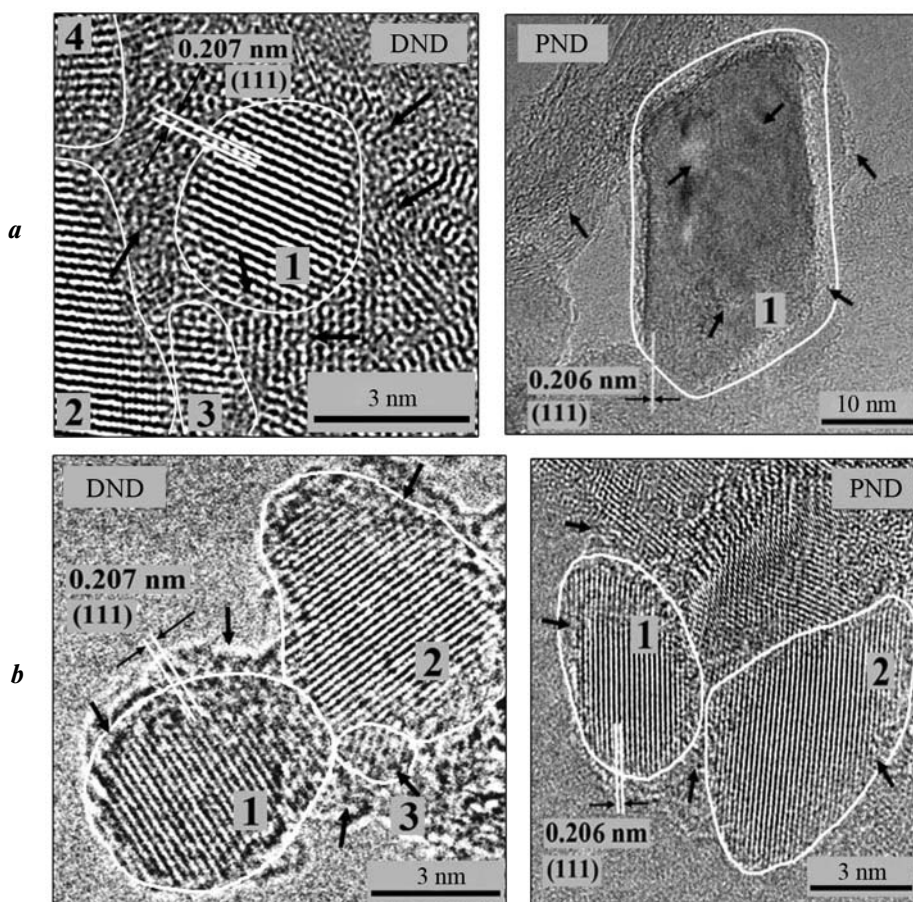


Fig. 7. The high-resolution images of primary particles of the samples of DND and PND nanopowders before annealing (*a*) and after heating in air at a temperature of 550 °C (*b*)

The numbers indicate the crystalline cores of diamond of primary particles of nanopowders, the arrows indicate the segments of graphite-like formations of carbon in the sp^2 -state and amorphous carbon in the sp^3 -state

Рис. 7. Изображения высокого разрешения первичных частиц образцов нанопорошков ДНА и ПНА до отжига (*a*) и после нагрева на воздухе при температуре 550 °C (*b*)

Цифрами помечены кристаллические ядра алмаза первичных частиц нанопорошков; стрелками обозначены фрагменты графитоподобных образований из углерода в sp^2 -состоянии и аморфного углерода в sp^3 -состоянии

of graphite, occupying the frequency range of 1400–1700 cm^{-1} with a center at 1577 cm^{-1} , decreased noticeably after annealing. In the Raman spectrum of DND sample before annealing, the diamond peak hardly stands out against the background of the intense broad *D* line of low-ordered carbon in sp^2 -state, while after annealing the diamond peak is clearly observed at a frequency centered at about 1328 cm^{-1} . These changes in the Raman spectra are indicative of the fact that the proportions of non-diamond carbon atoms in the sp^2 -state in the samples of PND and DND nanopowders decrease as a result of their oxidation with atmospheric oxygen during annealing in air.

Thus, XPS and Raman spectroscopy methods, as

well as the direct images obtained using high-resolution TEM, provide consistent results showing that during the annealing of PND and DND samples in air (starting from a temperature of 400°C), the selective removal of structural formations consisting primarily of non-diamond carbon in sp^2 -state and amorphous carbon in sp^3 -hybridized state.

Returning to Fig. 1, which shows the photographic images of nanopowders, let us note that the color of both the original samples of DND and PND nanopowder, and the samples annealed in air at $t = 550^\circ C$ correlates well with the relative content of structural formations of non-diamond carbon in sp^2 - and sp^3 -states in them. The high content of non-diamond car-

Table 7. The weight losses of PND and DND samples depending on the temperature and duration of their annealing in air and the basic processes occurring in nanopowder samples

Таблица 7. Потери массы образцов ПНА и ДНА в зависимости от температуры и длительности их отжига на воздухе и основные процессы, протекающие в образцах нанопорошков

t , °C	Time, h	Weight loss, %		The main processes occurring in the samples of diamond nanopowders during annealing in air
		PND	DND	
200	1	0.14	4.01	Desorption and removal of water molecules and volatile impurities [38–40]
300	2	0.30	5.08	
400	3	1.13	7.36	The oxidation of the smallest formations of non-diamond sp^2 -carbon and amorphous carbon in the sp^3 -state [4, 7, 21–23]
500	5	3.08	14.21	The oxidation of graphite-like sp^2 -carbon, amorphous carbon in the sp^3 -state, and small primary particles of nanopowders [4, 7, 33]
550	6	5.37	21.09	

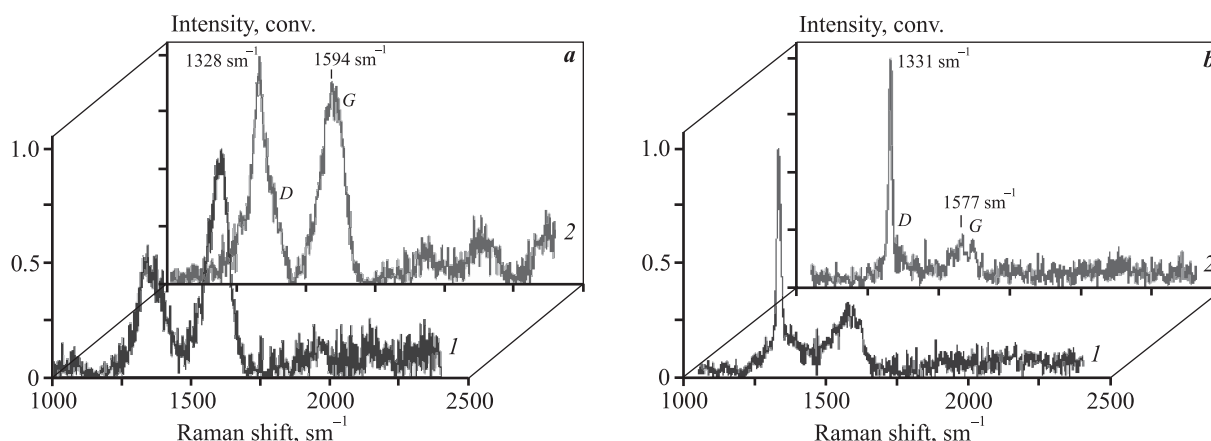


Fig. 8. The Raman spectra of the samples of PND (a) and DND (b) nanopowders before annealing (I) and after annealing in air at a temperature of 550 °C (2)

The spectra are adjusted by background subtraction and normalized to unity

Рис. 8. Спектры КР образцов нанопорошков ПНА (a) и ДНА (b) до отжига (I) и после отжига на воздухе при температуре 550 °C (2)

Спектры скорректированы путем вычитания фона и нормированы на единицу

bon in the original samples of diamond nanopowders contributes to their dark colour tint. The removal of structural formations of non-diamond carbon located both on the shell of the diamond core and in the space between adjacent primary particles during annealing in air causes a lighter color of PND and DND nanopowders.

The weight loss of samples of PND and DND nanopowders after their annealing in air. Table 7 shows that at an annealing temperature of 200 °C the weight loss of PND sample was 0.14 % of its initial value, and the

weight loss of DND sample sample accounted for 4.01 %.

The relatively high weight loss of DND sample upon heating in air compared to the one of PND sample is apparently caused by the higher value of its specific surface area, which is capable of adsorbing more water molecules and volatile impurities in the initial state.

As a result of annealing at $t = 300$ °C, the weight losses of PND and DND samples compared to their initial values accounted for 0.3 % and 5.08 %, respectively. In

addition to the removal of adsorbed water molecules and volatile compounds, the weight losses at this annealing temperature might also be caused by desulfuring and denitrogenation, the presence of sulfur- and nitrogen-containing compounds in the original samples is associated with the chemical purification of the original nanopowders using the mixtures of strong acids, containing H_2SO_4 and HNO_3 [38, 39].

At $t = 400$ °C, the weight losses of PND and DND samples increase noticeably and account for 1.13 and 7.36 %, respectively. A noticeable increase in the weight losses is caused by the beginning of the processes of oxidation and removal of small structural formations consisting of non-diamond carbon in sp^2 -state and amorphous carbon in sp^3 -hybridized state [4, 7].

In the case of $t = 500$ °C and 550 °C, the weight losses of the original PND and DND samples increase significantly. After annealing at temperatures of 500 °C and 550 °C, the original PND samples lost 3.08 % and 5.37 %, and the DND samples lost 14.21 % and 21.09 %, respectively. The increase in the weight losses of the samples at these temperatures is caused by active oxidation and removal of non-diamond carbon from them, which is reflected by the data of XPS and Raman spectra measurements, in particular, the change in the ratio of various forms of carbon sp^2/sp^3 (see Table 4).

Conclusion

A complex of modern methods was used in the course of the research aimed to study the impact of modification by annealing in air on the morphology, elemental and phase compositions, chemical state, and structure of primary particles of nanopowders obtained by the methods of grinding natural diamond and detonation synthesis. The annealing of nanopowder samples was performed at 5 given values of temperature: 200 °C, 300 °C, 400 °C, 500 °C and 550 °C.

It is shown that heat treatment in air at given values of temperature and heating time does not affect the elemental composition and atomic structure of primary particles of both DND and PND nanopowders. Using XPS and Raman spectroscopy methods, it has been established that annealing in air in the temperature range of 400–550 °C results in the removal of amorphous and graphite-like carbon atoms in sp^2 - and sp^3 -states from diamond nanopowders by oxidation with atmospheric oxygen. After annealing for 5 h at $t = 550$ °C, the relative number of non-diamond carbon

atoms in the sp^2 -state in the original DND nanopowder, containing about 33.2 % of non-diamond carbon atoms of the total number of carbon atoms, decreased to ~21.4 %. In this case, the relative number of carbon atoms in the sp^3 -state (in the diamond core lattice) and in the composition of oxygen-containing functional groups increased from ~39.8 % to ~46.5 % and from ~27 % to ~32.1 %, respectively. After annealing under the same conditions, their relative number in PND nanopowder, containing about 10.6 % of non-diamond carbon atoms in the sp^2 -state of the total number of carbon atoms before annealing, decreased to 7.1 %. The relative number of carbon atoms in the sp^3 -state increased from 72.9 to 82.1 %. The proportion of carbon atoms in the composition of oxygen-containing functional groups increased insignificantly (from 10.2 to 10.8 %) as well.

It is demonstrated that after annealing in air PND nanopowders exhibit a noticeable increase in the proportion of oxygen atoms in the composition of ester, carbonyl, and carboxyl functional groups compared to its content in the original sample. Whereas, in DND samples annealed in air, the proportion of oxygen atoms of the hydroxyl and carbonyl groups in the composition of ester, anhydride, and carboxyl groups somewhat decreases compared to the original sample. Besides, in DND samples after annealing, a slight increase in the proportion of oxygen atoms of the non-carbonyl group was recorded only in the composition of carboxyl, anhydride, and ester groups.

Acknowledgments: *The research was performed with the financial support from the Ministry of Education and Science of Russia within the frames of State Assignment for Project FSRG-2020-0017.*

Исследование выполнено при финансовой поддержке Минобрнауки России в рамках государственного задания по проекту FSRG-2020-0017.

References

1. Долматов В.Ю. Ультрадисперсные алмазы детонационного синтеза: свойства и применение. *Успехи химии*. 2001. Т. 70. No. 7. С. 687–708.
Dolmatov V.Y. Detonation synthesis ultradispersed diamonds: properties and applications. *Russ. Chem. Rev.* 2001. Vol. 70. No. 7. P. 607–626. DOI: 10.1070/RC2001v070n07ABEH000665.
2. Новиков Н.В., Богатырева Г.П., Волошин М.Н. Детонационные алмазы в Украине. *Физика тв. тела*. 2004. Т. 46. No. 4. С. 585–590.
Novikov N.V., Bogatyreva G.P., Voloshin M.N. Detonation

- diamond in Ukraine. *Phys. Solid State*. 2004. Vol. 46. No. 4. P. 600–605. DOI: 10.1134/1.1711432.
3. *Верещагин А.Л.* Структура и реакционная способность детонационных алмазов. *Юж.-сиб. науч. вестн.* 2017. Т. 18. No. 2. С. 24–30. <http://s-sibsb.ru/issues/51-2017-issues/issue-18/200-5>.
Vereshchagin A.L. Structure and reactivity of detonation diamonds. *Yuzhno-sibirskii nauchnyi vestnik*. 2017. Vol. 18. No. 2. P. 24–30 (In Russ.).
 4. *Osswald S., Yuchin G., Mochalin V., Kucheyev S.O., Gogotsi Y.* Control of sp²/sp³ carbon ratio and surface chemistry of nanodiamond powders by selective oxidation in air. *J. Am. Chem. Soc.* 2006. Vol. 128. No. 35. P. 11635–11642. DOI: 10.1021/ja063303n.
 5. *Плотников В.А., Демьянов Б.Ф., Макаров С.И., Черков А.Г.* Атомная структура нанокристаллов детонационного алмаза. *Фундам. пробл. соврем. материаловедения*. 2012. Т. 9. No. 4. С. 521–526.
Plotnikov V.A., Dem'yanov B.F., Makarov S.I., Cherkov A.G. Atomic structure of detonation diamond nanocrystals. *Fundamental'nye problemy sovremennogo materialovedeniya*. 2012. Vol. 9. No. 4. P. 521–526 (In Russ.).
 6. *Шарин П.П., Сивцева А.В., Яковлева С.П., Копырин М.М., Кузьмин С.А., Попов В.И., Никифоров Л.А.* Сравнение морфологических и структурных характеристик частиц нанопорошков, полученных измельчением природного алмаза и методом детонационного синтеза. *Известия вузов. Порошковая металлургия и функциональные покрытия*. 2019. No. 4. С. 55–67.
Sharin P.P., Sivtseva A.V., Yakovleva S.P., Kopyrin M.M., Kuz'min S.A., Popov V.I., Nikiforov L.A. Comparison of morphological and structural characteristics of nanopowder particles fabricated by grinding natural diamond and detonation synthesis. *Russ. J. Non-Ferr. Met.* 2020. Vol. 61. No. 4. P. 456–465. DOI: 10.3103/S1067821220040100.
 7. *Stehlik S., Varga M., Ledinsky M., Jirasek V., Artemenko A., Kozak H., Ondic L., Skakalova V., Argentero G., Pennycook T., Meyer J.C., Fejfar A., Kromka A., Rezek B.* Size and purity control of HPHT nanodiamonds down to 1 nm. *J. Phys. Chem. C*. 2015. Vol. 119. No. 49. P. 27708–27720. DOI: 10.1021/acs.jpcc.5b05259.
 8. *Плотников В.А., Демьянов Б.Ф., Макаров С.В., Богданов Д.Г.* Примесная подсистема детонационного наноалмаза. *Фундам. пробл. соврем. материаловедения*. 2013. Т. 10. No. 4. С. 487–492.
Plotnikov V.A., Dem'yanov B.F., Makarov S.V., Bogdanov D.G. Impurity detonation nanodiamond subsystem. *Fundamental'nye problemy sovremennogo materialovedeniya*. 2013. Vol. 10. No. 4. P. 487–492 (In Russ.).
 9. *Sharin P.P., Sivtseva A.V., Popov V.I.* X-rays photoelectron spectroscopy of nanodiamonds obtained by grinding and denotation synthesis. *Tech. Phys.* 2021. Vol. 66. No. 2. P. 275–279. DOI: 10.1134/S1063784221020183.
 10. *Yongwei Zhu, Zhijing Feng, Baichun Wang, Xianyang Xu.* Dispersion of nanodiamond and ultra-fine polishing of quartz wafer. *China Particuology*. 2004. Vol. 2. No. 4. P. 153–156. DOI: 10.1016/S1672-2515(07)60046-3.
 11. *Hirata A., Igarashi M., Kaito T.* Study on solid lubricant properties of carbon onion produced by heat treatment of diamond cluster or particles. *Tribol. Int.* 2004. Vol. 39. P. 899–905. DOI:10.1016/j.triboint.2004.07.006.
 12. *Zhao X., Wang T., Li Y., Huang L., Handschuh-Wang S.* Polydimethylsiloxane/nanodiamond composite sponge for enhanced mechanical or wettability performance. *Polymers*. 2019. Vol. 11. No. 6. P. 948–960. DOI: 10.3390/polym11060948.
 13. *Afandi A., Howkins A., Boyd I., Jackman R.* Nanodiamonds for device applications: An investigation of the properties of boron-doped detonation nanodiamonds. *Sci. Rep.* 2018. Vol. 8. No. 1. P. 1–10. DOI: 10.1038/s41598-018-21670-w.
 14. *Hsu S-H., Kang W.P., Davidson J.L., Huang J.H., Kerns D.V. Jr.* Nanodiamond vacuum field emission integrated differential amplifier. *IEEE Trans. Electron Devices*. 2013. Vol. 60. No. 1. P. 487–493. DOI: 10.1109/TED.2012.2228485.
 15. *Тверитинова Е.А., Житнев Ю.Н., Кулакова И.И., Маслаков К.И., Нестерова Е.А., Харланов А.Н., Иванов А.С., Савилов С.В., Лунин В.В.* Влияние структуры и свойств поверхности на каталитическую активность наноалмаза в конверсии 1,2-дихлорэтана. *Журн. физ. химии*. 2015. Т. 89. No. 4. С. 680–687.
Tveritinova E.A., Zhitnev Yu.N., Kulakova I.I., Maslakov K.I., Nesterova E.A., Kharlanov A.N., Ivanov A.S., Savilov S.V., Lunin V.V. Effect of structure and surface properties on the catalytic activity of nanodiamond in the conversion of 1,2-dichloroethane. *Russ. J. Phys. Chem. A*. 2015. Vol. 89. No. 4. P. 680–687. DOI: 10.1134/S0036024415040251.
 16. *Lin Y., Sun X., Su D., Centi G., Perathoner S.* Catalysis by hybrid sp²/sp³ nanodiamonds and their role in the design of advanced nanocarbon materials. *Chem. Soc. Rev.* 2018. Vol. 47. No. 22. P. 8438–8473. DOI: 10.1039/C8CS00684A.
 17. *Яковлев Р.Ю., Соломатин А.С., Леонидов Н.Б., Кулакова И.И., Лисичкин Г.В.* Детонационный наноалмаз — перспективный носитель для создания систем доставки лекарственных веществ. *Рос. хим. журн.* 2012. Т. 56. No. 3–4. С. 114–125.

- Yakovlev R.Yu., Solomatin A.S., Leonidov N.B., Kulakova I.I., Lisichkin G.V.* Detonation nanodiamond — a perspective carrier for drug delivery systems. *Russ. J. Gen. Chem.* 2014. Vol. 84. No. 2. P. 379—390. DOI: 10.1134/S1070363214020406.
18. *Huang H., Pierstorff E., Ho D., Osawa E.* Active nanodiamond hydrogels for chemotherapeutic delivery. *Nano Lett.* 2007. Vol. 7. No. 11. P. 3305—3314. <https://doi.org/10.1021/nl071521o>.
 19. *Schrand A.M., Dai L., Schlager J.J., Hussain S.M., Osawa E.* Differential biocompatibility of carbon nanotubes and nanodiamonds. *Diam. Relat. Mater.* 2007. Vol. 16. No. 12. P. 2118—2123. <https://doi.org/10.1016/j.diamond.2007.07.020>.
 20. *Tsai L.-W., Lin Y.-C., Perevedentseva E., Lugovtsov A., Priezhev A., Cheng C.-L.* Nanodiamonds for medical applications: interaction with blood in vitro and in vivo. *Int. J. Mol. Sci.* 2016. Vol. 17. No. 7. P. 1111 (17). DOI: 10.3390/ijms17071111.
 21. *Денисов С.А., Дзидзигури Э.Л., Спицын Б.В., Соколина Г.А., Болдырев Н.Ю.* Очистка и модификация продукта детонационного синтеза алмаза. *Уч. записки Петрозав. гос. ун-та. Сер. Физ.-мат. науки.* 2011. No. 2. С. 89—98.
Denisov S.A., Dzidziguri E.L., Spitsyn B.V., Sokolina G.A., Boldyrev N.Y. Purification and modification of the product of detonation synthesis of diamond. *Uchenye zapiski Petrozavodskogo gos. un-ta. Ser. Fiziko-matematicheskie nauki.* 2011. No. 2. P. 89—98 (In Russ.).
 22. *Чиганов А.С.* Селективное ингибирование окисления наноалмазов в технологии очистки. *Физика тв. тела.* 2004. Т. 46. No. 4. С. 605—606.
Chiganov A.S. Selective inhibition of the oxidation of nanodiamonds for their cleaning. *Phys. Solid State.* 2004. Vol. 46. No. 4. P. 620—621. <https://doi.org/10.1134/1.1711436>.
 23. *Korepanov V.I., Hamaguchi H., Osawa E., Ermolenkov V., Lednev I., Etzold B., Levinson O., Zousman B., Eprella C.P., Chang H.-C.* Carbon structure in nanodiamonds elucidated from Raman spectroscopy. *Carbon.* 2017. No. 121. P. 322—329. <https://doi.org/10.1016/j.carbon.2017.06.012>.
 24. *Scofield J.H.* Hartree-slater subshell photoionization cross-sections at 1254 and 1487 eV. *J. Electron Spectrosc. Relat. Phenom.* 1976. Vol. 8. No. 2. P. 129—137. DOI: 10.1016/0368-2048(76)80015-1.
 25. *Орлов Ю.Л.* Минералогия алмаза. 2-е изд. М.: Наука, 1984.
Orlov Yu.L. Diamond mineralogy. Moscow: Nauka, 1984 (In Russ.).
 26. *Гурин В.А., Габелков С.В., Полтавцев Н.С., Гурин И.В., Фурсов С.Г.* Кристаллическая структура пирографита и каталитически осажденного углерода. *Вопр. атом. науки и техники. Сер. Физика радиац. поврежденных и радиац. материаловедение.* 2006. Т. 89. No. 4. С. 195—199.
Gurin V.A., Gabelkov S.V., Poltavtsev N.S., Gurin I.V., Fursov S.G. Crystal structure of pyrographite and catalytically deposited carbon. *Voprosy atomnoi nauki i tekhniki. Ser. Fizika radiatsionnykh povrezhdenii i radiatsionnoe materialovedenie.* 2006. Vol. 89. No. 4. P. 195—199 (In Russ.).
 27. *Штольц А.К., Медведев А.И., Курбатов Л.В.* Рентгеновский анализ микронапряжений и размера областей когерентного рассеяния в поликристаллических материалах. Екатеринбург: УГТУ—УПИ, 2005. https://study.urfu.ru/Aid/Publication/328/1/Shtolts_Medvedev_Kurbatov.pdf
Shtols A.K., Medvedev A.I., Kurbatov L.V. X-ray analysis of microstresses and sizes of coherent scattering regions in polycrystalline materials. Ekaterinburg: UGTU—UPI, 2005 (In Russ.).
 28. *Андреев В.Д., Созин Ю.И.* Структура ультрадисперсных алмазов. *Физика тв. тела.* 1999. Т. 41. No. 10. С. 1890—1892.
Andreev V.D., Sozin Y.I. Structure of ultradisperse diamonds. *Phys. Solid State.* 1999. Vol. 41. No. 10. P. 1736—1739. <https://doi.org/10.1134/1.1131077>.
 29. <http://xpspeak.software.informer.com/4.1>.
 30. *Алексенский А.Е., Осипов В.Ю., Вуль А.Я., Бер Б.Я., Смирнов А.Б.* Оптические свойства слоев наноалмазов. *Физика тв. тела.* 2001. Т. 43. No. 1. С. 140—145.
Aleksenskii A.E., Osipov V.Y., Vul' A.Y., Ber B.Y., Smirnov A.B. Optical properties of nanodiamond layers. *Phys. Solid State.* 2001. Vol. 43. No. 1. P. 145—150. DOI: 10.1134/1.1340200.
 31. *Fang C., Zhang Yu., Shen W., Sun Sh., Zhang Zh., Xue L., Jia X.* Synthesis and characterization of HPHT large single-crystal diamonds under the simultaneous influence of oxygen and hydrogen. *Cryst. Eng. Comm.* 2017. Vol. 19. No. 38. P. 5727—5734. DOI: 10.1039/C7CE01349C.
 32. *Qi M., Xiao J., Cheng Y., Wang Zh., Jiang A., Guo Y., Tao Z.* Effect of various nitrogen flow ratios on the optical properties of (Hf : N)—DLC films prepared by reactive magnetron sputtering. *AIP Adv.* 2017. Vol. 7. No. 8. P. 085012. DOI: 10.1063/1.4993631.
 33. *Швидченко А.В., Жуков А.Н., Дидейкин А.Т., Байдакова М.В., Шестаков М.С., Шнитов В.В., Вуль А.Я.* Электрические свойства поверхности монокристаллических частиц детонационного наноалмаза, полученных отжигом агломератов в атмосфере воздуха. *Коллоид. журн.* 2016. Т. 78. No. 2. С. 218—224. DOI: 10.7868/S0023291216020142.

- Shvidchenko A.V., Zhukov A.N., Dideikin A.T., Baidakova M.V., Shestakov M.S., Shnitov V.V., Vul' A.Ya. Electrical properties of the surface of single-crystal particles of detonation nanodiamond obtained by annealing agglomerates in air. *Kolloidnyi Zhurnal*. 2016. Vol. 78. No. 2. P. 218—224 (In Russ.).
34. Araujo M.P., Soares O.S.G.P., Fernandes A.J.S., Pereira M.F.R., Freire C. Tuning the surface chemistry of graphene flakes: new strategies for selective oxidation. *RSC Adv*. 2017. No. 7. P. 14290. DOI: 10.1039/c6ra28868e.
35. Li H., Xu T., Wang C., Chen J., Zhou H., Liu H. Effect of relative humidity on the tribological properties of hydrogenated diamond-like carbon films in a nitrogen environment. *J. Phys. D: Appl. Phys.* 2005. Vol. 38. P. 62—69. DOI: 10.1088/0022-3727/38/1/011.
36. Полянская Е.М., Таран О.П. Исследование функциональных групп на поверхности окисленного углеродного материала Сибунит методами кислотно-основного титрованияи РФЭС. *Вестн. Томск. гос. ун-та. Химия*. 2017. No. 10. С. 6—26. DOI: 10.17223/24135542/10/1.
- Polyanskaya E.M., Taran O.P.* Study of functional groups on the surface of the oxidized carbon material Sibunit by acid-base titration and XPS. *Vestnik Tomskogo gos. un-ta. Khimiya*. 2017. No. 10. P. 6—26 (In Russ.).
37. Rey A., Faraldos M., Bahamonde A., Casas J.A., Zazo J.A., Rodríguez J.J. Role of the activated carbon surface on catalytic wet peroxide oxidation. *Ind. Eng. Chem. Res.* 2008. Vol. 47. No. 21. P. 8166—8174. DOI: 10.1021/ie800538t.
38. Богданов Д.Г., Макаров С.В., Плотников В.А. Десорбция примесей при нагреве детонационного наноалмаза. *Письма в ЖТФ*. 2012. Т. 38. No. 4. С. 89—95.
- Bogdanov D.G., Makarov S.V., Plotnikov V.A.* Thermo-desorption of impurities from detonation nanodiamond. *Tech. Phys. Lett.* 2012. Vol. 38. No. 4. P. 199—202. <https://doi.org/10.1134/S1063785012020198>.
39. Плотников В.А., Богданов Д.Г., Макаров С.В., Богданов А.С. Сорбционные и десорбционные свойства детонационного наноалмаза. *Изв. вузов. Химия и хим. технология*. 2017. Т. 60. No. 9. С. 27—32. DOI: 10.6060/tcct.2017609.1y.
- Plotnikov V.A., Bogdanov D.G., Makarov S.V., Bogdanov A.S.* Sorption and desorption properties of detonation nanodiamond. *Izvestiya vuzov. Khimiya i khimicheskaya tekhnologiya*. 2017. Vol. 60. No. 9. P. 27—32 (In Russ.).
40. Кощеев А.П., Горохов П.В., Громов М.Д., Перов А.А., Отт У. Химия поверхности модифицированных детонационных наноалмазов различных типов. *Журн. физ. химии*. 2008. Т. 82. No. 10. С. 1908—1914.
- Koshcheev A.P., Gorokhova P.V., Gromova M.D., Perova A.A., Ott U.* The chemistry of the surface of modified detonation nanodiamonds of different types. *Russ. J. Phys. Chem. A*. 2008. Vol. 82. No. 10. P. 1708—1714. DOI: 10.1134/S0036024408100129.

UDC 669.1 : 620.1

DOI dx.doi.org/10.17073/1997-308X-2022-4-84-92

Features of the impact of hot isostatic pressing and heat treatment on the structure and properties of maraging steel obtained by selective laser melting method

© 2022 г. **A.O. Kayasova, E.A. Levashov**

National University of Science and Technology (NUST) «MISIS», Moscow, Russia

Received 19.07.2022, revised 27.07.2022, accepted for publication 28.07.2022

Abstract: Using the SLM method in a nitrogen blanket with heating to a temperature of 200 °C, samples were obtained at a position of 0° against the build plate. The effect of the hot isostatic pressing (HIP) and heat treatment (HT: hardening + aging) on the structure and mechanical properties of maraging steel CL50 WS was studied (the Russian analogue is ChS4 grade). To analyze the effect of post-processing on the strength characteristics (σ_b , $\sigma_{0.2}$, δ , ψ), tensile tests were conducted. Their results indicated high values of strength and ductility. It has been established that as a result of HT in the steel structure, in addition to α -Fe, γ -Fe, dispersed precipitates of the NiTi₃ strengthening phase are formed, the identification of which was carried out by high-resolution transmission electron microscopy. Through the NiTi₃ intermetallic phase, the steel has acquired increased tensile strength and yield strength required for the production of critical components and parts for highly loaded turbomachine disks. The change in the porosity of the samples before and after the HIP was analyzed. The microstructure of the samples and the changes that occur under the influence of various post-processing options are studied. The fine-grained homogeneous structure obtained by combining the SLM, HIP and HT provided optimal strength and ductility. Analysis of fractures after mechanical testing showed that the samples after post-processing are destroyed according to the viscous-pitting mechanism with the formation of a neck.

Keywords: selective laser melting, maraging steels, HIP, heat treatment, microstructure, phase composition, mechanical properties.

Kayasova A.O. — postgraduate student of the Department of powder metallurgy and functional coating (PM&FC) of National University of Science and Technology (NUST) «MISIS» (119049, Russia, Moscow, Leninskii pr., 4).
E-mail: NKayasova@gmail.com.

Levashov E.A. — Dr. Sci. (Eng.), prof., acad. of the Russian Academy of Natural Science, chair of the Department of PM&FC of NUST «MISIS», head of the Scientific-Educational Centre of SHS of MISIS—ISMAN.
E-mail: levashov@shs.misis.ru.

For citation: Kayasova A.O., Levashov E.A. Features of the impact of hot isostatic pressing and heat treatment on the structure and properties of maraging steel obtained by selective laser melting method. *Izvestiya Vuzov. Poroshkovaya Metallurgiya i Funktsional'nye Pokrytiya* (Powder Metallurgy and Functional Coatings). 2022. Vol. 16. No. 4.

P. 84—92 (In Russ.). DOI: dx.doi.org/10.17073/1997-308X-2022-4-84-92.

Особенности влияния горячего изостатического прессования и термообработки на структуру и свойства мартенситно-старееющей стали, полученной методом селективного лазерного сплавления

А.О. Каясова, Е.А. Левашов

Национальный исследовательский технологический университет (НИТУ) «МИСиС», г. Москва, Россия

Статья поступила в редакцию 19.07.22 г., доработана 27.07.22 г., подписана в печать 28.07.22 г.

Аннотация: Методом селективного лазерного сплавления (СЛС) в среде азота при подогреве до температуры 200 °C получены образцы в положении 0° относительно плиты построения. Изучено влияние горячего изостатического прессования (ГИП) и термообработки (ТО: закалка + старение) на структуру и механические свойства мартенситно-старееющей стали CL50 WS (российский аналог — ЧС4). Для анализа влияния постобработки на прочностные характеристики (σ_b , $\sigma_{0.2}$, δ , ψ) проведены испытания на разрыв. Их результаты показали высокие значения прочности и пластичности.

Установлено, что в результате ТО в структуре стали, помимо α -Fe, γ -Fe, образуются дисперсные выделения упрочняющей фазы NiTi_3 , идентификацию которой проводили методом просвечивающей электронной микроскопии высокого разрешения. Благодаря интерметаллидной фазе NiTi_3 , сталь приобрела повышенные предел прочности и предел текучести, требуемые для производства ответственных узлов и деталей высоконагруженных дисков турбомашин. Проанализировано изменение пористости образцов до и после ГИП. Исследованы микроструктуры образцов и изменения, происходящие под влиянием различных вариантов постобработки. Мелкозернистая однородная структура, полученная при сочетании СЛС, ГИП и ТО, обеспечила оптимальные показатели прочности и пластичности. Анализ изломов после механических испытаний показал, что образцы после постобработки разрушаются по вязко-ямочному механизму с образованием шейки.

Ключевые слова: селективное лазерное сплавление, мартенситно-стареющие стали, горячее изостатическое прессование, термическая обработка, микроструктура, фазовый состав, механические свойства.

Каясова А.О. — аспирант кафедры порошковой металлургии и функциональных покрытий (ПМиФП) НИТУ «МИСИС» (119049, г. Москва, Ленинский пр-т, 4). E-mail: NKayasova@gmail.com.

Левашов Е.А. — докт. техн. наук, проф., акад. РАЕН, зав. кафедрой ПМиФП НИТУ «МИСИС», директор Научно-учебного центра СВС МИСиС—ИСМАН. E-mail: levashov@shs.misis.ru.

Для цитирования: Каясова А.О., Левашов Е.А. Особенности влияния горячего изостатического прессования и термообработки на структуру и свойства мартенситно-стареющей стали, полученной методом селективного лазерного сплавления. *Известия вузов. Порошковая металлургия и функциональные покрытия*. 2022. Т. 16. No. 4. С. 84—92. DOI: dx.doi.org/10.17073/1997-308X-2022-4-84-92.

Introduction

High-strength maraging steel (MS) belongs to the group of high-alloy steel grades that are based on carbon-free martensite. Compared to classic carbon-free steels, maximum hardening is achieved by heat treatment (HT) in the aging mode due to the dispersion hardening of highly ductile martensite.

The worldwide experience in the application and operation of MS steels has proven that they provide a high degree of reliability, manufacturability and other advantages in comparison with carbon steels. The low hardness of low-carbon martensite contributes to good machinability and deformability in the initial and hardened states, while aging provides a high level of strength, ductility and permanent deformation. The hardening heat treatment of complex shaped thin-walled parts is accompanied by a small change in linear dimensions, i.e. no warpage is caused.

MS steels exhibit the feature of throughout hardenability at the austenitization temperature, i.e. martensitic structure formation is assured regardless of the cooling rate and cross-sectional dimension of a finished product or a part. Such steels are well deformed without heating during sheet stamping and rotary drawing and forging.

MS steel of ChS4 grade with strength $\sigma_V = 1950 \div \pm 2150$ MPa has increased ductility, especially under conditions of local deformation, and, as a consequence, lower sensitivity to stress concentrators, which ensures

higher reliability during operation under extreme loads compared to high-strength carbon steels treated for the equivalent strength.

The structure of carbon-free martensite in all grades of MS steel, including ChS4, belongs to the type of massive martensite, which differs from carbon martensite in the absence of tetragonality in the α -BCC lattice, high dislocation density, and the presence of a significant number of twins. This type of structure is not exposed to tempering and softening processes, but is only capable of intensive strengthening due to precipitation of dispersed phases.

In powder metallurgy, MS steel products are obtained from atomized alloy powders by thermoforming methods. This allows to reduce segregational heterogeneity as well as to ensure high strength properties. The parts produced by sintering exhibit high ductility, toughness and can be used under high-temperature contact conditions.

For the manufacture of geometrically-complex special-purpose products of MS steels, it is highly promising to use the technology of selective laser melting (SLM), which significantly reduces the production time and the material consumption. Interest in using MS steels in SLM technology is caused not only by a high complex of physical and mechanical properties, but also by almost complete absence of warping in the printing process due to the unique nature of the steel. The forma-

tion of the product during SLM is performed due to the successive melting and crystallization of layers of metal powder. Therefore, the formation of interfaces, which are a structural defect for this technology and may contain discontinuities, occurs.

The SLM process is characterized by such defects as an incomplete fusion of particles, a residual porosity, microcracks, high residual stresses, and a formation of supersaturated solid solutions. The presence of defects results in a decrease in the mechanical and operational properties of products. In this regard, the use of post-processing techniques, in particular hot isostatic pressing (HIP), is reasonable and economically feasible since it reduces residual porosity, heals structural defects, ensuring a fine-grained steel structure with the effect of dispersion hardening [1–8].

The purpose of this paper is to study the effect of HIP and heat treatment by aging on the structural phase transformations and properties of SLM samples made of maraging steel.

Research methodology

The metal powder of maraging steel of CL50 WS grade (Germany) was used for the research. Its Russian analogue is steel of ChS 4 grade. The chemical composition of CL50 WS alloy is presented below, wt.%:

Fe	Base	Si	≤ 0.1
Mo	4.5–5.2	Mn	≤ 0.15
Ni	17.0–19.0	P	≤ 0.01
Ti	0.8–1.2	S	≤ 0.01
Co	8.5–10.0	Cr	≤ 0.25
C	≤ 0.03		

The concentrations of gas impurities in the powder for oxygen, nitrogen and hydrogen are 0.146, 0.021 and 0.0075 wt.%, respectively. The particle size of the powder is in the range of 5–45 μm, while the distribution quantiles d_{10} , d_{50} and d_{90} are 17.7, 29.4 and 48.0 μm, re-

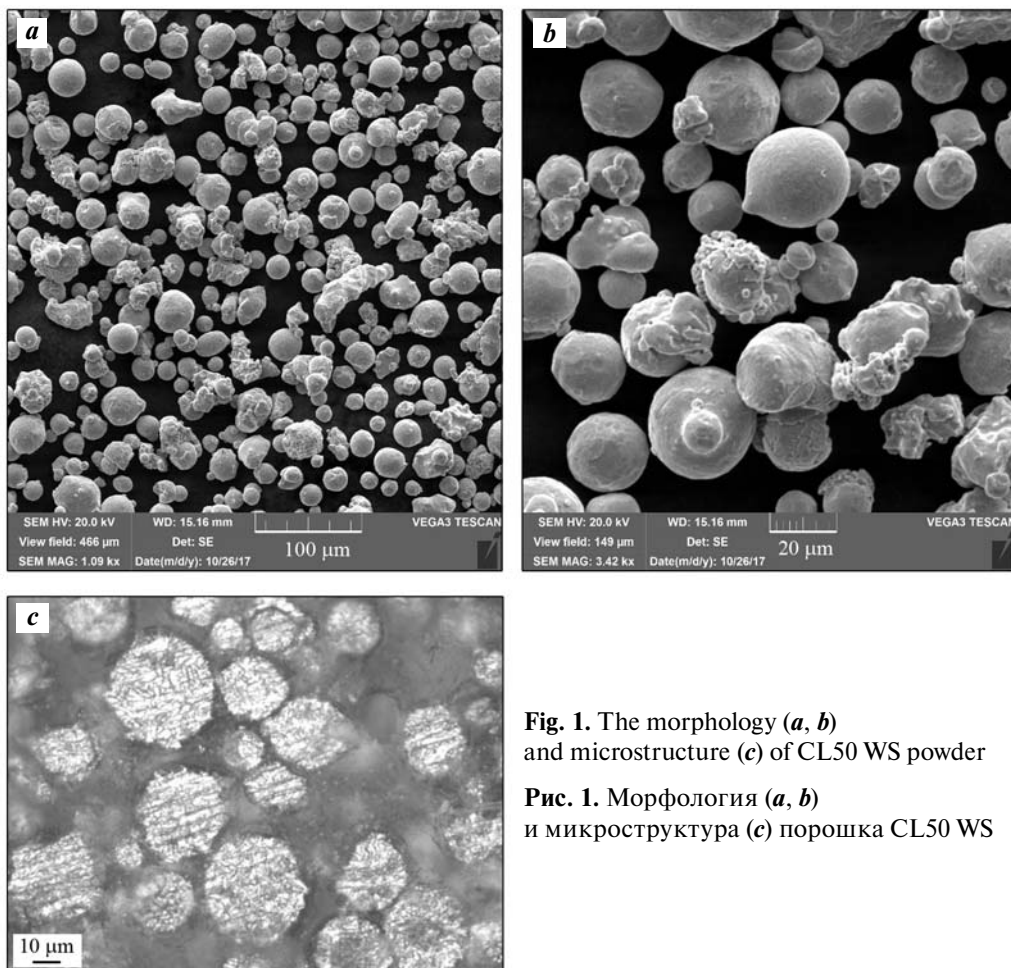


Fig. 1. The morphology (a, b) and microstructure (c) of CL50 WS powder

Рис. 1. Морфология (a, b) и микроструктура (c) порошка CL50 WS

spectively. The bulk density is 4.544 g/cm^3 . The powder contains irregularly shaped particles up to $50 \text{ }\mu\text{m}$ in size. There are satellites on the surface of individual particles (Fig. 1, *a, b*). The microstructure of the powder is represented by small dendritic crystals, no closed gas pores are detected (Fig. 1, *c*).

The samples were obtained on the «Concept Laser M2» machine (Germany) under a nitrogen blanket with the blanks being horizontally positioned against the build plate and subjected to the following process parameters: the thickness of the fused layer is $30 \text{ }\mu\text{m}$, the laser power is 180 W , the scanning speed is 800 mm/s , the temperature of the build plate during the printing process is $200 \text{ }^\circ\text{C}$. The control of blank samples was performed using XTH450 LC X-ray tomography system (Nikon Metrology, Japan) with a sensitivity of 0.1 mm .

The SLM samples were gasostated on ABRA HIRP 10/26-200-2000 unit (Sweden). The HIP mode consisted of heating to the hardening temperature and holding for 2 h at a constant pressure. Following the HIP, additional heat treatment was conducted in a chamber furnace with a blanketing atmosphere in two modes: HT1 — hardening followed by aging, HT2 — aging.

Porosity was determined by the layer-by-layer analysis in the cross section with the calculation of the average index for three layers with a step of 3 mm . Sections on samples for determining porosity and structural studies were made parallel (section YZ) and perpendicular (section XY) to the direction of synthesis.

To evaluate the mechanical properties of steel, cylindrical test-pieces were cut out of blanks for tensile tests (under GOST 1497-84, type IV, No. 8). The tests were conducted on «Shimadzu 100kN» unit (Japan), offset yield strength ($\sigma_{0.2}$), tensile strength (σ_V), percentage of elongation (δ) and percentage of reduction (ψ) were determined.

The fractographic analysis of fractures was performed on «Vega 3» scanning electron microscope (Tescan, the Czech Republic), and the study of the microstructure was performed on «Hitachi S-3400N» scanning electron microscope (Japan). The fine structure was studied by transmission electron microscopy (TEM) method on JEM-2100 instrument (Jeol, Japan), including *in situ* at high resolution. Foils for TEM were prepared by ion etching in «PIPS II System» (Gatan, United States).

Research results

The appearance of SLM blanks of MS steel is shown in Fig. 2.

The absence of discontinuities and cracks in the blanks was established using X-ray tomography (Fig. 3).

Hot isostatic treatment allowed to reduce the residual porosity from 0.43 to 0.20. The analysis of mechanical tests of samples in the state of SLM + HIP + HT1 demonstrated an increase in the yield strength by 58 % and tensile strength by 50 % relative to the state of SLM + HIP, and in the case of the state of SLM + HIP + HT2, the increase in these indicators was 58 % and 48 %, respectively. Thus, it has been established that heat treatment modes ensure optimal

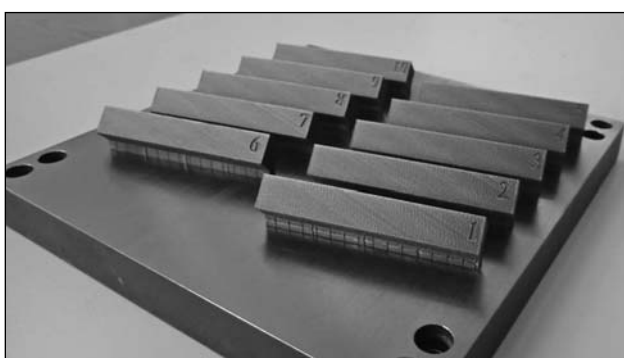


Fig. 2. The location of blanks on the build plate

Рис. 2. Расположение заготовок на плите построения

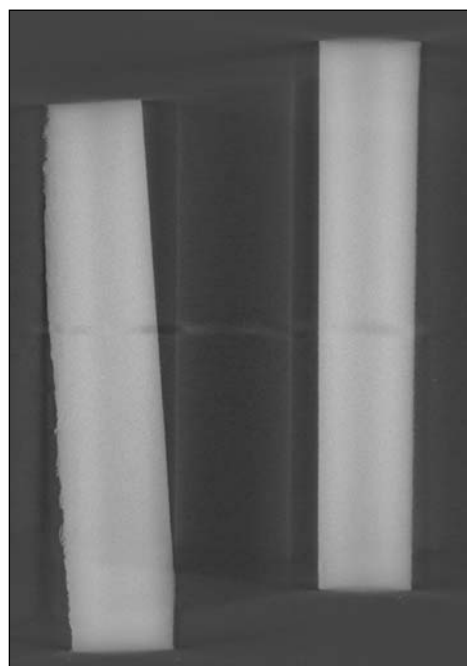


Fig. 3. The X-ray tomography of SLM samples

Рис. 3. Рентгеновская томография СЛС-образцов

indices of strength and ductility [9]. Fig. 4 shows the deformation curves for uniaxial tension of samples in the states of SLM + HIP + HT1, SLM + HIP + HT2, and SLM + HIP.

The samples subjected to post-processing under SLM + HIP + HT1 and SLM + HIP + HT2 modes are characterized by a uniform plastic deformation area and high strength and ductility.

A noticeable increase in strength and ductility was also observed for the samples in SLM + HIP state ($\psi = 58.9\%$). The obtained indices of percentage of reduction exceed the value for this steel in the state of hot-rolled and forged bar (TU 14-1-811-73, $\psi = 40\%$).

In works [10–12], it is shown that the mechanical properties of MS steel of 18Ni300 grade (the analogue of steel of 01KhN18L9M5TYu grade) in SLM state are in the following intervals: $\sigma_{0.2} = 500\div 900$ MPa, $\sigma_V = 800\div 1100$ MPa, $\delta = 10\div 30\%$, $\psi = 11\div 25\%$, in SLM + HT state ($t = 425\div 900$ °C) they are as follows: $\sigma_{0.2} = 370\div 1000$ MPa, $\sigma_V = 700\div 1200$ MPa, $\delta = 15\div 35\%$, $\psi = 20\div 50\%$. Thus, the mechanical properties

obtained for MS steel of CL50 WS grade correspond to the international standard.

Fig. 5 shows the microstructure of SLM sample after HIP with high structural homogeneity. There is no sub-grain structure typical for SLM samples that indicates the completion of the grain recrystallization process during HIP.

Aging after gasostatic processing also results in the formation of a uniform martensitic structure, but with a smaller grain size (Fig. 6). As a result of «martensitic» aging, the alloying elements form a plastic matrix phase being a substituted martensite reinforced with uniformly distributed high-strength dispersed precipitates of the excessive NiTi₃ intermetallic phase with an average crystallite size of 10 μm . The identification of this phase was confirmed by TEM method in an *in situ* study of structural transformations during heating of the lamella. The precipitation of NiTi₃ phase from a supersaturated solid solution begins at a temperature of 570 °C, which corresponds to the aging temperature (Fig. 7).

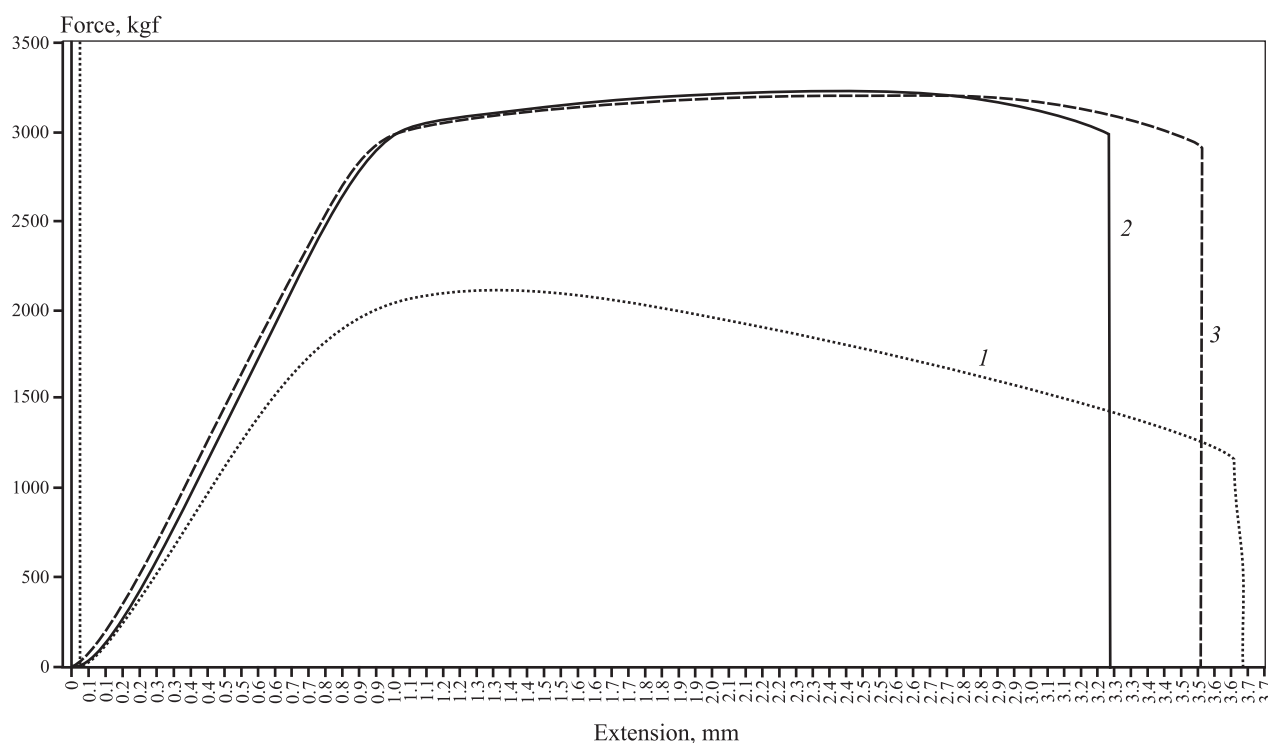


Fig. 4. The deformation curves in uniaxial tension of samples made of MS steel of CL50 WS grade depending on the type of post-processing

1 – SLM; 2 – SLM + HIP + HT1; 3 – SLM + HIP + HT2

Рис. 4. Деформационные кривые при одноосном растяжении образцов из МС-стали CL50 WS в зависимости от вида постобработки

1 – СЛС; 2 – СЛС + ГИП + ТО1; 3 – СЛС + ГИП + ТО2

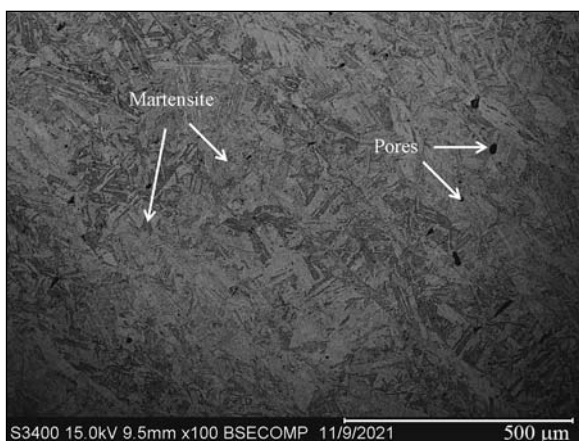


Fig. 5. The microstructure of MS steel in SLM + HIP state

Рис. 5. Микроструктура МС-стали в состоянии СЛС + ГИП

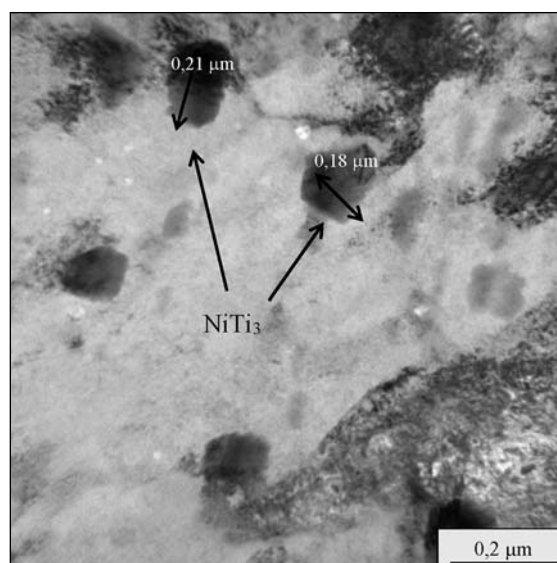


Fig. 7. TEM image of the precipitated phase

Рис. 7. ПЭМ-изображение выделившейся фазы

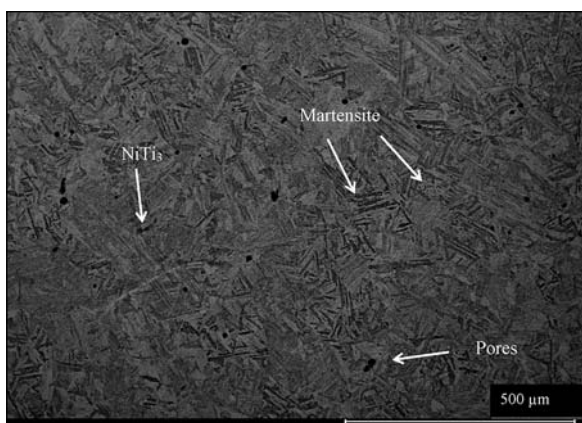


Fig. 6. The microstructure of MS steel in the state of SLM + HIP + HT2

Рис. 6. Микроструктура МС-стали в состоянии СЛС+ ГИП + ТО2

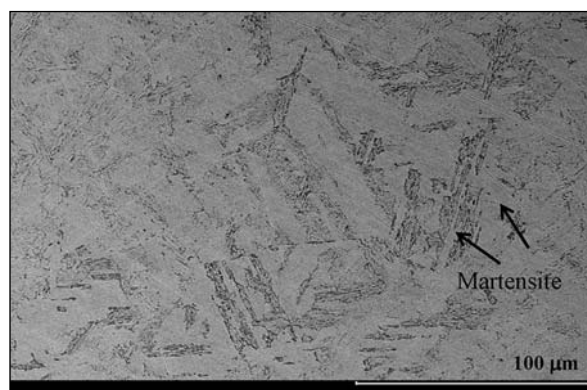


Fig. 8. The microstructure of SLM sample after HIP + HT1

Рис. 8. Микроструктура СЛС-образца после обработки ГИП + ТО1

Post-processing under HIP + HT1 mode also resulted in the formation of a hardening phase, however, additional hardening after HIP contributed to the coarsening of the martensitic structure (Fig. 8).

The studies of the fine structure of SLM samples by TEM method revealed the grains of NiTi₃ phase in the interdendritic space. As a result of calculating the parameters of crystal lattices of particles by Fourier transforms, the parameters of BCC-lattice $a = 0.210 \pm 0.247$ Å were determined at tabular values $a = 0.289 \pm 0.607$ Å. The formation of twins is specific for this type of steel (Fig. 9). A slight deviation of crystal lattice parameters of the identified phases from the tabular values is associ-

ated with the dissolution of alloying and impurity elements in them.

The fractographic analysis revealed that the samples are destroyed with necking, i.e. the plastic component of deformation prevailed, and the destruction proceeded from the surface. Initially, a viscous shear occurred, resulting in separation. The macroplastic fracture was formed by the shear mechanism. The micromechanism of destruction is a viscous-pitting one. This type of failure is typical for maraging steels, regardless of the method of obtaining the material [13–22]. Fig. 10 exhibits the micromechanism (a) and the appearance of fractures (b–d).

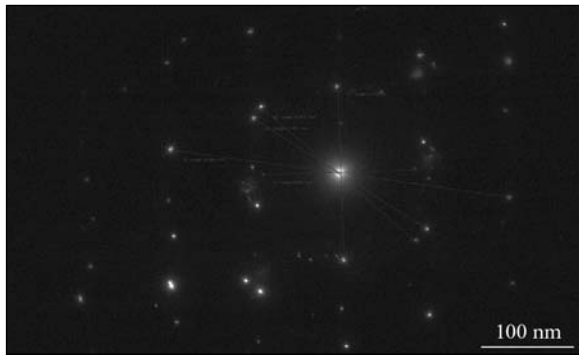


Fig. 9. The Fourier transforms separated from the surface of phase

Рис. 9. Фурье-трансформации выделившейся с поверхности фазы

Conclusions

1. In the process of hot isostatic pressing according to the selected modes, the subgrain structure of SLM samples of maraging steel is recrystallized with the formation of a homogeneous structure. As a result of aging, the alloying elements form a plastic matrix phase being a substituted martensite, dispersion-hardened by the precipitates of excessive phase $NiTi_3$.

2. HIP in combination with heat treatment (hardening + aging) provides a 2-fold reduction in residual porosity and a 1.5-fold increase in tensile strength and offset yield strength.

3. The SLM samples made of MS steel are destroyed

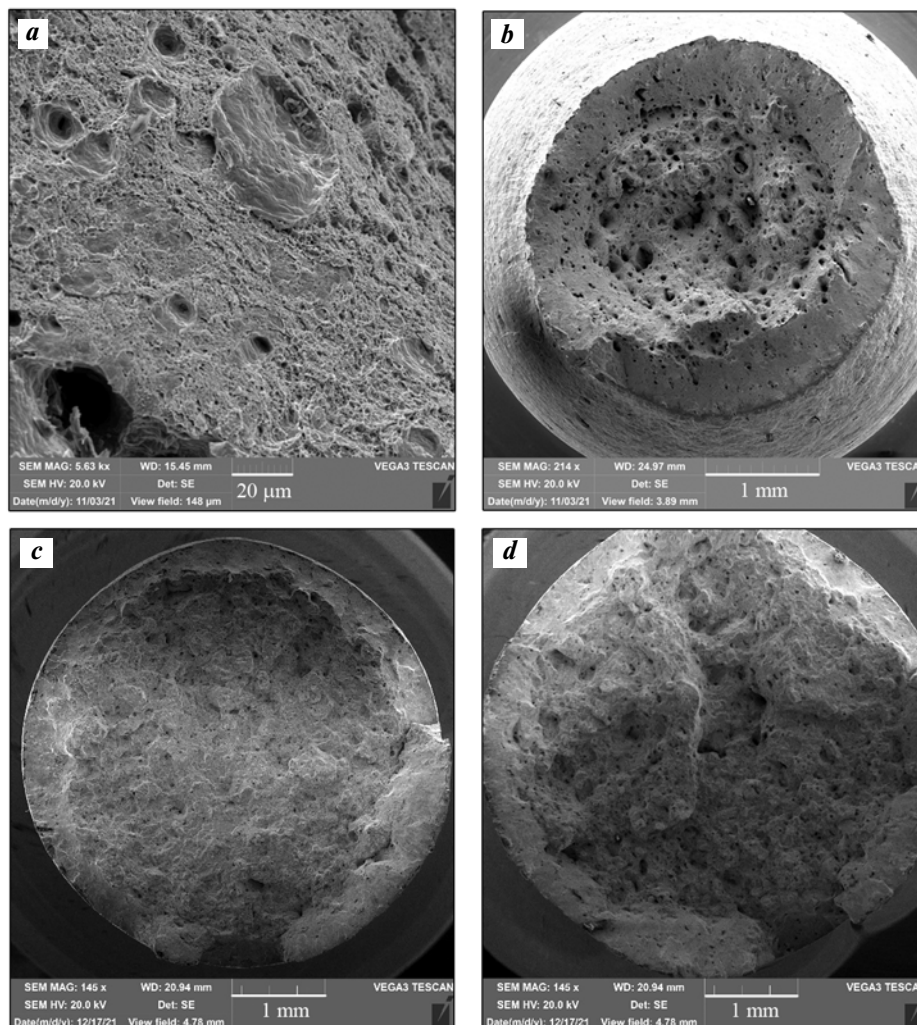


Fig. 10. The appearance of fractures

a — micromechanism; *b* — HIP; *c* — HIP, hardening and aging; *d* — HIP and aging

Рис. 10. Внешний вид изломов

a — микромеханизм; *b* — ГИП; *c* — ГИП, закалка и старение; *d* — ГИП и старение

with necking according to the viscous-pitting mechanism, which is typical for maraging steels, regardless of the method of their production.

Acknowledgments: *The work was performed with the financial support from the Russian Science Foundation (Project No. 19-79-10226).*

Работа выполнена при финансовой поддержке Российского научного фонда (проект № 19-79-10226).

References

1. Пикеринг Ф.Б. Физическое металловедение и разработка сталей. М.: Металлургия, 1982.
Pikering F.B. Physical metallurgy and development of steels. Moscow: Metallurgiya, 1982 (In Russ.).
2. Панов В.С., Чурилин А.М. Технология и свойства спеченных твердых сплавов и изделий из них: Учеб. для вузов. М.: МИСиС, 2001.
Panov V.S., Churilin A.M. Technology and properties of sintered hard alloys and products from them. Moscow: MISIS, 2001 (In Russ.).
3. Бабич Б.Н. Металлические порошки и порошковые материалы. М.: Экомет, 2005.
Babich B.N. Metal powders and powder materials. Moscow: Ekomet, 2005 (In Russ.).
4. Раковский В.С., Силаев А.Ф., Ходкин В.И., Фаткуллин О.Х. Порошковая металлургия жаропрочных сплавов и тугоплавких металлов. М.: Металлургия, 1974.
Rakovskii V.S., Silaev A.F., Hodkin V.I., Fatkullin O.Kh. Powder metallurgy of heat-resistant alloys and refractory metals. Moscow: Metallurgiya, 1974 (In Russ.).
5. Либенсон Г.А., Лопатин В.Ю., Комарницкий Г.В. Производство металлических порошков. Т. 1. Формование и спекание порошков: Учеб. для вузов. М.: МИСиС, 2001.
Libenson G.A., Lopatin V.Yu., Komarnitskii G.V. Production of metal powders. Vol. 1. Formation and sintering of powders. Moscow: MISIS, 2001 (In Russ.).
6. Акименко В.Б., Гуляев И.А., Калашникова О.Ю., Секачев М.А., Гаврилов В.А., Гаврилов С.А. Железные и легированные порошки в России — промышленные технологии и перспективные разработки. В сб.: *Инженерия поверхности. Новые порошковые композиционные материалы. Сварка*. Ч. 1. Под ред. П.А. Витязь. Минск: Институт порошковой металлургии, 2011. С. 60—65.
Akimenko V.B., Gulyaev I.A., Kalashnikova O.Yu., Sekachev M.A., Gavrilov V.A., Gavrilov S.A. Iron and alloyed powders in Russia — industrial technologies and advanced developments. In: Surface engineering. New powder composite materials. Welding. Pt. 1. Ed. P.A. Vityaz'. Minsk: Institut poroshkovoi metallurgii, 2011. P. 60—65 (In Russ.).
7. Оглезнева С.А. Материаловедение и технологии современных и перспективных материалов: Учеб. пос. Пермь: Изд-во Перм. нац. иссл. политех. ун-та, 2012.
Oglezneva S.A. Materials science and technology of modern and promising materials. Perm': Izd-vo Perm. nats. issled. politekhn. un-ta, 2012 (In Russ.).
8. Ильющенко А.Ф., Савич В.В. Порошковая металлургия — одна из первых аддитивных технологий. В сб.: *Аддитивные технологии, материалы и конструкции: Матер. науч.-техн. конф.* (Гродно, 5—6 октября 2016 г.). Гродно: ГрГУ, 2016. С. 20—30.
Ilyushchenko A.F., Savich V.V. Powder metallurgy is one of the first additive technologies. In: Additive technologies, materials and structures: Proc. sci.-tech. conf. (Grodno, 5—6 Oct. 2016). Grodno: GrGU, 2016. P. 20—30 (In Russ.).
9. Геров М.А., Каясова А.О., Терентьев В.Ф., Просвирнин Д.В., Колмаков А.Г. Механические свойства и особенности разрушения высокопрочной мартенситно-старееющей стали, полученной селективным лазерным сплавлением. *Деформация и разрушение материалов*. 2021. No. 9. С. 2—10.
Gerov M.V., Kayasova A.O., Kolmakov A.G., Prosvirnin D.V. Mechanical properties and fracture of high-strength maraging steel fabricated by selective laser melting. Russ. Metall. (Metally). 2022. No. 4. P. 309—315. DOI: 10.1134/S0036029522040139.
10. Ullah R., Akmal J.S. Anisotropy of additively manufactured 18Ni300 maraging steel: threads and surface characteristics. *Procedia CIRP*. 2020. Vol. 93. P. 68—78.
11. Kucerova L., Zetkova I., Jenicek S., Burdova K. Hybrid parts produced by deposition of 18Ni300 maraging steel via selective laser melting on forged and heat treated advanced high strength steel. *Add. Manuf.* 2020. Vol. 32. P. 100—111.
12. Караваяев А.К., Пучков Ю.А. Исследование структуры и свойств сплава ALSI10MG, полученного методом селективного лазерного сплавления. *Вестн. МГТУ им. Н.Э. Баумана. Сер. Машиностроение*. 2020. No. 5. С. 71—85.
Karavaev A.K., Puchkov Yu.A. Study of the structure and properties of the ALSI10MG alloy obtained by selective laser melting. Vestnik MGTU im. N.E. Baumana. Ser. Mashinostroenie. 2020. No. 5. P. 71—85 (In Russ.).
13. Deng H., Qiu W., Cao S., Chen L., Hu Z., Wei Y., Xia Z., Zhou L., Cui X., Tang J. Heat-treatment induced mic-

- rostructural evolution and enhanced mechanical property of selective laser melted near beta Ti–5Al–5Mo–5V–3Cr–1Zr alloy. *J. Alloys Compd.* 2021. Vol. 858. Art. 158351.
14. Богачев И.А., Сульянова Е.А., Сухов Д.И., Мазалов П.Б. Исследование микроструктуры и свойств коррозионно-стойкой стали системы Fe–Cr–Ni, полученной методом селективного лазерного сплавления. *Тр. ВИАМ.* 2019. No. 3 (75). С. 3–13.
Bogachev I.A., Sul'yanova E.A., Sukhov D.I., Mazalov P.B. Investigation of the microstructure and properties of corrosion-resistant steel of the Fe–Cr–Ni system obtained by selective laser alloying. *Trudy VIAM.* 2019. No. 3 (75). P. 3–13 (In Russ.).
 15. Nigon G.N., Isgor O.B., Pasebani S. The effect of annealing on the selective laser melting of 2205 duplex stainless steel: Microstructure, grain orientation, and manufacturing challenges. *Opt. Laser Technol.* 2021. Vol. 134. Art. 106643.
 16. Rasa T., Anderson J., Svensson L.-E. Microstructure of selective melted alloy 718 in As-manufactured and post heat treated condition. *Proc. Manuf.* 2018. P. 450–458.
 17. Yang W., Zhang X., Ma F., Dong S., Jiang J. Selective laser melting of 1.2738 mold steel: densification, microstructure and microhardness. *Mater. Res. Express.* 2021. Vol. 8. Iss. 1. Art. 016525.
 18. Tan C., Zhou K., Ma W., Zhang P., Liu M., Kuang T. Microstructural evolution, nanoprecipitation behavior and mechanical properties of selective laser melted high-performance grade 300 maraging steel. *Mater. Desing.* 2017. Vol. 134. P. 23–34.
 19. Hong Y., Dong D.D., Lin S.S., Wang W., Tang C.M., Kuang T.C., Dai M.J. Improving surface mechanical properties of the selective laser melted 18Ni300 maraging steel via plasma nitriding. *Surf. Coat. Technol.* 2021. Vol. 406. Art. 126675.
 20. Sun H., Chu X., Liu Z., Gisele A., Zou Y. Selective laser melting of maraging steels using recycled powders: A comprehensive microstructural and mechanical investigation. *Metall. Mater. Trans. A.* 2021. Vol. 52. Iss. 5. DOI: 10.1007/s11661-021-06180-1. P. 52.
 21. Mayer H., Schuller R., Fitzka M., Tran D., Pennings B. Very high cycle fatigue of nitrided 18Ni maraging steel sheet. *Int. J. Fatig.* 2014. Vol. 64. P. 140–146.
 22. Yin S., Chen C., Yan X., Feng X., Jenkins R., O'Reilly P., Liu M., Li H., Lupoi R. The influence of aging temperature and aging time on the mechanical and tribological properties of selective laser melted maraging 18Ni-300 steel. *Add. Manuf.* 2018. Vol. 22. P. 592–600.